Crashworthiness of Composite Sandwich Structures

PhD Thesis

Andrew John Davies

April 2002

Centre for Composite Materials, Imperial College of Science, Technology & Medicine

A thesis submitted to the University of London in accordance with the requirements of the degree of Doctor of Philosophy

ABSTRACT

The main objective of the present study was to investigate the in-plane crushing behaviour of CFRP-faced sandwich structures.

A survey of relevant literature on energy absorption was undertaken and the topic of in-plane crushing of sandwich panels was decided upon. The initial experimental work focused on obtaining progressive crushing of the panels whilst maximising their energy absorbing potential. Structural parameters such as face thickness, core thickness, lay-up and the effect of the triggering mechanism on energy absorption were studied.

Having discovered that a large percentage of the energy absorbed by the panels was in crushing the sandwich panels faces, an investigation was undertaken to see whether the failure modes seen could be replicated in smaller more economical specimens representing just the sandwich panel faces.

Small specimens of the same lay-up, thickness, etc. as the sandwich faces were manufactured and tested in a similar manner to the sandwich panels. It was seen that small specimens of the face skins tested in a "back-to-back" configuration failed in a very similar manner to that observed in the full sandwich tests. The small specimen tests were also used to investigate parameters such as loading plate friction, stacking sequence and the un-supported length of the specimen.

Complementary tests were also done to assess the energy absorbed in tearing of the face skins and debonding the faces of the sandwich panel from the core, two energy absorbing mechanisms likely to happen in a real structure.

Finally, various sizes of sandwich cruciform structures representing the intersection points of load-carrying beams in an aircraft subfloor fuselage structure were manufactured and tested. A linear relationship between cruciform size and parameters such as energy absorption and peak crush load was seen. An outline theoretical analysis of the failure of the face skins and the sandwich specimens was proposed.

ACKNOWLEDGEMENTS

There are many people I would like to thank for helping to make my thesis possible. Firstly, I would like to thank my supervisors Prof. Frank Matthews, Dr Paul Robinson and Prof. Paul Curtis who guided me through the trials and tribulations with good advice and good humour. I would also like to thank Prof. Paul Curtis and DERA for very kindly funding me with an EPSRC Case Award.

I should like to thank Hexcel Composites for providing the materials for the project.

For spending time and listening to my ideas, I would like to thank Rafael and Pedro and the staff of the Composite Centre.

For making usable pieces of equipment and test pieces, from my ideas, I would like to thank Sean, Ray and Gary. I would also like to thank John O'Leary for his patience in videoing the crush tests and John Churchward for advising me on test machines.

Lastly, I would like to thank Emily for putting up with me for those years, and my parents for humouring me when I decided to do the PhD.

CONTENTS

LIST OF FIGURES

Chapter 3

Chapter 4

Chapter 5

Chapter 6

Appendix B

Appendix C

LIST OF TABLES

NOMENCLATURE

AE	Crush force efficiency
A_o	Original cross-sectional area
a	Delamination length
B	Beam width
C	Compliance
D	Inside circular tube diameter
d	Beam thickness
d_c	Frustrum diameter
E_{abs}	Absorbed energy
E_s	Specific energy
F	Axial force
$F_{(avg)}$	Average force
F_o	Load to overcome resisting torque
$F_{(peak)}$	Peak force
G^*	Fracture toughness
G_{Ic}	Mode 1 fracture toughness
G_{IIc}	Mode 2 fracture toughness
k_{fi}	Foundation stiffness
L_c	Central crack length
L_i	Fibre bundle length
l_o	Compacted specimen length
l_s	Original specimen length
M_i	Crush mode indicator
m	mass of structure
N	Loading block correction factor
n*	Number of splits
P	Load
P_{sus}	Sustained load
R_{ad}	Fracture energy

r_o	Flange radius
r_i	Drum radius
S	Stroke
S_2	Shell shortening distance
SE	Stroke efficiency
SSCS	Specific sustained crush stress
T	Number of trials
T*	Average peel torque
t	Wall thickness
α_1	Angle formed between the height and external side of the wedge
α_2	Angle formed between the height and internal side of the wedge
δ	Load point displacement
ε_{ci}	Failure strain
ε_{fi}	Foundation failure strain
μ_1	Coefficient of friction between frond and platen
μ_2	Coefficient of friction between wedge and frond
θ	Semi-apical angle of the frustrum
σ	Stress
σ_{cr}	Critical stress
σ_o	Tensile fracture stress

CHAPTER 1

INTRODUCTION

1.1 Introduction

The aim of the work detailed in this thesis was to determine the energy absorbing potential of carbon/fibre-epoxy composite sandwich structures when subjected to in-plane compressive loading. The inclusion of composite materials in aerospace vehicles is increasing, especially with regard to primary load bearing structures. Composite materials offer considerable advantages over their metallic counterparts in terms of weight and fabrication costs, but also, more importantly, they offer the designer a way of tailoring a specific part to maximise strength for example, whilst minimising mass by placing the load bearing structures where they are most needed.

The experimental work carried out for this thesis concentrated on evaluating a specific type of composite material, namely the sandwich structure. The definition of a sandwich structure being "a construction comprising of a combination of dissimilar simple or composite materials, assembled and intimately fixed in relation to each other so as to use the properties of each separate component to the structural advantage for the whole assembly" [1].

A sandwich element is a special form of a laminated composite and consists of three main parts; two thin, strong, stiff and relatively high density facings separated by a thick, light and weaker core. The faces and core are adhesively joined in order to transfer the loads between the components. The advantages given by this design may be summarised thus: high stiffness and strength-to-weight ratios and integration of functions such as thermal and acoustic insulation, and high energy absorption capability.

In an aircraft crash the first event is often the contact of the landing gear with the floor, followed by the bottom of the fuselage contacting the ground. The subfloor beams, located between the cargo floor and the bottom of the fuselage deform. Crash-

induced loads can be transmitted from the subfloor beams to the rest of the aircraft. If the fuselage is not designed to carry these loads then failure of the aircraft is possible. It has been found to be expensive to design crashworthy vehicle structures using composite materials due to the inherently high research and development costs [(2)]. The problem stems from the nature of the crush process. Energy absorption is not a property, like elastic modulus or strength, which can be measured easily using coupon specimens. Instead, energy absorption is very sensitive to the form of the structure of which the material is a part.

Simple analytical calculations are typically utilised to design conventional composite structures. Development of sufficient data to establish a statistically valid design database for sandwich structures would be both cost and time prohibitive. An alternative to a database would be to develop simple calculations to predict the failure modes of simple sandwich structures with various geometries subjected to in-plane loading conditions.

An in-depth understanding of the cause and effect relationships of crash energy absorption in composite materials and structures is necessary, prior to the development of a method to predict the energy absorption capabilities of sandwich structures. It was seen that although work had been undertaken on the in-plane crushing of various structural geometries, the crushing of sandwich panels was not widely reported.

In this project the failure modes and energy absorbing processes of carbon fibre/epoxy sandwich specimens of increasing size and complexity were studied. Initially carbon epoxy faced, aluminium alloy cored sandwich panels were tested and then specimens which evaluated the failure modes seen in the sandwich faces were tested. Finally sandwich cruciform structures representing the intersection points of fuselage beams were evaluated (Figure 1.1). This last research topic is important as these intersection points act as areas of high stiffness which can, on the aircraft impacting with the ground, penetrate into the cabin area of the aircraft which is unacceptable from a safety point of view.

Once the response of sandwich structures to in plane loading has been understood, and analytical tools have been developed, efficient use of these structures to absorb crash energy can be achieved.

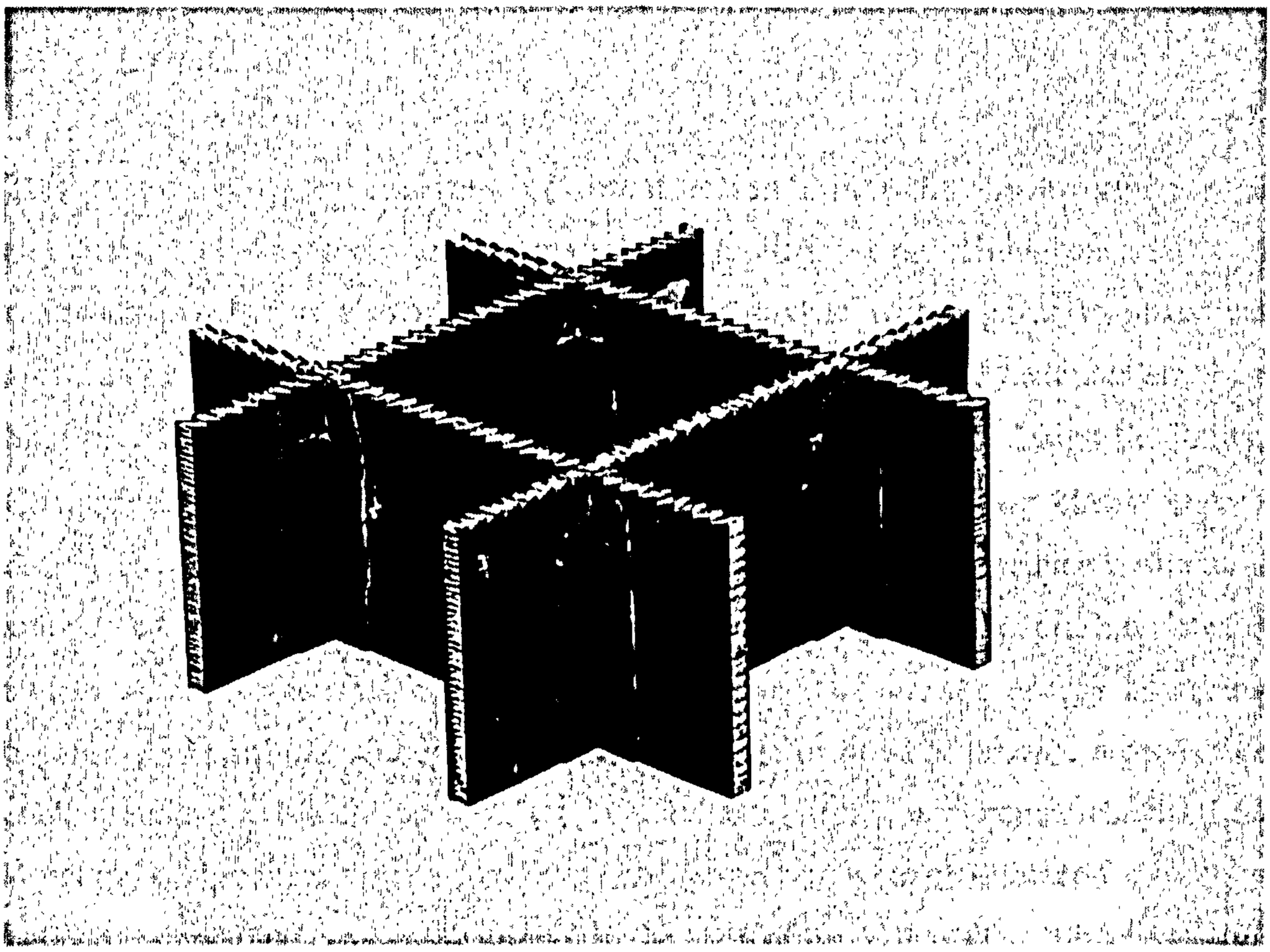

Figure 1.1 Cruciform structure

CHAPTER 2

LITERATURE REVIEW

2.1 Introduction

This section provides a review of recent research into the crashworthiness of structures, including tubes and beams manufactured from monolithic materials and sandwich panels. It also reports on the work to date with regards to analytical modelling of such structures. The major advantages of composite materials are their high specific strength and stiffness properties in combination with design flexibility. Composite materials also have considerable potential for absorbing kinetic energy during a crash [3]. Composites offer a unique combination of reduced structural weight and improved vehicle safety. They exhibit at least equivalent crash resistance to metals, and sometimes better [3]. Crash resistance covers the energy absorbing capability of crushing structural parts as well as the demand to provide a protective shell around the vehicle occupants (structural integrity). In aeronautics, the first structural design requirements for better crash protection were established for military helicopters and light fixed-wing aircraft in the form of the MIL-STD-1290A [4].

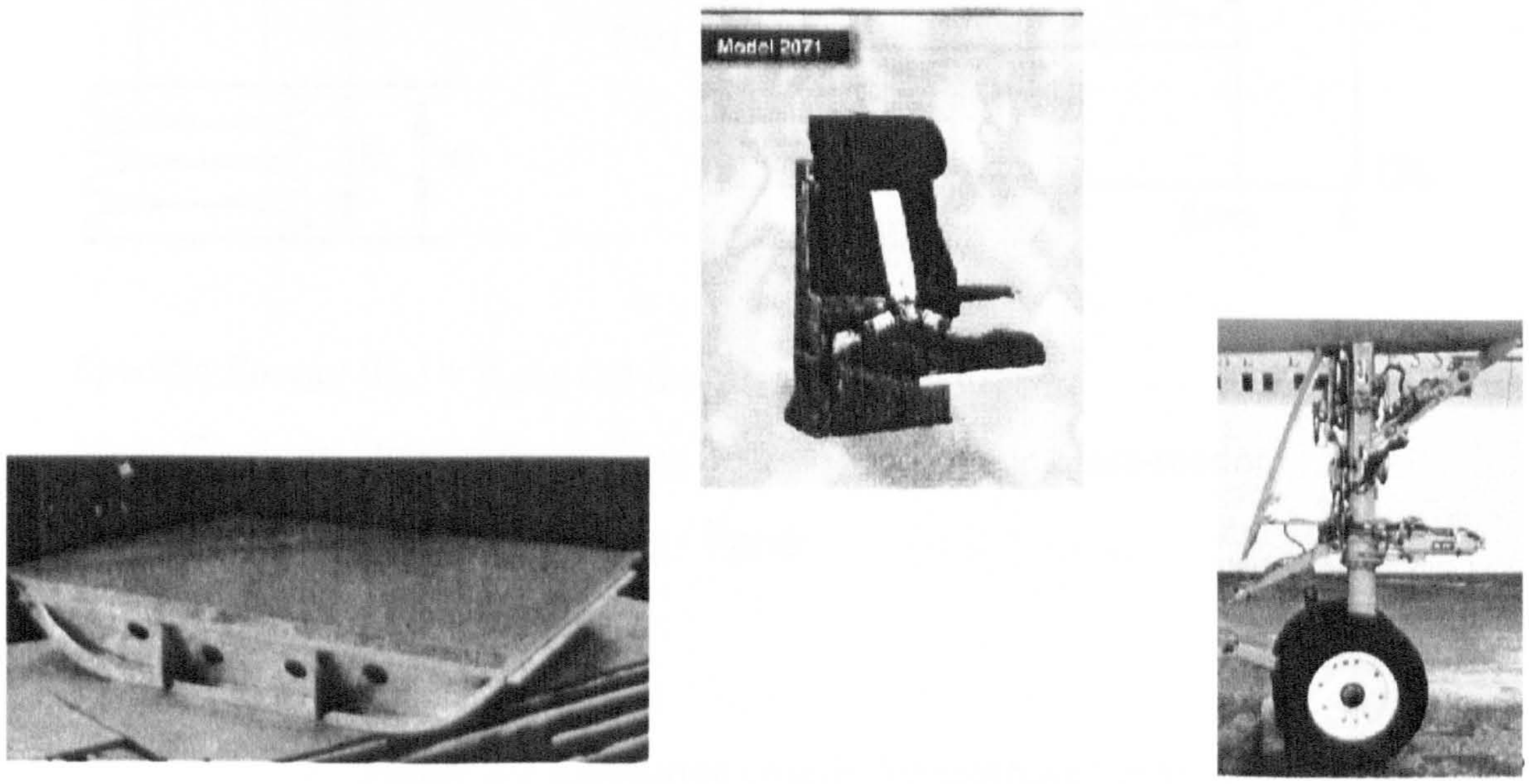

Figure 2.1 Systems approach to crashworthiness [5]

In an aircraft crash many structural items must act together to reduce the deceleration forces on occupants and to provide a protective shell around the occupied area. Especially important to the absorption of the vertical and horizontal components of the crash force are the following three structural areas [5]: - the landing gear, seat structure, and subfloor structure (Figure 2.1). The landing gear and seat structures are commonly composed of simple tubular structural members for which extensive impact energy absorption studies have already been conducted.

2.2 Criteria for Describing Crushing Behaviour

A terminology has been developed to describe and compare the energy absorption performance of collapsing or crushing material specimens or structural parts (Figure 2.2). The evaluation criteria are derived basically from the force-deflection curve and the absorbed energy, which is the area under this curve. The crushing characteristics typically have three stages: (a) initiation; (b) collapse by crushing or folding; and (c) compacting or "bottoming out".

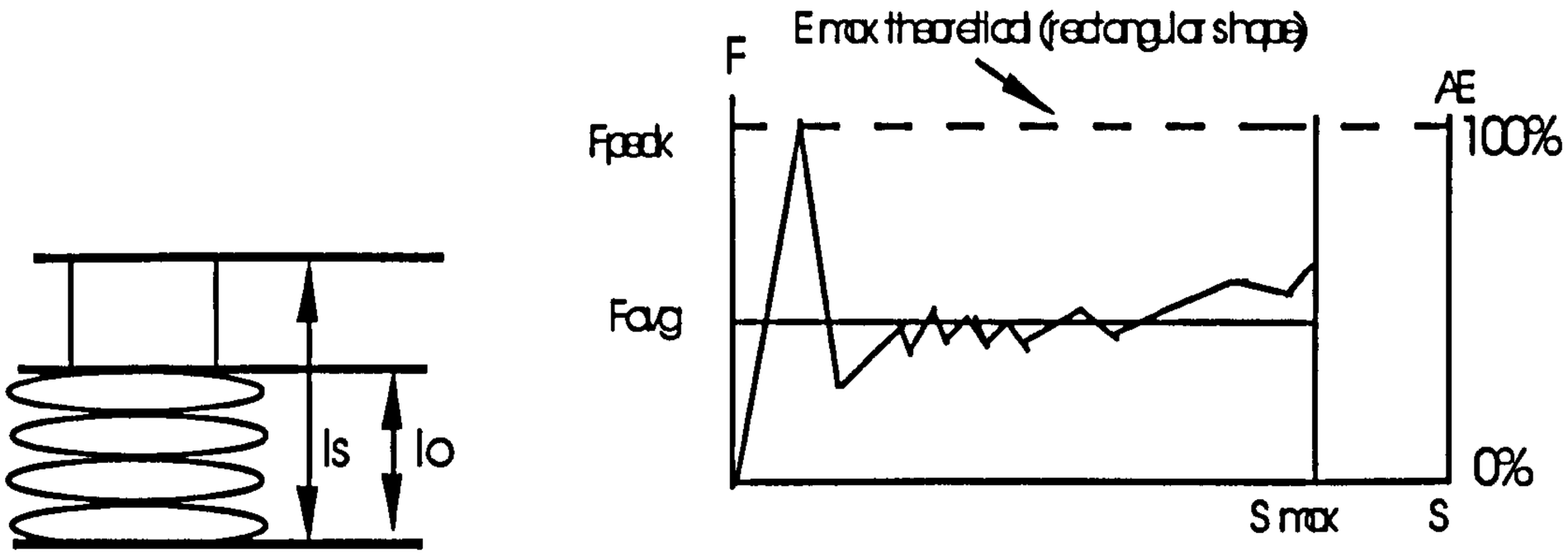

Specific Energy (E_s) = E_{abs} / $m_{destroyed}$ [kJ/kg]

Mean Crushing Stress = $\sigma_{cr} = F_{avg} / A_o$; A_o is original cross-section

Crush Force Efficiency $AE = F_{avg} / F_{peak}$

Stroke Efficiency $SE = l_s / l_o$

Figure 2.2 Evaluation criteria for crushing behaviour

2.2.1 Specific Energy

The specific energy relates the absorbed energy to the mass of the absorber or structure, and is therefore an important criterion for lightweight designs. As can be seen from Figure 2.2 Kindervater et al [3] define specific energy as absorbed energy divided by mass. Kindervater et al state that often only the crushed mass of the absorber is taken into account. However, in more complex structures the crushed mass is difficult to determine, and therefore the complete mass of the structure would be used. It is not stated how the specific energy will be altered by the measurement of different masses.

2.2.2 Mean Crushing Stress and Sustained Crushing Load

For an absorber sustaining an axial load, F, rather than a bending load, the crushing stress is calculated as the average crush force (F_{avg}) (a mean value about which the force oscillates) divided by the original cross-sectional area of the absorber. High values of crushing stress are required to absorb energy when impacted by large masses. The specific sustained crushing stress (SSCS) is a useful measure of energy absorbing capability often used in the literature; this is the average crushing load divided by the product of the cross-sectional area and the density of the absorber.

2.2.3 Crush Force Efficiency

The crush force efficiency value relates the average crush force, F_{avg}, to the maximum force, F_{peak}, of the crush characteristic. The highest force occurs normally in the initiation phase. An absorber that exhibits a rectangular force-deflection curve (ideal-plastic)(Figure 2.2) and theoretical maximum energy absorption has a crush efficiency of 100%. Lower values than this indicates force peaks during crushing.

2.2.4 Stroke Efficiency

The stroke efficiency, SE, is the ratio of the stroke, S, at compaction of the absorber to the initial length of the absorber. High ratios indicate efficient use of the material for a given absorbed energy. In structures with crushing modes, the fragmented and compacted debris can limit the amount of stroke leading to a low stroke efficiency, but not necessarily low energy absorption [3].

2.2.5 Post Crush Integrity

Post crush integrity is a measure of the residual structural capability of the structure.

2.3 Energy Absorption of Composite Plates and Tubes

2.3.1 Composite Failure and Energy Absorption Mechanisms

The importance of improved safety and crashworthiness in aerospace vehicles is evident through increased design requirements as specified by military standards [4]. To meet these requirements without severe weight penalties, designers of military aircraft are approaching vehicle crashworthiness from a systems approach i.e. using landing gear, fuselage structure and seats in combination to absorb energy. With the increased emphasis on lightweight vehicles the use of composite materials in aerospace and automotive structures has created a need to further understand the energy absorption characteristics of composite materials [4].

The material behaviour, the geometric parameters and the structural design govern structural crash resistance [3]. Owing to the brittleness of polymer composites reinforced by glass or carbon fibres, material plasticity is not really apparent. Basic fracture modes are fibre fracture, matrix fracture and fracture at the fibre/matrix interface in tension, compression and shear parallel and normal to the fibre direction.

On the laminate level, delaminations caused by shear or buckling of single layers or groups can also occur [6].

Crushing on the micro level is complex, and combinations of many mechanisms are apparent. The key mechanism of composite energy absorption under crush loading is formation of a microcrack pattern, which spreads across the laminate [6]. The formation of such a propagating front must be activated by a stress concentration where cracks first occur. The shape of the crush front generated by a so-called trigger or crush initiator (2.3.3.4) determines the level of crush force. The material properties, the laminate architecture, the trigger and the specimen geometry or structural configuration control the complex sequence of local cracking and fragmentation that occurs when a laminate is crushed [3].

Instability dominated failures caused by shell or Euler buckling lead generally to low energy absorption. Another important factor in the energy absorbing process is friction. Frictional forces act between the broken and sliding parts within the crush front, and between the crush platen surface and fragmentation debris. A set of basic crushing modes especially found in tubular absorbers [6] are (a) brittle fracturing, (b) lamina bending, (c) local buckling and transverse shearing (Figure 2.3a-d), a combination of (a) and (b), can also occur.

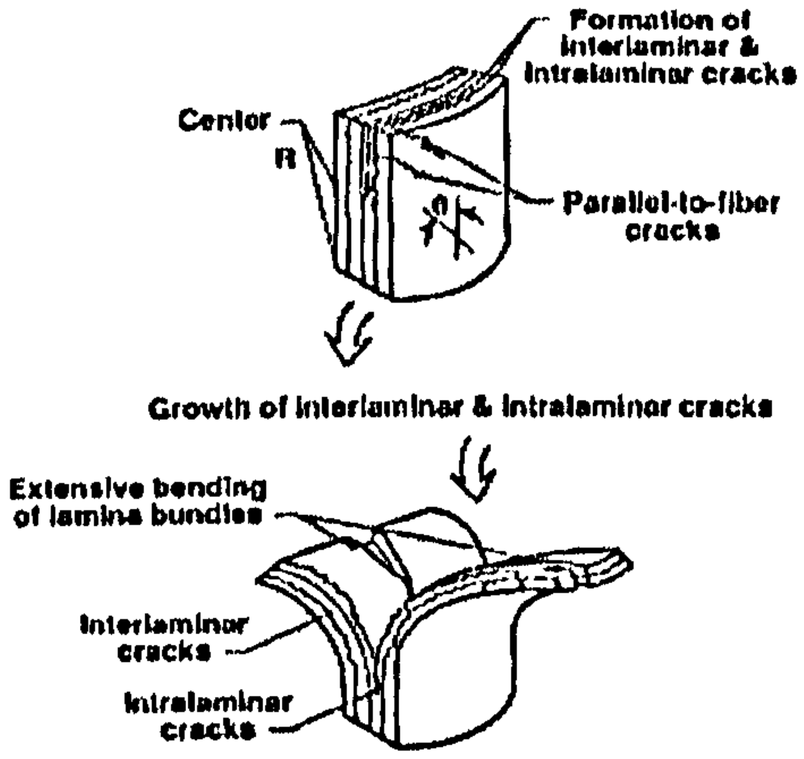

Figure 2.3a Typical basic crushing modes observed with tubes [3].

Brittle fracturing

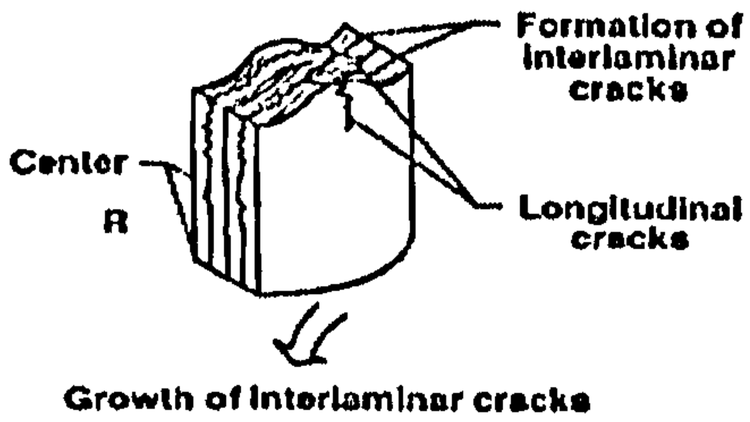

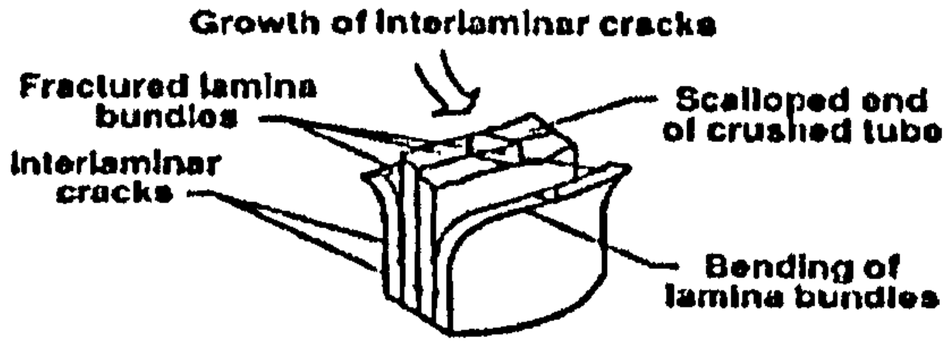

Figure 2.3b Lamina bending

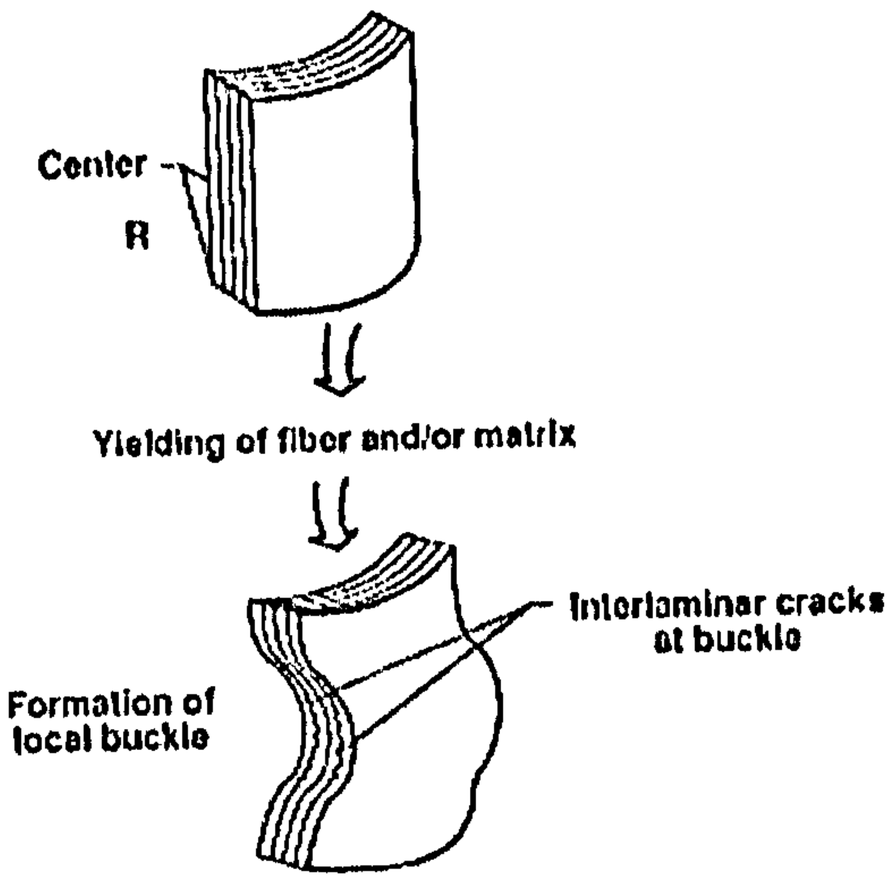

Figure 2.3c Local buckling

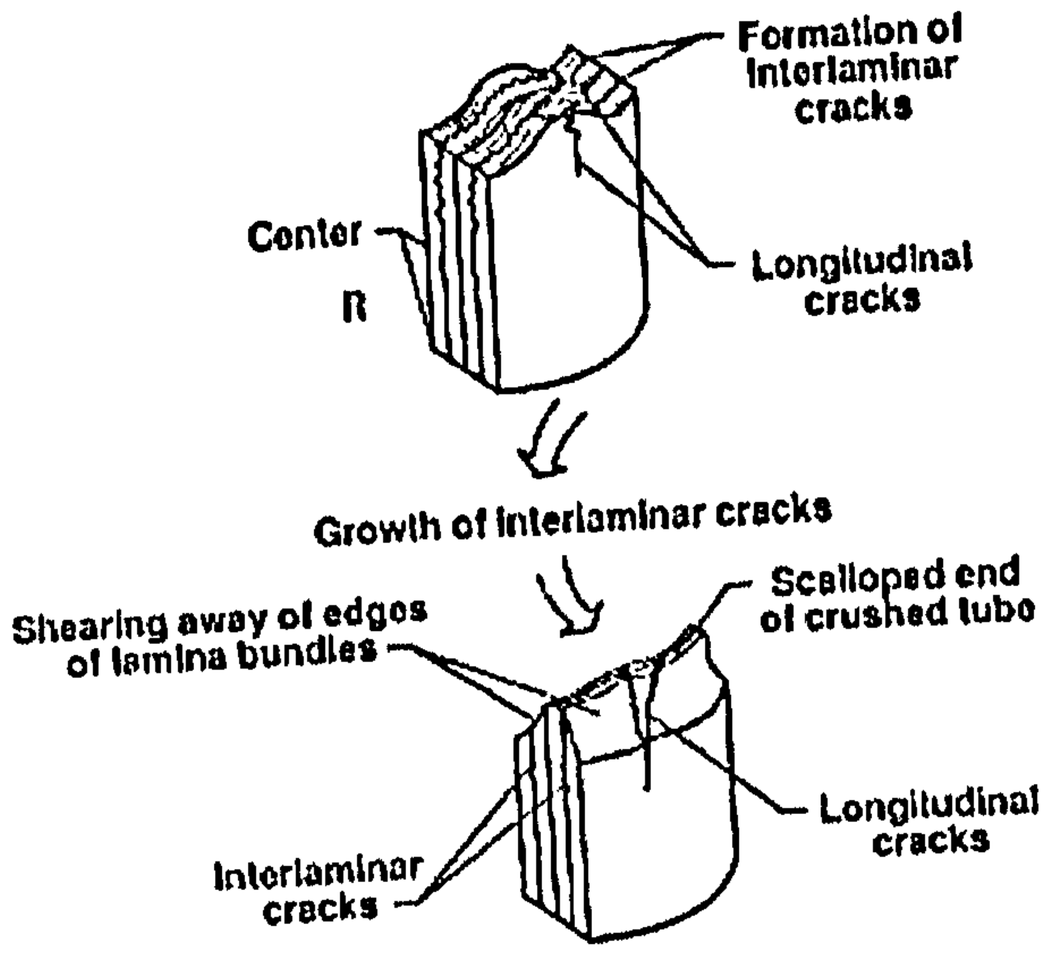

Figure 2.3d Transverse shearing

2.3.2 Energy Absorption of Composite Plates

The design of composite structures for crashworthiness is not well developed. Components such as tubes and beams that have complex shapes to suppress buckling and promote progressive crushing are expensive and difficult to fabricate with consistent results. Full-scale structural elements are generally tested as the relationship between full and sub-scale model energy absorption performance is not well understood, leading to high research and development costs [5].

A number of authors such as Lavoie et al [7-9], Vizzini et al [10,11] and Laananen et al [12,13] have investigated the crushing of plate type structures. Vizzini et al have investigated the energy absorption of composite plates under off-axis loads and also compared the energy absorption of plates with that of tubes and found comparable SSCS's and failure modes. Laananen et al have done work on developing an analysis methodology for predicting the energy absorbing capabilities of composite stiffeners based on crush tests of flat plate specimens. Ramany Bala Poubady et al [14] have worked on a similar problem using woven carbon fibre plates.

2.3.2.1 Quasi-static Crush Response.

Lavoie et al have developed a crush test fixture [9] for flat plate composite specimens. The test fixture illustrated in Figure 2.4 consists of a set of posts whose function is to guide the top platen. This platen is fitted with linear bearings for near frictionless travel on the guideposts. The posts, which provide support to the composite, are mounted on the lower platen and pass through clearance holes in the top platen. The specimen is in contact with, and supported by, knife-edges that fit into slots in the support posts. A collar is placed over each pair of support posts at their upper end to ensure that the specimen is supported along its entire length. Spreading of the support posts that would occur when a plate is crushed if the support posts were only cantilevered from the lower platen is eliminated.

The fixture has provided a method for screening candidate material systems, laminate stacking sequences, trigger systems and size scaling effects by being able to accommodate two sizes of plate. Three material systems were investigated; APC-2 (carbon fibre/PEEK), AS-4 / 3502 (carbon fibre/epoxy) and a hybrid AS-4/Kevlar 49/ 3502. All the materials used were in the form of unidirectional pre-pregs. The laminate stacking sequence was $[\pm 45°/0°_4/\pm 45°]_S$ for the APC-2 and the carbon fibre/epoxy baseline (1/2 scale) plates, and $[\pm 45°Kv/0°_4 carbon/\pm 45°Kv]_S$ for the hybrid baseline plates. Baseline plate dimensions were 76 x 51 x 2.2mm.

The full-scale plates had double the in-plane dimensions and thickness of the baseline plates. Thickness was scaled by ply-level and sublaminate-level approaches (Figure 2.5). The stacking sequence for ply-level scaled plates was $[45°_2/-45°_2/0°_8/45°_2/-45°_2]_S$, and for the sublaminate scaled plates was $[\pm 45°/0°_4/\pm 45°]_{2S}$. The stacking sequence for the carbon/Kevlar/epoxy full scale laminates were similar to the carbon/epoxy plates except that the 45° plies were Kevlar fibre/epoxy, instead of carbon /epoxy. Full scale plate dimensions were 102 x 152 x 4.3mm.

Table 2.1 summarises the quasi-static baseline test results of Lavoie et al [8] which are grouped by material system, laminate type and trigger mechanism, giving the crush initiation load, average crushing load, and the SSCS (specific sustained crushing

stress). The carbon fibre/PEEK baseline specimens had an average crushing load of 23.3kN while the carbon fibre/epoxy was 10.3kN. Plates were tested with both notched and steeple triggers. The different crush modes seen help to explain the differences in SSCS observed between the thermoplastic matrix material and the epoxy materials, and between the ply-level scaled and the sublaminate scaled plates. The energy absorption of the composite plates investigated was strongly related to the crush mode. There are four crush modes defined by Farley (see previously Figure 2.3). The preferred crush mode has been shown previously (Section 2.3.1) to depend on the constituent properties and stacking sequence and trigger mechanism.

Lavoie et al [7] found that a change in crush mode could be correlated with a change in matrix toughness. They also found that the crush mode of the sublaminate scaled APC-2 plate was similar to the most efficient transverse shear crushing mode. It was seen that the lamina bundles that resulted from short interlaminar cracks of length less than the plate thickness grew during crushing and did not shear off, so much as curl away. Little fracturing of fibres actually took place, except for a few 0° plies near the laminate core. There may well instead be matrix shear yielding at 45° to the load axis.

Table 2.1 Plate crush results [8]

MATERIAL Trigger Mechanism/ Scale**	No. of Tests	Crush Initiation Load (kN)	Average Crush Load (kN)	SSCS (Nm/g)
AS4/PEEK				
Steeple baseline	3	30.54	23.28	133.1
Steeple ply-level	3	27.27	14.13	81.2
Steeple sublam.	3	31.45	25.10	143.8
Notch baseline	3	31.59	24.62	140.7
Notch ply-level	3	23.61	15.55	89.4
Notch sublam.	3	31.01	27.60	158.7

Table 2.1 Plate crush results [8]

MATERIAL Trigger Mechanism/ Scale**	No. of Tests	Crush Initiation Load (kN)	Average Crush Load (kN)	SSCS (Nm/g)
AS4/3502				
Steeple baseline	4	15.49	10.30	62.9
Steeple ply-level	3	11.93	7.42	43.3
Steeple sublam.	3	15.67	10.38	60.5
Notch baseline	5	18.43	11.70	71.5
Notch ply-level	3	16.05	8.41	49.0
Notch sublam.	3	18.96	12.37	72.1
AS4/Kevlar/3502				
Steeple baseline	3	15.46	9.33	53.7
Steeple ply-level	2	11.84	6.89	40.9
Steeple sublam.	3	12.30	8.38	49.9
Notch baseline	2	17.39	9.61	55.3
Notch ply-level	2	15.15	7.28	43.4
Notch sublam.	4	16.59	8.86	52.7
** see Figure 2.5				

The ply-level scaled APC-2 (PEEK) plates crushed in the inefficient, lamina bending/crushing mode; this is usually characterised by extensive delamination. In the APC-2 plates laminae delaminated 15-35mm (i.e. four to nine times the plate thickness) into the plate and across its width before fracturing away, (unfortunately no clear pictures were available to illustrate this point). This explains why the energy absorption was only half that of the sublaminate scaled plates. All the APC-2 plates showed superior energy absorption compared with the other systems tested; this was attributed to the high interlaminar fracture toughness of the PEEK matrix. For PEEK-based materials G_{Ic} is of the order of ten times that of epoxy-based materials, which explains the substantial reduction in delamination observed in carbon fibre/PEEK as

compared to their epoxy matrix counterparts. Both the ply-level and sublaminate scaled carbon fibre/epoxy plates crushed mainly by delamination and lamina bending, with some fracturing of the inner plies in evidence.

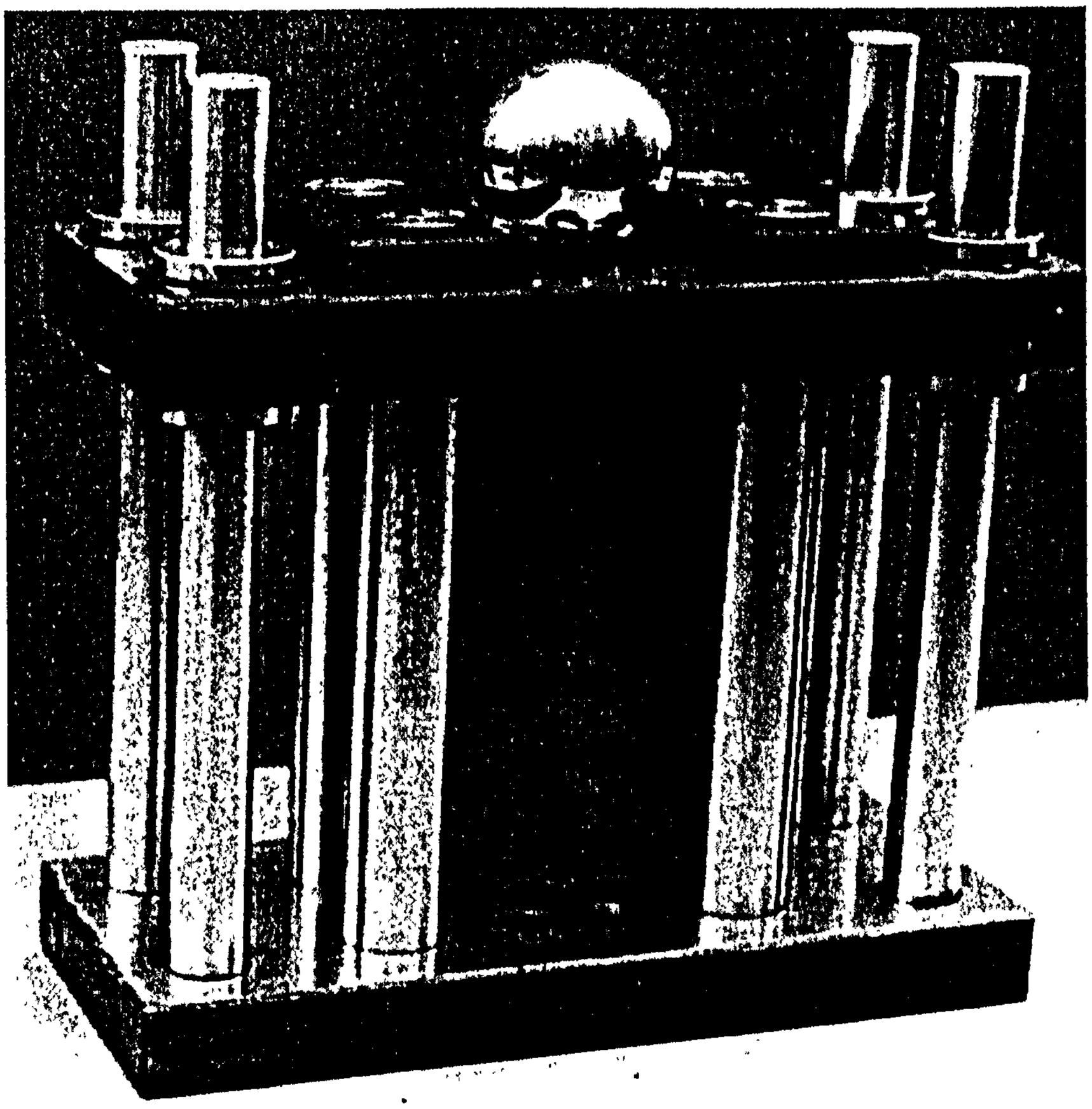

Figure 2.4 Crush test fixture

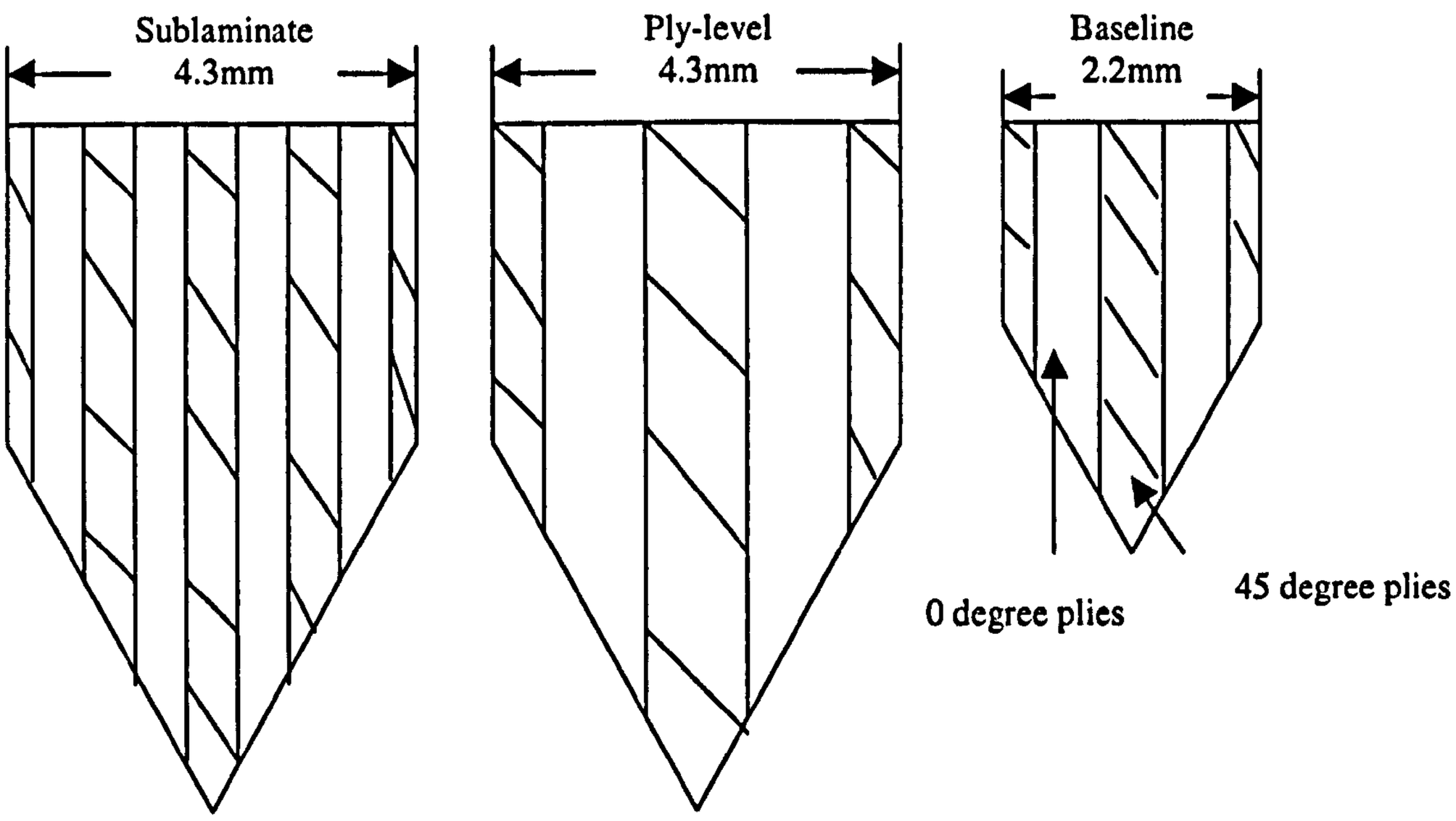

Figure 2.5 Thickness scaling approach: from baseline stacking sequence $[\pm 45/0_4/\pm 45]_s$, up to sublaminate $[\pm 45/0_4/\pm 45]_{2s}$, or ply-level scaled $[45_2/0_8/45_2/-45_2]_s$

It was found that the carbon fibre/Kevlar/epoxy plates had lower energy absorption than the carbon fibre/epoxy plates because the Kevlar fibres are weaker in compression, and much less stiff than carbon fibres, hence the Kevlar fibres were supporting less load than the carbon fibres. The carbon/epoxy and the hybrid plate crushed in the inefficient lamina bending mode (Figure 2.3).

2.3.2.2 Dynamic Crush Response

APC-2 plates when dynamically crushed using a drop tower [7] showed a decrease in energy absorption, compared with the quasi-static case, due to a transition to a less efficient crushing mode. This was attributed to a drop in matrix toughness at high strain rates, although Lavoie et al do not elaborate on this point. The energy absorption of the hybrid carbon/Kevlar/epoxy was seen to be almost rate insensitive. Dynamically crushed baseline and sublaminate scaled plates had crushing stress values very close to the ply-level scaled plates [9]. This is explained by the transition

of the former from an efficient energy absorbing mode characterised by short fractures, to the inefficient energy absorbing lamina bending/crushing mode dominated by delamination and ply-spreading (Figure 2.3). The carbon fibre/epoxy plates also showed reduced energy absorption when crushed dynamically, but to a lesser extent than those of APC-2. The reason for the reduced effect is that carbon fibre/epoxy plates already crush in the lamina bending mode when tested quasi-statically therefore, unlike the APC-2 there is no transition of crushing mode, the observed change in energy absorption is smaller.

The Kevlar plies in the hybrid plate were seen not to fragment. Crushed material accumulated in the knife-edges incorporated into the fixture, possibly acting as a constraint to ply spreading and so the load carried increased. In contrast it was seen that carbon fibre/epoxy plies fractured along the knife-edges as the delaminated plies spread. Large load spikes were observed during the dynamic crush response of the hybrid plate. These were thought to be an interaction between the fixture and the specimen that simulated the constraining action to spreading observed in crushing of tubes.

2.3.3 Energy Absorption of Composite Tubes

To develop an understanding of the energy absorbing behaviour of composite elements and how the numerous laminate parameters affect the crushing performance, many tests, both quasi-static and dynamic, have been performed, mostly on tubes. Below is a summary of the literature of the work published on tubes and how specific parameters alter their energy absorbing capabilities.

2.3.3.1 Effect of Material Properties

Thornton et al [15] concluded that the specific energy of commonly used reinforcing fibres tends to increase in the order of carbon < glass < aramid/other synthetic fibres. For the matrix the specific energy tends to increase in the order phenolic < vinyl ester < epoxy. A linear dependence of the specific energy upon the resin tensile strength and the modulus is also reported (Figure 2.6) [15]. Specific energy is taken to be the

energy absorbed divided by the mass of the amount of material destroyed in the crushing process (Figure 2.2).

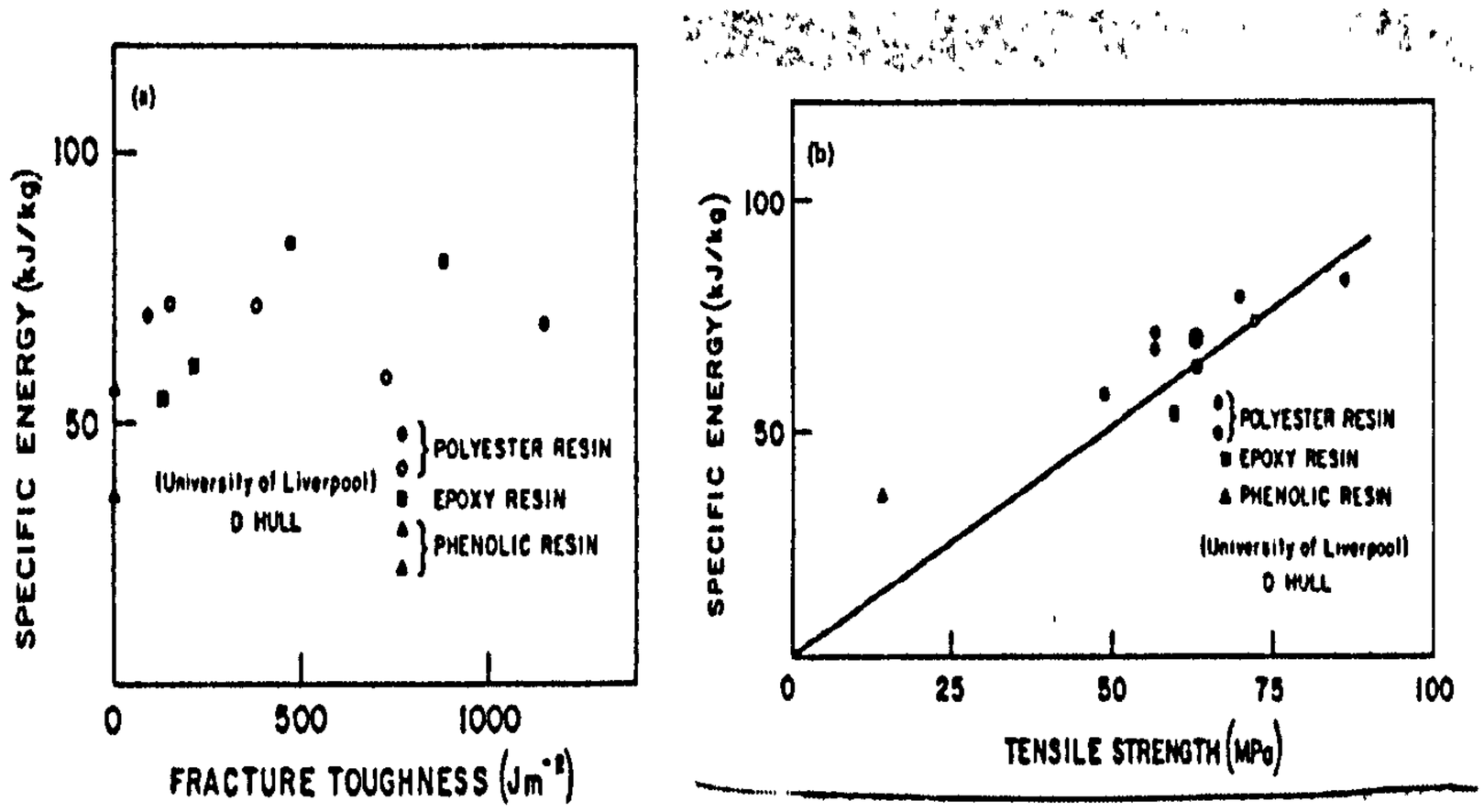

Figure 2.6 Variation in specific energy of glass-fibre composite tubes with a) resin fracture toughness and b) resin tensile strength [15]

2.3.3.2 Fibre Orientation

Tube ply orientation can affect energy absorption significantly. There is evidence that fibres oriented in the loading direction (tube axis 0°) increase the energy absorbing capability, especially in combination with inner and outer hoop layers (90° orientation) [16]. It has been found [3] that the following orientations produce high crush forces: - hoop layers at the outside (90°/0°), pure 90° and ±45° tubes, and orientations (± angle / 0°), but Kindervater et al did not elaborate on the above lay-ups. The influence of fibre orientation is more evident when brittle fracturing is seen (glass and carbon fibre reinforcements, hybrids). When tubes fail in local buckling (aramid and polyethylene fibre reinforcements), the influence of the fibre orientation is not as large.

2.3.3.3 Tube Geometry

Energy absorption with regard to the cross-sectional shape increases in the order rectangular<square<circular for tubes [15]. Farley [17] found that important parameters that affect energy absorption are the ratio of circular tube diameter D to wall thickness

t, or the ratio of square tube width W to wall thickness t. As the tube D/t and W/t decrease, energy absorption capability increases. Farley [17] does not state if there is a limit to this trend.

2.3.3.4 Trigger Mechanisms

Triggers are used to serve two purposes: (a) to initiate stable propagating crushing and (b) to reduce initial peak loads. In brittle fracturing modes, chamfer angles between 30° and 45° are recommended for stable crush initiation. Czaplicki et al [18] compared identical glass fibre-reinforced tubes with bevel and tulip triggers (Figure 2.7), and reported that up to 100% more energy per unit weight was absorbed by tulip triggered tubes. In addition to this, the crushing was more controlled and predictable using a tulip trigger. The primary difference in appearance between specimens crushed using the two triggers is the distance between the fracture lines (Czaplicki et al showed no diagrams to clarify this particular point). These are formed periodically after delamination cracks have penetrated between the surface glass mats and the uniaxial fibre bundles (Figure 2.8). The shorter distance between fracture lines for tulip triggered than for bevel triggered tubes results in the former having more fractures both within the glass mats and the unidirectional fibres, in addition to an increased regularity of fracture.

The difference in fracture line spacing seems to be the result of the type of crack pattern that is produced from the trigger. The pattern that results from triggering appears to persist for the entire crushing process. In addition to affecting the crushing load and energy absorption, the fracture behaviour appears to affect the load stability. The difference in crushing appeared to arise from the different abilities of the tubes to support load because of the different geometry of individual load carrying structures that resulted from triggering.

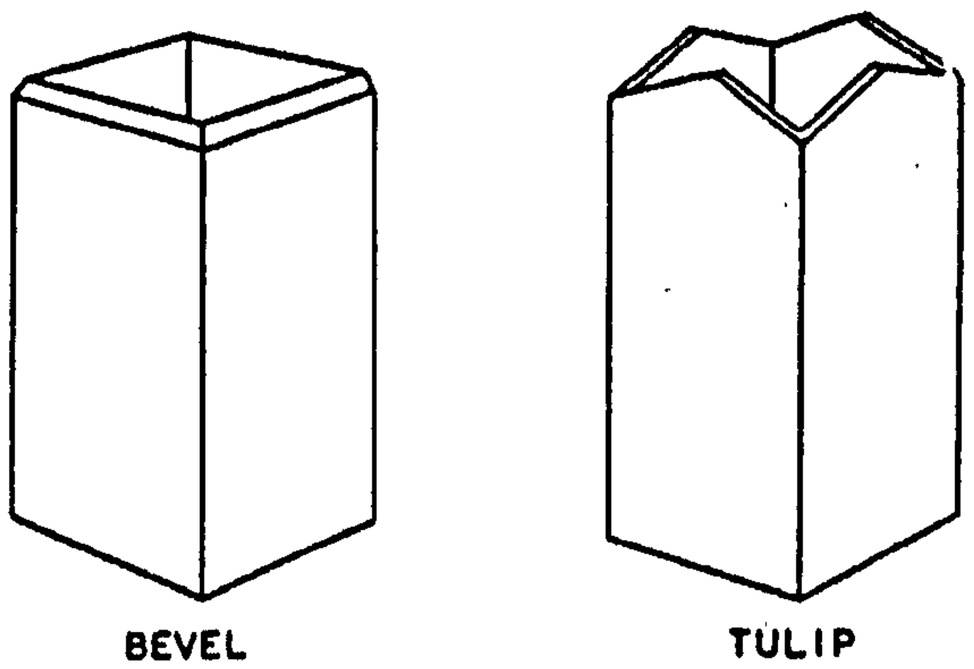

Figure 2.7 Bevel and tulip triggers [18]

By using a tulip trigger the force-deflection curve can be tailored to a predetermined shape. If the tube fails by buckling, then the trigger has no, or much less, influence compared with brittle fracturing.

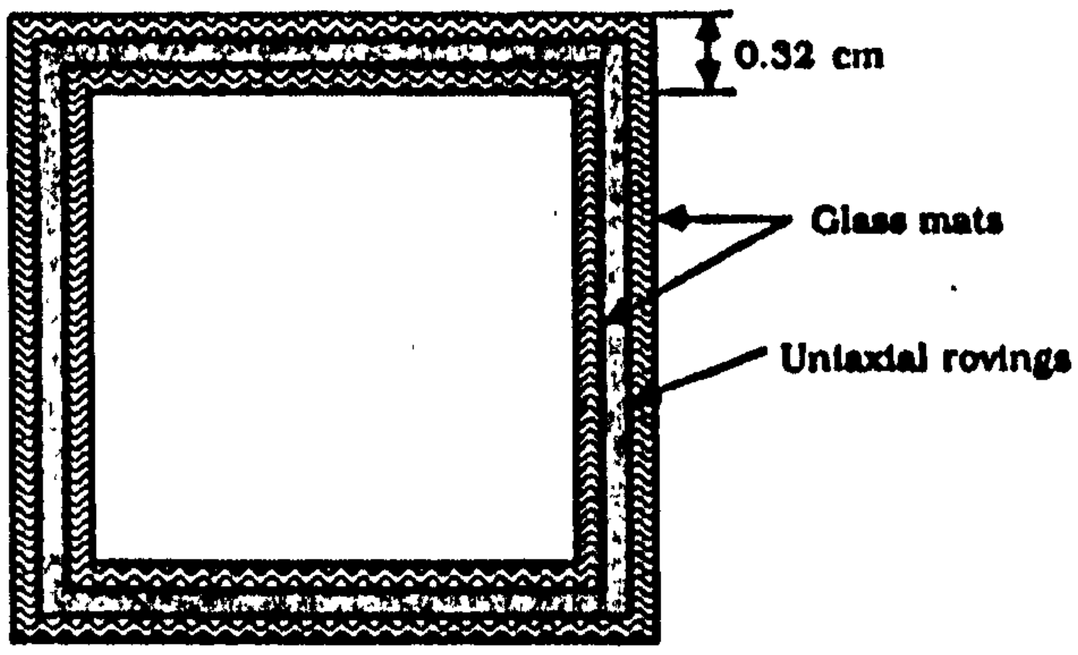

Figure 2.8 Schematic diagram of tube lay-up.

2.3.3.5 Rate Effects

Rate effects result from structural inertia and strain rate sensitivity of the mechanisms that control the crushing process. Therefore fibre or matrix strain rate sensitivity can influence crushing [3]. Owing to the different testing methods (hydraulically driven machines and drop towers), trends are difficult to interpret. With hydraulic machines the strain rates can be controlled, whereas with a drop tower a more realistic crash process is simulated, i.e. the strain rates are high at initial impact and zero at maximum stroke. For epoxy matrices, the specific energy increases with increase in strain rate, the magnitudes of the increase being less for carbon fibre-reinforced composites (about 2%) than for glass fibre-reinforced composites (about 20%) [15][19].

Work carried out by Farley [19] links the energy absorption of carbon fibre/epoxy and Kevlar fibre/epoxy tubes to crushing speed. The magnitude of the effects of crushing speed on energy absorption capability was determined to be a function of the mechanism that controls the crushing process. The effect of crushing speed on the energy absorption capability is related to whether the crushing of the trigger is determined by strain rate. With glass fibre-reinforced polyester plastics there is a decrease in specific energy with increase in rate (not specified), the magnitude of the decrease being about 30% [20]. Further work by Farley [21] establishes the influence of fibre and matrix maximum strain at failure on the energy absorption capability of carbon fibre-reinforced composite material. The higher the strain to failure of a particular composite system, the higher the energy absorbing capability it possessed. Tests carried out by Farley et al [21] showed that as the matrix failure strain is increased, so interlaminar cracking is reduced. The reduced interlaminar cracking results in the fracture crushing mode rather than the bending crushing mode, and hence more energy is absorbed.

2.3.3.6 Temperature

If operating temperature changes then the resin properties control the changes in energy absorption, and the effect can be directly related to the matrix behaviour which will be related to the glass transition temperature of the resin. Most reinforcing fibres do not change mechanical properties within their operating temperature range (-40°C

to 120°C)[3]. Changes in temperature affect the crush characteristics of composites primarily through the changes in resin properties. For epoxy matrices a decrease in specific energy becomes particularly noticeable at temperatures above 150°C, for polyester matrices the decrease occurs at temperatures above 120°C [3].

2.4 Energy Absorption of Sandwich Panels.

2.4.1 The Sandwich Concept

During the past decades technical development has been heading towards more and more sophisticated and optimised structural design in the pursuit of increased performance and improved economy [22]. This has been achieved by utilising new materials, e.g. fibrous composites, ceramics and new alloys, but also by using new structural concepts. One of the new structural concepts that has found increasing use in recent years is sandwich construction. This concept is based on the use of a combination of particular materials in order to fulfil the desired mechanical and physical requirements. The feature of sandwich construction is the opportunity, through efficient design, to utilise each constituent to its practical limit.

The definition [1] for a structural sandwich is " a construction comprising of a combination of dissimilar simple or composite materials, assembled and intimately fixed in relation to each other so as to use the properties of each separate component to the structural advantage for the whole assembly".

A sandwich element is a special form of a laminated composite and consists of three main parts; two thin, strong, stiff and relatively high density facings separated by a thick, light and weaker core. The faces and core are adhesively joined in order to transfer the loads between the components (Figure 2.9). The advantages given by this design may be summarised thus: high stiffness and strength-to-weight ratios and integration of functions such as thermal and acoustic insulation, and high energy absorption capability [22]. Such structures are particularly good in flexure.

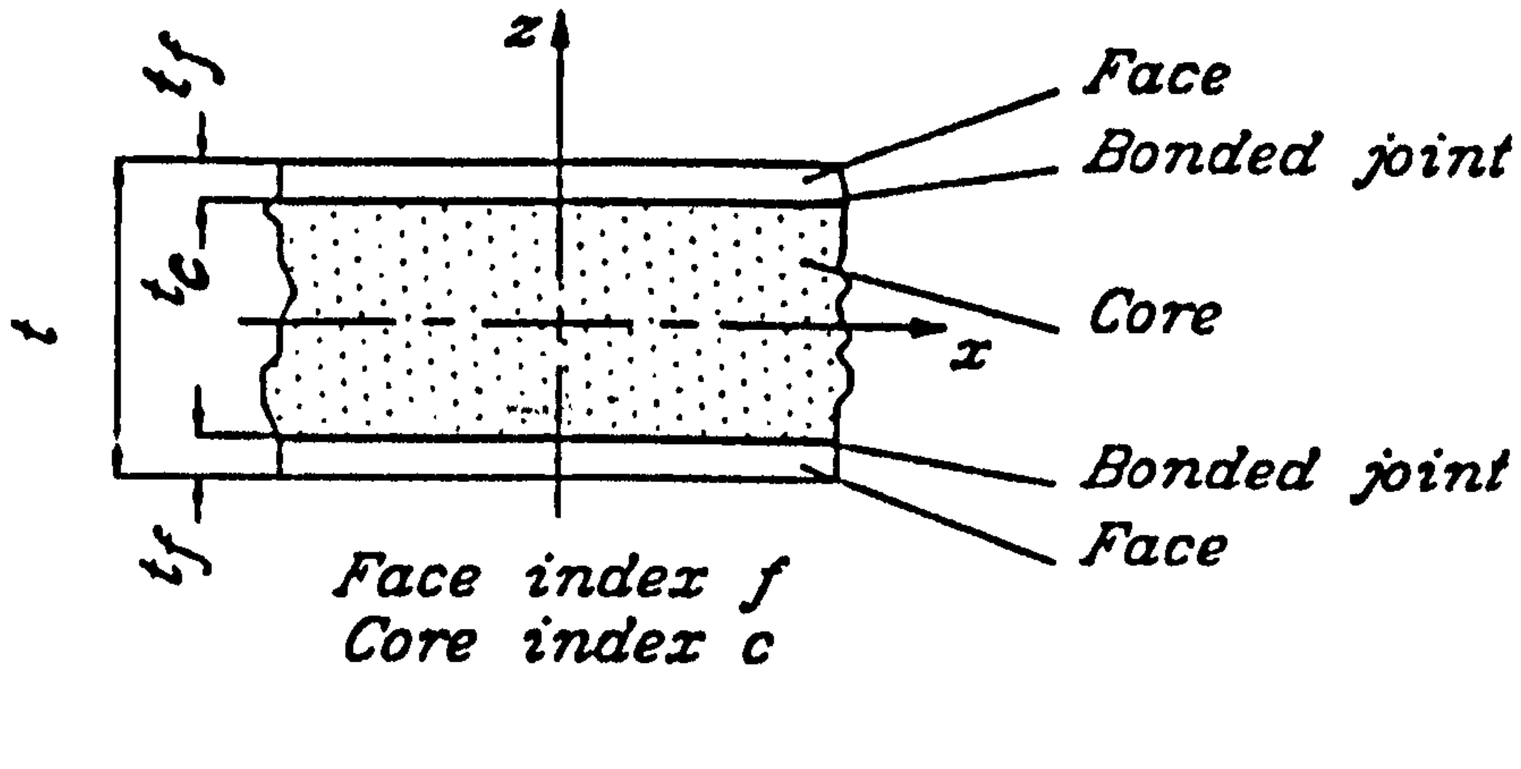

Figure 2.9 Sandwich concept

Improvements in structural crashworthiness, a critical consideration in many engineering applications, must be accomplished within certain constraints, such as limits on force transmission and/or deformation. If only small deformations are permitted, then large amounts of momentum transfer and force levels must be expected, which may be unacceptable. Conversely, if large permanent deflections are tolerable, a limit can be set on the magnitude of the force transmitted. This objective can be achieved by employment of sandwich components that dissipate energy mainly by localised crushing of the core and bending, crushing and stretching of the facings.

With careful choice of the material and thickness of the three components of the sandwich, as well as the geometry of the cellular structure, it is possible to simultaneously design for a desired peak transmitted force and the amount of energy that can be usefully absorbed per unit area. The practical limit of this dissipation is reached when the cellular core has been completely crushed either through the thickness, or in plane. Further loading is resisted by force levels corresponding to the core material acting as if it were solid (Figure 2.10).

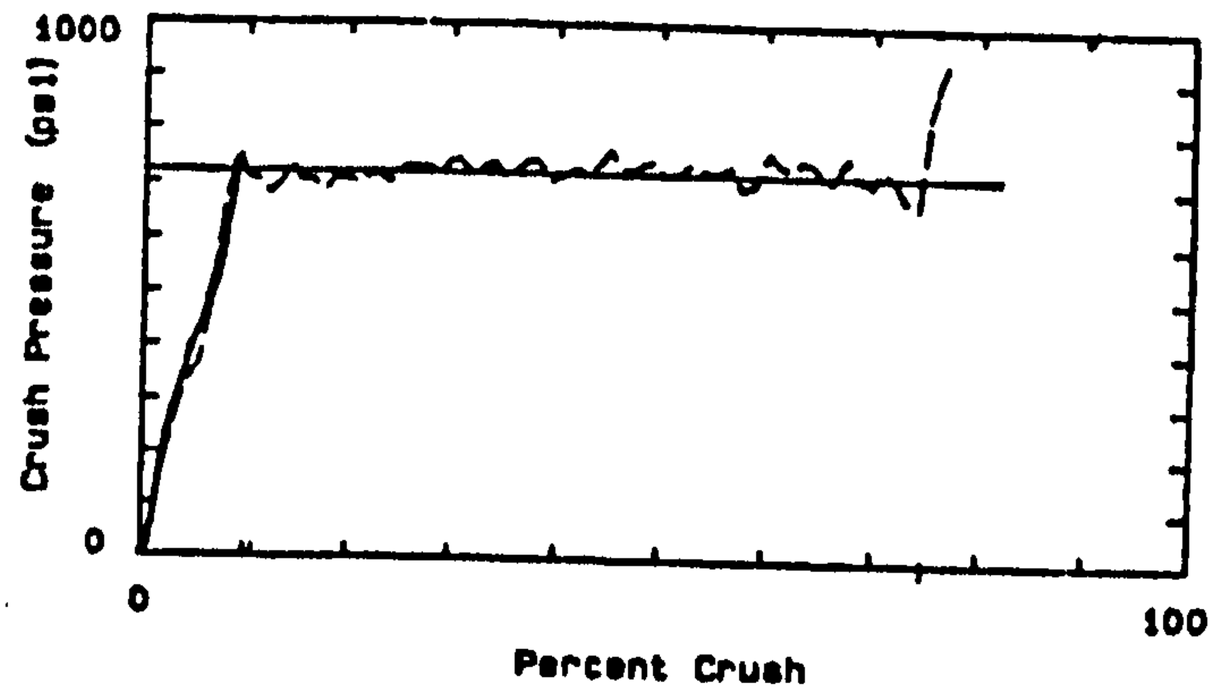

Figure 2.10. Pressure-crush curve for aluminium honeycomb showing densification onset [23]

2.4.2 In-Plane Loading of Sandwich Panels

Brachos et al [24] have published work on the analysis of edge loaded sandwich panels. It has been found experimentally by these authors that the presence of a core in structures like cylinders, etc. increased the energy absorption capability of these components in a manner similar to that illustrated by the classic problem of a column, or plate, on an elastic foundation (Figure 2.11). The modulus of the foundation represents the magnitude of the reaction of the foundation per unit surface area of the plate, per unit deflection of the plate. As the modulus of the foundation increases the axial load carrying capability increases, which also translates to an increase in energy absorption capability, although this also depends on deflection.

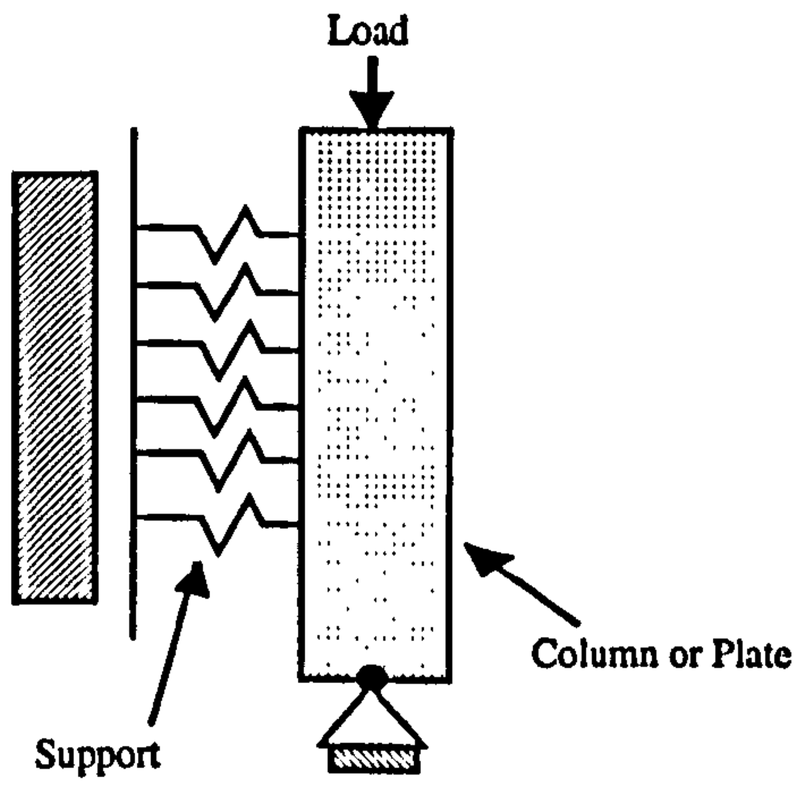

Figure 2.11 Column on an elastic foundation analogy

Flat sandwich plates were loaded in edgewise compression [24] between two crushing plates and crushed without any edge support, other than a bottom edge fixture which consisted of two metal angled stiffeners, held in place with two bolts (Figure 2.12). Loading the specimens resulted in information about the crushing behaviour of the plates as well as the load-displacement curves. It was found that not only did the core (balsa in this specific case) increase the buckling load of the faces, but, also controlled the failure mode by imposing a lamina bending mode (Figure 2.3). It was seen that initially the glass fibre/epoxy skins bent away from the core. During the initial deflection of the skins away from the core, they are still supported by the core, the face-to-core adhesive acting like a set of springs trying to pull the skins back. By altering the stiffness of the cores used, a different failure mode was obtained. If a soft flexible core was used the panel would fail in a local buckling mode. If the stiffness of the core was increased the panel would collapse in a local crushing mode with mode I fracture in the core.

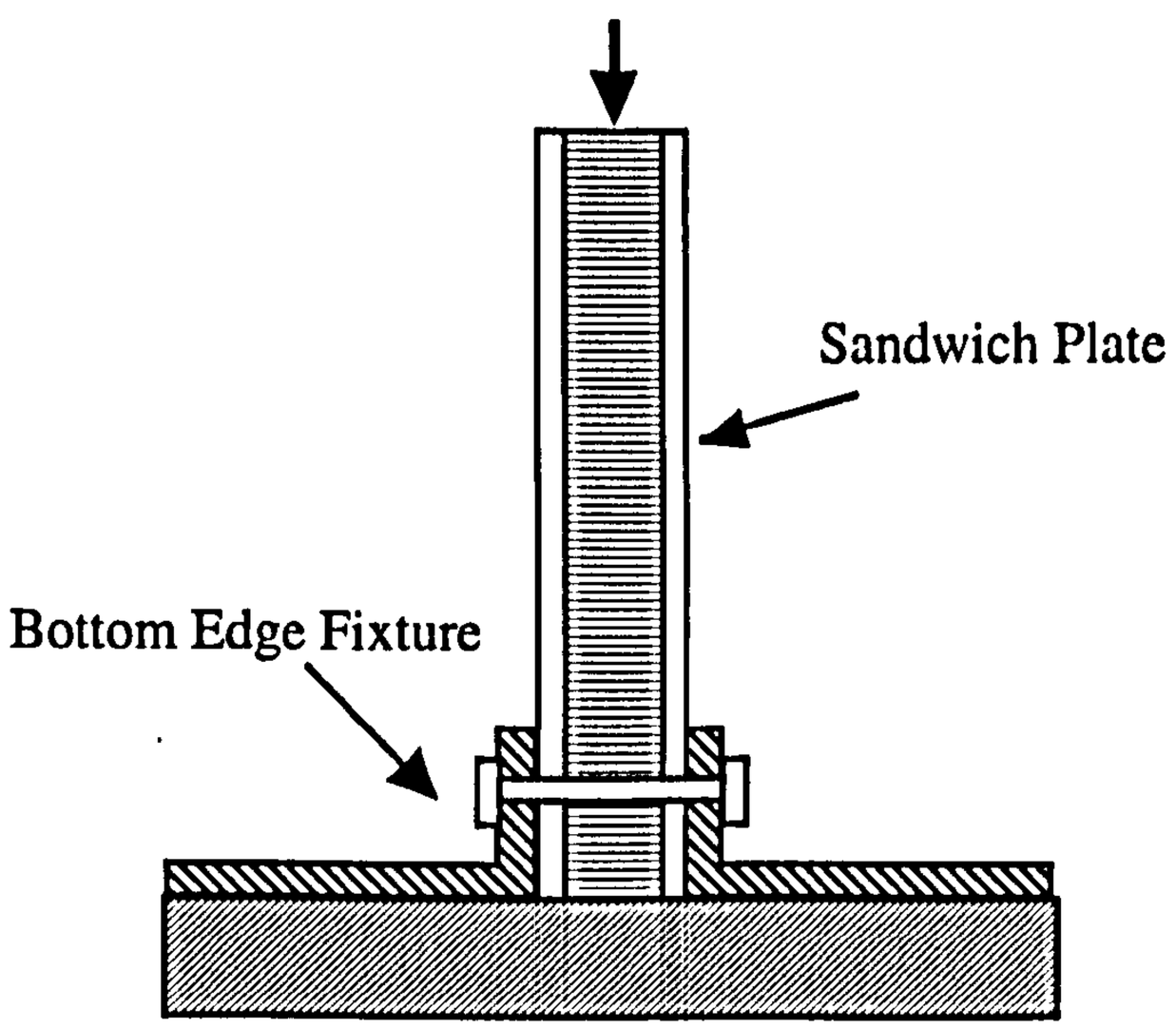

Figure 2.12 Edgewise compression rig

Brachos et al proposed a model to predict failure initiation (Figure 2.13). The model consists of an axially loaded beam on an elastic foundation. The top edge of the plate is free to move, the bottom edge is fixed. The mode of buckling of the beam is dependent on the length of the beam. The analysis for the model would be based on fracture mechanics, perhaps using the stress intensity factor at the tip of the crack in the balsa core during failure initiation.

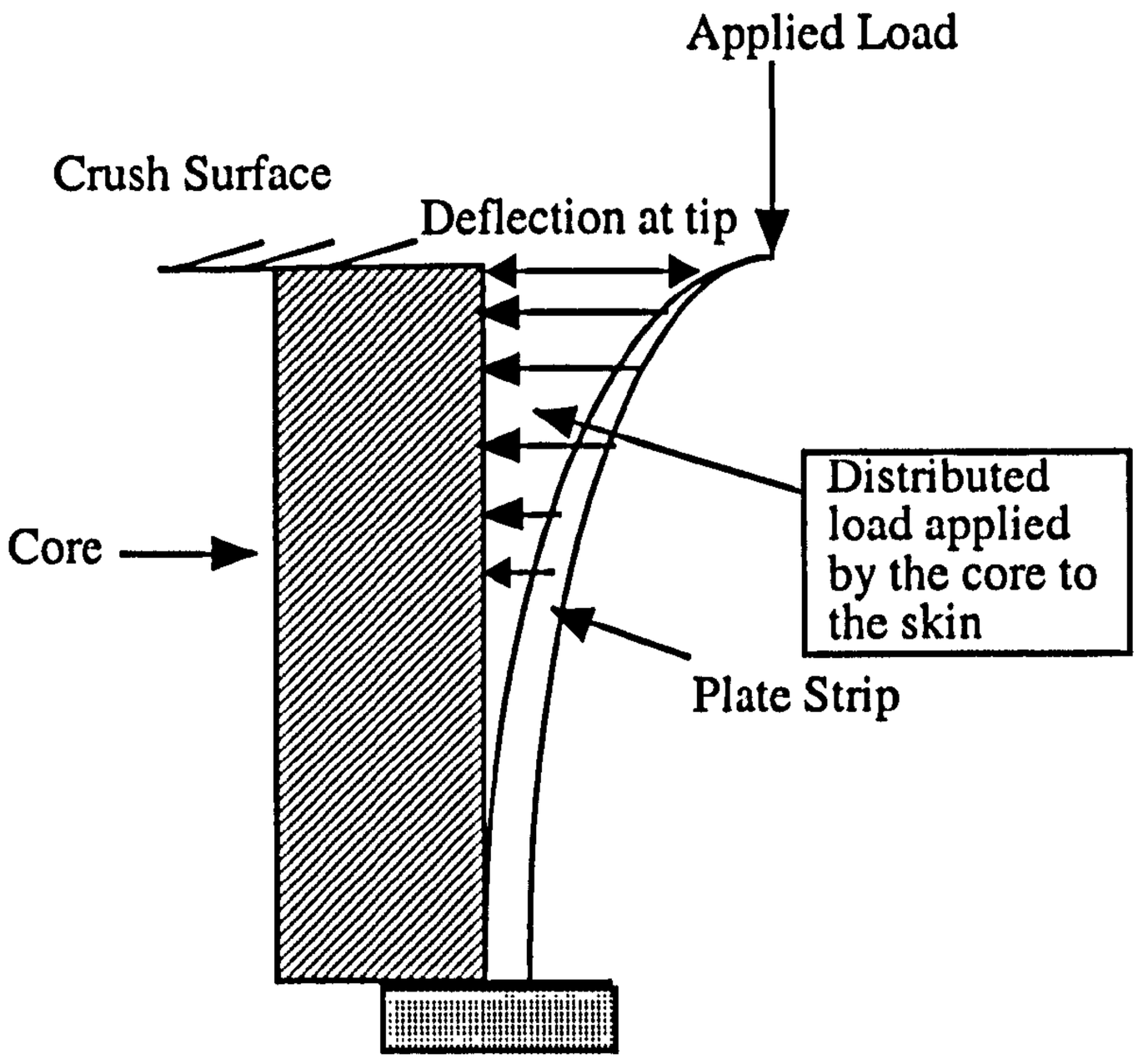

Figure 2.13 Schematic of skin deflection from core

2.5 Airframe Crash Resistance.

Crashworthiness is a complex subject involving human tolerance, the crash environment (impact surface, terrain, aircraft velocities and attitudes), seats and restraints, cabin environment, post-crash fire, landing gear, and the airframe structure. In addition the type of aircraft will affect the crashworthiness design approach. For example, to provide control of decelerative loads of seated occupants in a vertical impact, a different design approach would probably be used for a large transport aircraft compared with a light fixed-wing general aviation aircraft or a helicopter. The large transport structure having considerable depth of crushable under-floor

structure may not require energy-absorbing landing gear and seats. On the other hand, light fixed-wing aircraft and helicopters having relatively little crushable under-floor airframe structure would require energy absorption in the landing gear and seats, as well as in the fuselage structure, to prevent injury to occupants in potentially survivable crashes (Figure 2.14) [25].

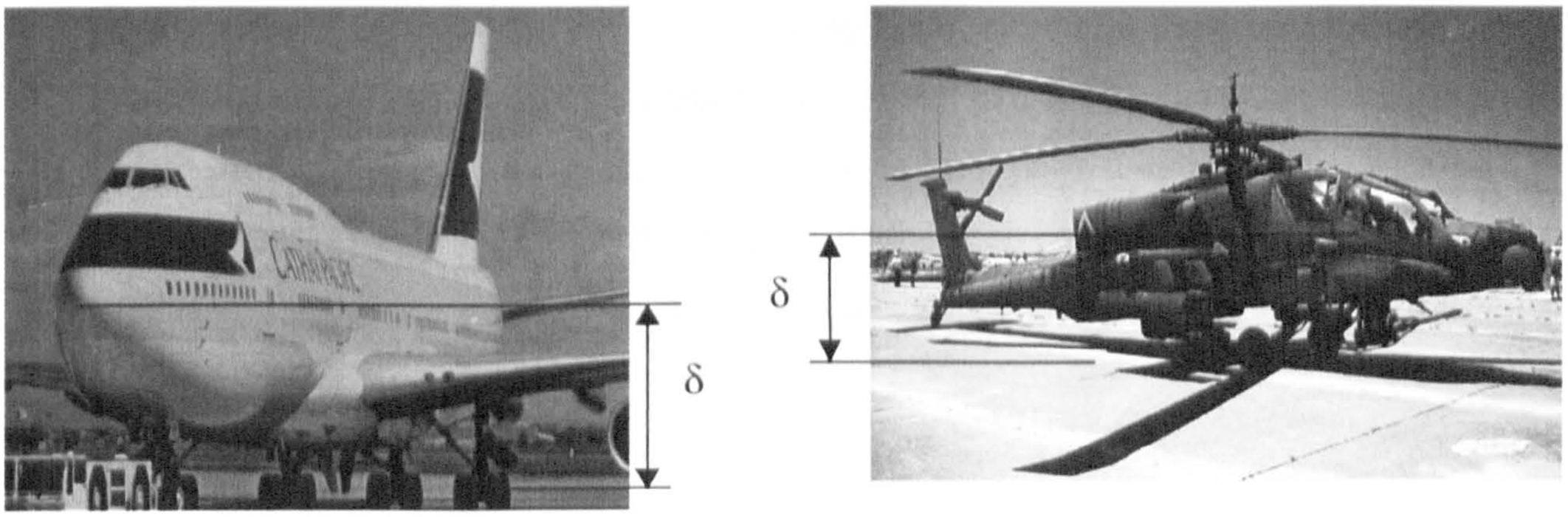

Figure 2.14 Energy absorption concept for various aircraft

For aircraft and helicopters, the kinetic energy is dissipated in the distance delta.

The basic requirements for crash resistant subfloors can be summarised as follows [3]:

-

- Distribution of ground-to-floor reaction and seat loads so as not to destroy structure(s).
- Limitation of the decelerative forces by structural deformation with a "controlled load" concept;
- Maintenance of cabin floor structural integrity.
- Minimisation of cost and weight penalties, a dual function structural concept. Load-carrying capability for normal operation, energy absorption for crash cases.

2.5.1 Composite Airframe Crash Resistance

Structural frames are frequently used above the cabin floor for high mass retention (transmission, engines, rotor hubs, etc.) and to provide a suitable survival volume in a crash situation. Frames deforming plastically offer the possibility of load-limiting concepts for large overhead masses. High energy absorption with composites has been obtained for compressive loading where brittle fracturing of the composite into sublaminates occurs. Under tensile or bending loads, structural integrity may be lost at initial fracture, and energy absorption can be low. To assure post-crush integrity, carbon fibre composite structures can be hybridised with tougher fibres such as Kevlar or polyethylene [25]. With only limited actual crash response information available, the need exists to examine generic composite structures under crash loading.

2.5.2 Sine Wave Beams

Sine wave beams are one of the most efficient subfloor design concepts yet developed in that they combine high load carrying capability, high energy absorption in the web direction, and good structural integrity by using hybrid lamination techniques. The sine wave web (or corrugated web) is commonly chosen as a structural member to study as it represents a realistic configuration directly usable in designs [26]. While tubes can be tested under well controlled conditions, and the energy absorption results used as material properties in designs, sine wave beam testing is required to confirm the validity of using such energy absorption data in the design process. As mentioned previously, one of the most important methods of achieving high energy absorption performance with brittle materials is the triggering and stabilisation of an efficient failure mode.

2.5.2.1 Trigger Mechanisms

Work done by Hanagud et al [27] used three differing types of triggered sine wave specimen, namely full width ply drop off, notched and chamfered end (Figure 2.15). The results obtained showed that specimens with a small trigger exhibited higher energy absorption, independent of the shape of the trigger. The larger the trigger used

the greater the loss in energy absorption capability. Thus a small trigger can initiate and promote efficient failure modes, but using too large a trigger can lead to a rapid loss of performance. Hanagud et al [27] reported no differences in the failure modes in the various specimens used in their study when looked at with the naked eye, which is suprising. It is believed that the differences in energy absorption were related to the micromechanical effects of the trigger on the failure mode, leading to failure mode differences at the micro level. Jimenez et al [28] have also carried out work on the triggering of structural components and have reported that small differences in trigger geometry such as bevel angle can have a large effect on the energy absorbed.

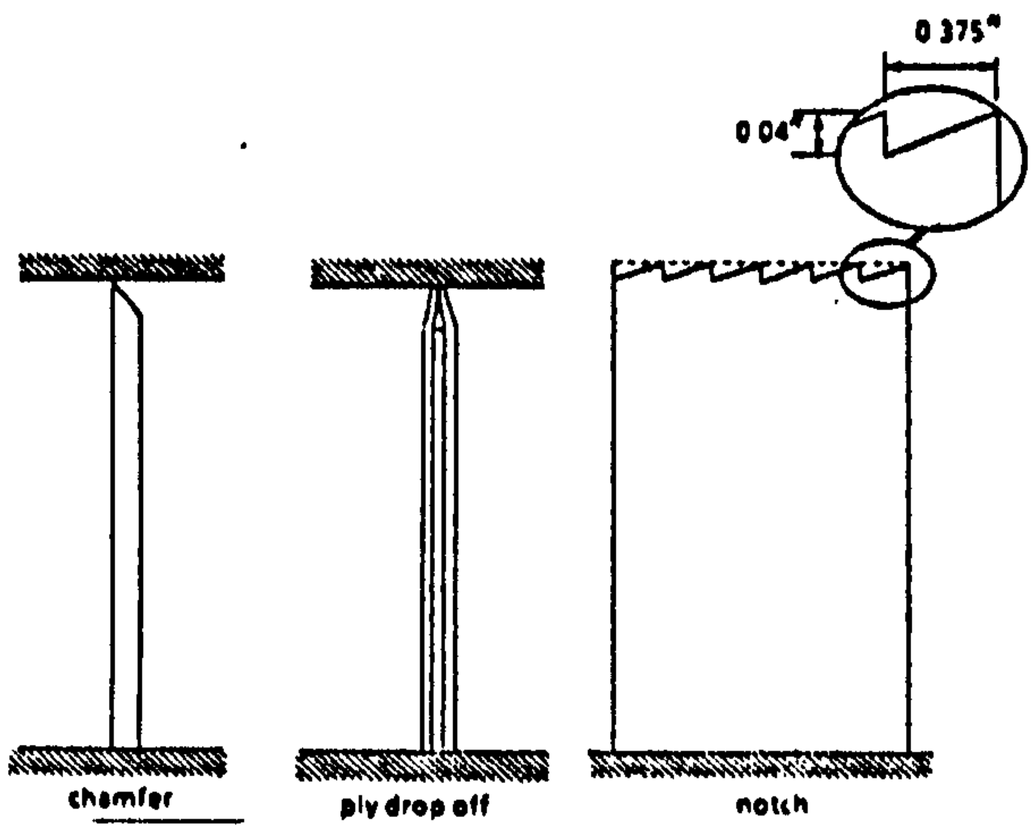

Figure 2.15 Trigger types [27]

2.5.2.2 Wave Count (Specimen Width) Effects

The sine wave specimen exhibits certain features that can be found in tubular specimens, which have been widely studied. However, there are certain features that the sine wave beam does not share with a tube, one such feature being the width of the web (Figure 2.16). A web with large width would not suffer from edge effects, but as the width of the web is decreased boundary effects brought about by these edges will occur. Hanagud et al [27], concluded that there was a very slight decrease (< 10%) in energy absorption as the width of the specimen was decreased by a factor of 3 i.e. the specimen was reduced in width from a 3 wave specimen to a one wave specimen. This was attributed to the boundary effects of the stress free sides. The specimens

used in these tests were composed of tangentially joined circular arc segments as in Figure 2.16.

2.5.2.3 Included Angle (Effective Amplitude) Effects

The effective amplitude of the web waviness is an important geometric parameter since it defines the gross width-to-thickness of the web (Figure 2.16 and 2.17). A flat plate geometry was considered as one extreme, 180° another extreme. The flat plate underwent global buckling resulting in almost zero energy absorption [27]. The other angles tested were 180°, 150°, 120°, 90° and 60°, the specimens all being 89mm high and 1, 2 or 3 waves wide. There was no significant difference in energy absorption from 180° to 90°. The 60° specimen absorbed minimal amounts of energy. The failure mode was global, indicating the existence of a stability boundary in the range of 60° to 90°, where the failure mode switches from efficient crushing to inefficient buckling global failure. Hanagud et al [27] gave no indication of which triggering mechanism was used apart from one of the three shown in Figure 2.15.

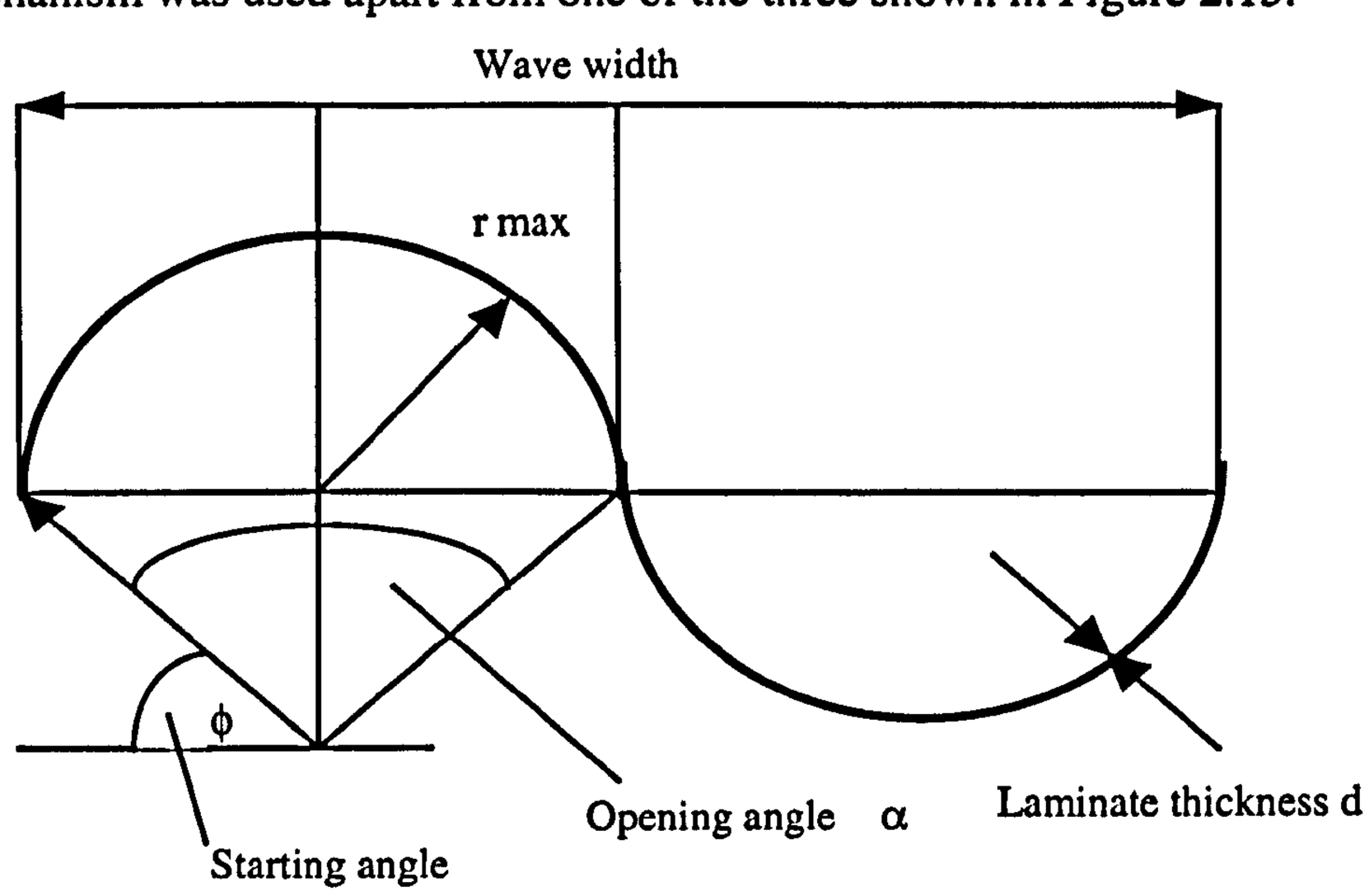

Figure 2.16 Sine web terminology [3]

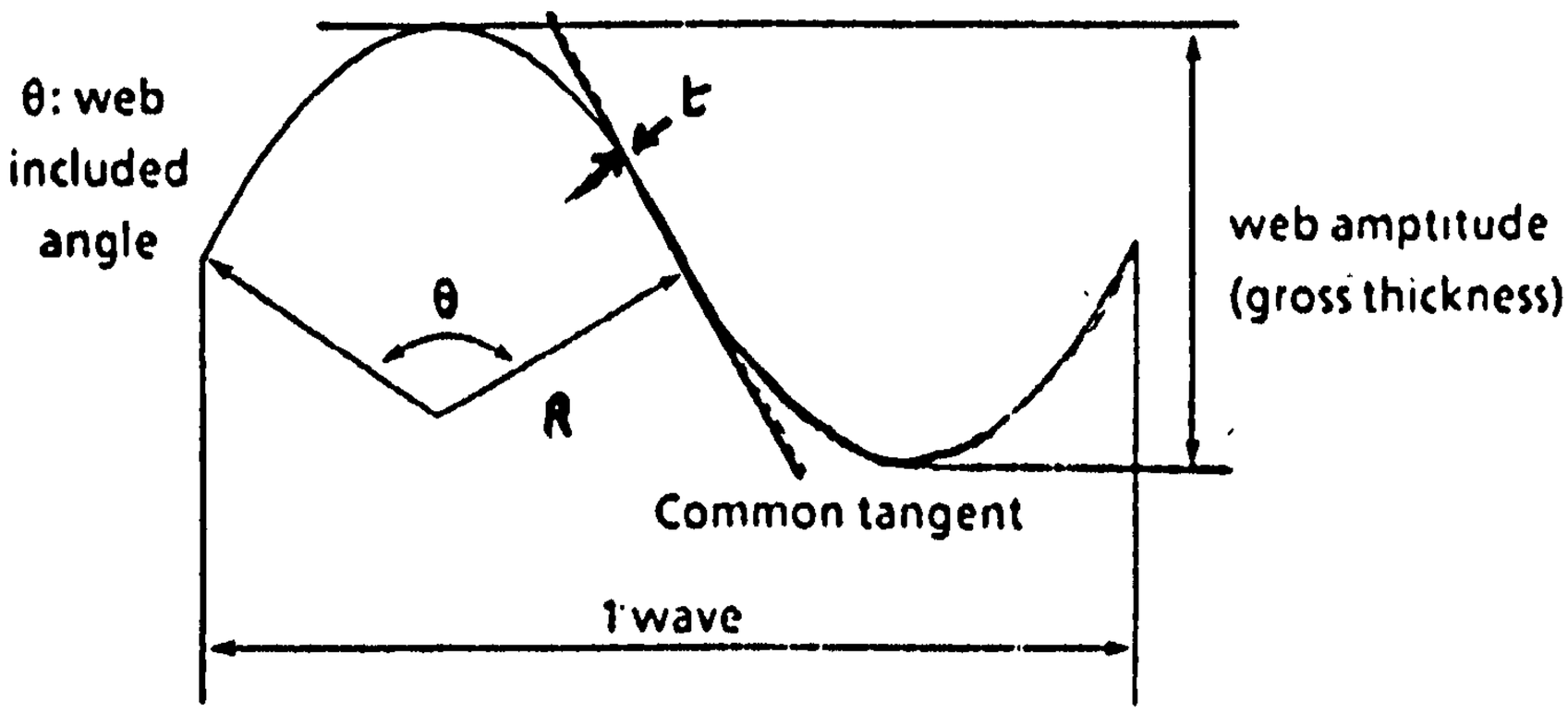

Figure 2.17 Included angle (gross thickness) effect [27]

2.5.2.4 Hybridisation Influence and Crushing Characteristics

Carbon fibre-reinforced laminates under compressive loading can have extremely high energy absorption capabilities, but disintegrate completely into small laminate fragments [3]. To increase their post-crush structural integrity, laminates can be hybridised with tougher fibres such as Kevlar or high performance polyethylene. This hybridisation however results in lower laminate stiffness due to the lower compression moduli of the synthetic fibres. Hybridisation can be accomplished by altering the laminate stacking sequence or by using intraply woven fibres. The sine webs' energy absorption capacity is good, approaching that of composite tubes. Both of these elements have the same failure modes. Sine wave elements incorporating Kevlar tended to fail in a buckling-crushing mode. As the amount of carbon was increased, the failure mode transitioned to the desirable rolling-fragmentation type (Figure 2.18) and the absorbed energy increased.

Figure 2.18 Rolling-fragmentation type of failure [16]

A beam section with a sinusoidal-shaped web when compressed shows a high initial peak failure load followed by a sharp load drop. However, during the fragmentation and folding of the web, the crush force magnitude is almost constant. It is not clear however how Kindervater et al [3] calculated the mean load curve (Figure 2.19).

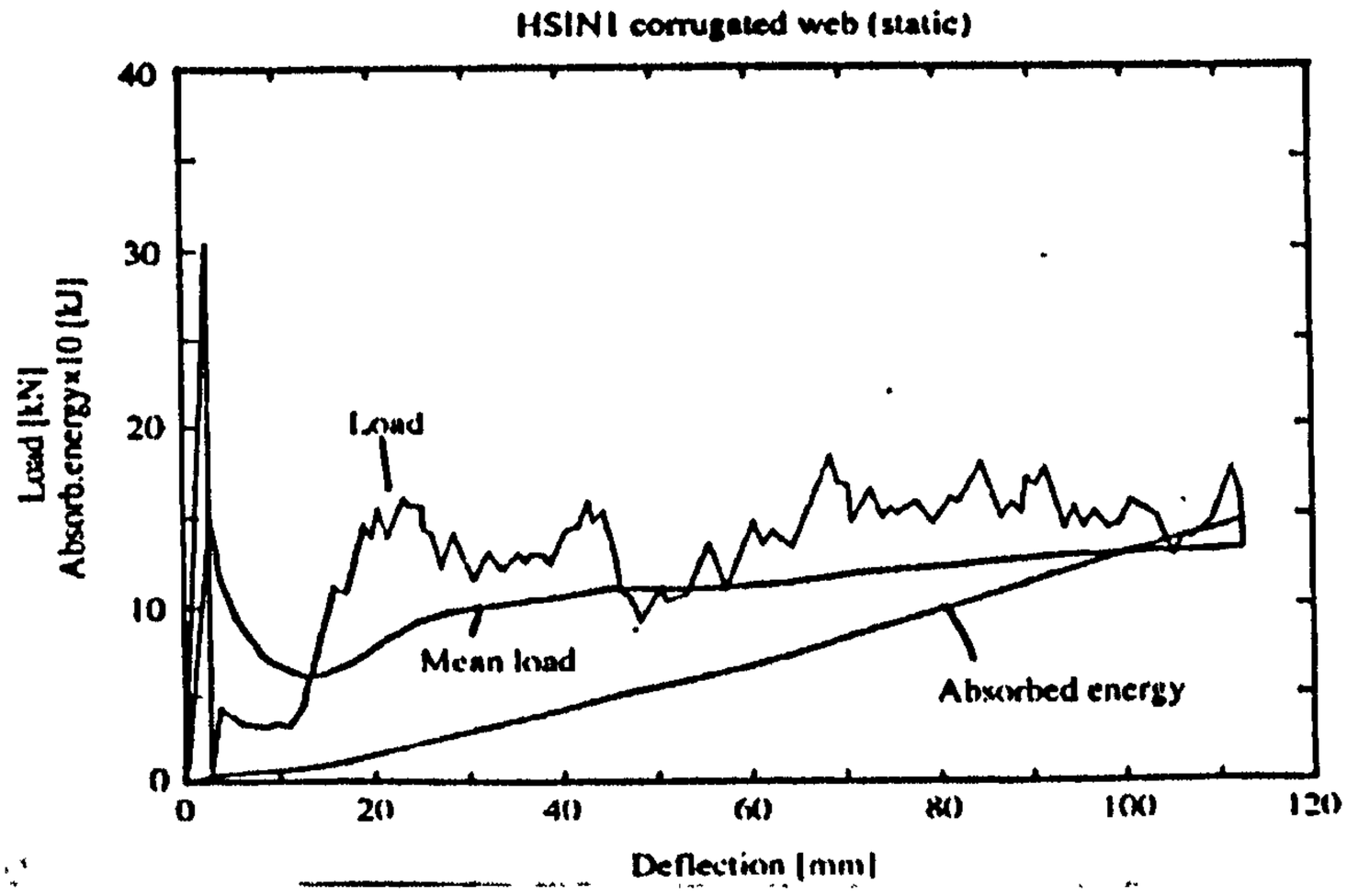

Figure 2.19 Hybrid sine wave web; typical load-deflection curve [3]

In reference [3] Kindervater et al. tested pure AFC (aramid fibre composite) and CFC (carbon fibre composite) sine web beams and various AFC/CFC hybrid configurations. The hybridisation was accomplished by either alternating pure AFC and CFC laminae in the stacking sequence, or by using intraply woven AF/CF fabric laminae in combination with 1-3 CFC midlayers orientated in the loading direction (HSIN 1-3). All the beam webs were subjected to dynamic drop tests at 10m/s. The dynamic specific crush stresses were not consistently higher than the static test results. The phenomena that caused these stress inconsistencies are related to the failure modes that develop in each case. If the sine wave beam crushes in a controlled uniform manner then the stresses will be higher than if the specimen fails non-uniformly.

The pure AFC web elements had higher dynamic crushing stresses due to the development of a uniform local buckling (folding) failure mode. For the hybrid elements and the pure CFC the dynamic crushing stresses were lower than the static values, caused by irregular brittle fractures in the CFC portion. However, two hybrid web (HSIN 2 and 3) configurations had more regular dynamic failure modes (local laminate bending) which resulted in higher specific stresses compared with static stresses. The energy absorption performance of an AFC/CFC hybrid sine wave beam configuration (HSIN 2) was compared with an "equivalent" aluminium beam with a corrugated web. Although both beam webs had the same mass, the composite element absorbed twice the energy.

2.5.3 Stringer Stiffened Beam Sections

Further work on aircraft subfloor sections has been carried out [26] and also considerable work has been undertaken on helicopter subfloor structures [25][29][31][32]. Bannerman et al [26] present results for the energy absorption properties of composite stringer stiffened, sandwich and integrally stiffened (sine wave web) beam sections, Figure 2.20. Quasi-static and impact crush tests were performed to determine the effects of material and construction variables. Failure modes, specific energies of absorption, crush load uniformities, impact effects, and failure trigger mechanism effects were discussed and compared with aluminium elements. The results showed that the composite beam integrally stiffened with a sine wave web had higher energy

absorption capabilities than the other types of specimens under crash conditions. The results obtained showed that composite energy absorption characteristics could be as good as aluminium and, by paying close attention to the constituent materials and construction methods, as well as the trigger mechanism can be considerably better than aluminium.

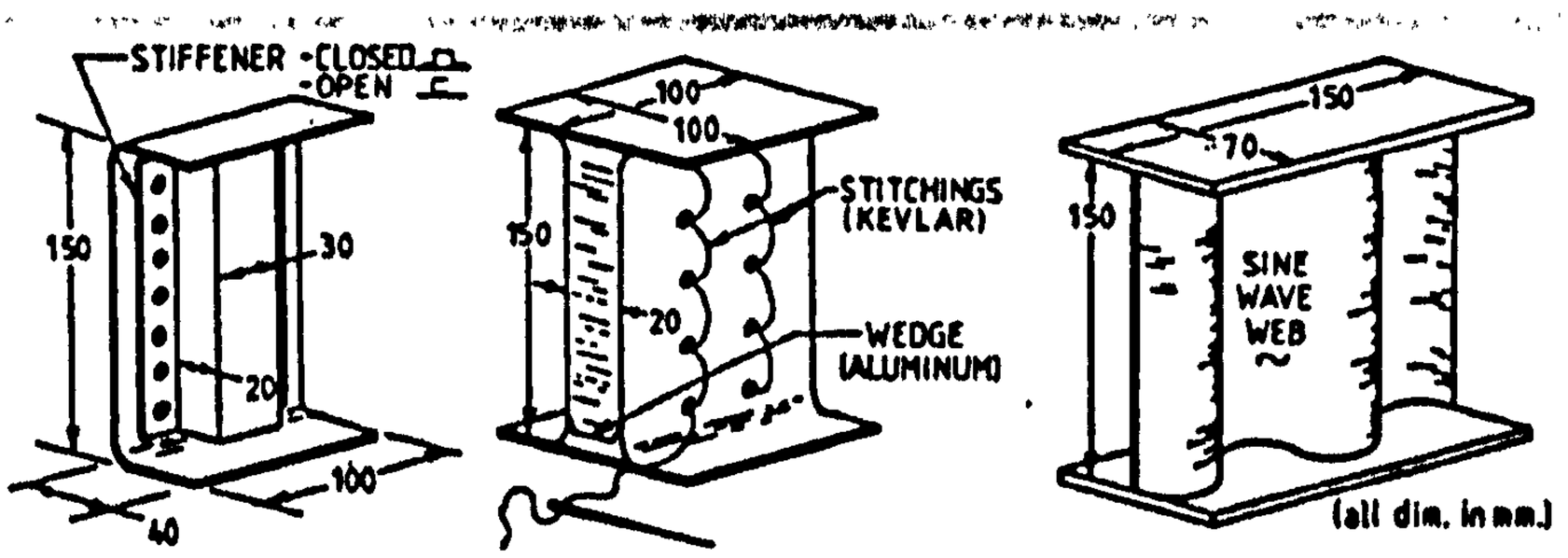

Figure 2.20 Test specimens [26]

For this stringer stiffened type of beam section (Figure 2.20) there are two elements which contribute to the energy absorption process, i.e. the stiffener and the panel. The panels stiffened with an open "C"-shaped stiffener failed by column buckling and hence absorbed little energy. The "closed hat" type stiffener was found to be a very good energy absorber. However, the panel section due to the influence of the panel on the failure mode affected the performance of the stiffener. It was found by Bannerman et al [26] that with the addition of Kevlar fibres to the panel, the panel and the stiffener crumpled in a similar manner to each other and hence high specific energy resulted. As increasing amounts of carbon fibres were incorporated into the panel (Bannerman et al do not specify how much) the specific energy dropped and a change in panel failure mode became apparent. The panel failed in a brittle manner forcing the stiffener to do likewise. As more carbon fibres were added to panels the stiffness increased and the failure shape became more irregular, however the superior energy absorbing capabilities of the carbon began to show and the specific energy began to increase again. The best static results were obtained for an element, which consisted of a small amount of glass fibre in the carbon panel.

2.5.4 Sandwich Elements

Bannerman et al [26] found that due to the stiffness-to-height characteristics of the sandwich sections under consideration, the sections tended to fail by a simple buckling mode, or by a ballooning type failure where the core split up the middle. Neither of these failures absorbed a lot of energy (Figure 2.21). Various techniques were investigated to initiate and propagate stable failure modes. The techniques included vertical rows of Kevlar stitches through the beam section, and an aluminium wedge placed at the radius (Figure 2.20). These additions were intended to produce a rolling fracture failure mode as seen for aluminium tubes by McGehee [33]. Although the results obtained were considerably better than those for aluminium alone, they were still poor in comparison with the stringer stiffened sections. Two other techniques were investigated to try to obtain more complex crushing shapes. These were a single horizontal row of Kevlar stitching added to the centre of the web, and a third laminate sandwiched between two Nomex cores. Again the results obtained were far better than those obtained for simple aluminium sandwiches but fell short in achieving the energy absorbing capacity of stringer stiffened sections.

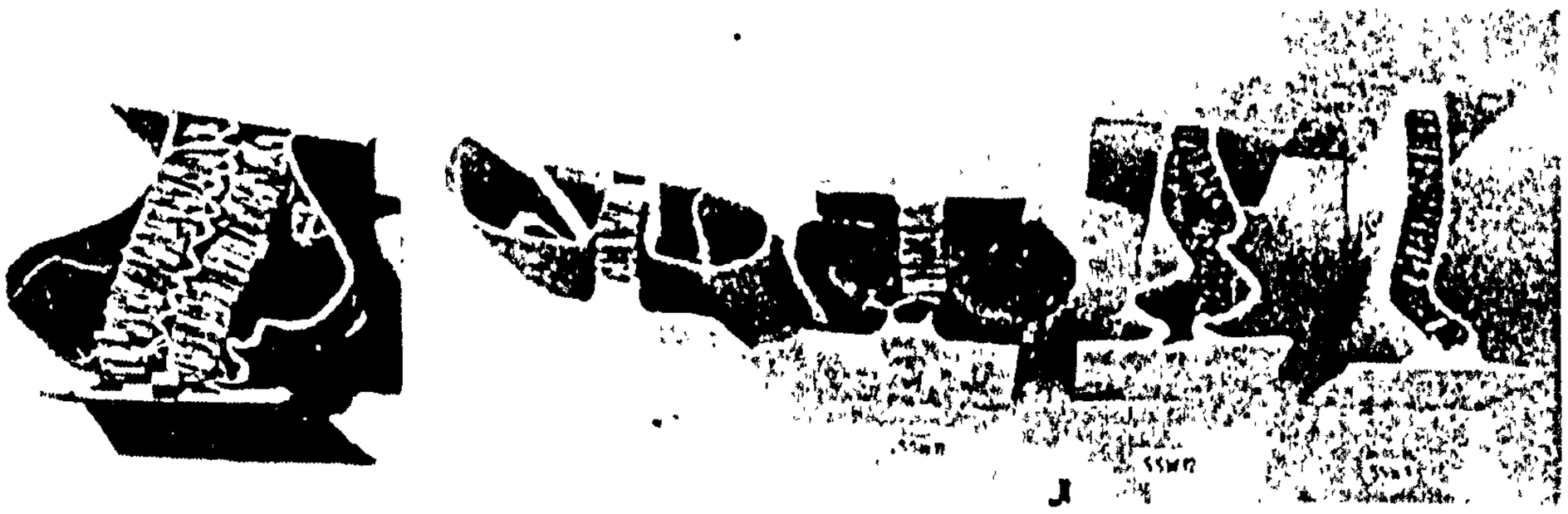

Figure 2.21 Typical sandwich element failure modes [26]

2.5.5 Aircraft Subfloor Intersections (Node Point Areas or Cruciforms)

Structural intersections of keel beams, landing gear frames and side shell frames represent structural "hard points" under crash loading within the framework of the subfloor [34]. These intersections are areas of high load transfer. Crash simulations with aircraft subfloors indicate that "hardpoint" areas in subfloor frameworks generate high acceleration pulses at the cabin floor level and create dangerous inputs to the seat/occupant system. Structural elements at intersection areas which are designed to carry shear and bending loads react very stiffly in a compressive crash situation i.e. they tend not to crush, but pierce the floor. Investigations with metal aircraft subfloor structures [25] have demonstrated the effectiveness of reducing the stiffness of these "hard points". The reduction in stiffness was accomplished by, amongst others, a "notched corner" concept (Figure 2.22).

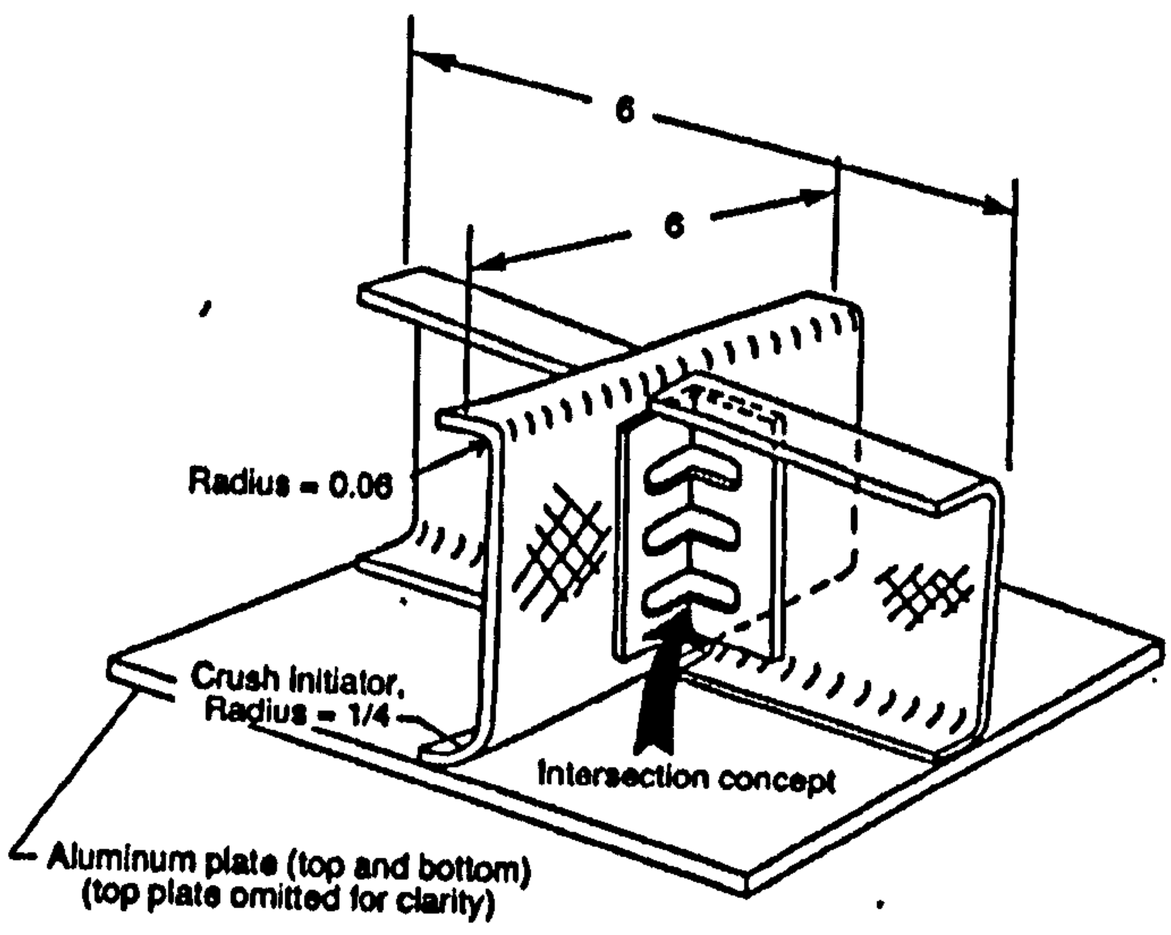

Figure 2.22 Notched corner concept [34]

Jones et al [35] tested quasi-statically forty one composite specimens of aircraft subfloor intersections (cruciforms) to determine the effects of geometry and material on the energy absorbing behaviour, failure characteristics and post-crush integrity of the specimens (Figure 2.23). The cruciforms were constructed of 12-ply ($[\pm 45]_6$) laminates of either Kevlar fibre 49/934 or AS-4/934 carbon fibre/epoxy in heights of 10, 20 and 30cm. The geometry of the specimens varied in the design of the

intersection attachment angle. Four different geometries were tested. They were tapered without cutouts (TWOCO), tapered with cutouts (TWCO), straight without cutouts (SWOCO) and straight with cutouts (SWCO)(Figure 2.23).

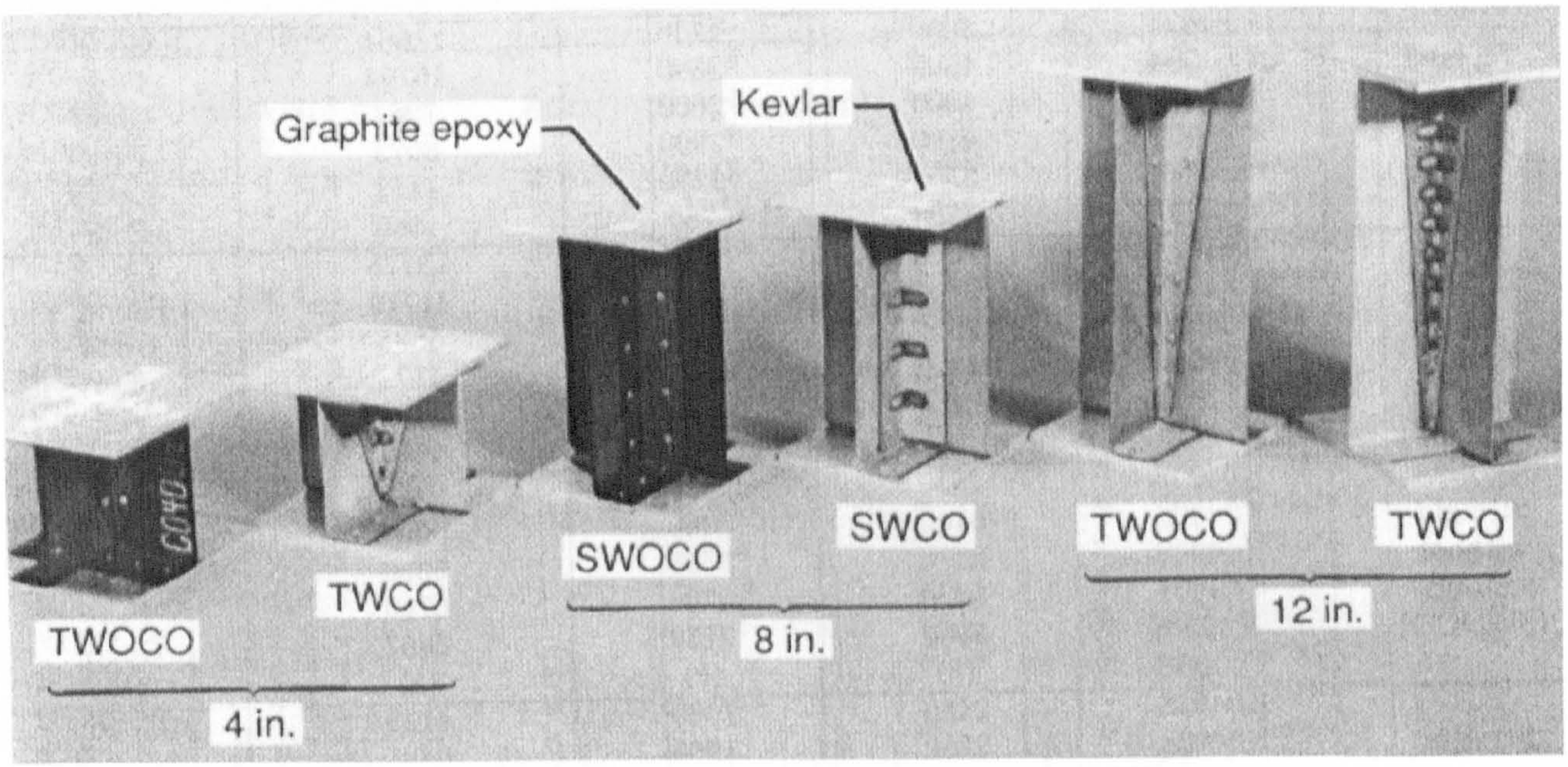

Figure 2.23. Typical cruciforms

The performance of the samples was evaluated on peak load, sustained crushing loads, specific energy absorption, ratio of peak loads to sustained loads (see Section 2.2), and a subjective evaluation of structural integrity following the crushing tests. The following conclusions were drawn: -

- Local failure modes with multiple buckling are necessary to achieve high energy absorption efficiency for the intersection concepts.
- Structural integrity was maintained with the plastic-like behaviour of the Kevlar material. Structural integrity was not achieved with the brittle carbon epoxy system.
- A tapered attachment angle concept applied to the subfloor intersections provided the best performance for peak loads, sustained crushing, specific energy absorption, and structural integrity.
- Attachment concepts with cutouts in the web of the intersections tended to reduce the various performance parameters more than the concepts without cutouts.

- The cutouts led to undesirable delaminations in both the angles and the webs of the Kevlar specimens, thus reducing the overall efficiency of the concepts.

Although the above conclusions were made, Jones et al [35] did not produce any design methodology to optimise the geometry for maximum energy absorption. Further work by Kindervater et al [3][34] examined several triggering concepts for cruciforms. Starting from a baseline aluminium cruciform, other aluminium and composite cruciforms having single and multiple notched edged joints, corrugated edge joints, and cruciforms with increasing amounts of Kevlar fibre at the mid-section of the cruciform, were studied (Figure 2.24). A moderate initial stiffness and then a constant or slightly increasing crush force level, in addition to post-crush structural integrity, were seen as the major design goals for good energy absorption.

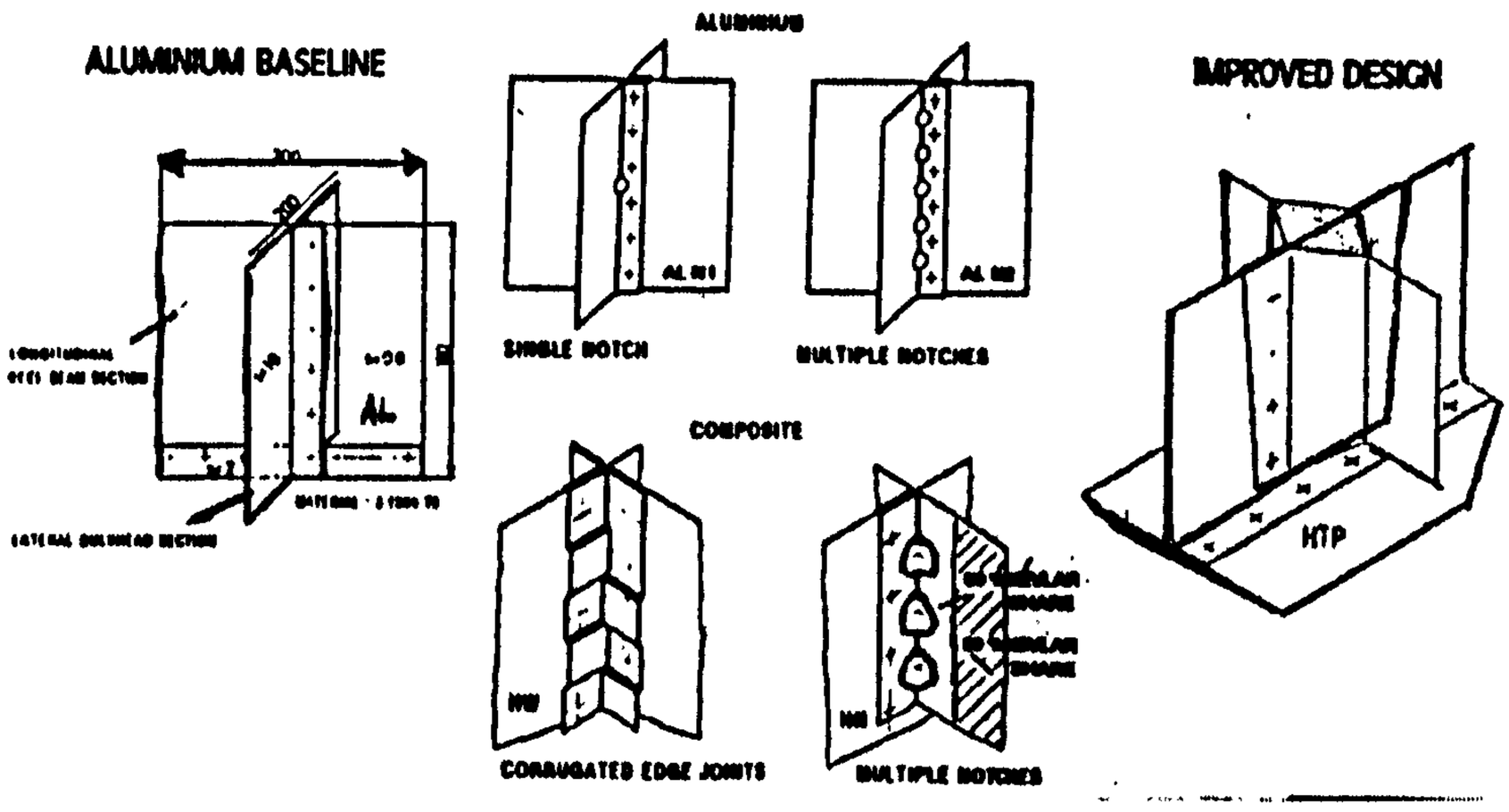

Figure 2.24 Triggering concepts for cruciforms [35]

As can be seen from Figure 2.25 Kindervater et al. [3] found that a carbon/Kevlar fibre hybrid cruciform with corrugated edge joints (HW) had comparable absolute energy absorption to an aluminium part with one centre notch (AlN1). It is not mentioned however whether the cruciforms were comparable in other ways, such as stiffness. The HW element was found still to have a high initial load peak (Figure 2.25). Further design improvements led to the hybrid cruciform variant (HTP). This consisted of a column-like midsection formed by a Y-shaped split of the shear web laminate, an integral bevel trigger at the bottom of the shear webs, and tapered edge

joints at the keel beam attachment. In several static and dynamic crush tests it was found to absorb 3 to 4 times the energy of the other elements. The dynamic HTP-element force-deflection curve showed an almost ideal shape for crush response at the cabin floor level.

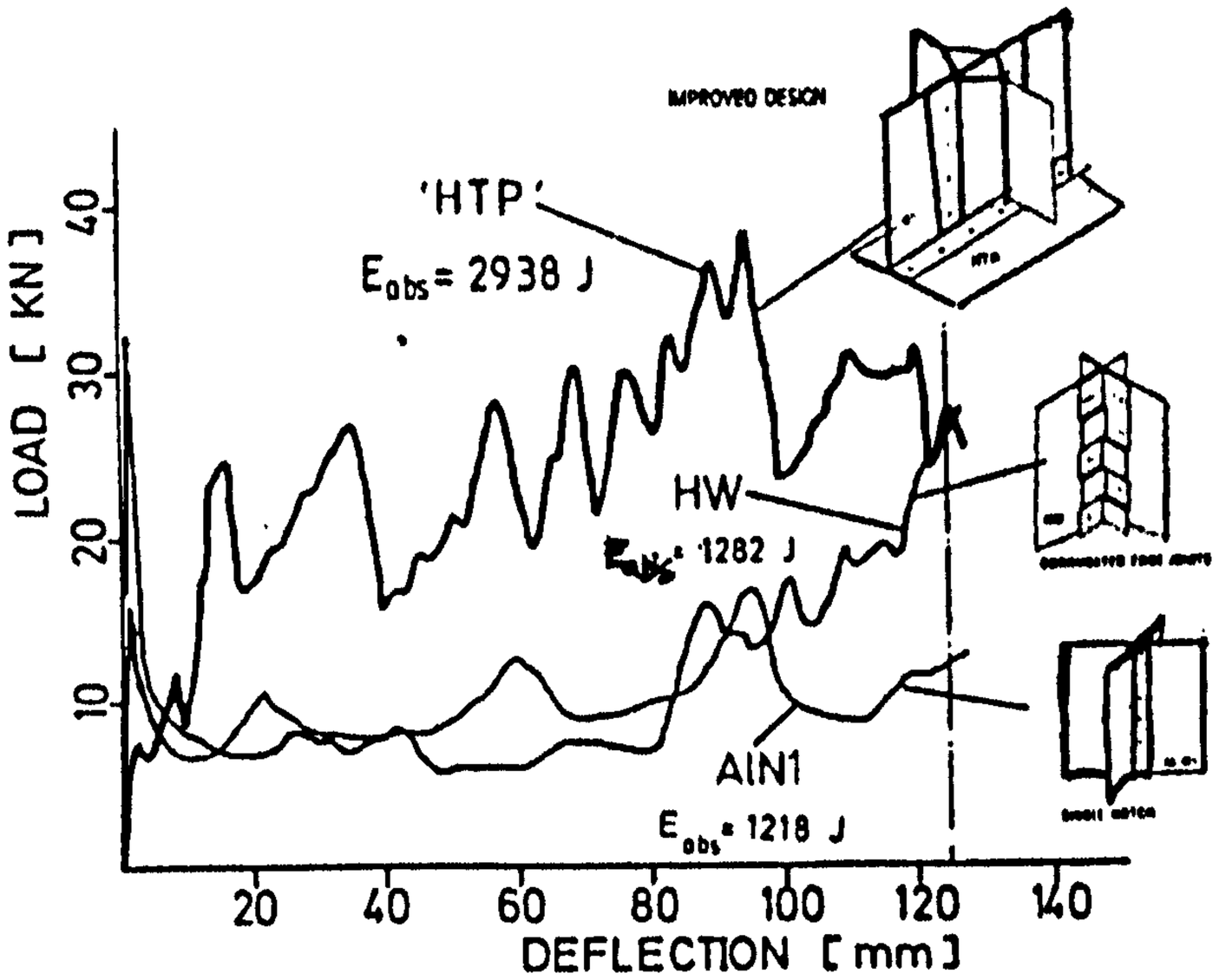

Figure 2.25 Static load-deflection curves of different trigger variants [3].

As well as confirming the conclusions of Jones et al [35] above, Kindervater also concluded the following points:-

- Multiple notching of the cruciforms for peak load reduction results in low energy absorption.
- Pure carbon fibre/epoxy cruciforms have high energy absorption and high weight saving (30%) compared with aluminium, but disintegrate completely during crushing. Hybrid elements have weight savings between 15-20%.
- Composite cruciforms show the same or even much higher (HTP element) absolute energy absorption compared with metal elements.

2.5.6 Airframe Subfloor Structures

Besides carrying the normal flight and ground loads, the airframe structure should absorb a significant amount of impact energy and still maintain a protective shell when a crash occurs. When designing a crashworthy airframe structure there are many factors to consider. Of prime importance is the design of the airframe to maintain structural integrity and a habitable space for the occupants. The airframe structure should incorporate a high strength protective shell or cage around the occupants. This structure should provide roll-over strength, a strong support structure for restraint of large mass items and seats, as well as maintain stability of exits for emergency access. The forward fuselage structure should be designed to minimise ploughing i.e. entry of the nose area of the aircraft into the ground, and to absorb energy during longitudinal impacts. In addition, the crushable structure should be multipurpose; i.e. it should be able to absorb as much energy as possible in a crash as well as being a structural part, otherwise the overall structure will become too heavy.

The primary objective of Cronkhite et al.[25] was to develop crashworthy design concepts suitable for the floor sections of light aircraft. The primary emphasis in designing the floor structure was to ensure that structural integrity was maintained so that the seats and the occupants would be retained and a protective shell would be provided in a crash. Any floor damage that may occur could result in the seats coming loose during a crash, subjecting the occupants to secondary impact with the structure that could result in injury. The design philosophy chosen for the floor sections is shown in Figure 2.26 and consists of a strong structural floor with a crush zone underneath. The structural floor is a 5cm deep platform designed to carry loads and moments imposed by the seat/occupant and to maintain seat-to-structure integrity without breaking up, heaving or decreasing the cabin volume. The energy absorbing subfloor is about 15cm deep, and is designed to distribute the loads to the upper floor as uniformly as possible and to collapse in a controlled manner to absorb as much impact energy as possible, at or near human tolerance levels.

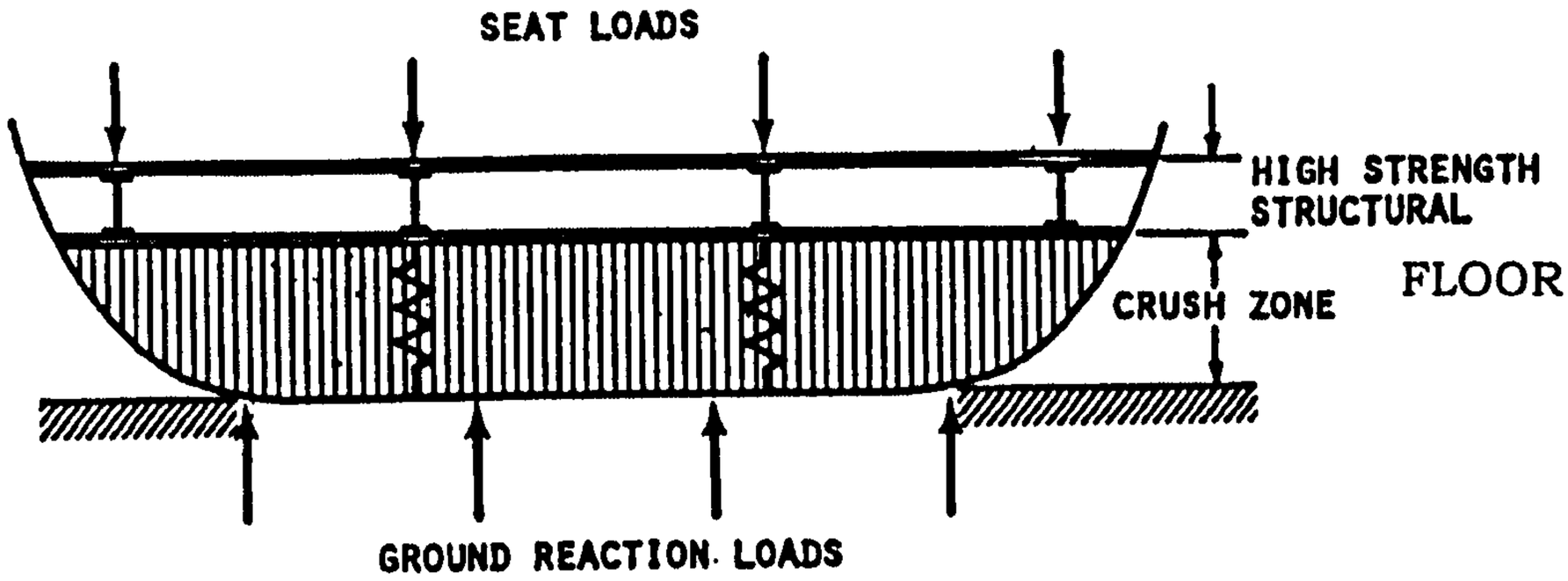

Figure 2.26 Lower fuselage design philosophy [25]

When designing the crush zone, the crushing load developed during a crash must not exceed the structural capability of the airframe, but it must be sufficiently high so that the maximum energy is absorbed. As Figure 2.27 shows, the load-deflection curve for a conventional structure is generally characterised by a high peak load. This load will tend to destroy the aircraft floor. The peak load is followed by a severe drop in load-carrying capability, which usually coincides with the structure becoming unstable and then failing. The result of this instability is low energy absorption. Conversely the ideal crush would have a controlled peak load that lies within the structural capability of the floor and is rectangular in shape indicating that it has maximum energy absorption, as indicated by the "controlled load concept" in Figure 2.27.

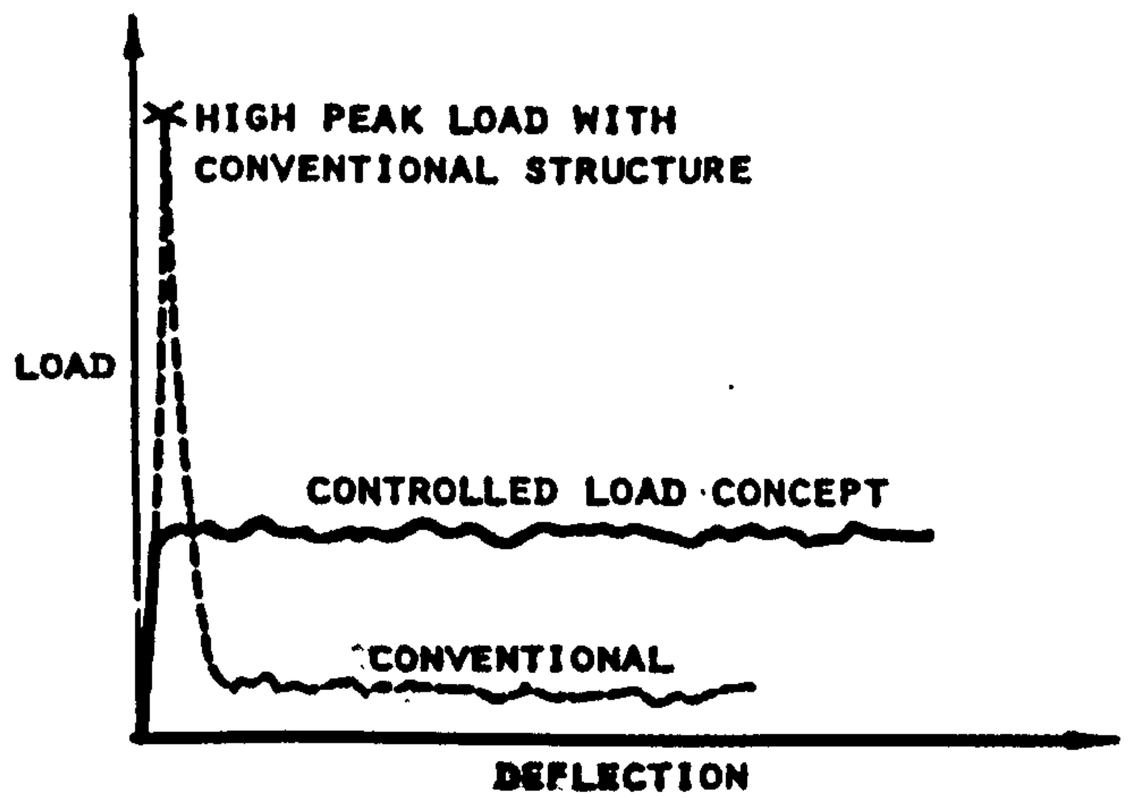

Figure 2.27 Crush zone load-deflection characteristics [25]

After reviewing the energy absorbing concepts available and considering their incorporation into a fuselage structure, Cronkhite et al [25] initially selected the following five (Figure 2.28). Jackson et al [31] and Bisagni [32] have investigated similar structures: -

- Deformable Keel Web - This concept absorbs energy by plastic deformation of the keel beam web (Figure 2.29).
- Corrugated Sandwich Web - This concept absorbs energy by deforming corrugated webs plus crushing of the foam filler.
- Corrugated Web/Notched Corners/Foam - This concept absorbs energy primarily by crushing foam and has structurally tailored notched corners to reduce load spikes at the intersections of longitudinal keel beams and lateral bulkheads.
- Corrugated Half-Shell - This concept absorbs energy by bending deformation of a curved corrugated shell.
- Foam-Filled Cylinder - This concept absorbs energy by crushing foam with the cylinder walls needed primarily for web shear strength.

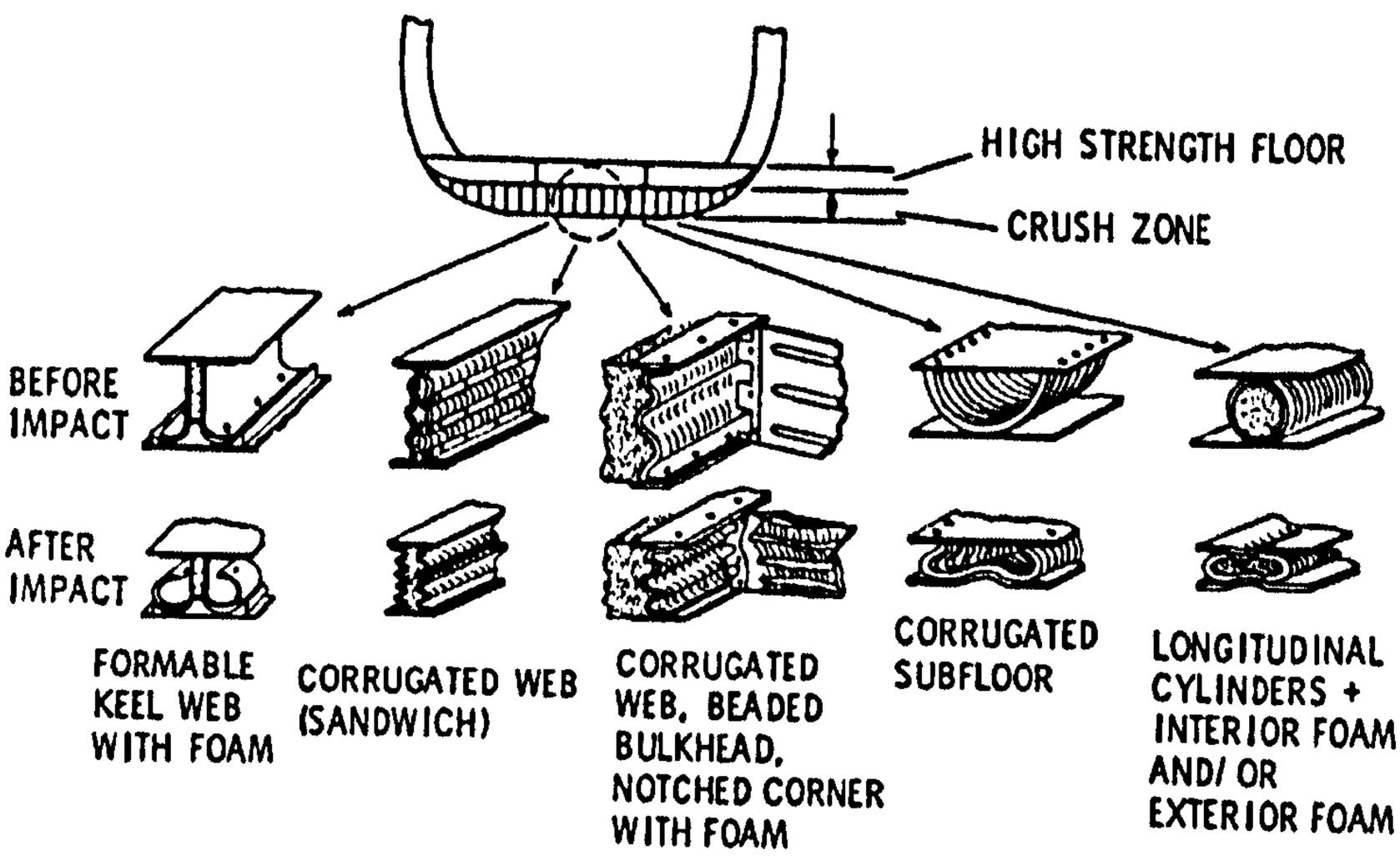

Figure 2.28 Lower fuselage load-limiting, energy-absorbing concepts [25]

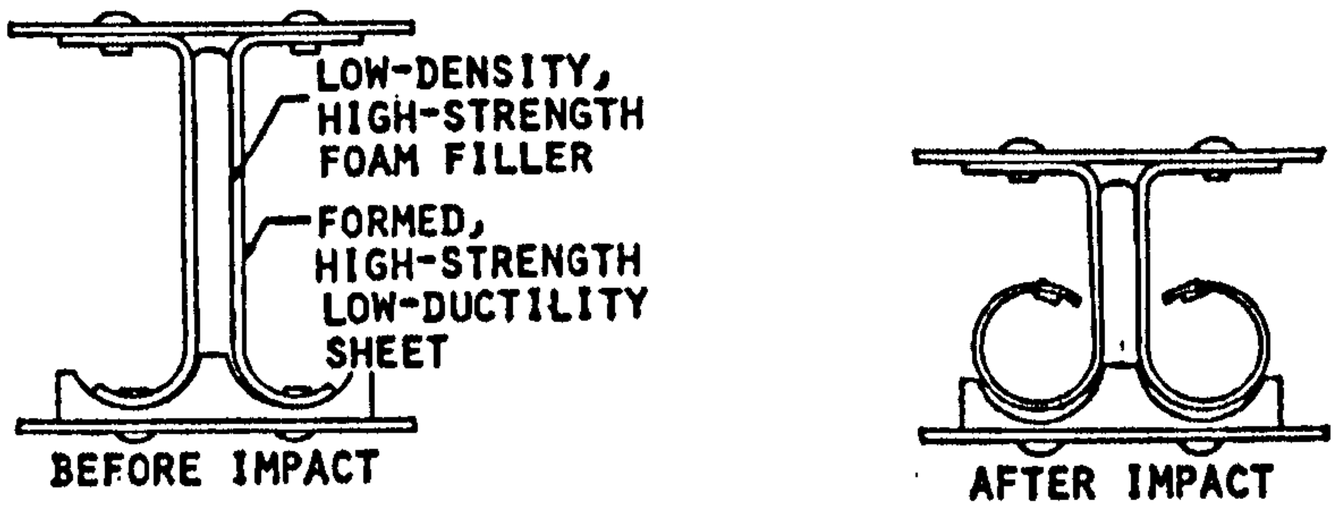

Figure 2.29 Energy absorbing keel beam concept [24]

However when all of the design goals were considered i.e. the concept should be: -

- Multipurpose (used for airframe strength and stiffness as well as energy absorption).
- Perform well under combined loading with various aircraft pitch and roll attitudes at impact while maintaining a protective shell and reacting concentrated loads from seats and other large masses.
- Practical from a cost and producibility viewpoint.

The original five designs considered were changed [25] (Figure 2.30): -

1) Canted bulkheads with conventional intersections (all frames are canted at an angle of 30° from vertical to promote their collapse for vertical impacts).
2) The corrugated half-shell.
3) The corrugated web with notched corner intersections.
4) The foam filled cylinder
5) Notched corner intersections with conventional webs.

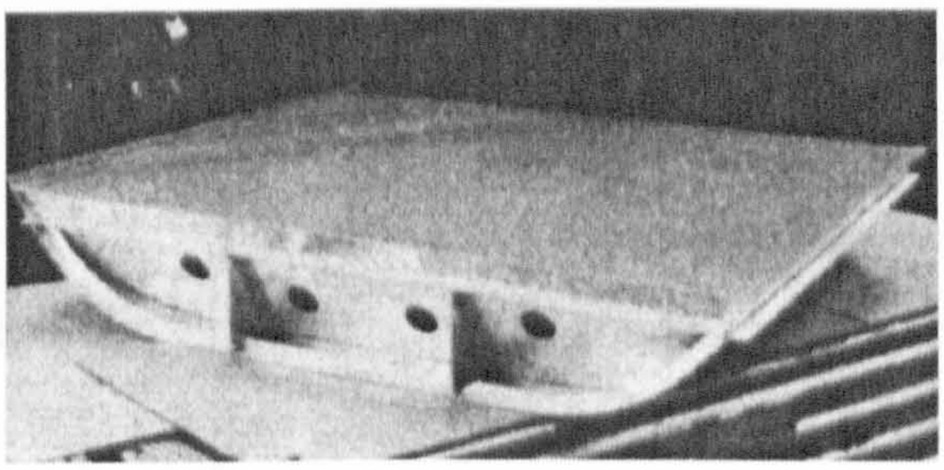

Canted Bulkheads

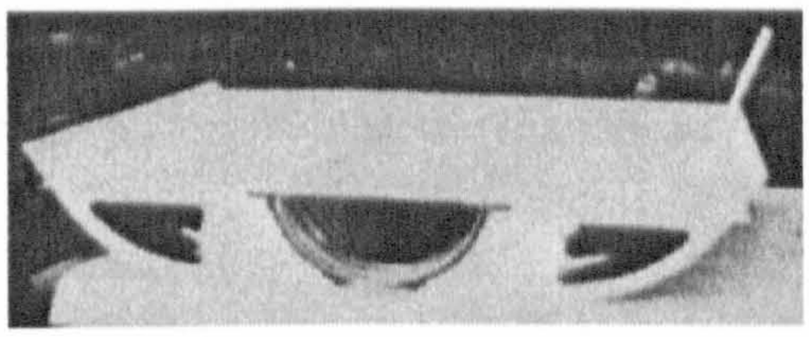

Corrugated Half-Shell

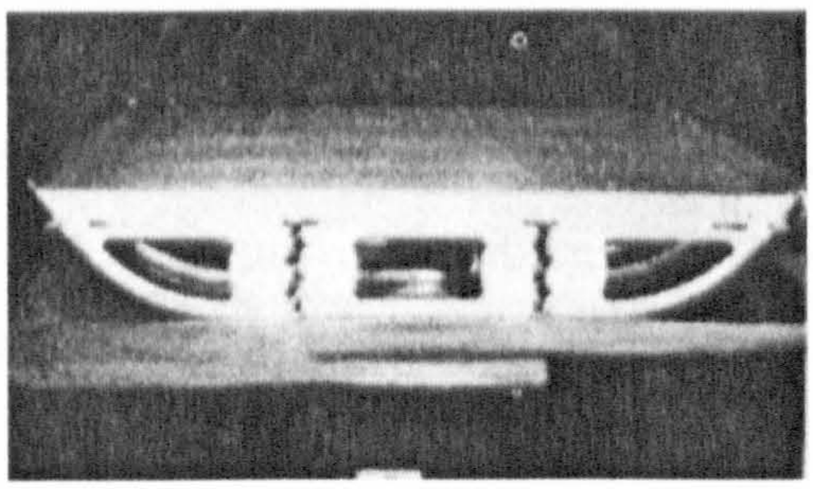

Corrugated Webs

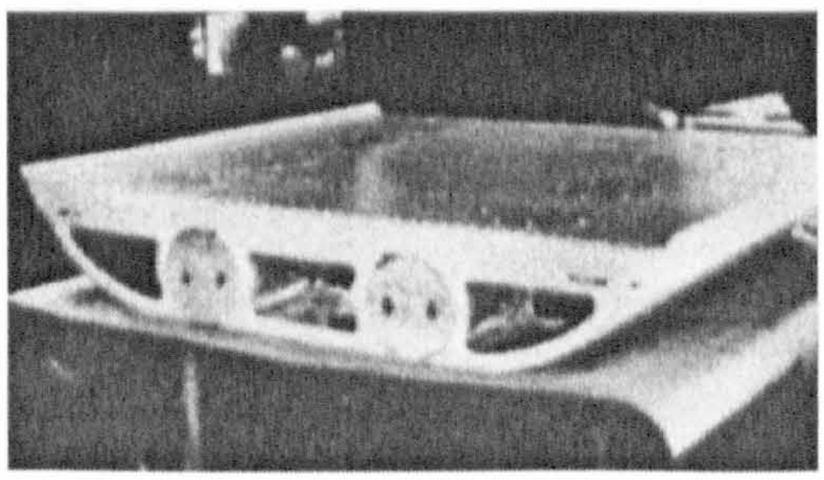

Foam-Filled Cylinders

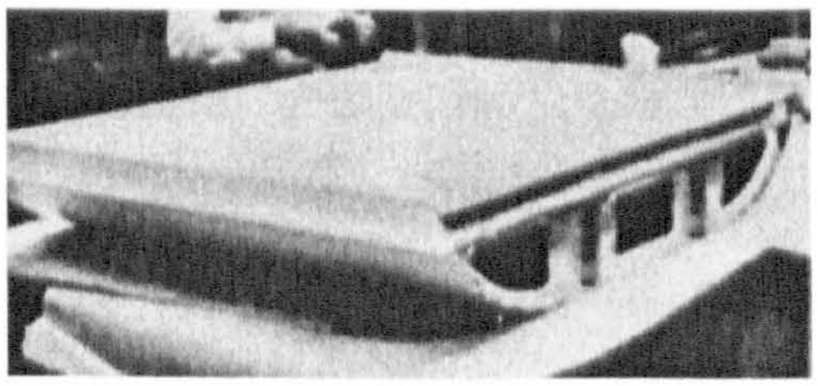

Notched Corners

Figure 2.30 Complete fuselage floor test sections [25]

The fourth and fifth concepts were considered to be minimum modifications to conventional airframe structures, whilst the others are more unconventional. Each of the above concepts were incorporated into a floor test section that featured a seat-supporting structural floor or platform with an energy-absorbing crush zone underneath. The concepts were tested both statically and dynamically. For most of the concepts it was found that it was possible to control the dispersion of loads to the structural floor. High energy absorption and good structural integrity were also found. The lightest concepts were found to be those that efficiently utilised the existing structure for energy absorption rather than those that incorporated redundant add-on materials such as foam.

Experimental static load-deflection data and dynamic deceleration response for the five concepts indicated that the floor sections performed well throughout the loading cycle, that is structural integrity and residual strength of the subfloors was maintained [25]. The data also indicated that the corrugated beam-notched corner and corrugated half shell were more effective in providing an essentially constant limit load with displacement than were the notched corners, foam filled cylinders and canted bulkhead subfloors. It was thought however that further design iterations could perhaps alleviate the undesirable characteristics of the less effective sections.

2.6 Analytical Failure Predictive Methods

The destructive nature of the energy absorption tests described previously would suggest that the cost of manufacturing and testing in terms of both time and money might become an important consideration in any given investigation. Any methods which can successfully predict the failure mode and hence, ultimately, the energy absorption capability of a component would be beneficial.

The majority of work conducted to date has been on axially loaded tubes [36]. However, other components have been investigated, namely conical shells [37] automotive frame rails [38] and square tubes [39]. Laananen and Bolukbasi [12,13] have undertaken predictive work on plates and stiffeners, Brachos et al [24] worked on edge-loaded sandwich panels.

Farley and Jones [40] describe a procedure based on an equation similar to the buckling load equation for a column on an elastic foundation. They used this to predict whether a change in energy absorption of a composite tube occurred as a result of changes in geometry or material properties. The following equation was used to calculate the sustained crushing force, P_{sus}.

$$P_{sus} = \sum_{i=1}^{n} \frac{N_i (EI)_i \varepsilon_{ci} + \frac{K_{fi}\varepsilon_{fi}}{M_i}}{L_i (G/t)_i}$$

The above equation contains six main variables. The internal tube dimensions-to-wall thickness ratio G/t, the laminate bundle length L_i (where a lamina bundle is composed of single lamina or multiple laminae, the bundles acting as columns to resist the applied load). M_i is the crush mode indicator, it indicates which term, column or foundation has the potential to affect the crush force. The number of laminate bundles n, the bending stiffness EI, the failure strain ε_{ci} and the foundation failure strain, ε_{fi} .K_{fi} is the foundation stiffness component of the *i*th bundle The parameter N_i was used to describe the general crushing mode. Lamina bundles that exhibited a lamina bending crushing mode would have a value of N_i between 0 and 1, but less than the N_i of lamina bundles that crush in a transverse shearing mode; tubes that crush in a local buckling mode would have an N_i approximately equal to 1.

Mamalis et al [37] have conducted work on the theoretical analysis of the stable collapse mechanism of conical thin-walled shells, crushed under axial compression. The total energy dissipated for a circular frustrum deformed a distance s, is given by the equation below. The proposed theoretical model was experimentally verified, it was very efficient for predicting the energy absorption capabilities for conical shells.

$$W_T = [1/(1-\mu_1+\mu_1 s_2/s)]\{[0.8.t.k.\sigma_\theta \pi[d_c+(s-s_1)\tan\theta]$$
$$/\cos\theta][(s-s_2)[\mu_2(1/\cos\alpha_1+1/\cos\alpha_2)-\mu_1(\tan\alpha_1+\alpha_2+2\mu_2)]$$
$$+[(\alpha_1+\theta)/\cos\alpha_1][0.4.t/(\cos\alpha_1\cos\theta)+s-s_2]+[(\alpha_2-\theta)/\cos\alpha_2]$$
$$[0.4.t/(\cos\alpha_2.\cos\theta)+s-s_2]]+R_{ad}[(s-s_1)\pi[d_c+(s-s_1)\tan\theta$$
$$+\pi(L_c/\cos\theta)(d_c+L_c\tan\theta]+n^*(t/2)G^*s\}$$

Where as shown in Figure 2.31, μ_1 is the coefficient of friction (static or dynamic) between the frond and platen. μ_2 is the coefficient of friction (static or dynamic) between the wedge (wedge formed by crush debris) and the fronds, t is the shell wall thickness, k is a constant. σ_θ is the tensile fracture stress, α_1, is the angle formed by the height and the external side of the wedge and α_2 the angle formed by the height and the internal side of the wedge. The related shell shortening is denoted by s_2, 0 is the semi-apical angle of the frustrum, L_c is the central crack length, d_c is the frustrum diameter at the crack tip, related to the position of the crack initiation. R_{ad} is the fracture energy required to fracture a unit area of interface between two adjacent layers and is calculated by using fracture theory [41], n^* is the number of splits and G^* the fracture toughness.

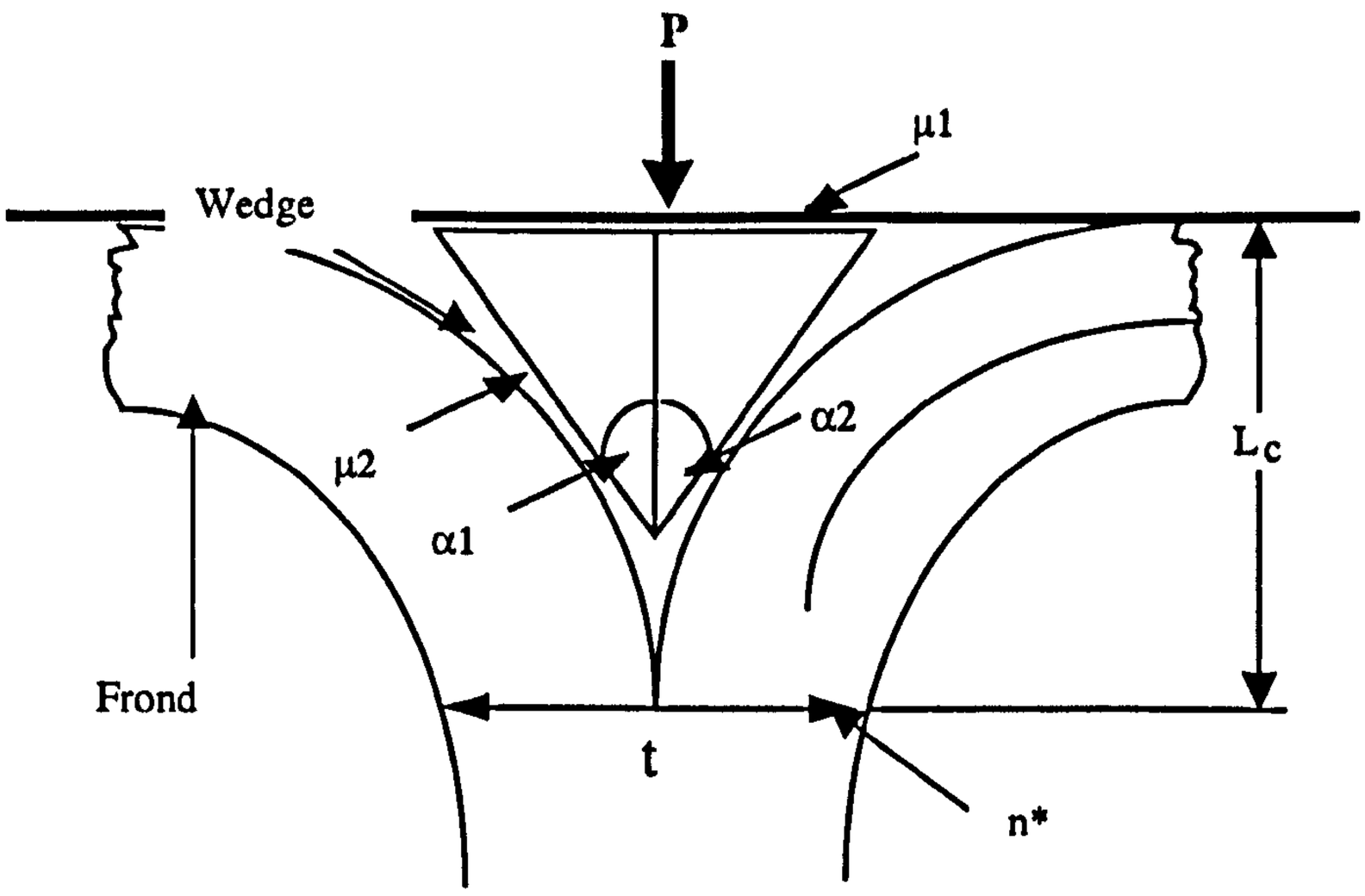

Figure 2.31 Configuration of circular tube crush zone

Mamalis et al [37] have reported similar theoretical predictions for the energy absorbing capabilities of square and circular tubes, frustra and hourglass sections [37-39].

Hulway and Wineman [42] report on a model to allow the prediction of crush performance based on a limited number of material properties. The technique proposed considered progressive crushing to be a fracture process. Fracture mechanics concepts were used rather than failure analysis modelling to predict the forces required for crush propagation. Strain energies of the crushing structure in its deformed shape, along with mode I, II and in-plane strain energy release rates were related to the work needed to continue the crushing process. To verify what was predicted analytically, experimental results were obtained for flat composite strips undergoing crushing to propagate a centreline delamination in a mode I fracture. The experimental and the predicted results were in good agreement. The models were then modified to account for the presence of mode II and in-plane fracture, which commonly occur in axially crushed composite tubes. These models were reasonably accurate in their prediction of the crush forces. Although, these models seem to demonstrate good agreement between experimental and theoretical results, to simplify the analysis a deformed shape for the specimen was assumed and hence the accuracy of the results depends very much on how a real specimen would behave compared with the model.

Continuing the theme of modelling the failure mechanism in tubes as a mode I failure with a centreline delamination, Kendall [41,43] developed a technique to calculate the force needed to propagate a long crack down a beam when loaded in a mode I style [37]. He also reported on a peel method for determining the interfacial fracture energy G_{Ic} or, as described by Kendall, R_{ad} [43].

Laananen and Bolukbasi [44] investigated the energy absorption behaviour of composite stiffeners subjected to axial compression. A nonlinear finite element approach was used to model the sustained crushing of the elements, and a progressive failure model implemented as part of the analysis to enable investigation of the fundamental crushing mechanisms. The progressive failure model was based on linear elastic fracture mechanics for prediction of crack growth, and a set of failure

criteria for predicting fibre/matrix failures that were caused by large deformations. Friction between the specimen and the crushing surface was included in the model. A semi-empirical methodology was developed for prediction of the energy absorption capability of composite stiffeners based on flat plate crush tests and an understanding of the fundamentals of the energy absorption process.

Friction between the crushing structure and the crush surface was identified by the finite element analysis as having a large effect on the energy absorption process in composite laminates. It was found that the energy absorption of flat plate specimens increased by 50% when the specimen crushed on a rough (μ=0.4 (rather than a smooth surface (μ=0.2). The non-linear finite element analysis performed was able to predict the failure mechanisms in the sustained crushing phase of the energy absorption process.

2.7 Conclusions

Continued research has been carried out on the subject of crashworthiness since the 1950's, and well over 500 publications on this topic are to be found in library databases. It was the intent of this literature review to survey all the relevant available information, especially papers from 1980 onwards.

Whilst compiling this review, it was found that certain areas of work had been extensively covered whereas other areas had very little work published on them. The crashworthiness and energy absorption of woven tubes is a widely covered subject and numerous papers by a variety of authors have been published. In contrast to this, the area of energy absorption of sandwich panels is a subject where a greater understanding of the energy absorption mechanisms of sandwiches and cores would be useful in furthering the topic of crashworthiness.

Although, there has been some published work on the static and dynamic loading of sandwich plates. The plates were both simply and fully supported, the investigation concentrated on the through-thickness behaviour of flat plates, in particular on changing the core and facing materials to establish what effect this had on the energy absorption of the sandwich panel. The only literature found during the review on in-plane compression testing of sandwich panels was the work by Brachos et al [24] who researched balsa cored sandwich panels with glass fibre-reinforced plastic facings.

Similarly, NASA and other organisations have published a great deal of work on the crashworthiness of airframes and aircraft subfloors. Generic elements such as sine wave beams, stringer stiffened beam sections, cruciforms and sandwich beams were reported on. Although, for all of the above elements, the energy absorption and failure modes were reported on, almost all of them lacked a detailed investigation into what factors controlled the crushing process and hence what ultimately influenced energy absorption Hull et al [16] being an exception.

To conclude, after reviewing the available literature the following points can be drawn. There is a large amount of work already published on tubular structures. The understanding that exists for tubes such as the effect of fibre orientation, geometry

and trigger mechanism on energy absorption can be used for structures such as sandwich configurations to increase their energy absorption characteristics. Likewise, there are papers published that show the energy absorption potential of sandwich panels, but there is scope for developing more complicated sandwich configurations such as cruciforms and box sections for aircraft subfloors. There is lacking from the published literature for a comprehensive study of the energy absorption mechanisms, which take place when sandwich panels are crushed in the in-plane direction. These mechanisms would ideally be studied using video techniques to build up a picture of the crushing process.

To begin with in the current project an investigation of the energy absorption characteristics of flat sandwich panels will be undertaken. Parameters such as face thickness, core thickness, trigger mechanism, facing material, will be altered and the panels tested quasi-statically to see what effect these parameters have on the energy absorption capability of the panels. As there are many such parameters to investigate analytical techniques such as Taguchi methods will be used to optimise the number of experiments needed. From the literature reviewed it seems that the key to successful energy absorption is to obtain progressive crushing of the panel, which in turn relies on the design of the triggering mechanism, sandwich panel support and crush plate geometry which influences the crushing process. Therefore, work will be carried out using existing trigger mechanisms to understand their workings and to see if these can be improved upon. Once we have understood the factors that influence crushing and energy absorption in a sandwich panel we will use the knowledge gained to study and design more representative elements such as cruciforms, which will be manufactured and tested.

CHAPTER 3

SANDWICH STRUCTURE MANUFACTURE

3.1 Introduction

Before work on the crushing of sandwich structures was undertaken a list of parameters which it was thought might contribute to the energy absorption mechanisms in composite faced sandwich panels was compiled.

3.2 Initial Parameters

Facings.

Fibre material (e.g. carbon, Kevlar).

Matrix.

Volume fraction.

Modulus of the fibre and matrix, strain to failure of the fibre and matrix.

Lay-up.

Stacking sequence.

Fracture toughness of the matrix

Thickness of the faces.

Fibre architecture for faces (e.g. pre-preg, woven or braided material).

Core.

Core material (e.g. honeycomb such as aluminium, Nomex, or a foam such as polyurethane or poly-vinyl chloride).

Core thickness.

Density of foam core if used.

Cell dimensions if a honeycomb.

Cell wall thickness.

Adhesive.

Adhesive type for core-to-face bonding.

Co-cured or secondary bonding sandwich panel manufacture.

Type of Loading.

Static or dynamic loading.

In-plane or through the thickness testing of sandwich panel.

Striker geometry.

Structural.

Trigger mechanism type.

Due to the large number of parameters obtained it was decided to try to limit the number of parameters using Taguchi software (Appendix A).

3.3 Final Parameters

The panels used to manufacture the sandwich specimens, face skin specimens and the initial set of four single cruciform structures were manufactured from HTA/913 and had the parameters shown in Table 3.1. Due to material availability, the remaining three single cruciform structures, two double cruciform structures and one quadruple cruciform structure tested were manufactured from T300/914. The parameters of this pre-preg are detailed in Table 3.2.

It was initially thought that it would be beneficial to study several types of honeycomb and pre-preg system to see whether factors such as fibre modulus, resin fracture toughness, different cell sizes and cell wall thicknesses would have any influence on the energy absorption of the sandwich panels. However, due to the shortage of suitable materials to manufacture all the relevant specimens needed, it was decided to limit to four the number of parameters studied initially, namely: - facing thickness, core thickness, lay-up and inclusion of trigger mechanism. To further minimise the number of parameters it was decided to limit the material to carbon

fibre/epoxy pre-preg, and due to material limitations only two thicknesses of honeycomb were available. This meant that initially almost all of the available material parameters such as cell size, fibre modulus had been fixed. Two different types of lay-up were initially investigated, these were quasi-isotropic $\{(-45°, 0°, 90°,+45°)_S\}_n$ and uni-directional, representing two very different lay-ups. Two face skin thicknesses (1mm and 3mm) were investigated.

The core material chosen for the sandwiches was Aeroweb Type 5052 aluminium alloy honeycomb. Ultimately two different thicknesses of honeycomb were used for the initial single sandwich panel specimens i.e. 10mm and 20mm thick. Initially the cell size and cell wall thicknesses for these two cores were nominally the same (for cell dimensions see table below). All the panels were initially manufactured with additional adhesive between the facings and the core in the form of one layer of adhesive film each side of the core, although this was later doubled (see Section 3.4), and the panels were co-cured. All the specimens, whether small coupons, sandwich panels or cruciforms were tested quasi-statically in an in-plane orientation. The trigger mechanism used was of the saw-tooth variety. Table 3.3 details the sandwich structure parameters used.

Elastic Properties		Strength Properties (MPa)	
E_1 (GPa)	130	σ_{1t}^u	1650
E_2 (GPa)	4.65	σ_{1c}^u	1100
E_3 (GPa)	4.65	σ_{2t}^u	60
G_{12} (GPa)	4.65	σ_{2c}^u	200
G_{23} (GPa)	4.65	σ_{3t}^u	----
G_{31} (GPa)	----	σ_{3c}^u	----
ν_{12}	0.35	τ_{12}^u	100
ν_{21}	----	τ_{23}^u	----
ν_{23}	----	τ_{31}^u	100
ν_{13}	----		

Table 3.1 Mechanical property data (UD carbon/epoxy HTA/913).

Elastic Properties		Strength Properties (MPa)	
E_1 (GPa)	139	σ_{1t}^u	1490
E_2 (GPa)	9.5	σ_{1c}^u	1402
E_3 (GPa)	9.5	σ_{2t}^u	46
G_{12} (GPa)	5.2	σ_{2c}^u	215
G_{23} (GPa)	3.2	σ_{3t}^u	46
G_{31} (GPa)	5.2	σ_{3c}^u	215
ν_{12}	0.32	τ_{12}^u	79
ν_{21}	0.02	τ_{23}^u	79
ν_{23}	0.5	τ_{31}^u	79
ν_{13}	0.32		

Table 3.2. Mechanical property data (UD carbon/epoxy T300/914).

Parameter	Fixed
Face material	Carbon fibre,
Fibre architecture i.e. pre-preg, woven	Unidirectional pre-preg.
Matrix material	Epoxy
Matrix volume fraction	35-40%
Core material	Aluminium honeycomb (Aeroweb Type 5052)
Honeycomb cell size	3.175mm (1/8") *
Cell wall Thickness	0.035mm
Separately made / co-cured	Co-cured
Static or dynamic loading	Static
Through-thickness or in-plane tested	In-plane tested (0°direction)
Quasi-isotropic stacking sequence (when used)	$\{(-45°,0°,90°,+45°)_s\}_n$
Parameter	**Variable**
Facing thickness	1mm and 3mm (8 and 24 layers) nominal thickness.
Core thickness	10mm and 20mm
Lay-up	Quasi-isotropic and unidirectional
Trigger mechanism	Saw tooth trigger and no-trigger

Table 3.3 Final sandwich panel parameters

*Due to a change in honeycomb supplier some of the sandwich panels tested subsequently had a honeycomb cell size of 6.350mm (¼").

3.4 Laminate Production

In this section the procedures used to manufacture the laminated plates for the sandwich skins and the face skin specimens are detailed, along with the subsequent method used to produce the sandwich panels and any subsequent machining of the panels.

The laminated plates were manufactured from unidirectional pre-impregnated carbon fibre material supplied by Hexcel Composites in 300mm wide rolls and of cured nominal thickness of 0.125mm. When not in use the rolls were kept refrigerated at -18°C to extend their shelf-life. Before use the pre-preg was removed from the freezer and left to thaw for a minimum of 4 hours to avoid condensation in the finished article. While the plates were being manufactured care was taken to avoid any entrapped air, and so after each pre-preg layer had been added the panel was compressed using a mangle. Once the plates had been assembled they were stored in a freezer until they were ready to be cured. The plates manufactured were 300 x 300 mm in size and had a cured nominal thickness of either 1 or 3mm.

3.4.1 Laminate Curing

The manufacturing method for laminates that ensures the most even finish is autoclave curing. An autoclave ensures that the components are subjected to uniform temperature and pressure. The laminated face skins manufactured for this project were made via this route.

The autoclave set-up used is depicted in Figure 3.1. The Duralumin pressure plate and the wooden dams ensured that the laminated plate remained dimensionally stable during the curing process and that a uniform pressure was exerted on the laminate. The plate was thick enough to avoid bending and as such the plate used for the curing of the laminates was 2 mm thick. To avoid adhesion between the curing laminate plates the pressure plate and the table, Melenex® sheet which are non sticking films, were used.

The HTA/913 pre-preg was a 120°C curing system for 1 hour and the T300/914 system was a 180°C curing system for 1 hour.

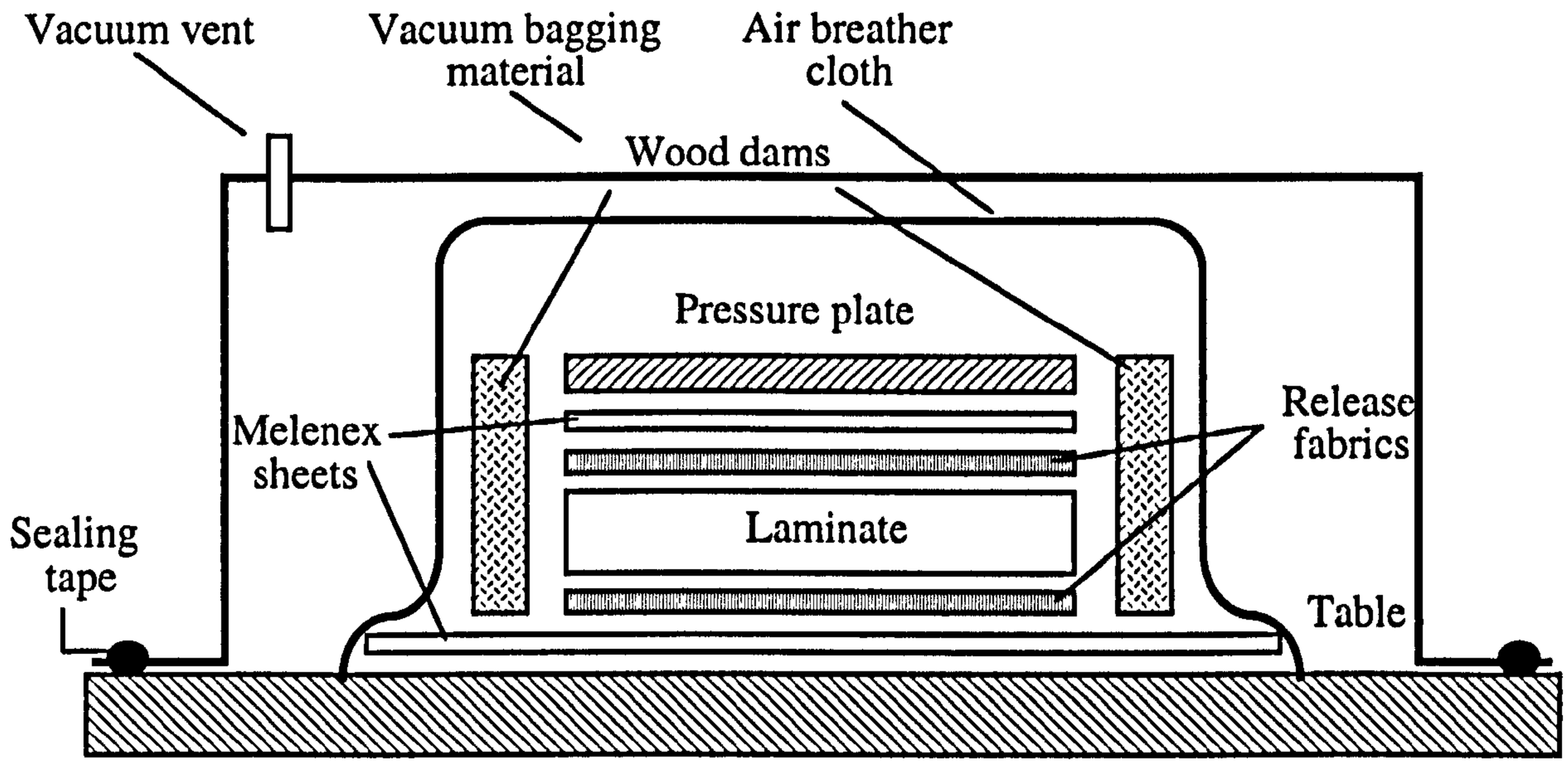

Figure 3.1 Autoclave lay-up

3.5 Sandwich Panel Production

To bond the faces of the sandwich panel to the aluminium honeycomb core an epoxy adhesive film was used. The adhesive cured at the same temperature as the pre-preg. The nominal uncured thickness of the adhesive film was 0.1mm. The adhesive was stored similarly to the pre-preg to prolong its usable life and was defrosted for a similar length of time before use – see Section 3.4.

To manufacture the sandwich panels the pre-preg faces were layed up in an identical manner to that for the face skin specimens. To bond the pre-preg faces to the sandwich panel the procedure outlined below was used (see also Figure 3.2).

A piece of adhesive film was cut to a size slightly larger than the un-cured plates i.e. 310mm x 310mm. The backing paper was removed from one side of the un-cured pre-preg and the adhesive film applied to the pre-preg. This procedure was repeated for the other un-cured face of the sandwich panel. To transfer the adhesive film from its backing paper to the pre-preg, the pre-preg face plus adhesive film were placed on an aluminium plate and put between the platens of a press heated to 100°C, and slight pressure applied for 30 seconds. Melenex® film was used to protect the platen faces from any adhesive that may have been squeezed from between the backing paper in the transfer process. After 30 seconds the faces were removed from the press and left to cool.

A similar process was repeated on the aluminium honeycomb; adhesive film was applied to either side of the core and the core plus adhesive film placed in the press. Care was taken when applying pressure not to compress the core. After 30 seconds the aluminium core plus adhesive was removed and left to cool. The backing paper was removed from both faces of the sandwich panel and from the core. It was noted that the honeycomb core cell size had an effect on the amount of adhesive transferred from the backing paper to the core: - a smaller cell size giving a larger effective area for the adhesive to adhere to. Once the backing paper had been removed from both components, the faces were placed on to the core. Care was taken to ensure that both

faces matched up with one another and were orientated in the correct way in relation to the ribbon direction of the core.

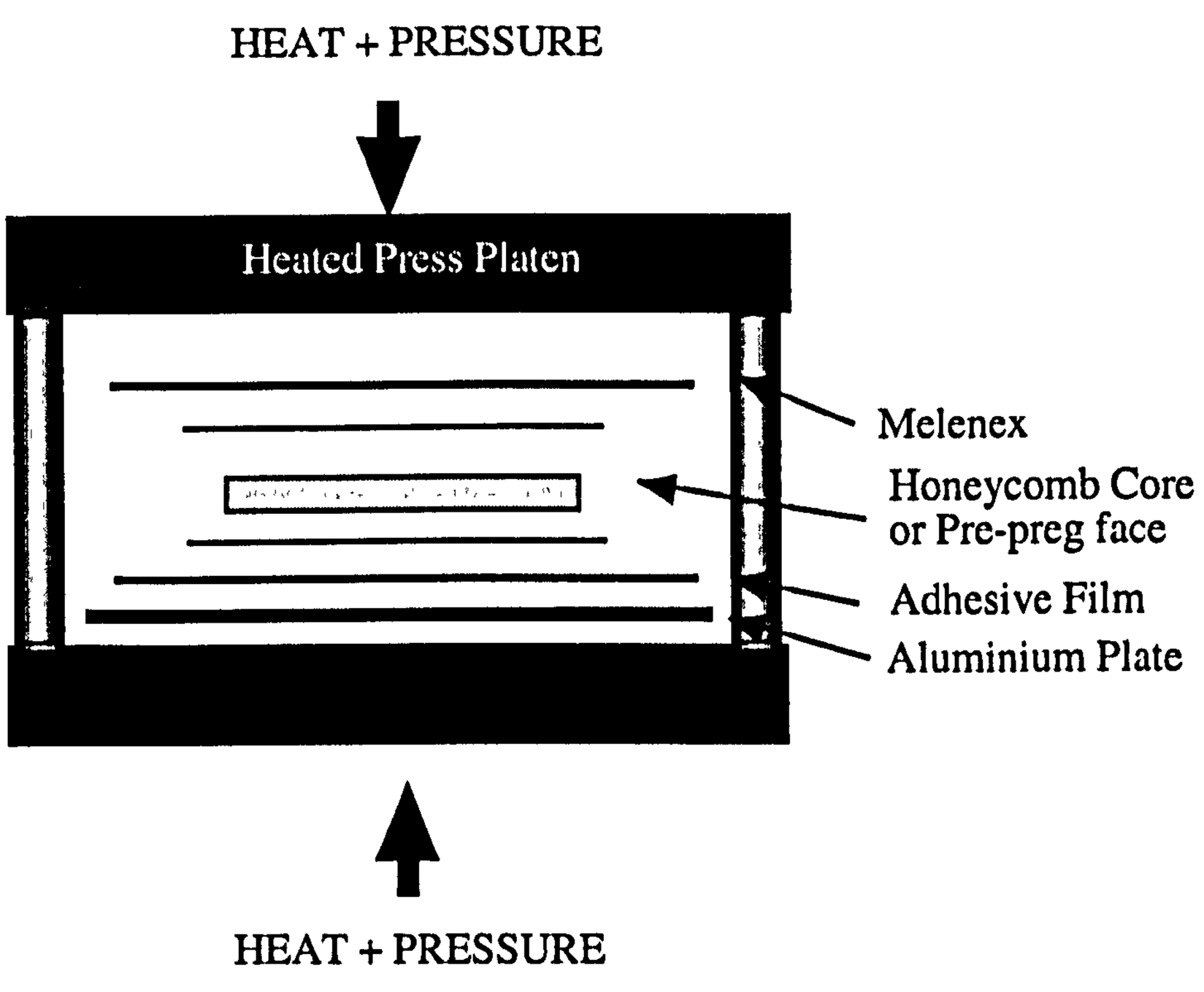

Figure 3.2 Adhesive film transfer technique

3.6 Saw-Tooth Trigger Mechanism

The saw-tooth trigger mechanism was machined using a rotating cutting head (Figure 3.3). Several sandwich panels at a time were clamped together and machined. When the end panels of the block were machined the direction of the cutting head was reversed to avoid fibre breakage on the unsupported outermost faces. The dimensions of the saw-tooth triggers are shown in Figure 3.4.

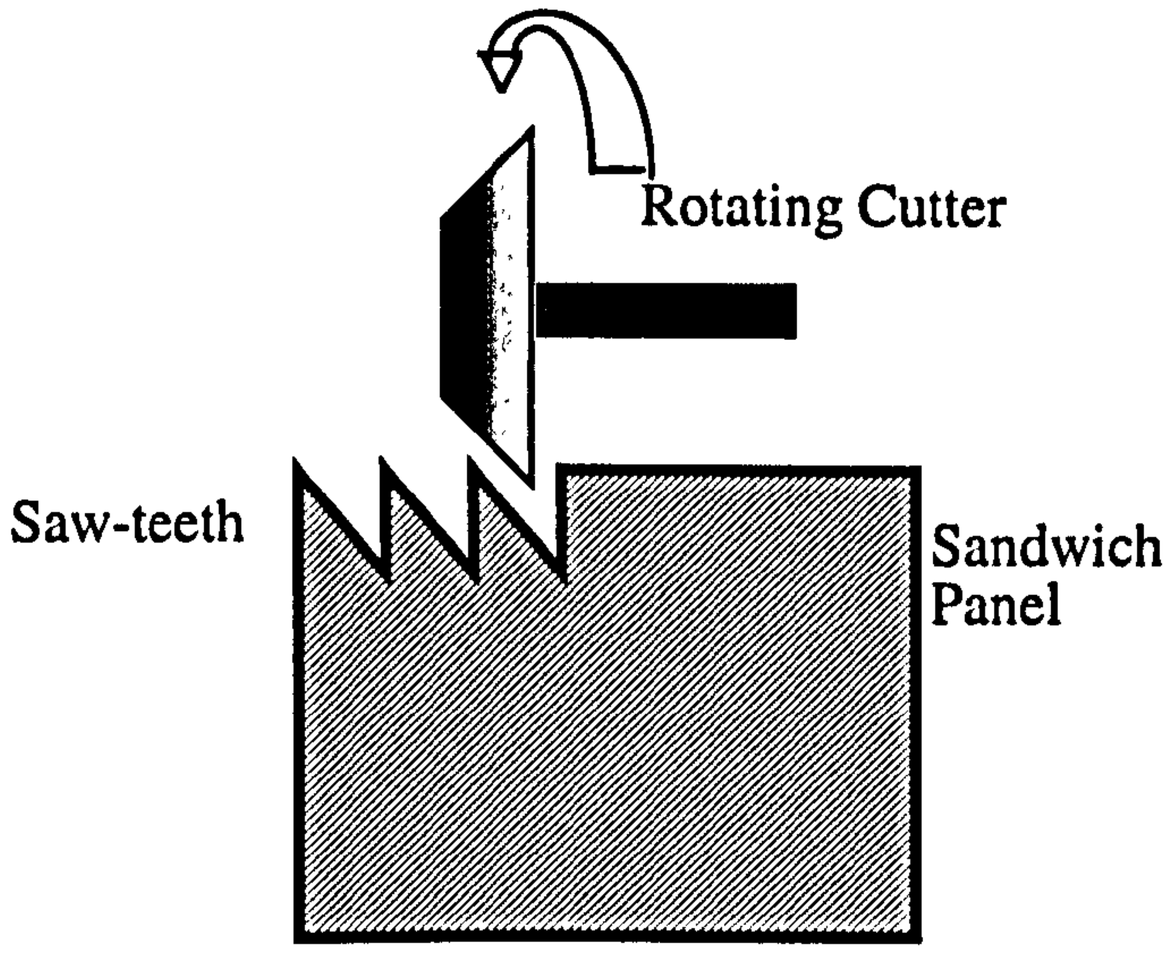

Figure 3.3 Saw-tooth machining

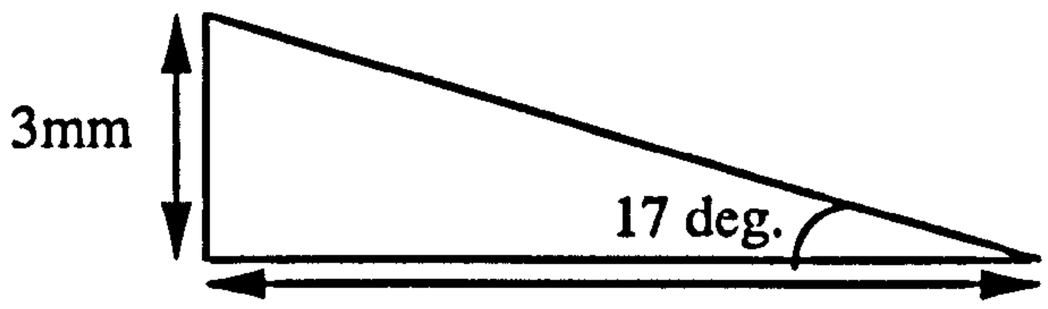

Figure 3.4 Saw-tooth dimensions

3.7 Small Specimen Manufacture

The small specimens were manufactured in an identical manner to the sandwich panel faces, as described in Sections 3.4 & 3.4.1.

3.8 Cruciform Manufacture

To manufacture the cruciforms the following steps were carried out: -

1) The sandwich panels were manufactured via the route outlined in Section 3.4. The sections that make up the cruciform were then cut to size (Figure 3.5).

2) The triggers were machined into the top of each panel.

3) The bases of the sandwich panels were machined flat.

4) The sections were joined together.

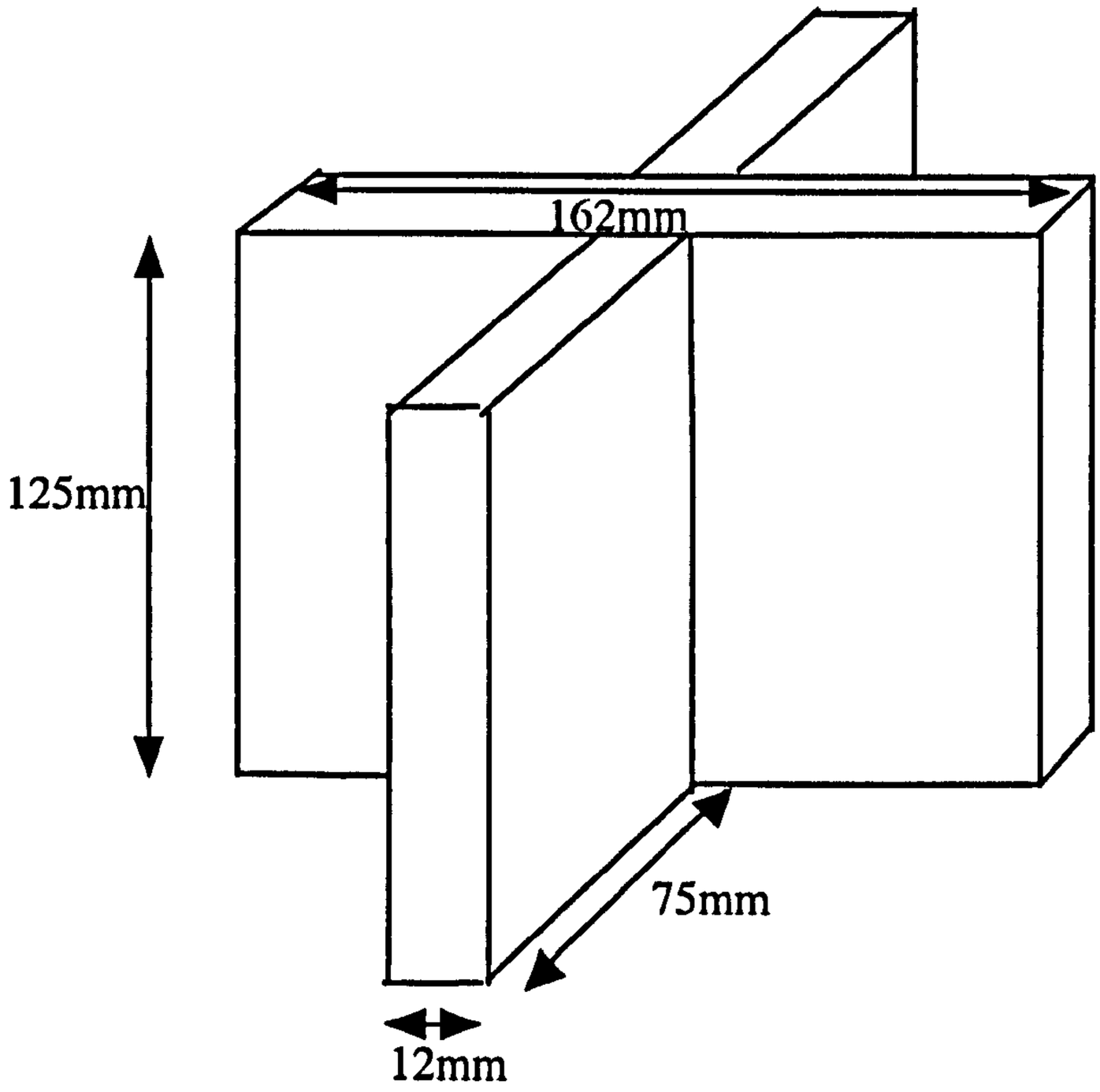

Figure 3.5 Single cruciform dimensions

The double cruciforms were 324mm long by 162mm wide i.e. each arm of the cruciform was 75mm long. Similarly for the quadruple cruciform, the length was again 324mm, as was the width.

3.9 Angle Stiffener Manufacture

To secure the individual sandwich panels together (Figure 3.6) into a cruciform structure, angle stiffeners were fabricated. Two pieces of aluminium section were used to form the stiffeners (Figure 3.6). The sections were 700mm in length and had side lengths of 25.4mm and 22.2mm and were 3.2mm thick. Both sections were covered in release fabric to stop adhesion with the pre-preg material. The stiffeners were made from the same pre-preg as the sandwich panel skins, and had a lay-up of $(-45°/0°/90°/45°)_{2S}$ with a nominal cured thickness of 2 mm.

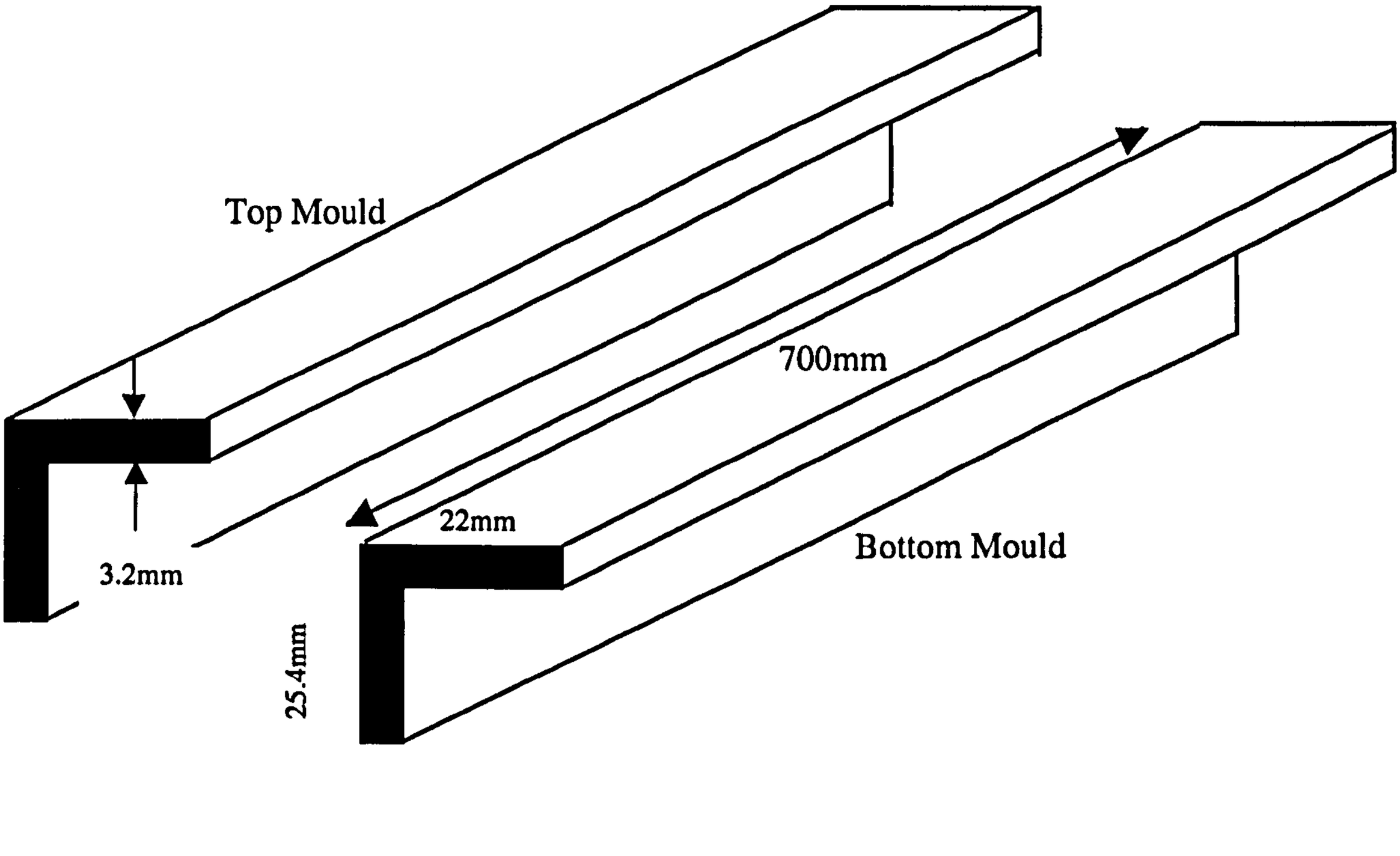

Figure 3.6 Stiffener moulds

To lay-up the stiffeners, strips of pre-preg 700mm x 70mm were cut out and laid-up four layers at a time in the correct stacking sequence. The four layer strip was then laid onto the mould as shown below in Figure 3.7 and pressure applied to the top mould. The whole assembly was then placed on a vacuum table for approximately 10 minutes to consolidate the pre-preg layers. This procedure was repeated until the stiffener lay-up was complete. The excess pre-preg was then trimmed off and the stiffener cured in an autoclave at 120°C or 180°C for 1hr following the cure schedule for the particular pre-preg used.

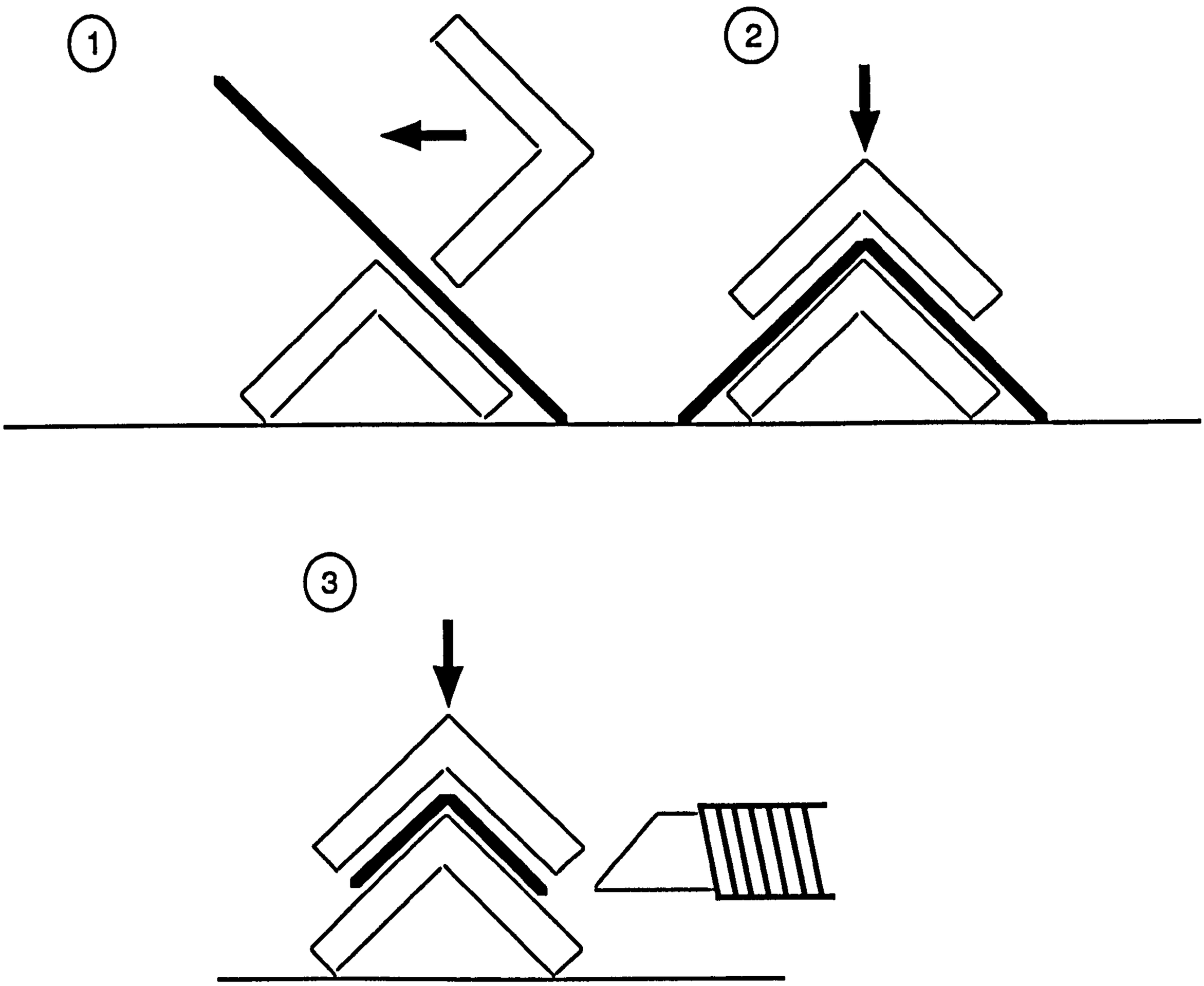

Figure 3.7 Forming of stiffeners

Once cured the stiffeners were deflashed and cut to size using a diamond saw. To adhere the stiffeners to the sandwich panel the back of the stiffeners and the

intersecting points of the cruciform (Figure 3.8) were grit blasted and cleaned with Freecoat®. The adhesive was applied to these prepared surfaces. The parts of the cruciform were glued together with Araldite® 2015, a high shear strength, two-part cold curing adhesive. The cruciform was correctly aligned so that the corners were at 90° to each other and held in place by clamps whilst the adhesive set.

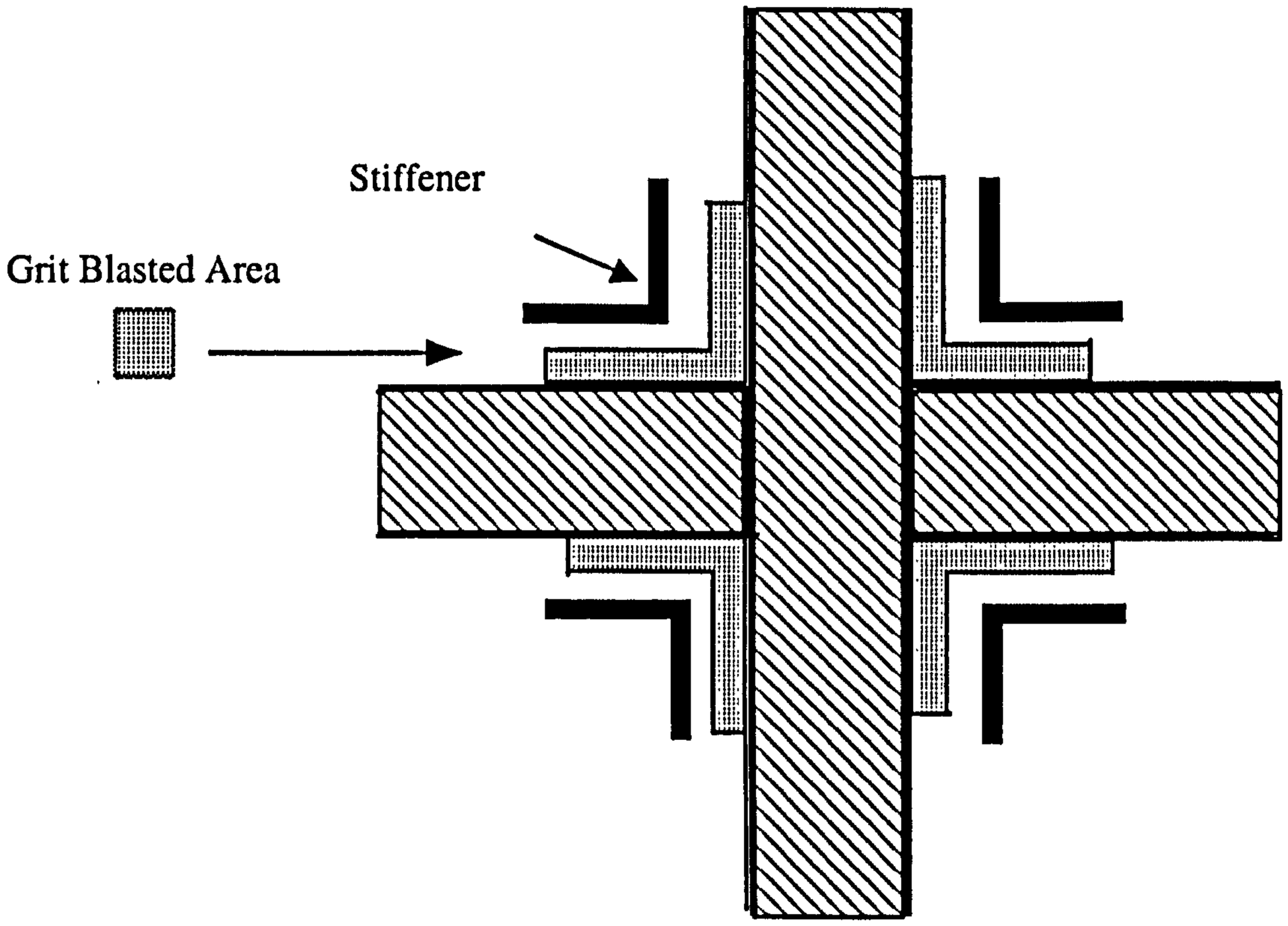

Figure 3.8 Grit blasted areas of cruciform

CHAPTER 4

IN-PLANE CRUSHING OF SANDWICH PANELS

4.1 Introduction

In this chapter, the crushing response of composite sandwich panels subjected to in-plane loading is presented. Included are descriptions of the different test rigs used, the crush modes, load-displacement behaviour and energy absorption characteristics. The findings from this initial set of sandwich panels crush tests were used to improve the testing of the subsequent cruciform structures. As can be seen from the following chapter, to maximise the energy absorption capability of sandwich structures when subjected to in-plane loading their failure modes had to be controlled. To achieve this specimen geometry, support conditions and crush plate fixture were investigated and reported upon in this chapter.

Twelve CFRP faced, aluminium cored sandwich panels of various configurations (specified by the Taguchi Array - Appendix A) were crush tested using the rig shown in Figure 4.1. Eleven of the samples were tested at 5mm/min and one was tested at 1mm/min. All of the specimens tested were 75mm wide and 80mm long. These dimensions were similar to those used by Lavoie [7]. The specimens were tested on an Instron universal testing machine fitted with a 100kN compression load cell. All of the samples were triggered at the bottom, the Instron crosshead moving downwards. The displacement values for the tests were obtained from the crosshead displacement. The displacements values recorded can only be used as a guide due to problems such as slight deflection of the crosshead or load cell under loading. A summary of the results for each sample is given below.

4.2 Test Results

Sample 1 — 3mm, quasi-isotropic face skins, 20mm thick aluminium core, no trigger. (Also see Appendix A).

The graph (Figure 4.20) depicts the crushing history for the sample. Crushing initiated at 45kN at which point a large reduction in load occurred. A quite regular pattern then developed of the load building up, and then fracturing of the sample causing the load to decrease once more. The magnitude of the load at the peaks (and troughs) of this oscillating load-displacement trace steadily increased as the displacement was increased from 6 to 21mm. At a displacement of 21mm a peak of 65kN was seen, which possibly may have been due to debris increasing the friction at the knife-edges and, hence, increasing the load.

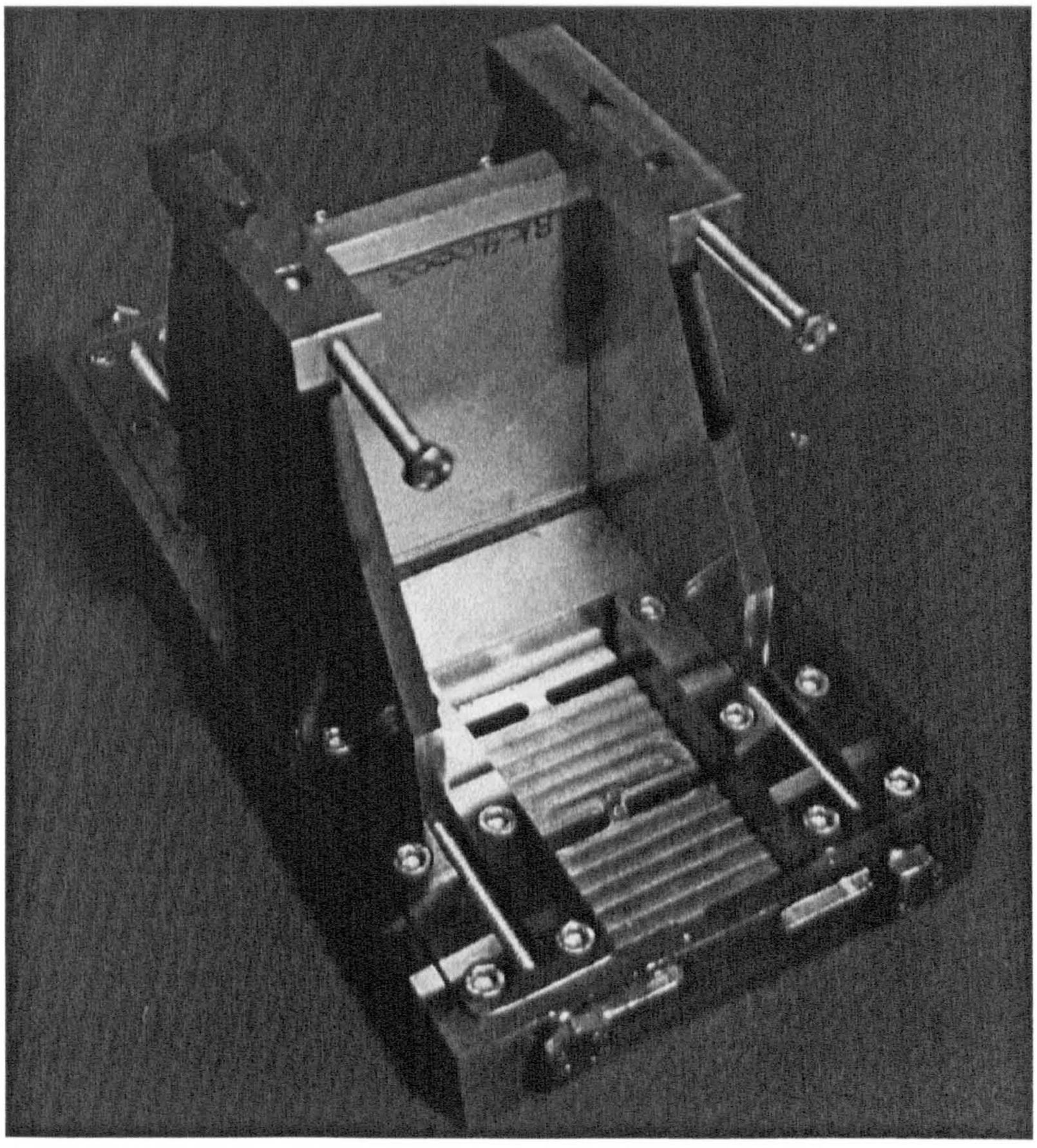

Figure 4.1 Crush rig

After this final peak, there was no longer an upward trend in the oscillating load-displacement trace, and the curve seemed to plateau and then start decreasing after a displacement of 32mm. The test was terminated at a displacement of 40mm. The

sample crushed from the top downwards. There were signs of friction between the sample and the knife-edges. (The specimen orientation in Figure 4.2 was for photographic purposes only).

Apart from the friction at the knife-edges the sample crushed as expected the faces underwent extensive delamination and peeled away from the core. The core appears to have crushed steadily, apart from where the sample had become jammed in the knife-edge, where both the facings and the honeycomb showed signs of tearing. It was difficult to see if there was any change in failure mode as crushing continued, because of the orientation of the test rig in the testing machine.

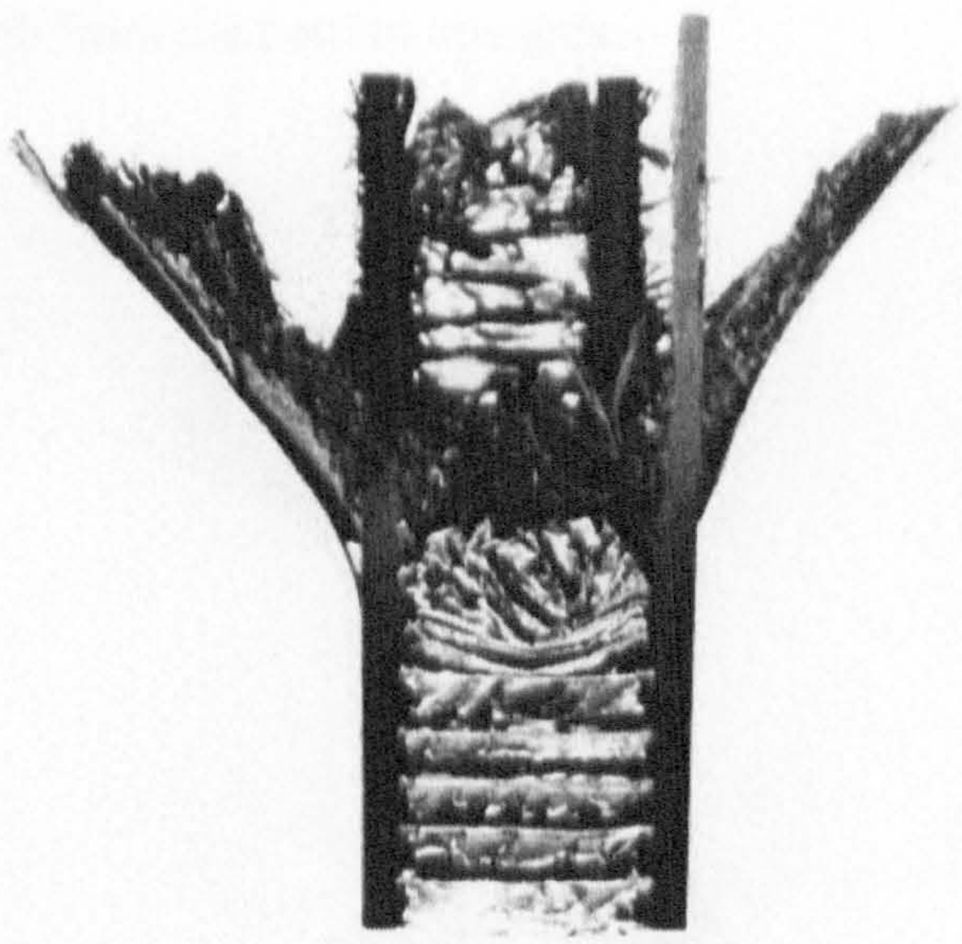

Figure 4.2 Sample 1

Sample 2 — 3mm, quasi-isotropic face skins, 10mm thick aluminium core, saw-tooth trigger mechanism. (Also see Appendix A).

Sample 2 crushed at the triggered end (top in Figure 4.3) at 65kN. The load rose steadily to peak at 95kN (Figure 4.21). Prior to this there was no evidence on the graph of any crushing. If this was true, then 5mm displacement in a sample of 80mm length equates to a strain of over 6%, which is clearly unlikely. The way in which the displacement was recorded, i.e. from the crosshead (as mentioned at the beginning of

this section), may well account for this. Before the triggers were fully crushed the crushing switched to the bottom of the sample (Figure 4.3) where 3mm of crushing occurred and was accompanied by a large decrease in load to 50kN. After 15mm displacement the load rose steadily to 75kN until at 22mm displacement a sudden drop in load was seen, down to a value of 25kN. This drop occurred as one of the face skins completely debonded (Figure 4.4). Although the face became debonded from the core (specimen held together for photo) it seemed to be held in the jig by the knife-edges. The crushing at this point started again at the bottom of the specimen with the load rising to a value of 50kN at a displacement of 33mm. Towards the end of the crush duration debris caused by the crushing process was seen to form a wedge between the bottom faces of the sample. The wedge had the effect of crushing the aluminium honeycomb from the bottom upwards.

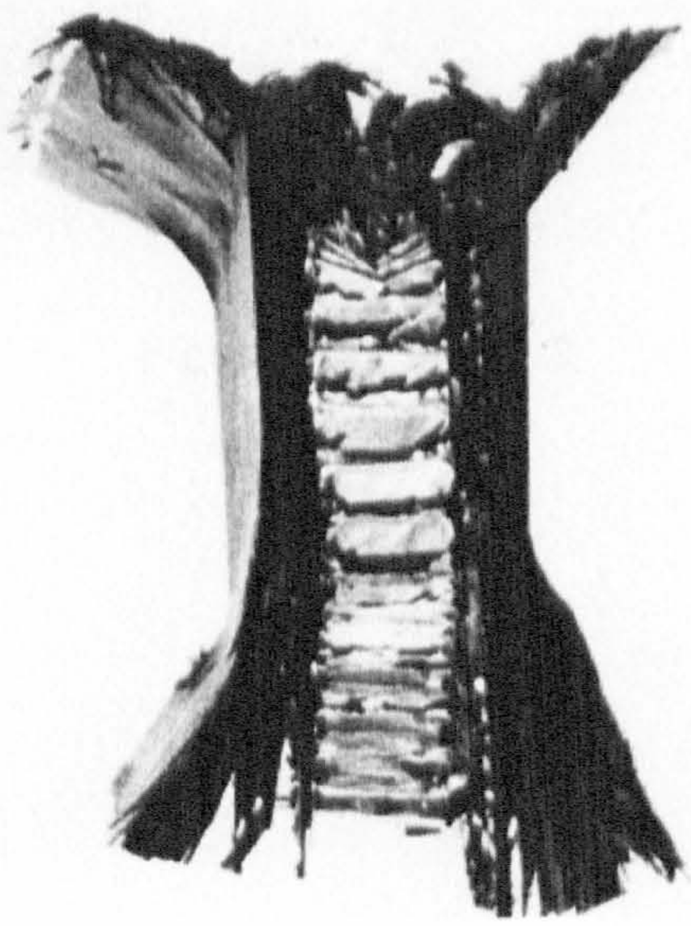

Figure 4.3 Sample 2

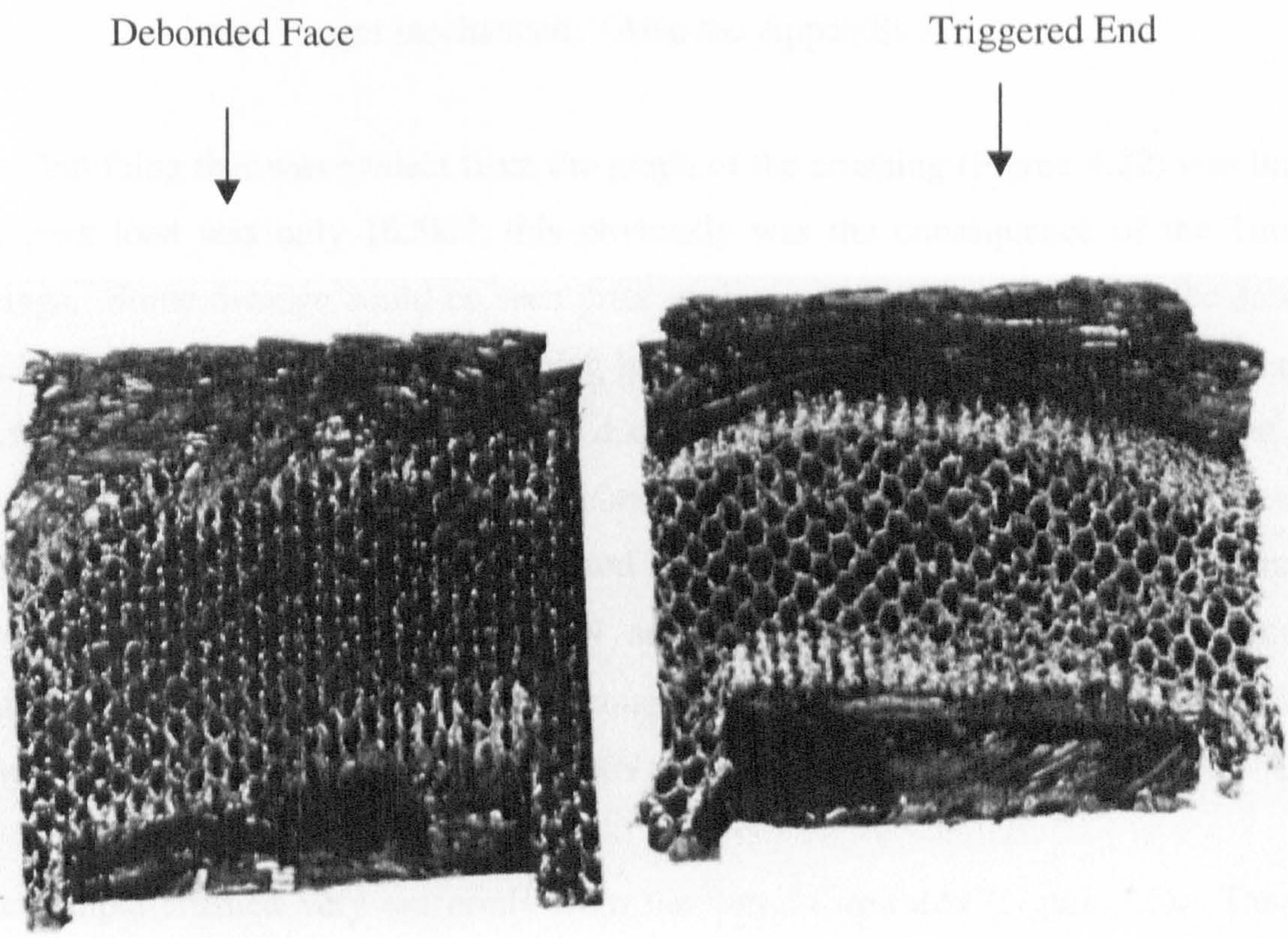

Figure 4.4 Sample 2

Sample 3. 1mm, quasi-isotropic face skins, 20mm thick aluminium core, saw-tooth trigger mechanism. (Also see Appendix A).

The first thing that was evident from the graph of the crushing (Figure 4.22) was that the peak load was only 16.5kN; this obviously was the consequence of the 1mm facings. Some damage could be seen prior to this, which was crushing of the saw-tooth trigger mechanism. Once crushing had started the load decreased to a value of 12.5kN, which corresponded to 10mm displacement. The load then increased at a steady rate until a value of 15.5kN was obtained at a displacement of 21mm. After an initial decrease the load then increased again, to a value of 13kN at 34mm displacement, finally dropping to 9kN at the termination of the test at 40mm displacement. The overall trend throughout the crush duration was slightly downwards, the load decreasing from 16kN to 9kN.

The sample crushed very uniformly from the bottom upwards (Figure 4.5). There seemed to be no friction problems between the knife-edges and the sample, the full width of the sample being crushed. The two outermost carbon fibre layers were left intact as they curled away from the crush 'zone'. All the other layers were crushed and formed a debris wedge. The aluminium honeycomb core crushed so that only 30mm of undamaged core remained at the end of the test.

Triggered End

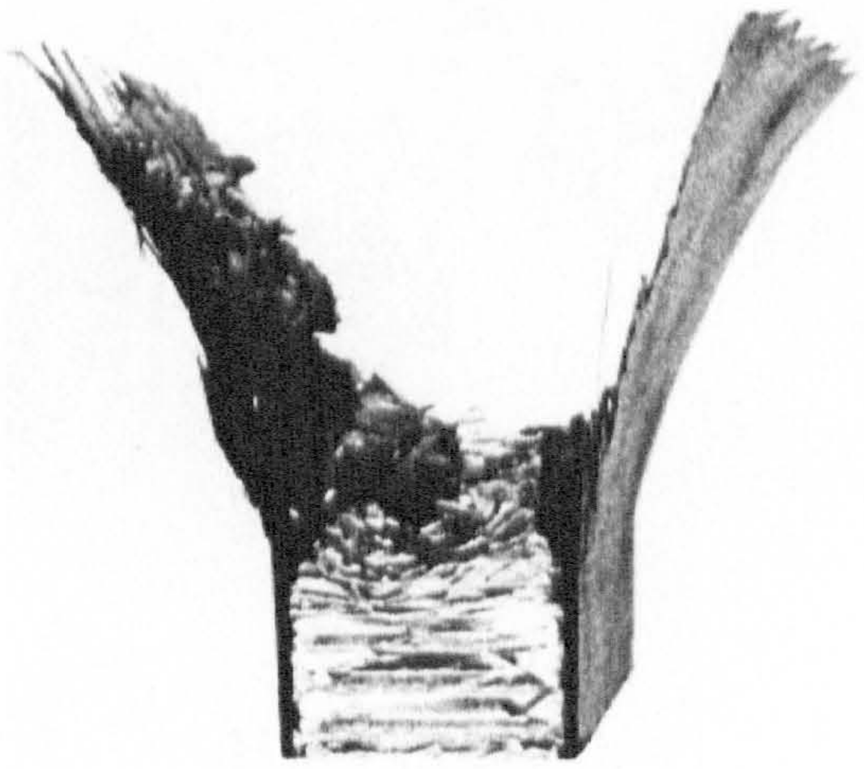

Figure 4.5 Sample 3

Sample 4. 3mm, unidirectional face skins, 20mm thick aluminium core, saw-tooth trigger mechanism. (Also see Appendix A).

The sample being unidirectional possessed high strength in the direction of crushing, taking a load of 66kN before the triggers started to crush. Evident in the crushed sample were signs of a large degree of friction at the knife-edges, the edges of the panel remaining uncrushed. This may have been bought about by the skins jamming in the knife-edges. Also evident was the fact that both faces had failed in through-thickness shear (Figure 4.6). Each of the faces seemed to have sheared into four distinct sections. Complete debonding of some parts of the faces was seen once shearing had taken place. A large reduction in load carrying capability can be seen from Figure 4.23 due to the above factors, the load decreasing from 65kN at the start of crushing to 5kN at its completion.

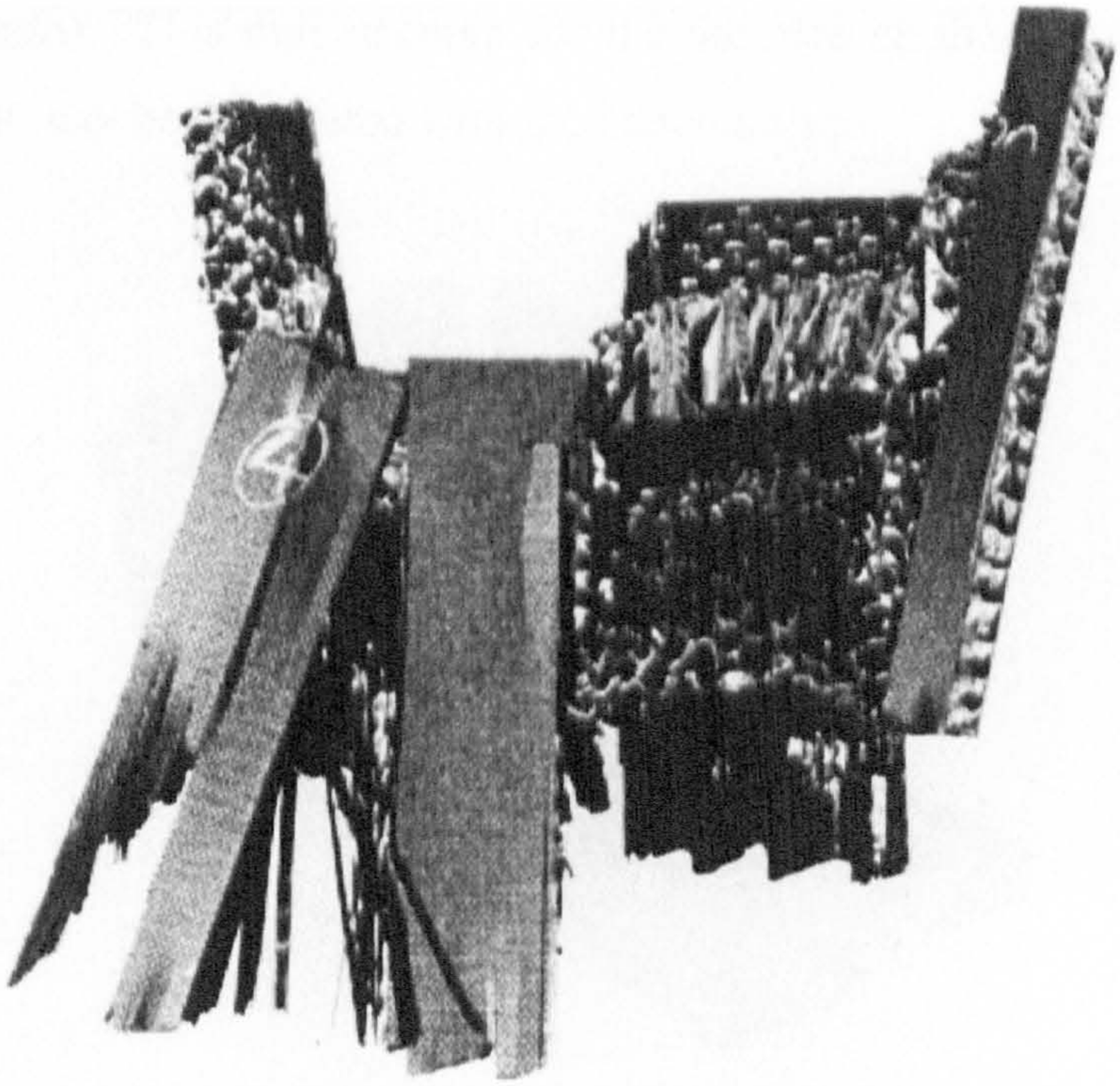

Triggered End

Figure 4.6 Sample 4

Sample 5. 3mm unidirectional face skins, 20mm thick aluminium core, no trigger mechanism. (Also see Appendix A)

Sample 5 was identical to Sample 4 apart from the absence of a triggering mechanism. Comparing the graphs for the two specimens (Figure 4.23 and 4.24) it was suprising that the sample with the saw tooth trigger achieved a higher peak load. As can be seen from Figure 4.24 the sample started to fail at a load of 36kN the load then decreasing to a value of 20kN. However, the load built up again to a value of 46kN before any more significant failures occurred.

At a displacement of 5mm the sample progressively crushed from the top downwards and the load decreased until the test was stopped at a displacement of 40mm, which corresponded to a load of 20kN. There was indication of friction at the knife-edges, the edges of the sample remaining uncrushed. As with Sample 4 the faces of the sandwich panel failed in through-thickness shear, although not as extensively, the faces splitting but not coming completely debonded from the core (Figure 4.7)(face removed for photo). This may account for the absence of sharp downward steps in the graph, which may be associated with face debonding.

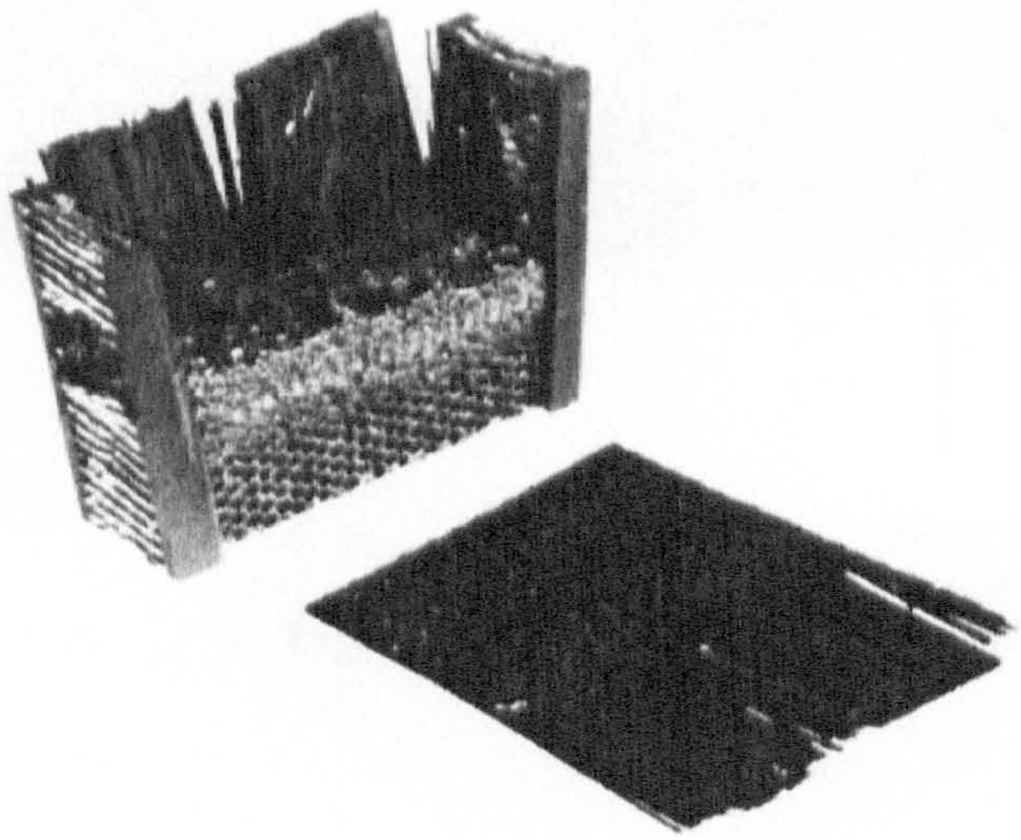

Figure 4.7 Sample 5

Sample 6. 3mm, unidirectional face skins, 10mm thick aluminium core, no trigger mechanism. (Also see Appendix A)

This sample was tested at 1mm min^{-1}. The graph for Sample 6 (Figure 4.25) was unlike any of the other twelve. The load increased to 95kN where at a displacement of 2.6mm fracture started to occur. At a displacement of 3.2mm, still at a load of 95kN, the sample underwent catastrophic failure, one entire face of the sandwich panel became debonded (see Figure 4.8). The sandwich panel at this point had lost almost all of its load carrying capacity and so the test was terminated at a displacement of 4mm.

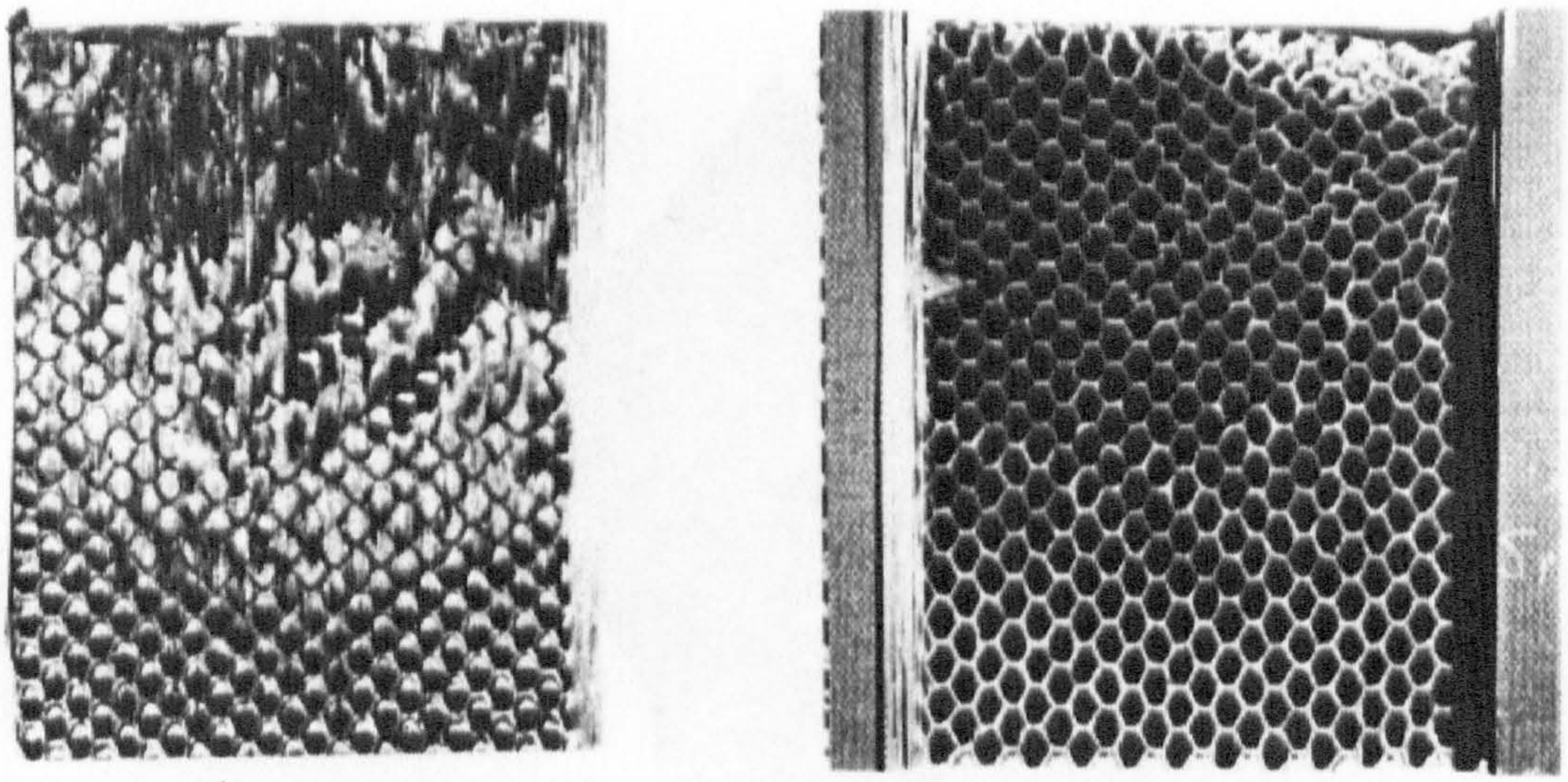

Inner surface of debonded face

Honeycomb surface exposed after face debonding

Figure 4.8 Sample 6

Sample 7 — 1mm, quasi-isotropic face skins, 10mm thick aluminium core, no trigger mechanism. (Also see Appendix A).

The graph for the crushing of this sample (Figure 4.26) showed a peak load of 19kN. Once delamination of the sample started, for reasons that are unclear, the load dropped rapidly and a constant crushing load of approximately 7-8kN was recorded until the test was terminated at a displacement of 40mm. The sample crushed from the top downwards. Again a significant amount of friction seems to have occurred at the knife-edges where tearing of the faces and of the honeycomb was seen (Figure 4.9). The central portion of the sample crushed uniformly, as indicated by the graph.

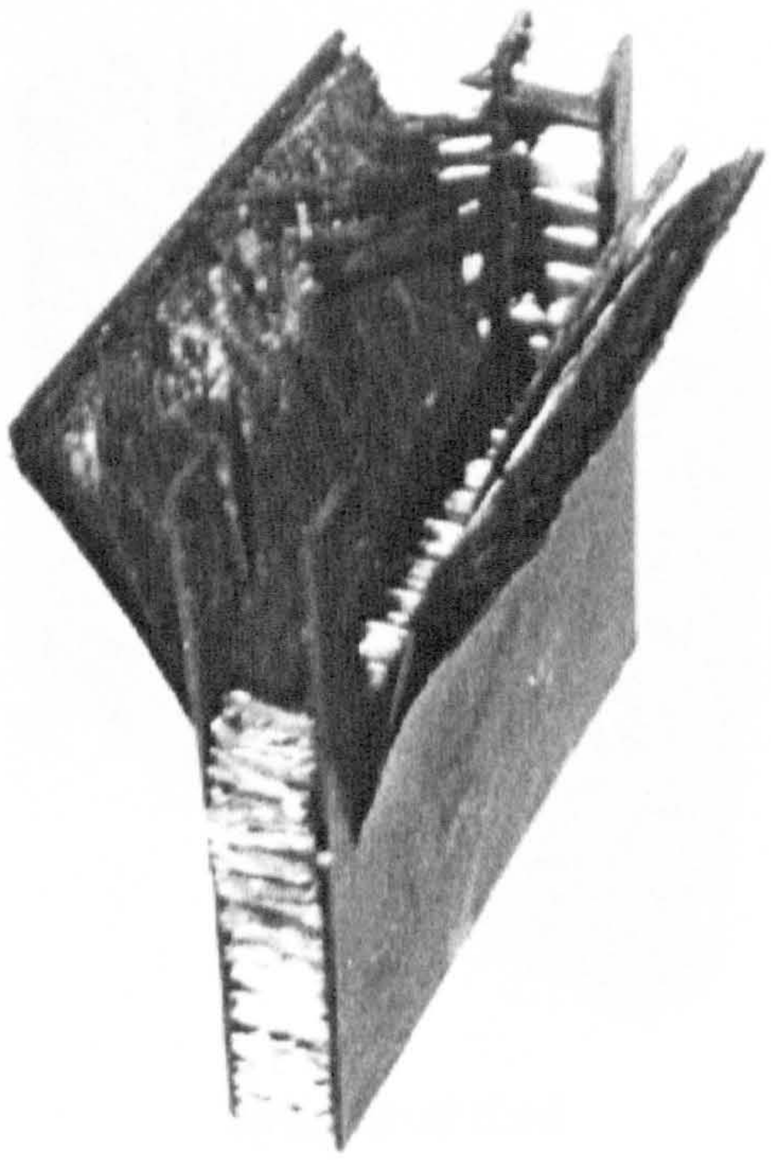

Figure 4.9 Sample 7

Sample 8. 1mm, unidirectional face skins, 10mm thick aluminium core, saw-tooth trigger mechanism. (Also see Appendix A).

Triggering was initiated at the bottom of the sample, i.e. once the tops of the triggers had been crushed, the crushing went back to the top of the sample (Figure 4.10). Again there seemed to be friction at the knife-edges where tearing of the sample occurred. The sample reached a peak load of 34kN (Figure 4.27). The faces of the sample delaminated and split. Although the splitting of the faces was quite extensive the but the faces remained attached to the specimens. The test was ended when the displacement had reached 40mm, at which point the load had dropped to a value of 5kN.

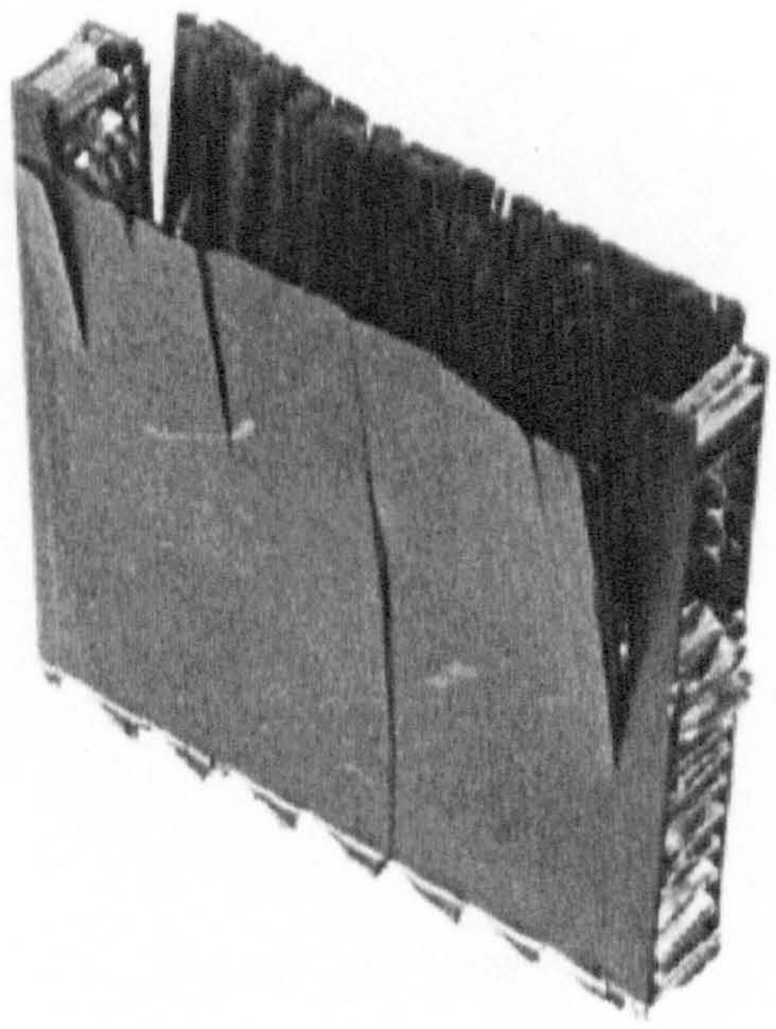

Triggered End

Figure 4.10 Sample 8

Sample 9 1mm, quasi-isotropic face skins, 20mm thick aluminium core, no trigger mechanism. (Also see Appendix A).

The crushing of this sample followed a similar trend to previous samples. The sample experienced a peak load of 17.5kN before crushing started from the top downwards (Figure 4.11) and the load dropped to a value of 8kN (Figure 4.28), before increasing rapidly again to 12kN possibly due to friction at the knife-edges. After this rise, the load decreased gradually and levelled out at a value of 6kN, this level being maintained until the test was ended at a displacement of 40mm.

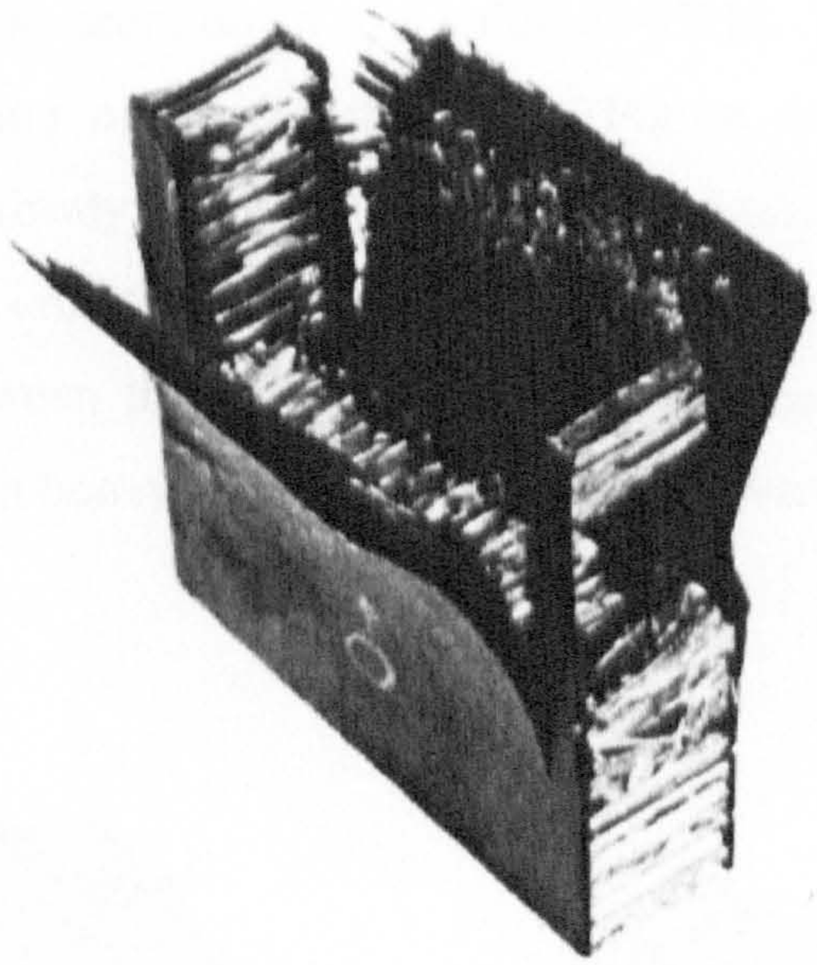

Figure 4.11 Sample 9

Sample 10. 3mm, quasi-isotropic face skins, 10mm thick aluminium core, saw-tooth trigger mechanism. (Also see Appendix A).

Sample 10 had an identical configuration to Sample 2. Comparing the two graphs (Figures 4.29 and 4.21) it can be seen that the traces follow the same general trend. From the graph for Sample 10 (Figure 4.29) it can be seen that the triggers initiated crushing at 62kN from the bottom upwards, the load rose steadily to peak at 85kN. Unlike Sample 2 (Figure 4.3) crushing continued from the bottom, there seemed to be no visible signs of friction at the knife-edges, the full width of the sample crushing. At 15mm displacement the load rose steadily to 72kN until at 23mm displacement a sudden drop in load was seen, down to a value of 45kN. The latter corresponded to the complete debonding of one of the faces (Figure 4.13). The face, although debonded, was held firmly in place by the knife-edges. Again, as in Sample 2 towards the end of the crush duration, debris caused by the crushing process was seen to form a wedge between the faces of the sample. The wedge had the effect of crushing the aluminium honeycomb from the bottom upwards.

Triggered End

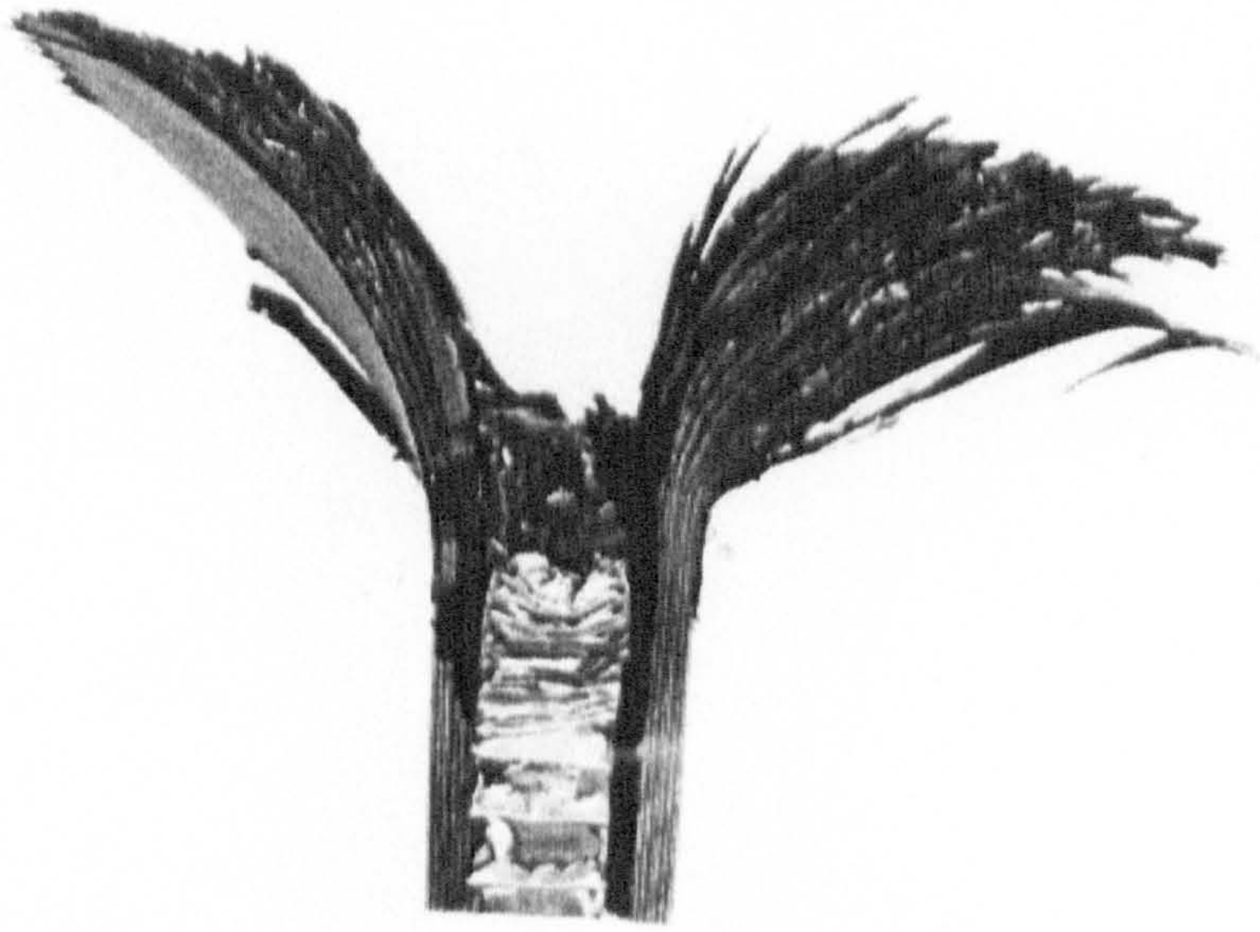

Figure 4.12 Sample 10

Debonded Face

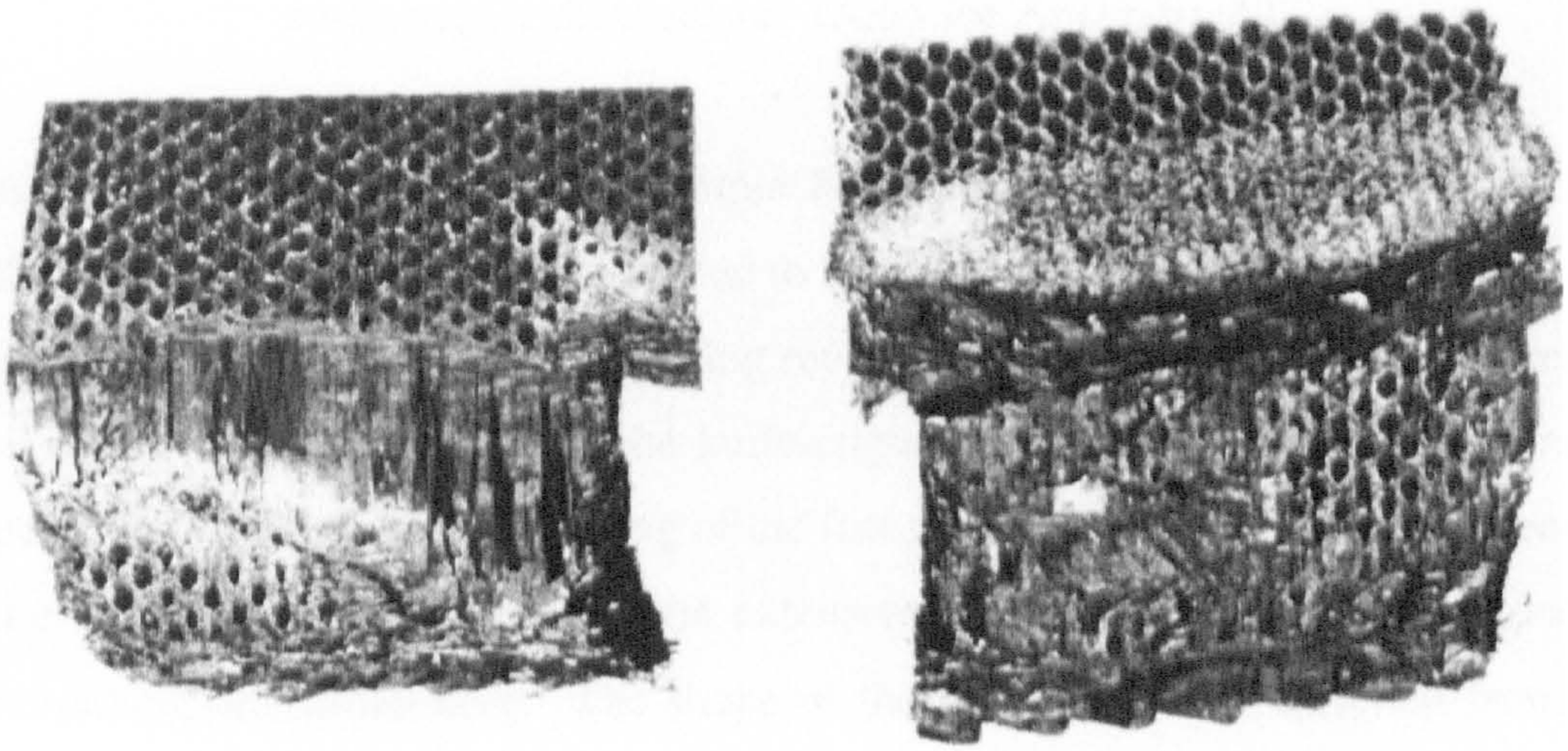

Figure 4.13 Sample 10

Sample 11. 1mm, unidirectional face skins, 20mm thick aluminium core, saw-tooth trigger mechanism. (Also see Appendix A).

Again, as seen previously for Sample 8, (same configuration apart from the core thickness) although the sample started to trigger from the bottom, once the tops of the triggers had been crushed the crushing reverted to the top of the sample. Once again, there seemed to be friction at the knife-edges (Figure 4.14). The sample reached a peak load of 27kN before splitting of the faces occurred (Figure 4.30). As previously, the splitting of the faces was quite extensive but the faces remained bonded to the remaining uncrushed core. The shape of the graph was very different from that of Sample 8 although the crushed samples look very similar. The load value throughout the crushing procedure remained high, a value of 16kN being recorded at the end of the test as compared with a value of 5kN for Sample 8.

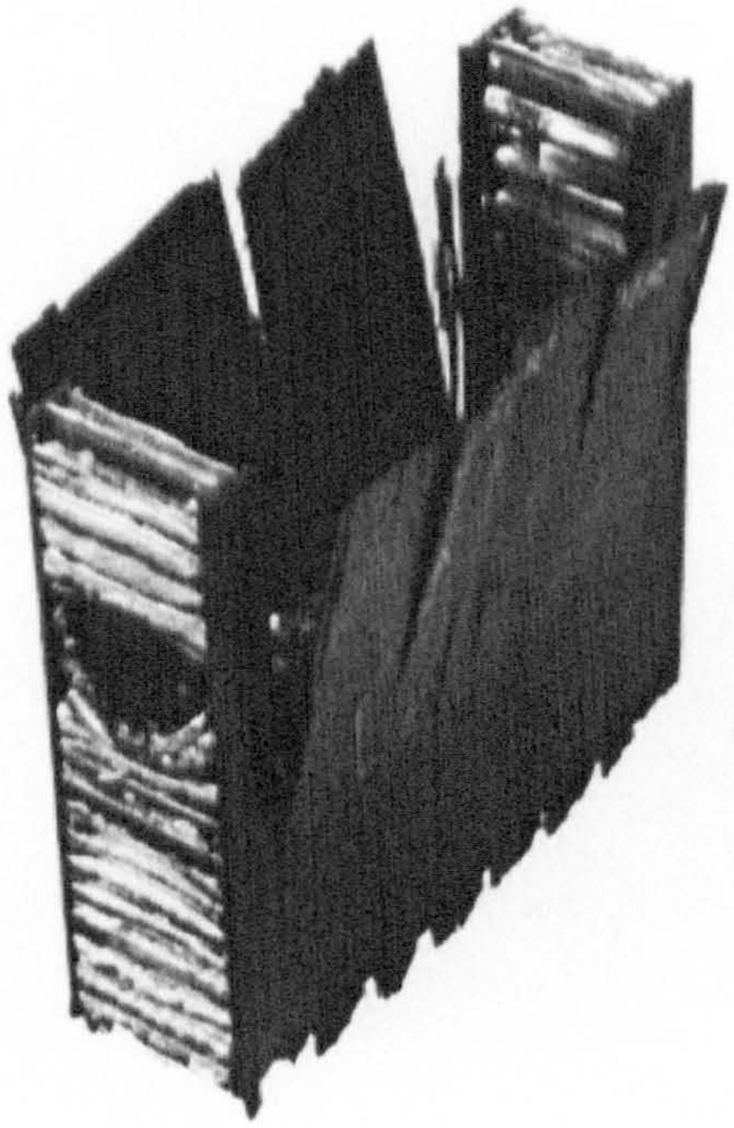

Triggered End

Figure 4.14 Sample 11

Sample 12. 1mm, unidirectional face skins, 10mm thick aluminium core, no trigger mechanism. (Also see Appendix A).

Again the specimen suffered from friction at the knife-edges (Figure 4.15). The sample crushed from the top downwards, the load reaching a peak of 27kN (Figure 4.31, p93) before delamination and splitting of the faces occurred. As observed for other specimens (e.g. Sample 8) the splitting of the faces was quite extensive. The load decreased from 27kN at the start to 11kN at the end of the test.

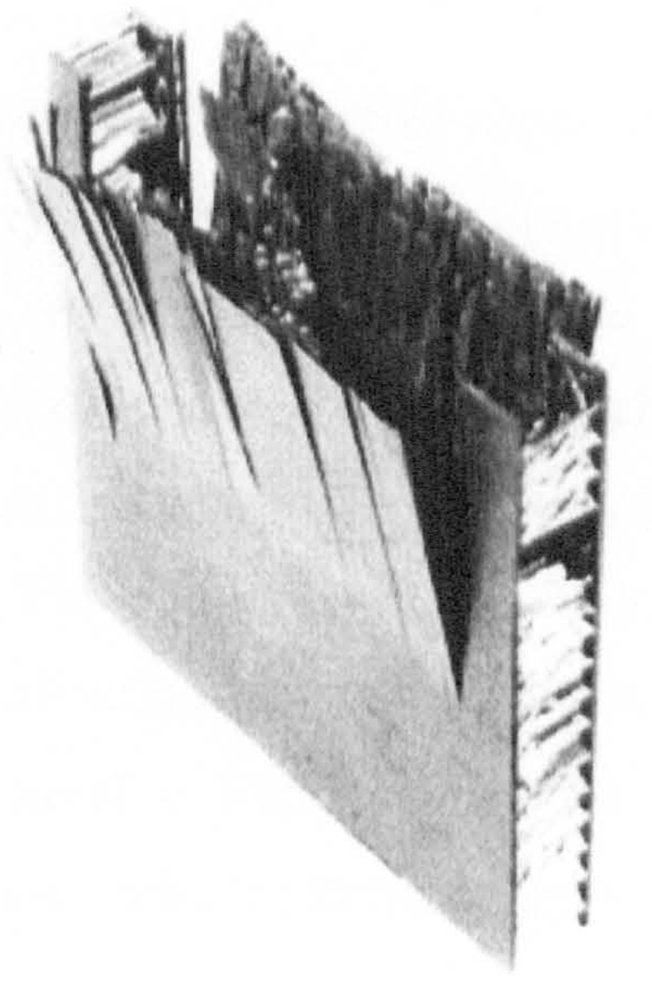

Figure 4.15 Sample 12

4.3 Conclusions of Initial Crushing Tests.

A number of conclusions can be drawn from this set of experiments. Firstly, it was found that when testing sandwich panels, rather than thin plates, the DERA rig (Figure 4.1) had several shortcomings which would affect the results. Primarily the rig was considered not to be sturdy enough. As the sandwich panel crushed, load was exerted on the knife-edges, due to through-thickness expansion of the sample. This resulted in the collars supporting the knife-edges deforming, as they were not stiff enough. The outcome of this was that a proportion of the load exerted by the testing machine was deforming the testing rig rather than crushing the sandwich panel and hence making the results erroneous.

The second shortcoming was that the knife-edges that provide support during crushing were an unnecessary feature when testing sandwich panels rather than thin plates. It was established whilst testing, that if the knife-edges were tightened sufficiently to closely support the sandwich panel, and also to stop the support collars from falling off, then an additional mechanism i.e. tearing of the facings at the knife-edges would be introduced. The additional tearing made the response, i.e. the energy absorbed by crushing, difficult to quantify. In contrast, if the knife-edges were not tightened and the sandwich panel was allowed to crush downwards, debris from the crushing panel became jammed under the knife-edges increasing friction, which could cause misleading results.

The third point to conclude from the above testing was the role of trigger mechanisms in the crushing of the samples. Of the six specimens that had saw-tooth triggers machined in them, three initiated crushing but three did not. The three that did not work were on unidirectional samples. The triggers began to crush so that the point of the saw-tooth had been flattened. This flattened zone seemed to prevent any further crushing at the triggered edge and crushing reverted to the other end of the sample. In contrast the triggers on the quasi-isotropic specimens worked fairly well, the graphs showing some initial reduction in peak loads. The triggers may have produced progressive crushing had the samples been dynamically tested, with the test duration being only fractions of a second.

The fourth point is that the crushing characteristics as far as could be ascertained for the two lay-ups i.e. unidirectional and quasi-isotropic were as follows:- The unidirectional facings tended to stay more intact but debonded from the sandwich core so little debris was produced. All of the unidirectional specimens (triggered or not) crushed from the top downwards. The quasi-isotropic samples because of their lay-up, created more debris, and in the samples that crushed across their full width, a debris wedge could be seen forming.

It was difficult to be very precise about the effect of the parameters, which were investigated in this series of experiments as not enough data was produced. If time allowed several specimens of the same type would have been tested to access variability. Inconsistent friction effects may also have masked the true significance of the results. However the following points can be drawn from the tests (Also see results Appendix A): -

- Energy absorption was shown to increase with increasing face skin thickness.
- In general, quasi-isotropic specimens absorbed more energy than unidirectional specimens.
- The effect of the aluminium honeycomb core thickness on the energy absorption was difficult to quantify due to friction effects. If anything, the energy absorbed by the 10mm thick core specimen was higher than the 20mm thick core specimen.
- The trigger mechanism worked when friction at the knife-edges was not a large factor, the triggers initiated crushing on quasi-isotropic specimens but not on unidirectional specimens.

4.4 Simplified Rig

Due to the problems with the test rig used in the initial crushing tests, it was decided to switch to a simpler piece of apparatus as shown in the diagram overleaf (Figure 4.16). In this new test rig the specimen was "built in" at the lower edge to prevent crushing from the bottom end, and a compressive load applied at the upper edge. No knife-edge supports were used on the vertical edges. However, the U-shaped channel and the packing strips provided 40mm of support for the specimen, leaving 40mm of

the length unsupported. Using this new apparatus two specimens were initially tested.

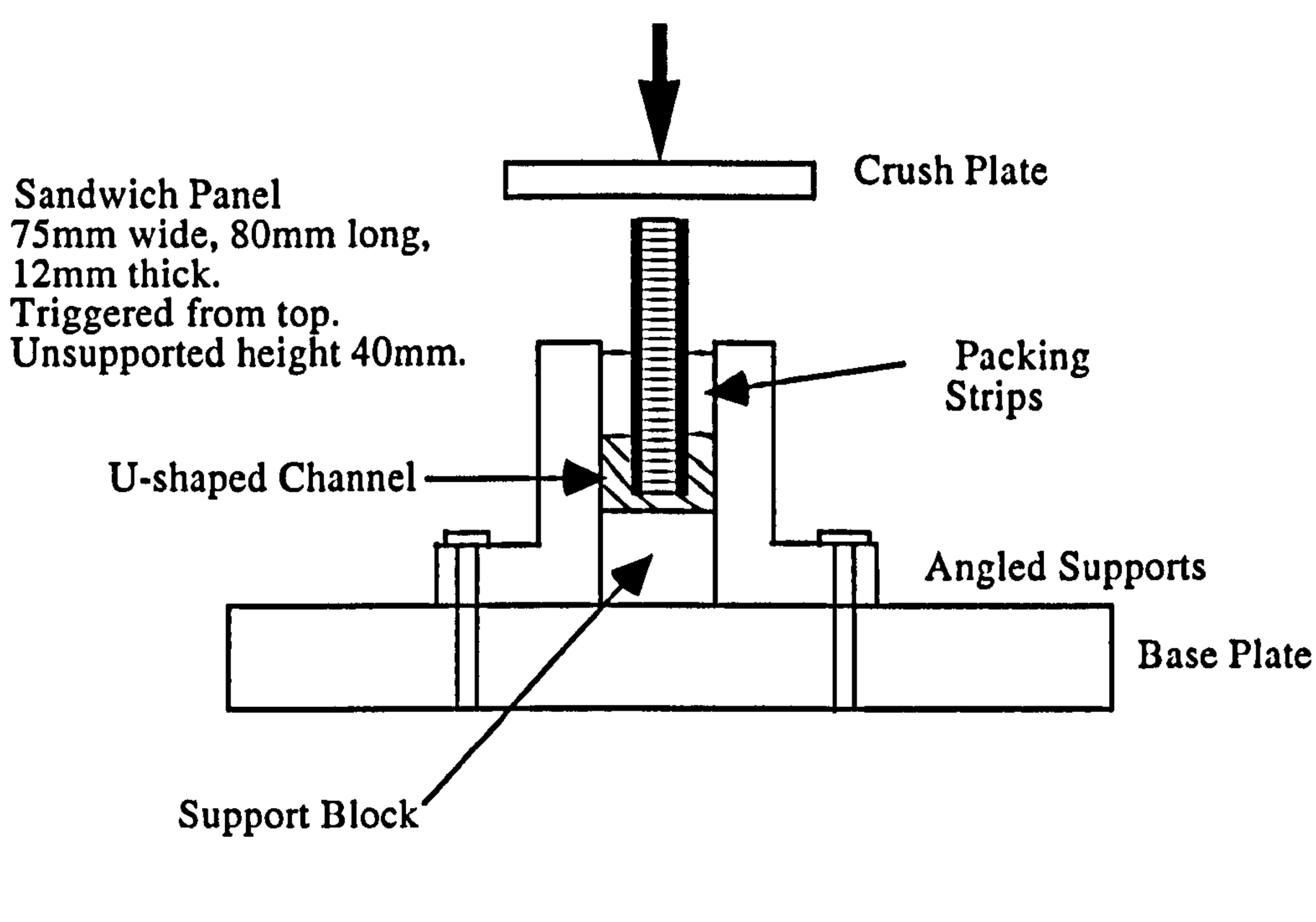

Figure 4.16 Simplified test rig

Sample 1. 1mm, quasi-isotropic $(-45^{\circ}, 0^{\circ}, 90^{\circ}, +45^{\circ})_S$ face skins, 10mm thick aluminium core, no trigger mechanism.

As the sample was un-triggered, when load was applied to the top of the sample failure occurred by debonding of the facings from the core, leading to the core buckling. A close examination of the faces after the load had been removed revealed that delamination had been initiated on the top edge of the faces.

Sample 2. 1mm, quasi-isotropic $(-45^\circ, 0^\circ, 90^\circ, +45^\circ)_S$ face skins, 10mm thick aluminium core, saw tooth trigger mechanism.

Sample 2 was initiated with a saw-tooth trigger at the top of the specimen. Crushing was initiated by the trigger and continued with the peeling away of the faces. The crushing occurred across the whole width of the specimen. An observation seen during this particular test was that if the specimen was supported too near the top, then the crush front was inhibited and ultimate failure of the specimen took place prematurely. A balance between enough support and too much support was needed. (No load-displacement results were available for these two tests due to a data acquisition failure).

4.5 Samples Using New Honeycomb Geometry.

After the above specimens had been tested a new batch of aluminium alloy honeycomb was purchased, unfortunately the same size cell size as previously was not available. The cell size of the new honeycomb was 8.50mm (in the ribbon direction) by 6.60mm, compared with 4.0mm by 2.75mm. The cell wall thickness remained unchanged. Specimens were manufactured with the new honeycomb and testing was resumed. Four out of the five specimens tested failed by face debonding. On close inspection of the failed samples it was discovered that the bonding between the carbon fibre facings and the aluminium honeycomb was insufficient due to the increase in honeycomb cell size compared with the previous samples. Ideally a fillet of adhesive would be formed up the walls of the honeycomb core (Figure 4.17).

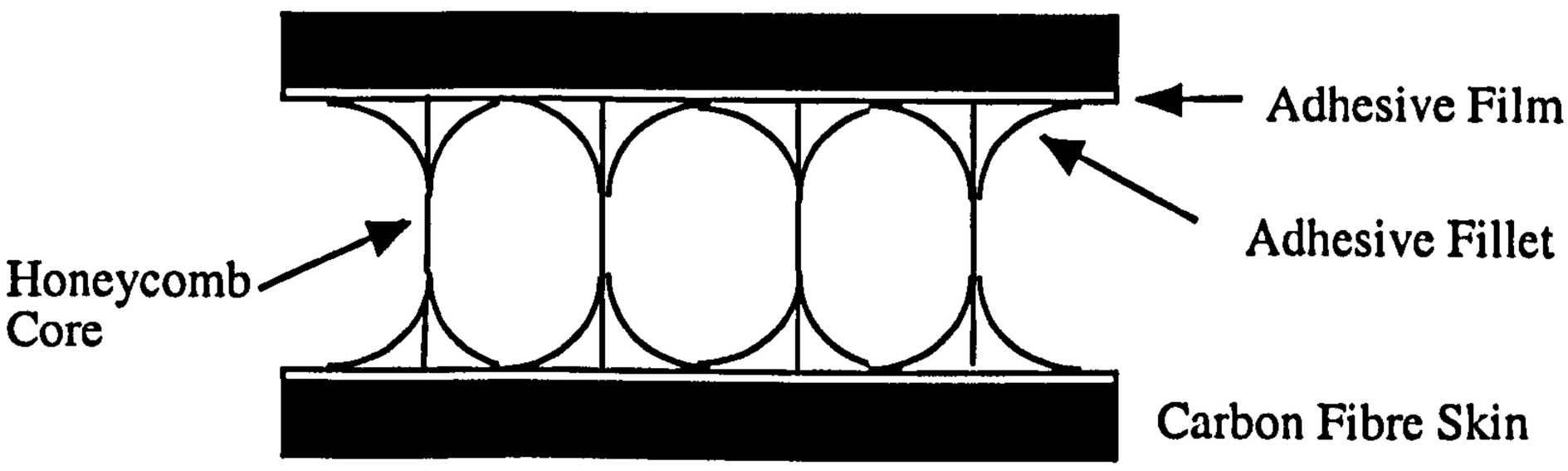

Figure 4.17 Adhesive fillet

The problem was eliminated by doubling the thickness of adhesive film used during the manufacture of the samples. Due to a shortage of adhesive film only three more samples were manufactured. Care was taken when testing these samples not to over support. This meant that the crush front could move ahead of the actual physical crushing without hindrance by the packing strips, therefore 40mm of progressive crushing took place rather than debonding of the faces. Figures 4.32 and 4.33 are two traces from similar samples with the following configuration:- Facing thickness 1mm, lay-up quasi-isotropic, stacking sequence $(-45^\circ, 0^\circ, 90^\circ, +45^\circ)_S$, Core thickness 10mm, Trigger mechanism saw-tooth.

When the two traces were compared with previous traces for similar samples the total energy absorbed was seen to be lower. This may have been because there are no losses due to friction at the knife-edges in the new test rig.

Five more specimens with an identical configuration to those above were manufactured except that a new batch of resin film was used. This adhesive film was $100gsm^{-1}$ compared with $75gsm^{-1}$ used previously.

Out of the five specimens tested, four out of five specimens failed to crush significantly. Examination of the saw-tooth trigger mechanisms showed that the inner half of the face-skin had crushed inwards (Figure 4.18(2)).

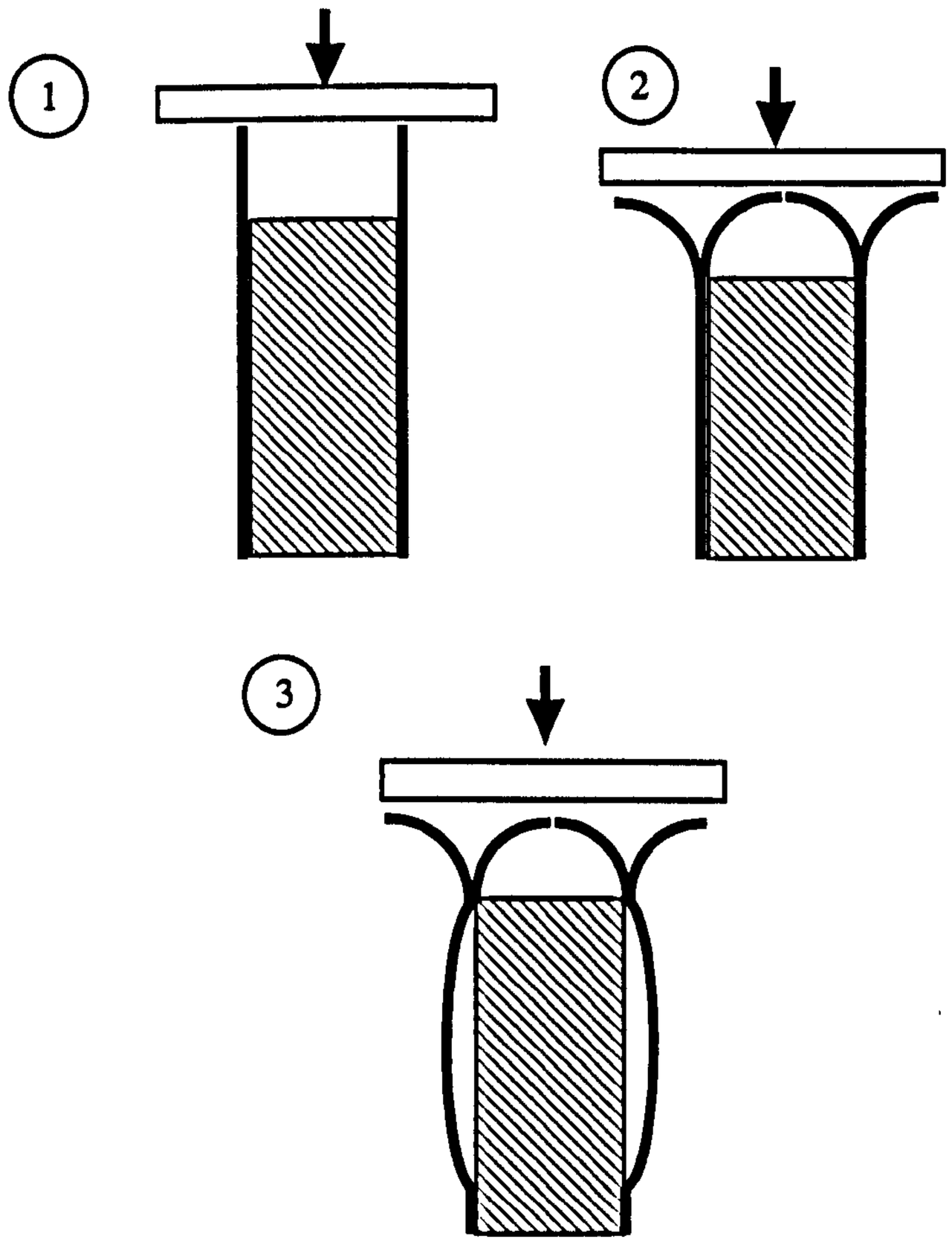

Figure 4.18 Sandwich panel failure modes

The inward crushing of the trigger caused the faces of the sandwich panel to become debonded and "balloon off" (Figure B.1 Appendix B) leading to premature failure and minimal energy absorption, (Figure 4.18(3)). To overcome this problem a new crush plate was designed to cause the desired "rolling fragmentation" failure. An angled plate was decided upon to encourage the trigger mechanisms to crush outwards. It was initially decided to machine a plate with a 5° chamfer, as it was hoped this would push the triggers outwards when crushed and lead to progressive failure of the faces.

A specimen with the usual configuration was clamped into the testing rig and the chamfered plate attached to the loading plate with a series of bolts. Care was taken to ensure that the plate was aligned so that the both faces of the sandwich panel crushed equally (Figure 4.19).

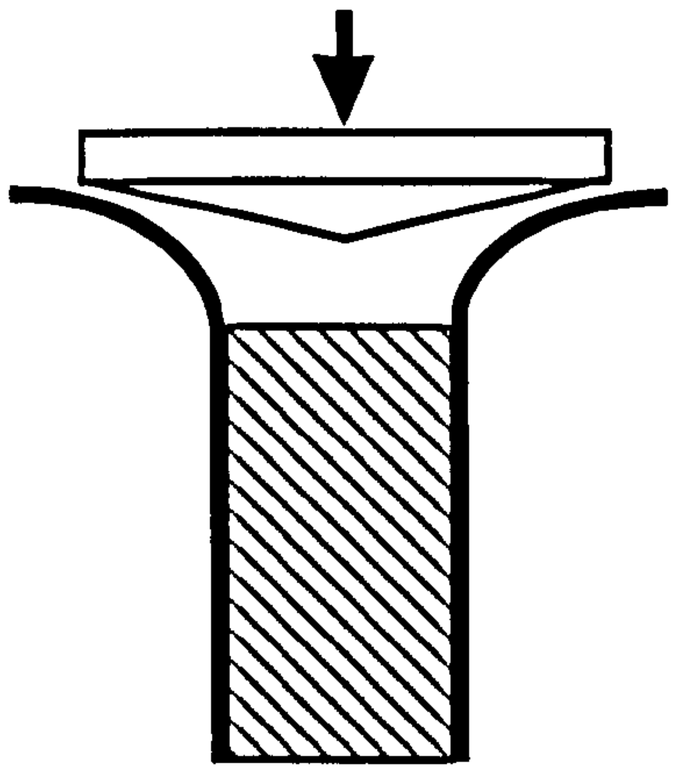

Figure 4.19 Chamfered crush plate

The panel was tested, but it was found that the angle was too steep and the faces became debonded from the honeycomb core. The chamfer angle was ground down to 2° and the experiment repeated. The specimen tested using the 2° chamfered plate failed progressively (Figures B.2 and B.3 Appendix B). The load-displacement curves were similar to Figures 4.32 and 4.33 although, due to the chamfered crush plate, the peak loads were slightly lower.

4.6 Conclusions

In this chapter the response of CFRP faced, aluminium honeycomb cored sandwich panels to in-plane crushing was examined. Initially twelve sandwich panels of different face and core thicknesses and face lay-up were tested, with or without a triggering mechanism. The panel parameters were specified by the Taguchi Array described in Appendix A. The Taguchi method of analysis was used as a screening method to see which of the sandwich panel parameters had the greatest effect on the energy absorbing capabilities.

Due to the test rig used initially to crush these panels, the frictional effect of the knife-edges masked all but the most obvious of changes in the panel parameters, i.e. changing the skin thicknesses from 1mm to 3mm could be seen to have the largest effect on energy absorption.

As outlined in the chapter the twelve panels failed in many different ways, not all of them in a manner suitable to maximise the energy absorption potential of the sandwich panel. It was seen that the crush rig used over-supported the panels. The knife-edges effectively introduced other energy absorbing mechanisms that made it difficult to investigate the energy absorption of the sandwich panels. A simplified rig was designed which supported the panel at one end, and at the edges of the panel up to a distance of 40mm. The top of the panel was free to crush across its entire width.

Of the several specimens tested with the simplified rig, some crushed in the desired "rolling fragmentation" mode whilst others failed due to debonding of the faces. A closer examination of the failed specimens showed that the flat plate used to crush the trigger mechanisms could cause the sandwich panels to fail prematurely. If the triggers moved outwards when the load was first applied, then the sandwich panel would continue to fail in the desired manner. Conversely, if the triggers moved inwards then the panel would fail prematurely, the faces "ballooning off" and leading to low energy absorption. To encourage the triggers to crush outwards, the flat loading plate was replaced with one chamfered at an angle of 2° to the horizontal. The sandwich panels tested with the chamfered load plate failed progressively in the desired manner.

Throughout the many different testing configurations described in this chapter it has been seen that to achieve the desired failure modes a careful balance of many different parameters must be achieved. Level of support, bond strength between the faces and the core, and the manner in which the crushing is initiated and subsequently continued were all seen to be crucial. With the development of the simplified crushing rig and chamfered loading plate, an apparatus has been developed to consistently crush sandwich panels in a manner to maximise their energy absorbing capabilities.

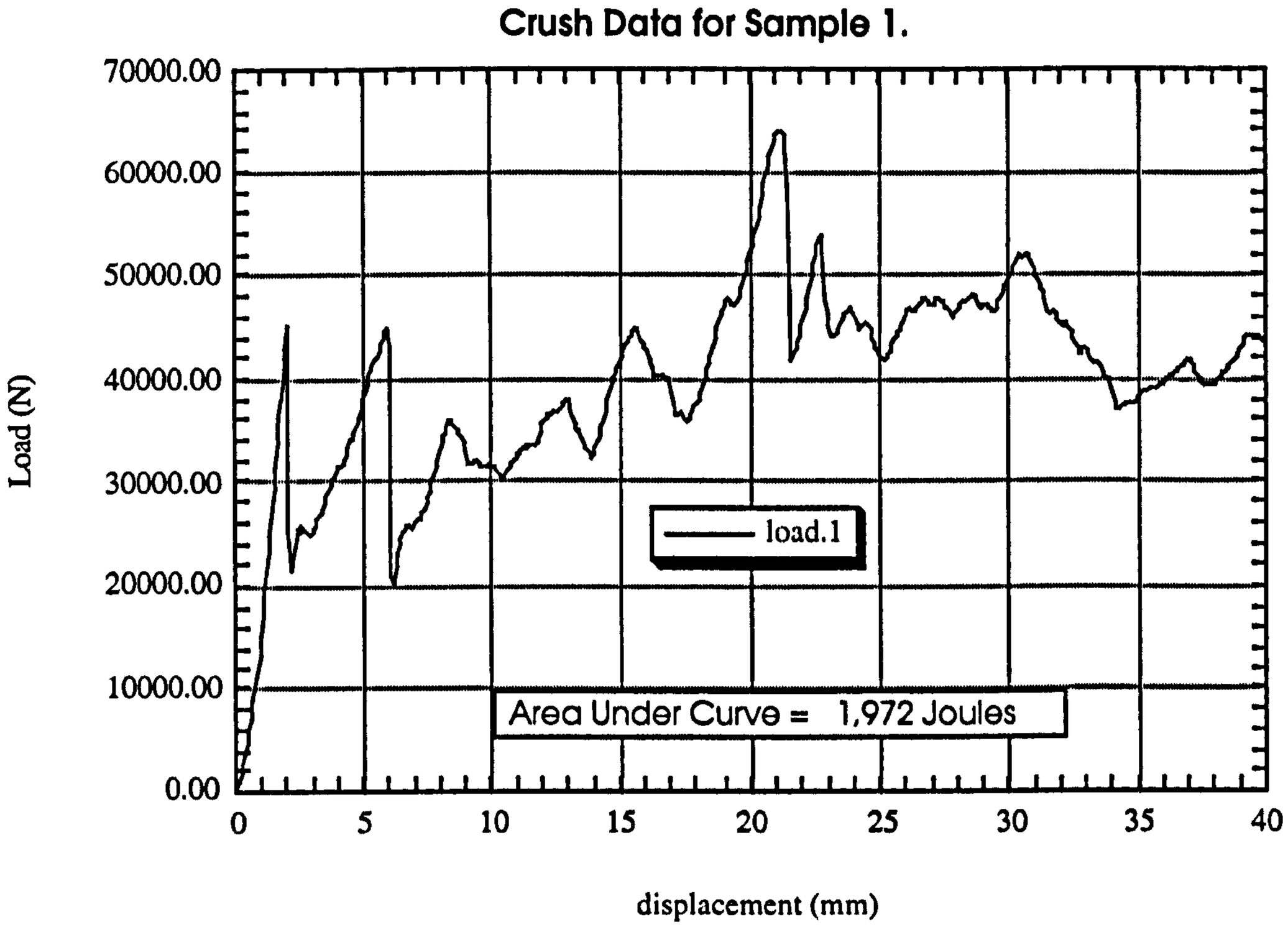

Figure 4.20 Crush Data from Sample 1

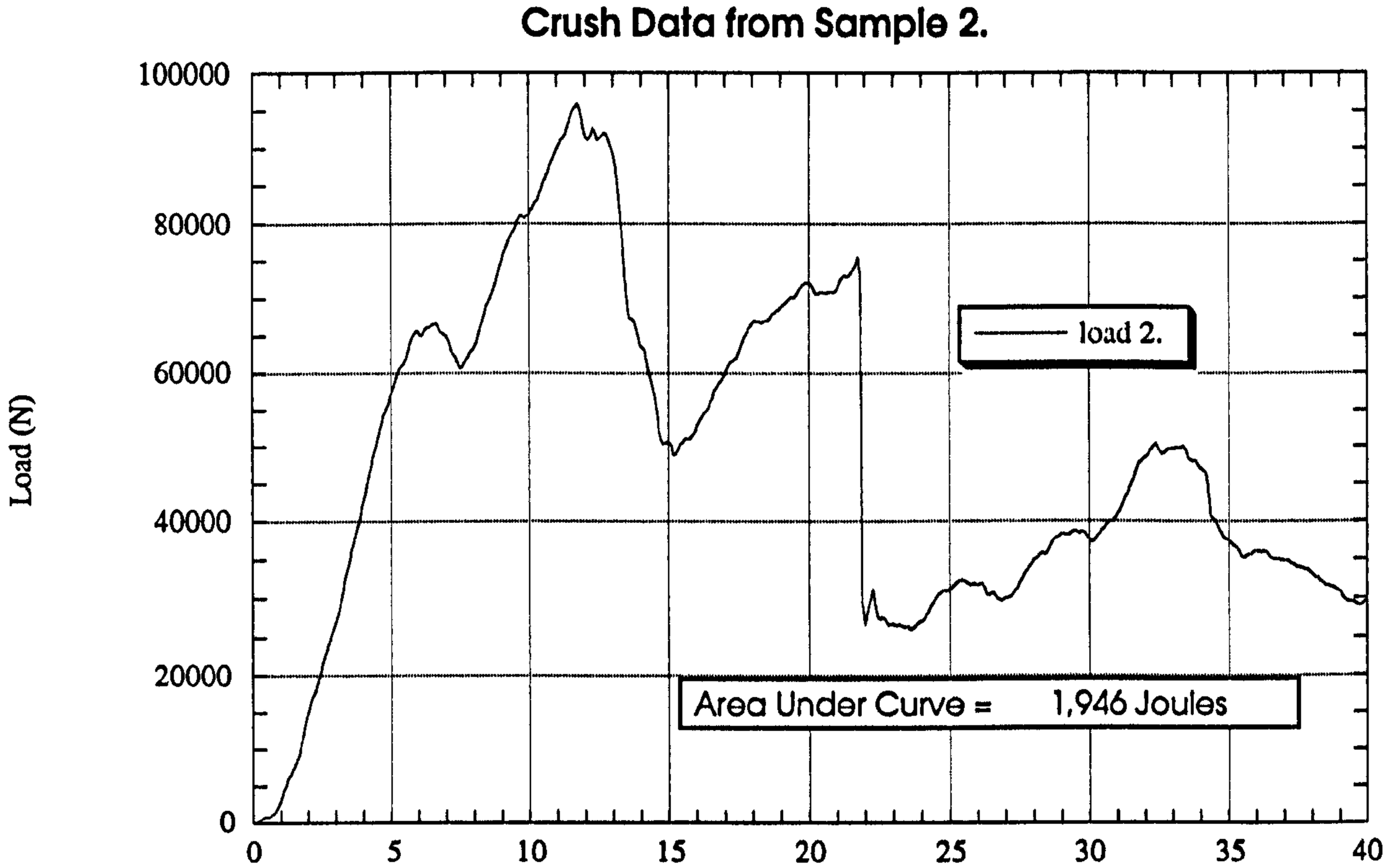

Figure 4.21 Crush Data from Sample 2

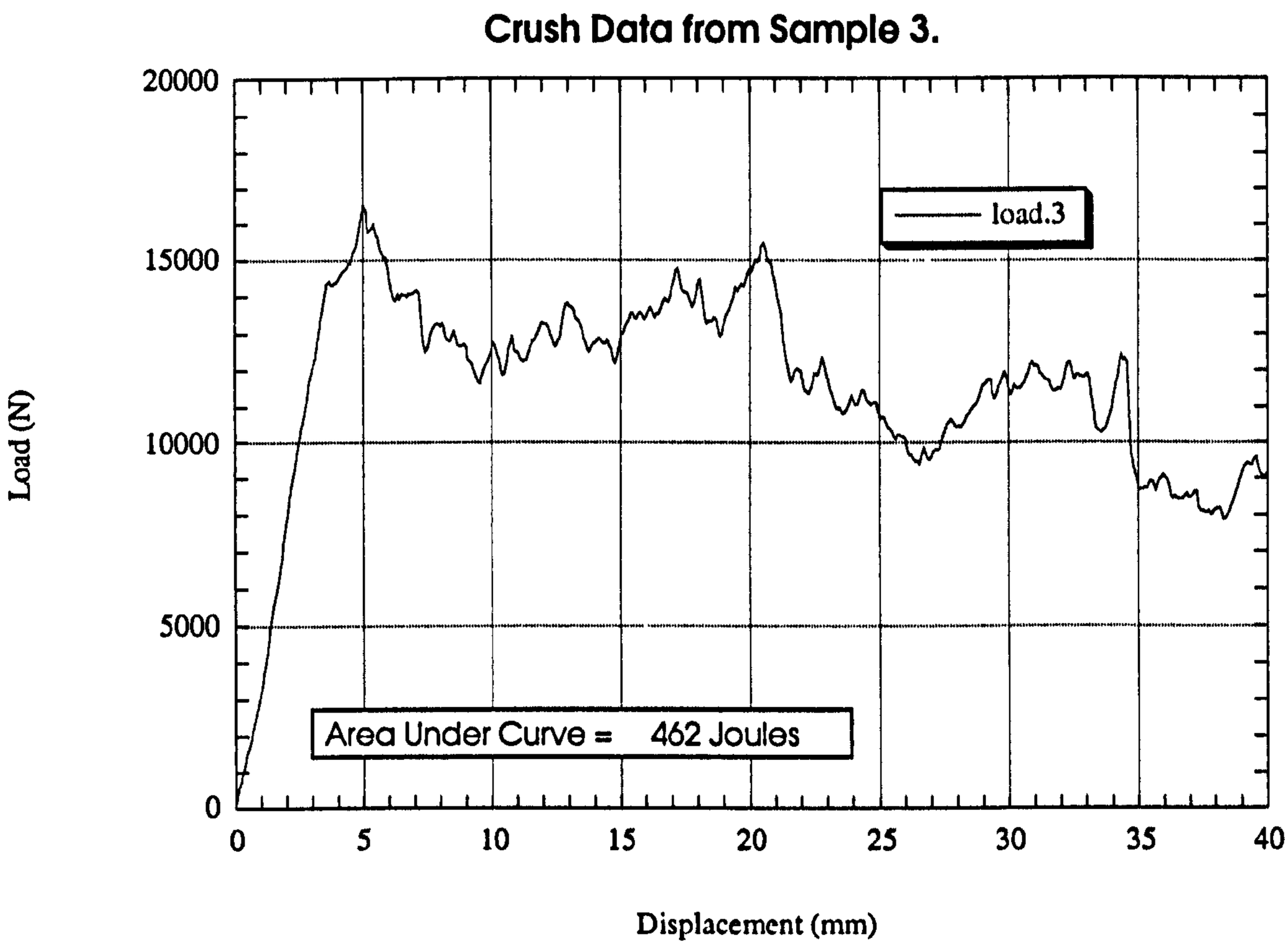

Figure 4.22 Crush Data from Sample 3

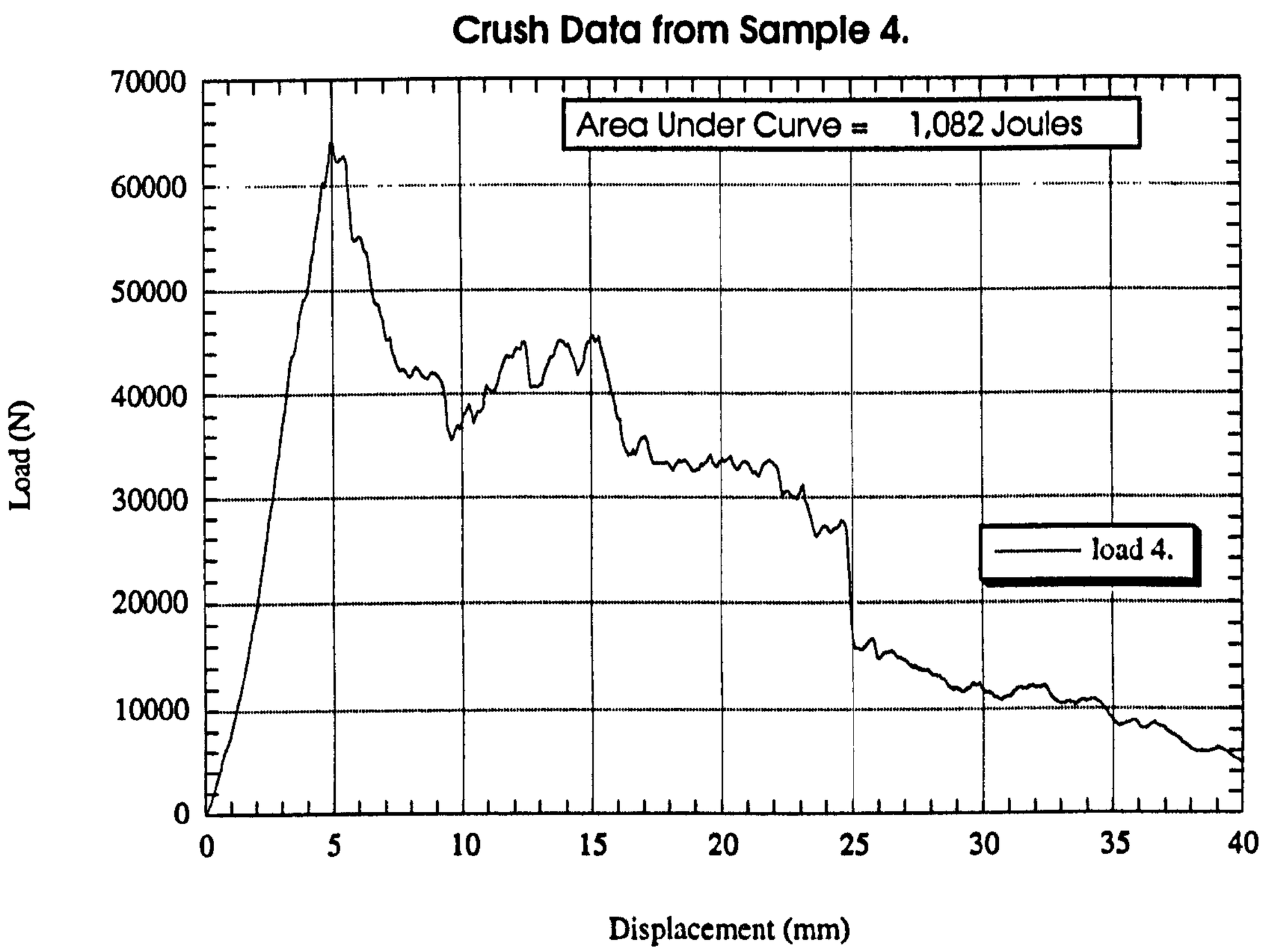

Figure 4.23 Crush Data from Sample 4

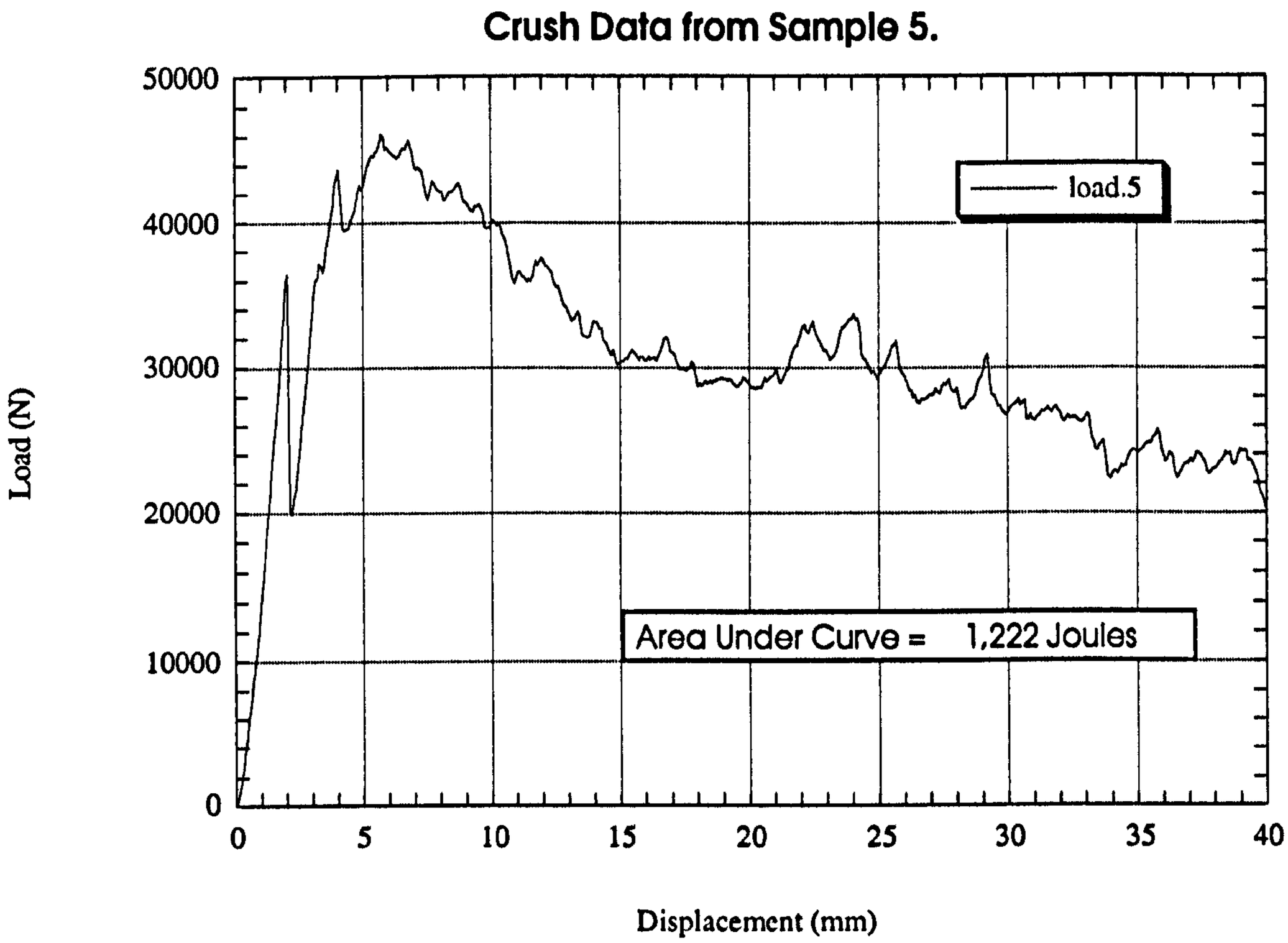

Figure 4.24 Crush Data from Sample 5

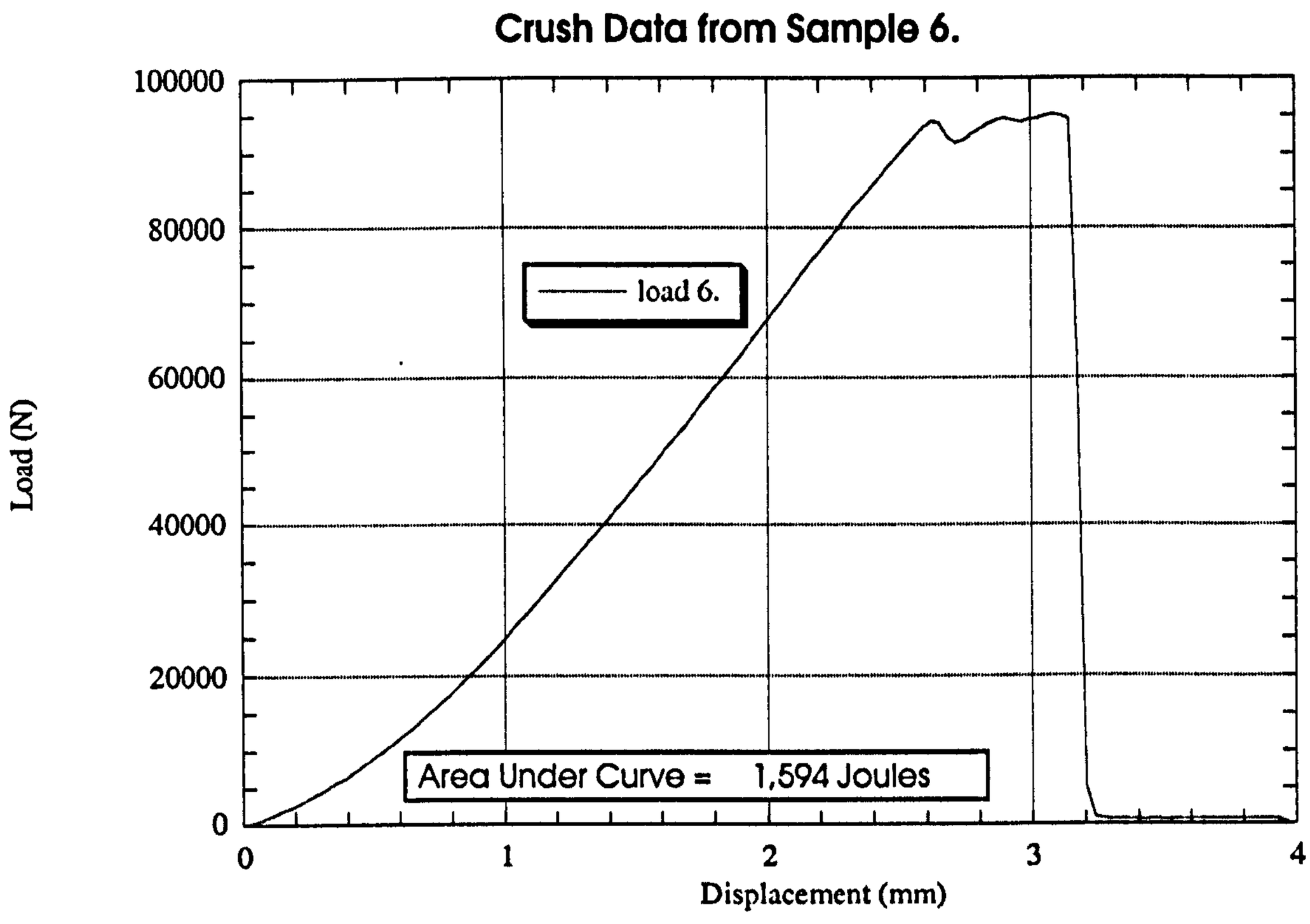

Figure 4.25 Crush Data from Sample 6

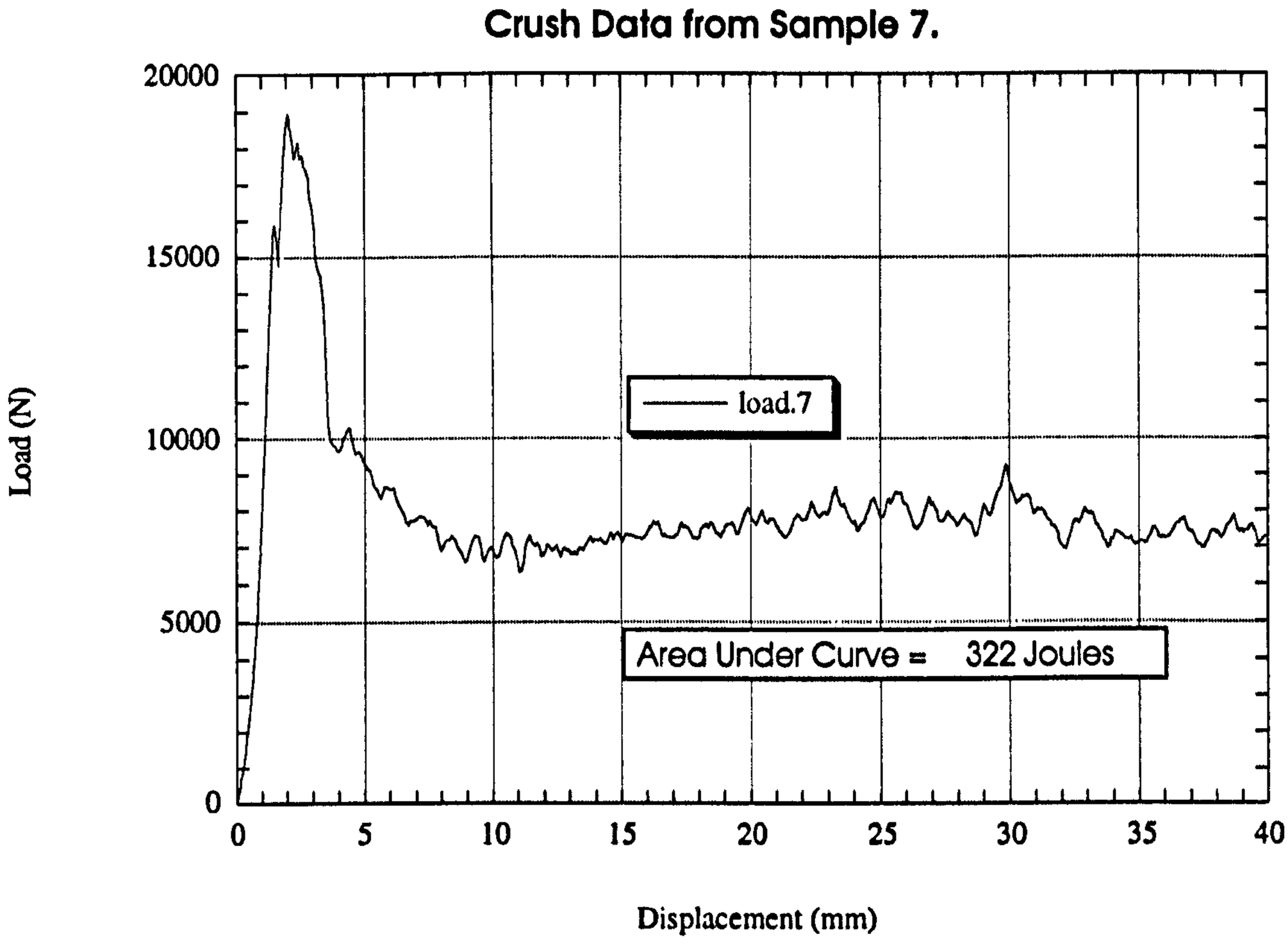

Figure 4.26 Crush Data from Sample 7

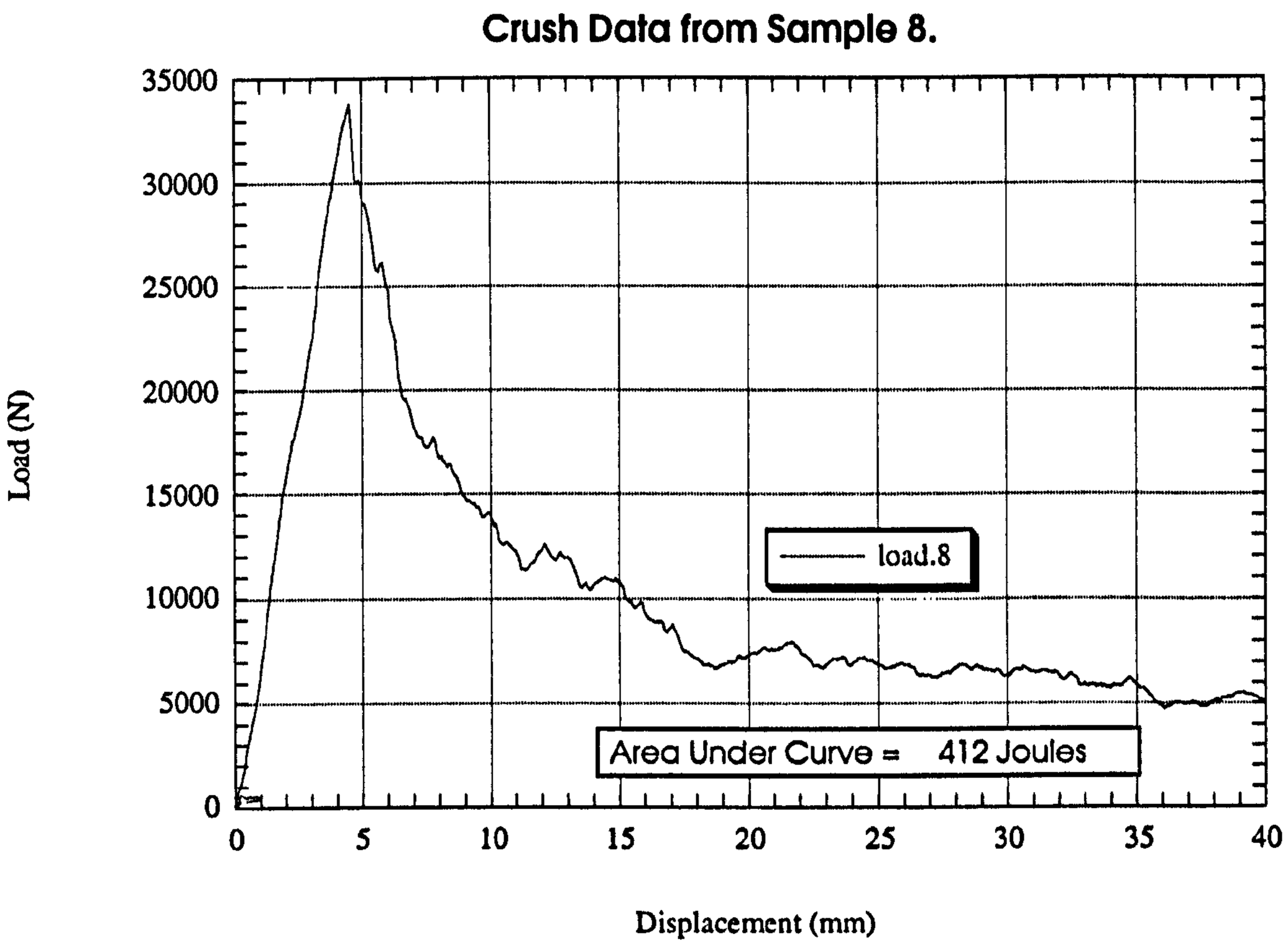

Figure 4.27 Crush Data from Sample 8

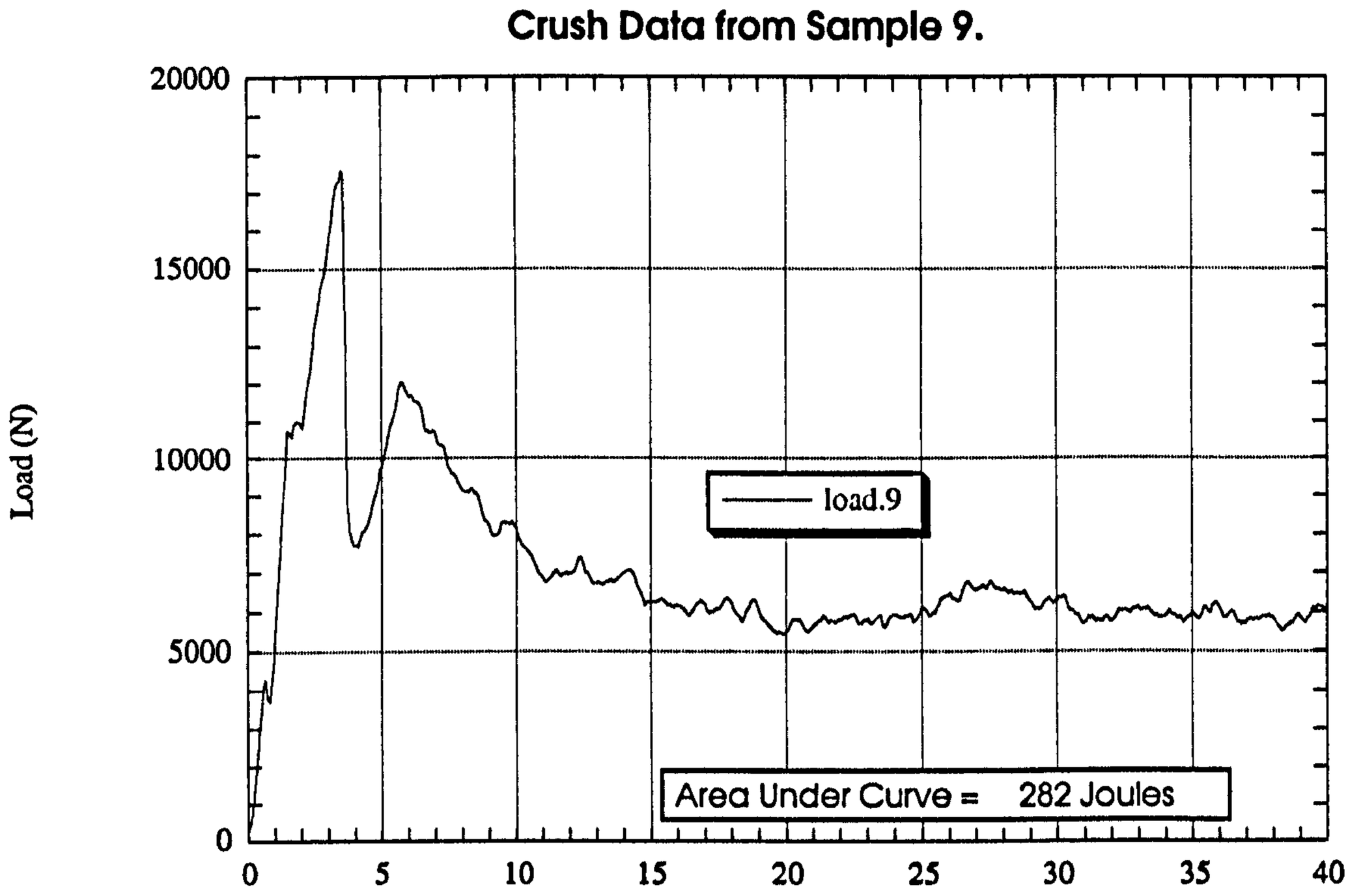

Figure 4.28 Crush Data from Sample 9

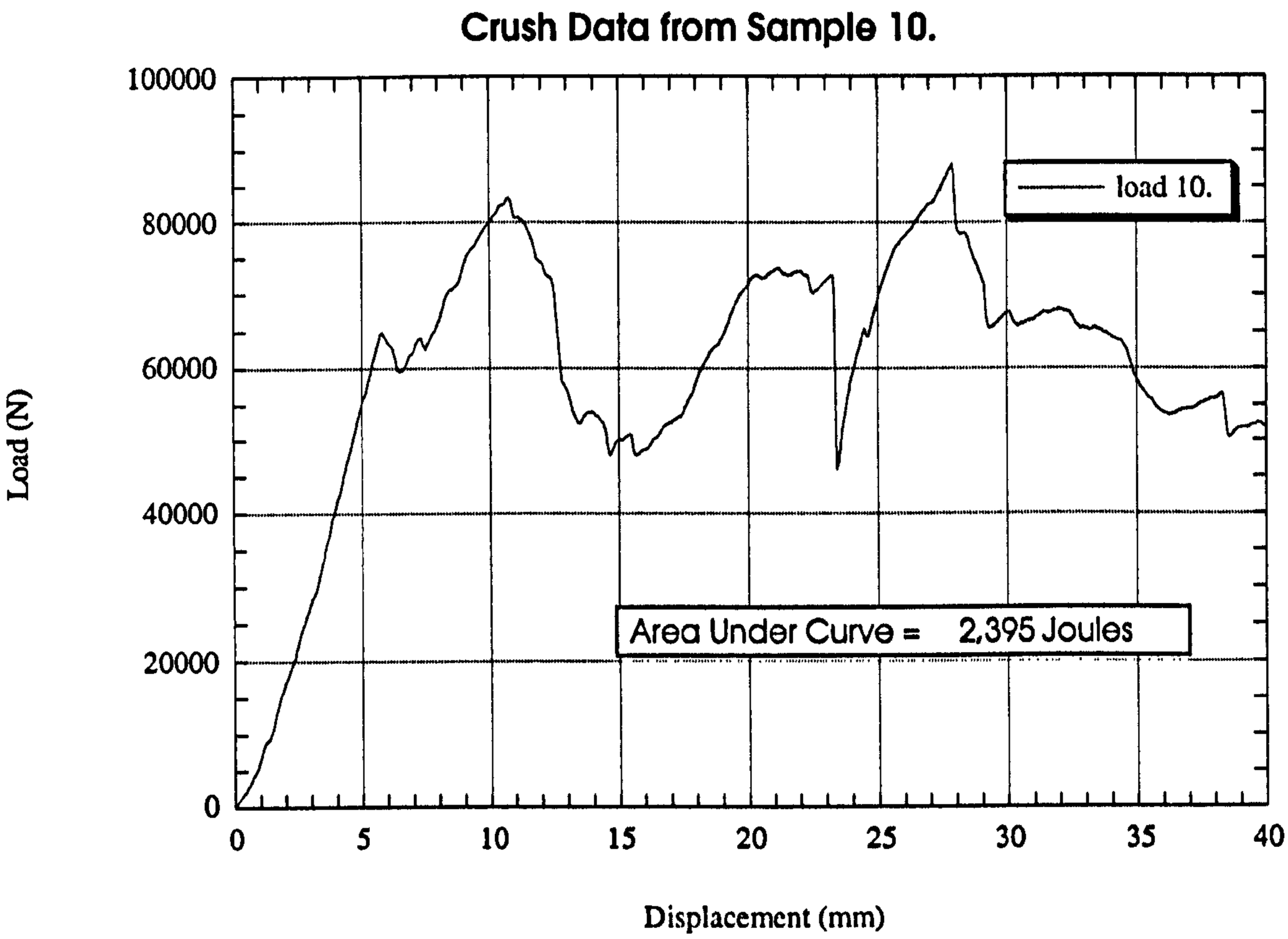

Figure 4.29 Crush Data from Sample 10

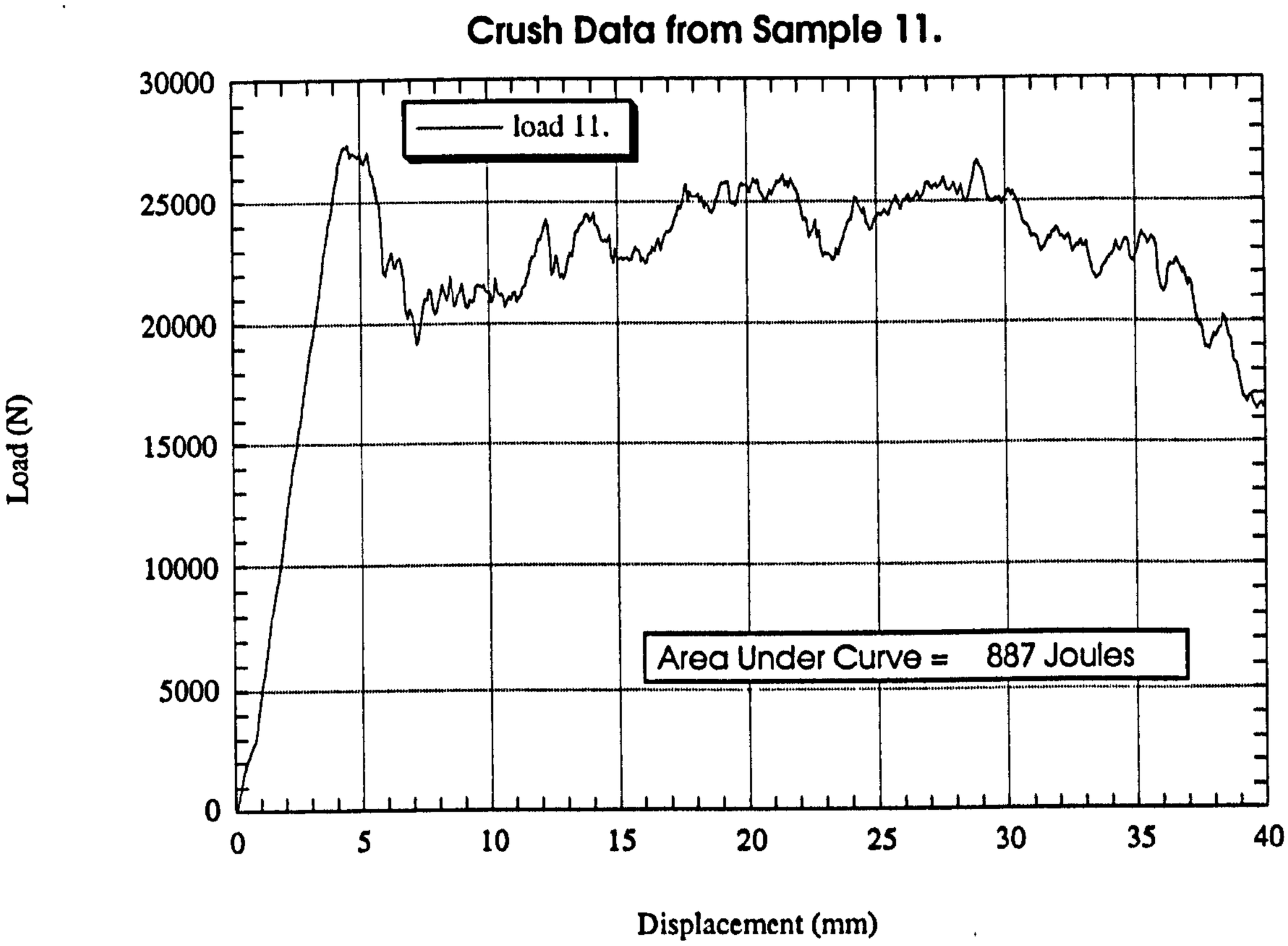

Figure 4.30 Crush Data from Sample 11

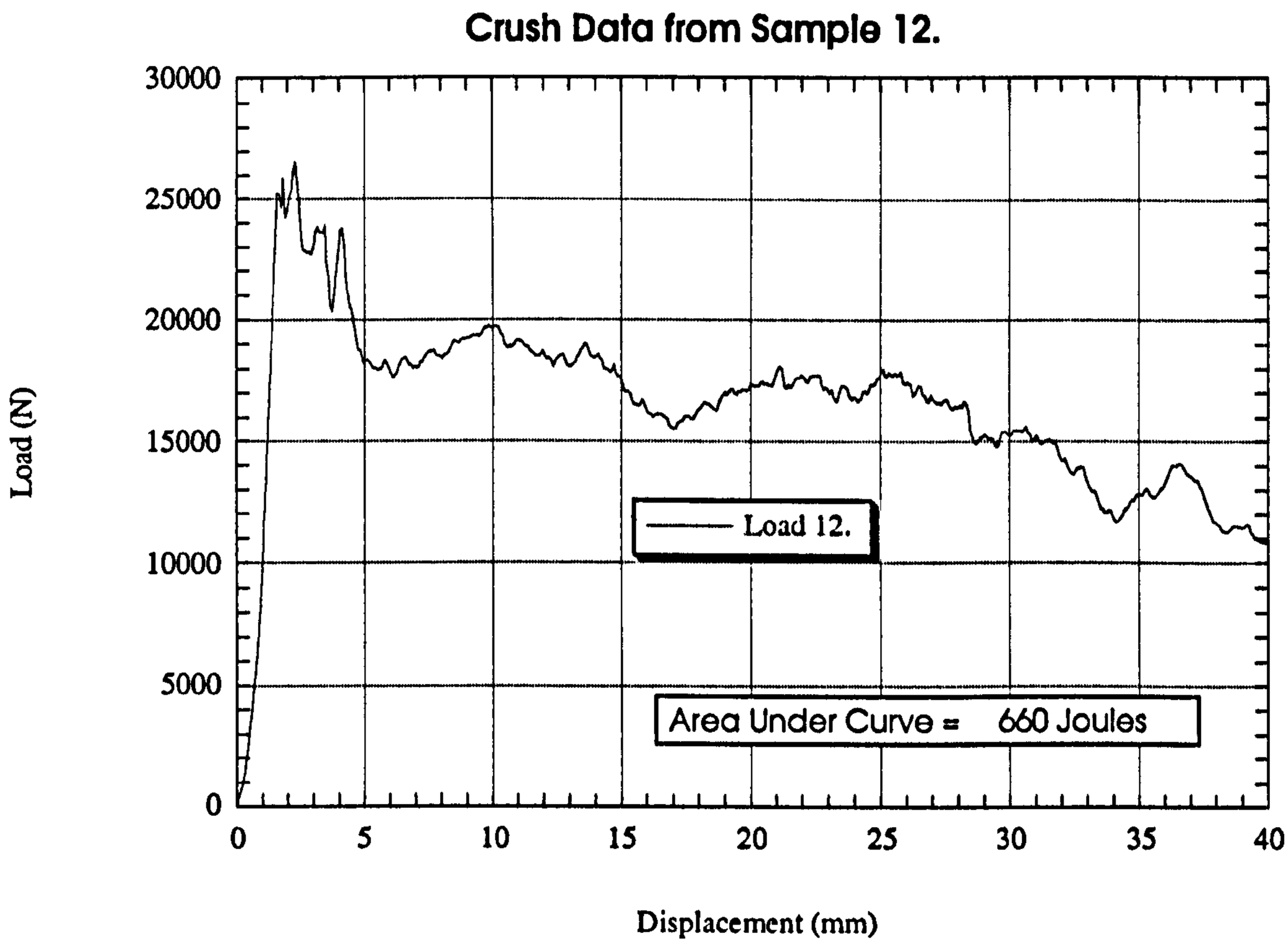

Figure 4.31 Crush Data from Sample 12

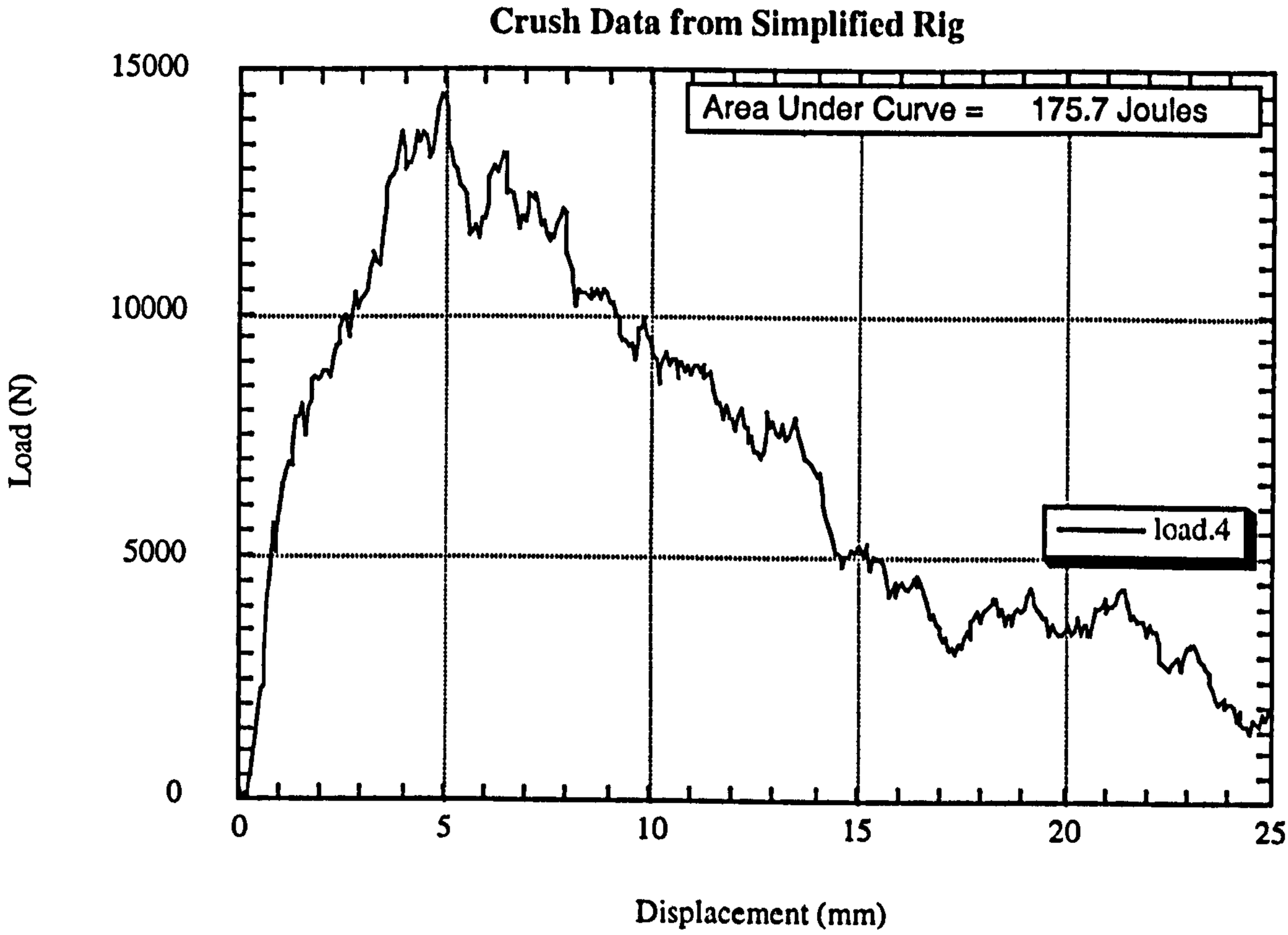

Figure 4.32 Crush Data from Simplified Rig

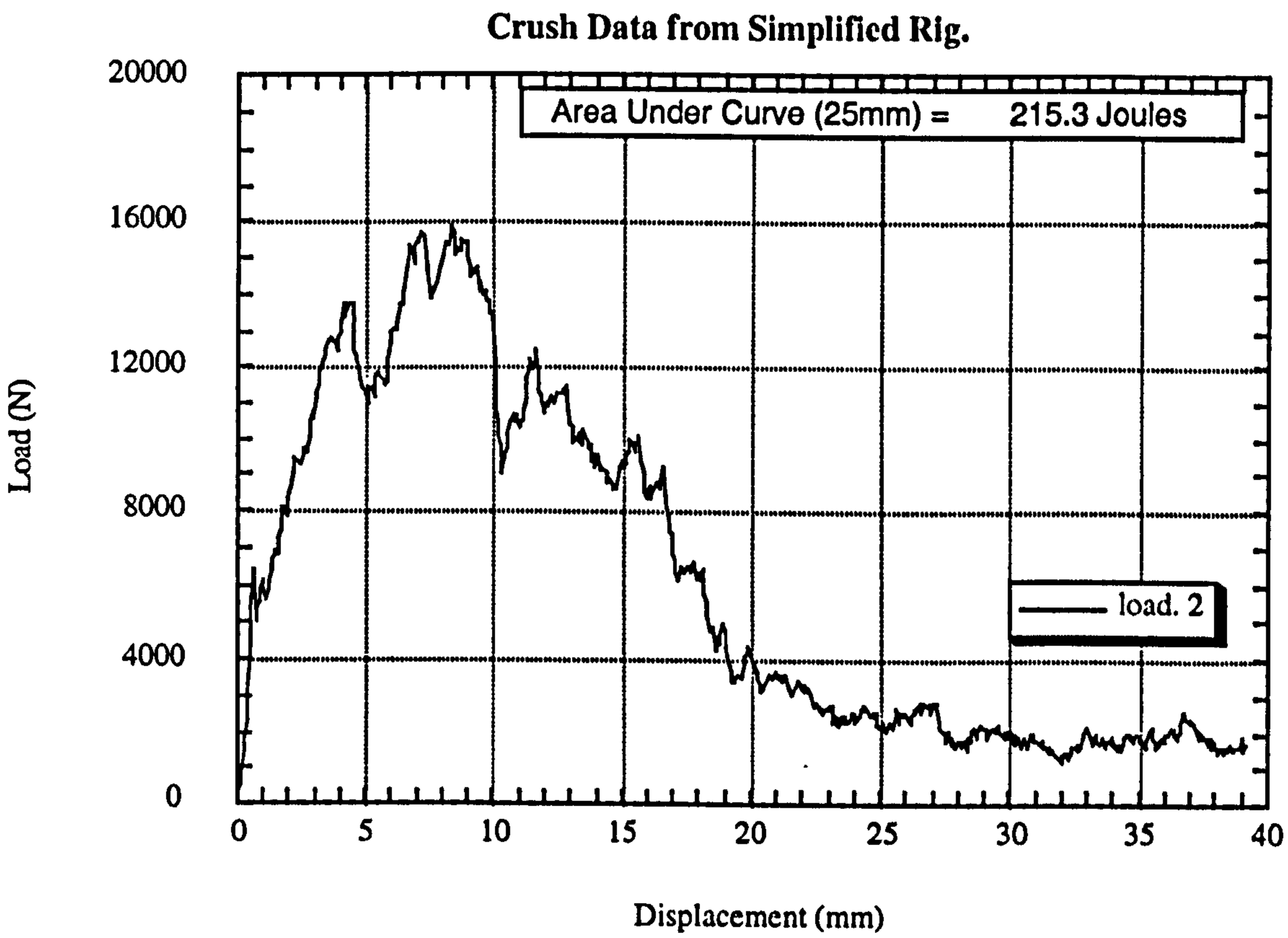

Figure 4.33 Crush Data from Simplified Rig

CHAPTER 5

INVESTIGATION OF THE COMPONENT ENERGY ABSORPTION MODES IN A SANDWICH PANEL

5.1 Introduction

In Chapter 4 sandwich panels of various skin and face thicknesses and face lay-ups were subjected to in-plane compressive loading. From these experiments it was seen that the sandwich panels failed by various failure modes, amongst these were face-to-skin debonding and face tearing. It was also seen that the faces of the sandwich panels absorbed the majority of the crush energy, the honeycomb core, although absorbing some energy through plastic deformation acted mainly to support the faces increasing the stability to the structure. In this chapter the failure modes described above were investigated. Firstly, the face skins of the sandwich panels were investigated. Further experiments were then conducted to ascertain the contribution of the face-to-core bonding face tearing and angled stiffener crushing.

The ideas in this chapter form a basis for ascertaining the component energy absorption modes seen in a sandwich panel. Using the ideas and techniques presented here the contribution of each energy absorption mode can be calculated. The energy absorption potential of a sandwich structure can be maximised without the need for crushing experiments on full scale sandwich structures that can be costly in terms of both money and time.

5.2 Face Skin Specimens

The failure mechanisms of the sandwich faces were investigated by using smaller specimens, which were easier and cheaper to manufacture than the sandwich specimens. These specimens represented the skins of the sandwich panel and as such were manufactured from the same HTA/913 pre-preg and some had the same $(-45°, 0°, 90°, +45°)_S$ stacking sequence. The samples were 10mm wide and 1mm thick and were tested using one end of a compression rig clamping fixture (Figure 5.1). The

majority of the tests were on specimens with 5mm of the overall 45mm length unclamped, some tests, however, were conducted on specimens with un-supported lengths ranging from 4-9mm. The specimens were crushed using the same 2° angled loading plate that was used to crush the sandwich panels. The plate was cleaned and coated with PTFE before each test. Parameters such as stacking sequence, un-supported length of specimen, and loading plate friction were studied using these small specimens, in parallel with test work on full size sandwich panels.

5.2.1 $(-45°, 0°, 90°, +45°)_S$ Stacking Sequence

Specimens with the same stacking sequence as the sandwich panel skins, i.e. $(-45°, 0°, 90°, +45°)_S$ and an un-supported length of 5mm, were crushed using the angled crush plate. Failure initiation occurred on one side of the specimen at the 0°/90° interface (Figure 5.2). From video evidence it was seen that the specimen split into three roughly equal sections (Figure B.4 Appendix B). One section remained upright and progressively crushed, the other two sections moved to the side (Figure 5.2). Table 5.1 shows the energy absorbed by the 5mm long specimens, the peak load and the average of the mean crushing loads experienced by the specimens during crushing. Typical load-displacement graphs are shown in Figures 5.23-5.33. The letters a, b and c are used to denote the series of tests showing $(-45°, 0°, 90°, +45°)_S$ stacking sequence.

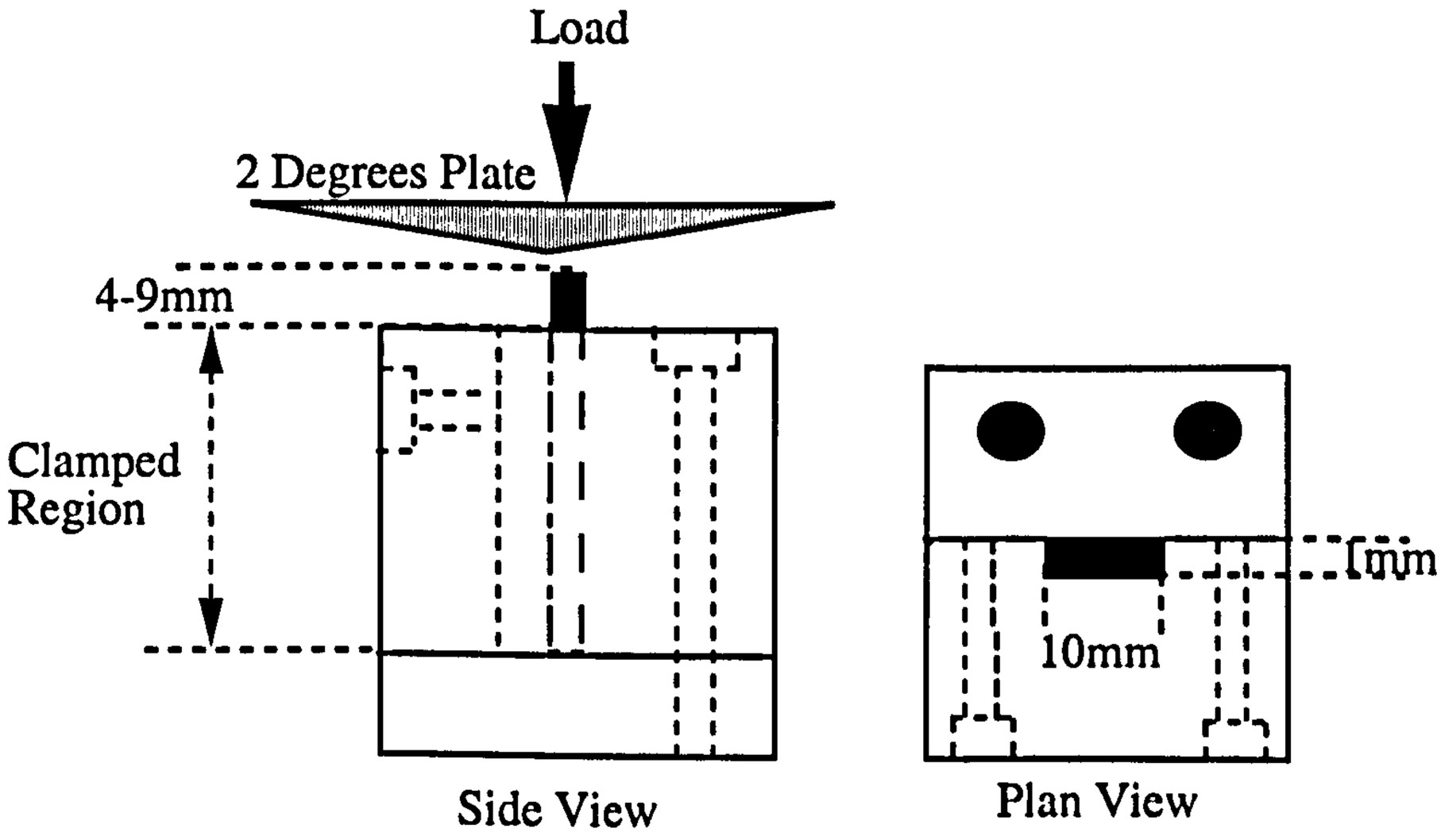

Figure 5.1 Clamping fixture

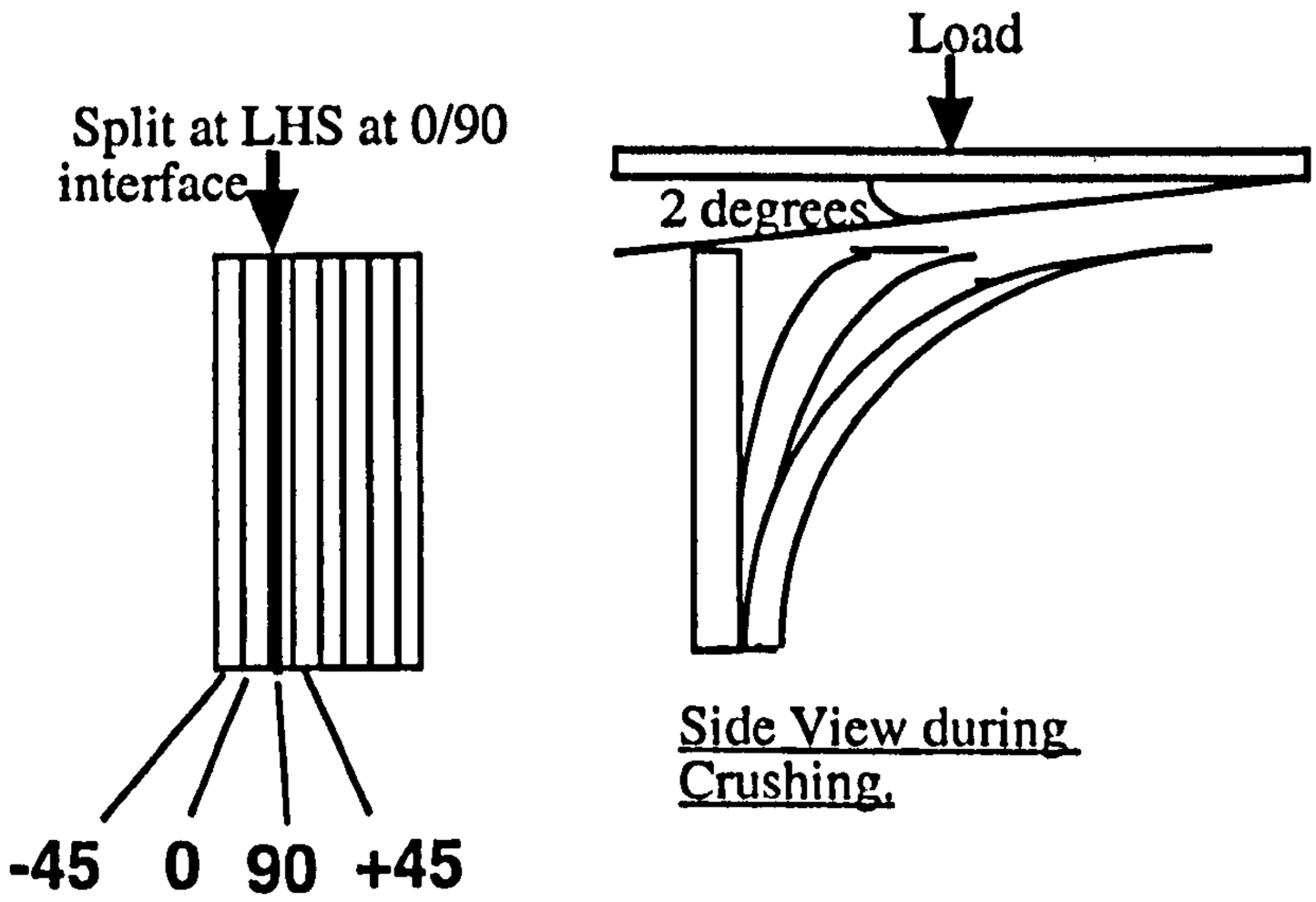

Figure 5.2 Failure mode for $(-45°, 0°, 90°, +45°)_S$ specimen

5.2.2 $(+45°, -45°, 0°, 90°)_S$ Stacking Sequence

The influence of stacking sequence on the energy absorption of the specimens was examined by crushing samples with the stacking sequence $(+45°, -45°, 0°, 90°)_S$. By having the + 45° and the – 45° together higher interlaminar shear stresses were induced in the samples and larger amounts of delamination occurred, leading to greater energy absorption (Table 5.1). The alternative stacking sequence increased the energy absorbed by the samples by an average of 41%. The failure mode of these samples was very different from that of the stacking sequence tested previously. Although, the initial crack was again on one side of the specimen (possibly an influence of the 2° angled crush plate), it appeared to start at the –45°/0° interface. Two laminae on each side of the specimen bent away from the main specimen which progressively crushed, which is clearly shown in Figure B.5 Appendix B. Typical load-displacement graphs are shown in Figures 5.34-5.37. The letter "s" is used to denote the series of tests showing $(+45°, -45°, 0°, 90°)_s$ stacking sequence.

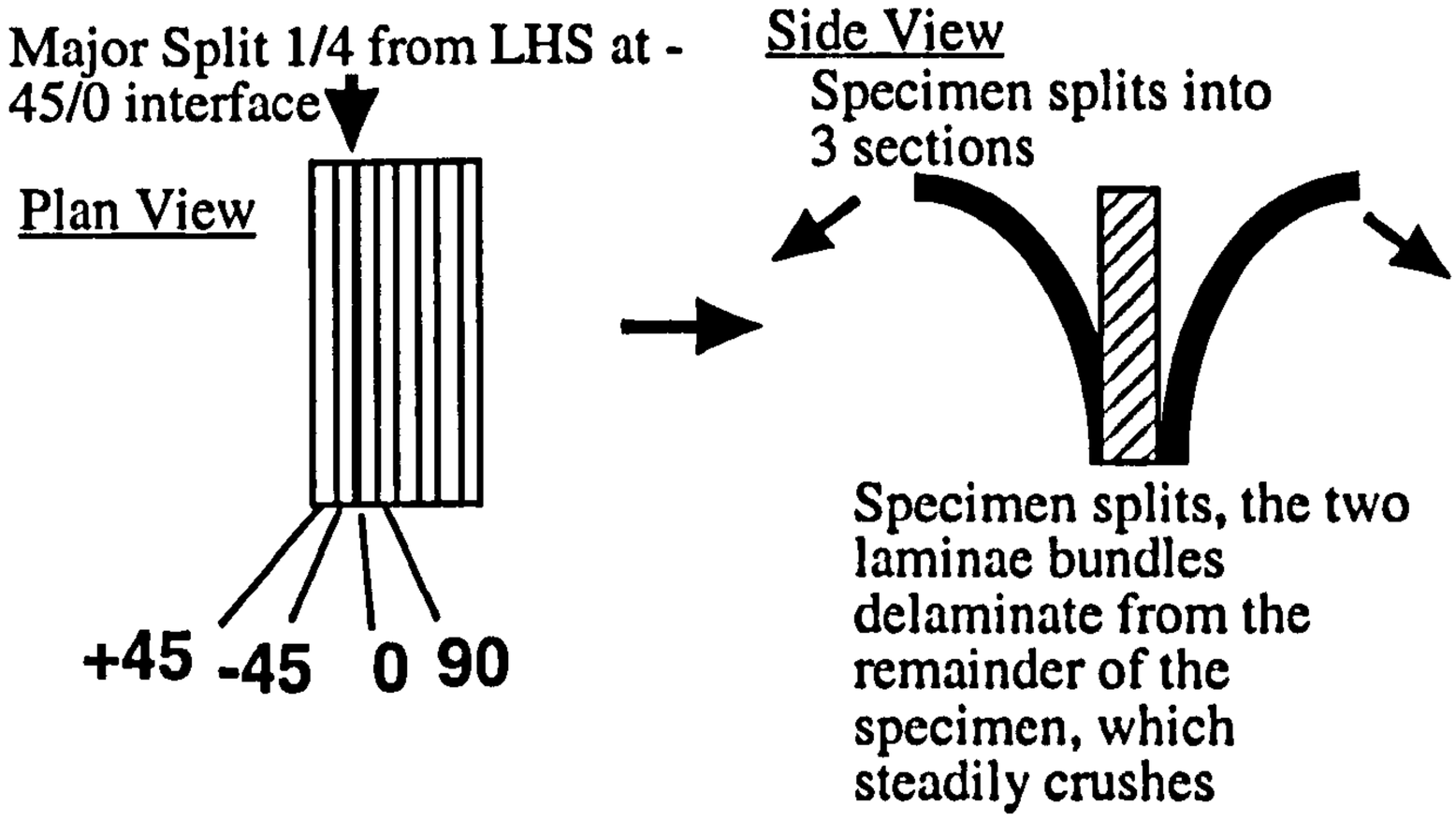

Figure 5.3 Failure mode for $(+45°, -45°, 0°, 90°)_S$ specimen

5.2.3 Effect of Loading Plate Friction

Specimens with the same stacking sequence as the sandwich panel skins, i.e. $(-45°, 0°, 90°, +45°)_S$ and an un-supported length of 5mm, were crushed using the angled crush plate. A series of tests was conducted where the crush plate was cleaned of any crush debris and sprayed with PTFE before each test, apart from two of the tests. It was seen that the "dirty" samples (Figures 5.38 & 5.39) exhibited a much higher peak load than the other tests in that series. To further investigate the effect of friction a second angled crush plate was machined and the surface of the plate was grit blasted to increase friction. The friction from this loading plate had a considerable effect on the overall energy absorbed by the specimen. Load-displacement graphs for these tests (Figures 5.40 & 5.41) showed the existence of an initial peak before the graph increased to a higher value where crushing of the sample occurred. The letter "d" is used to denote the series of tests showing "dirty" samples, "dr" for samples tested with grit blasted crushing plate. Results are shown in Table 5.1.

5.2.4 Effect of Unsupported Length

To investigate the effect of the unsupported length of the specimen, five different length specimens were tested namely, 4mm, 5mm, 6mm, 7mm and 9mm unsupported lengths. These samples had an identical lay-up to the above specimens and were also tested in a similar manner to previously, i.e. held in a compression fixture and

compressed using a 2° inclined loading plate. Apart from the 9mm unsupported length samples, when the samples had been crushed by their initial unsupported length they were moved upwards in the fixture by the same length again, and the crushing process was repeated. An aluminium spacer of the same dimensions as the unsupported section of sample was placed underneath the sample for support (Figure 5.4). It was hoped that the above procedure would show whether the plateau load recorded was a consequence of clamping the specimen, or whether the plateau load would decrease as the sample was raised and the next unsupported length of sample was crushed. From Figures 5.42 –5.45, it was seen that the plateau load stayed more or less constant as the sample was progressively crushed, raised and then crushed again. Table 5.2, summarises the results obtained.

The 4mm, 5mm and 6mm specimens failed in an identical manner to each other, i.e. crack initiation on one side of the sample, followed by a general bending/crushing mode. The 7mm unsupported length samples were seen to be starting to bend prior to crushing; this resulted in a different mode of failure. Three 9mm unsupported samples were tested. Two of these three samples failed in a bending/crushing mode (Figure B.6 Appendix B). The third sample crushed very little, just bending as the load was applied. Table 5.2 details the peak load, mean crush load and average stress of the specimens tested.

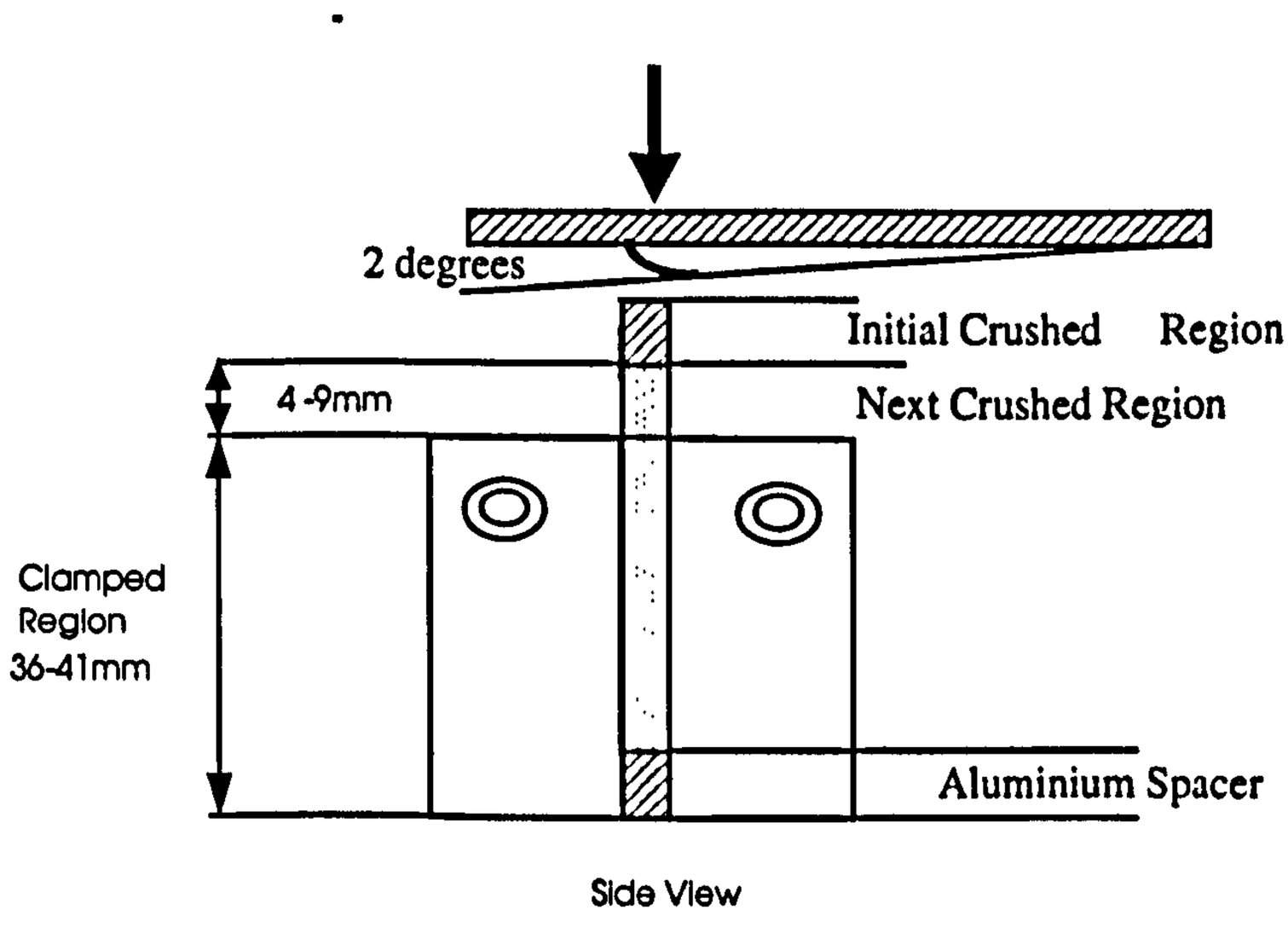

Figure 5.4 Fixture for testing effect of unsupported length

5.2.5 Discussion and Conclusions from Small Specimens Tests

The following conclusions were drawn from the numerous crush tests carried out on the small plate specimens representative of the faces of the full size sandwich panels (Results can be found in Tables 5.1-5.3).

a) Un-triggered small specimens with a 5mm unsupported length, having an identical stacking sequence to the sandwich panel faces, delaminated at the 0°/90° interface on the side of the sample as shown in Figure 5.2. The mean crushing plateau load of approximately 600N equates to a plateau stress of 60MPa (by dividing by the cross sectional area of the specimens i.e. $10mm^2$) in the small plate specimen. This compares with an average value of 27MPa for a skin of the sandwich panel samples tested in the simplified rig. The plateau loads were calculated using the Kaleidagraph software package. The energy absorbed by the small specimens, crushed by a distance of 2.5mm varied between 1.5 and 2.0 Joules. The peak load experienced by the specimen before crushing occurred varied between 2.5 and 2.9kN.

b) Un-triggered specimens with a 5mm unsupported length, but with an altered stacking sequence of $(+45°, -45°, 0°, 90°)_S$ were also tested. The initial delamination started at the -45°/0° interface on one side of the specimen. The specimen, as previously, split into three sections, however, in this case the central portion which remain upright consisted of four laminae. The outermost sections on each side of the specimen split symmetrically about the main central section. The specimens recorded peak loads much higher than those seen previously, i.e. 3.5 to 4.0kN. From video evidence it was seen that the extent of the delamination in these samples was much higher, leading to a larger amount of energy absorbed. On average, a value of 3.17 Joules was recorded, an increase of 41% over the previous stacking sequence. The plateau loads were also higher: 700 to 800N.

c) The effect of loading plate friction was studied on un-triggered specimens with a 5mm unsupported length and was found to have a large effect on the results. From previous tests it was noted that as failure was initiated in the sample this was accompanied by a large displacement of the top of the sample away from the incline.

As the friction was increased on the loading plate the specimen was seen to stay intact up to a higher load than with tests conducted with a smooth plate. The peak loads of the specimens tested ranged from 4.2 to 5.6kN, the plateau loads from 700 to 800N. The energies absorbed from a 2.5mm crushing displacement were high, ranging from 3.61 to 3.92 Joules.

d) When crushed previously, 5mm specimens only yielded 2.5 to 3mm of useful data before the influence of the clamping fixture became evident, causing the crushing load to rise steeply. To see whether the load plateau obtained on the crush plots was real, or influenced by the clamping conditions, after the first crush the specimens were raised by the amount initially un-supported. It was seen that the mean plateau load stayed constant. It was also seen that as the un-supported length was increased from 4mm to 7mm the peak load and the plateau load remained at a similar level of between 550 and 700N, and hence a corresponding average stress of 60MPa was recorded. It was only when the un-supported length was 9mm that any considerable difference was seen in failure mode and hence the results obtained. The average peak load obtained was then 1714N. However, the plateau loads were a lot lower, especially in the specimen that failed almost entirely by bending, the load being only 85N. In the 6mm specimens that failed in a bending/crushing mode the plateau loads averaged 363N, corresponding to a stress of 36MPa.

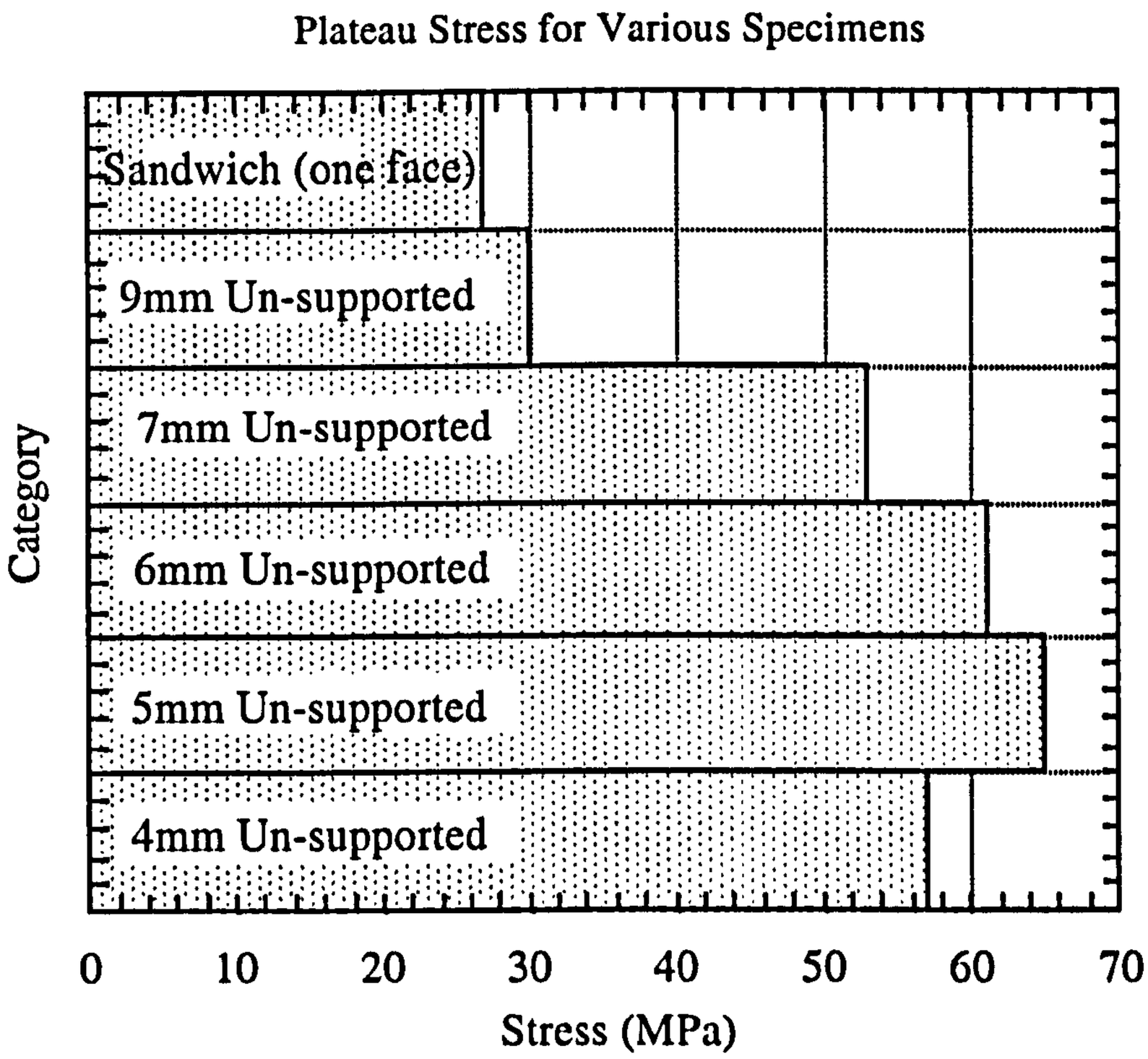

Figure 5.5 Comparison of plateau stresses for various specimens

The purpose of this work is to devise small test specimens, which have the same failure mode as the skins in the sandwich panel. In the sandwich panel tests the skin does have support from the honeycomb core, perhaps a back-to-back configuration would be more closely representative of this.

5.2.6 'Back-to-Back Specimens'

To represent the support conditions experienced by the skins of a sandwich panel, two un-triggered specimens with 6mm un-supported length were arranged back-to-back, with a layer of PTFE tape between them to reduce friction whilst crushing. 6mm specimen specimens were used because of specimen availability. The specimens provided support for each other against inward bending whilst crushing. The 2° tapered crush plate (Figures 5.6 & 5.7) was positioned symmetrically such that both specimens were identically crushed.

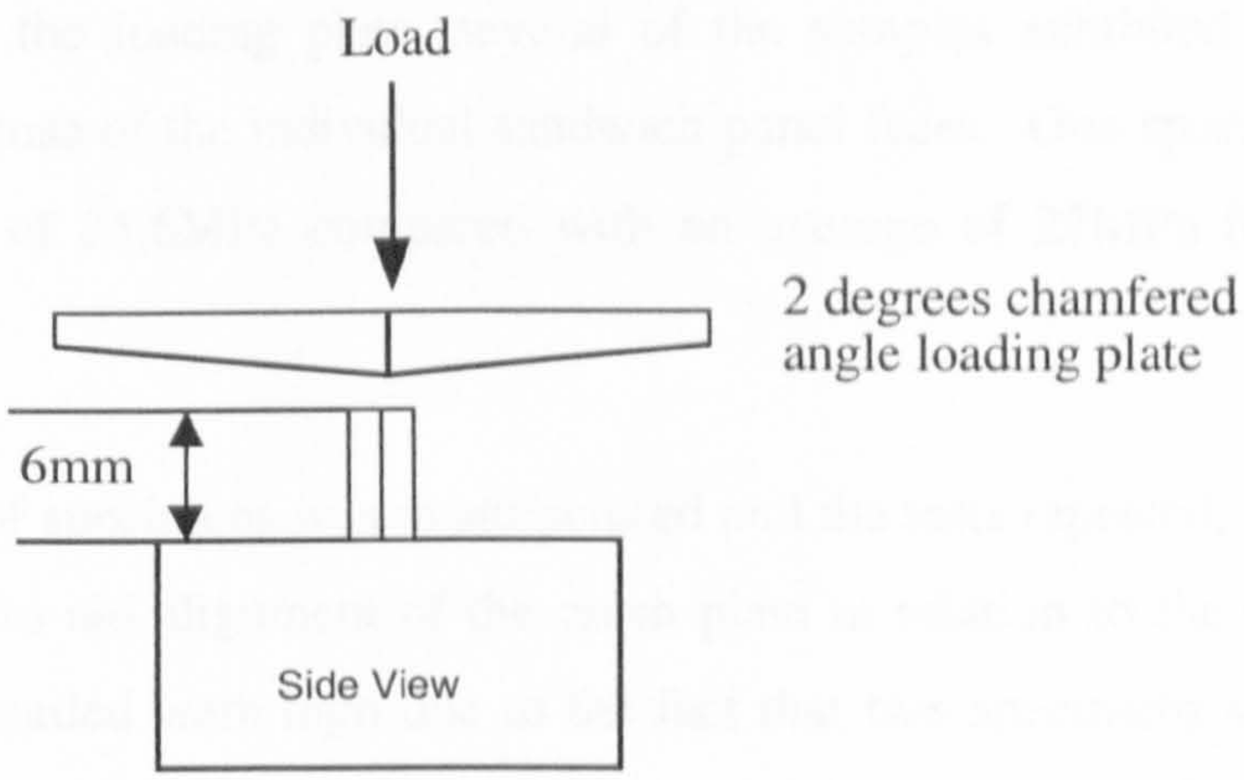

Figure 5.6 Diagram of test-rig used to test "Back-to-Back" specimens

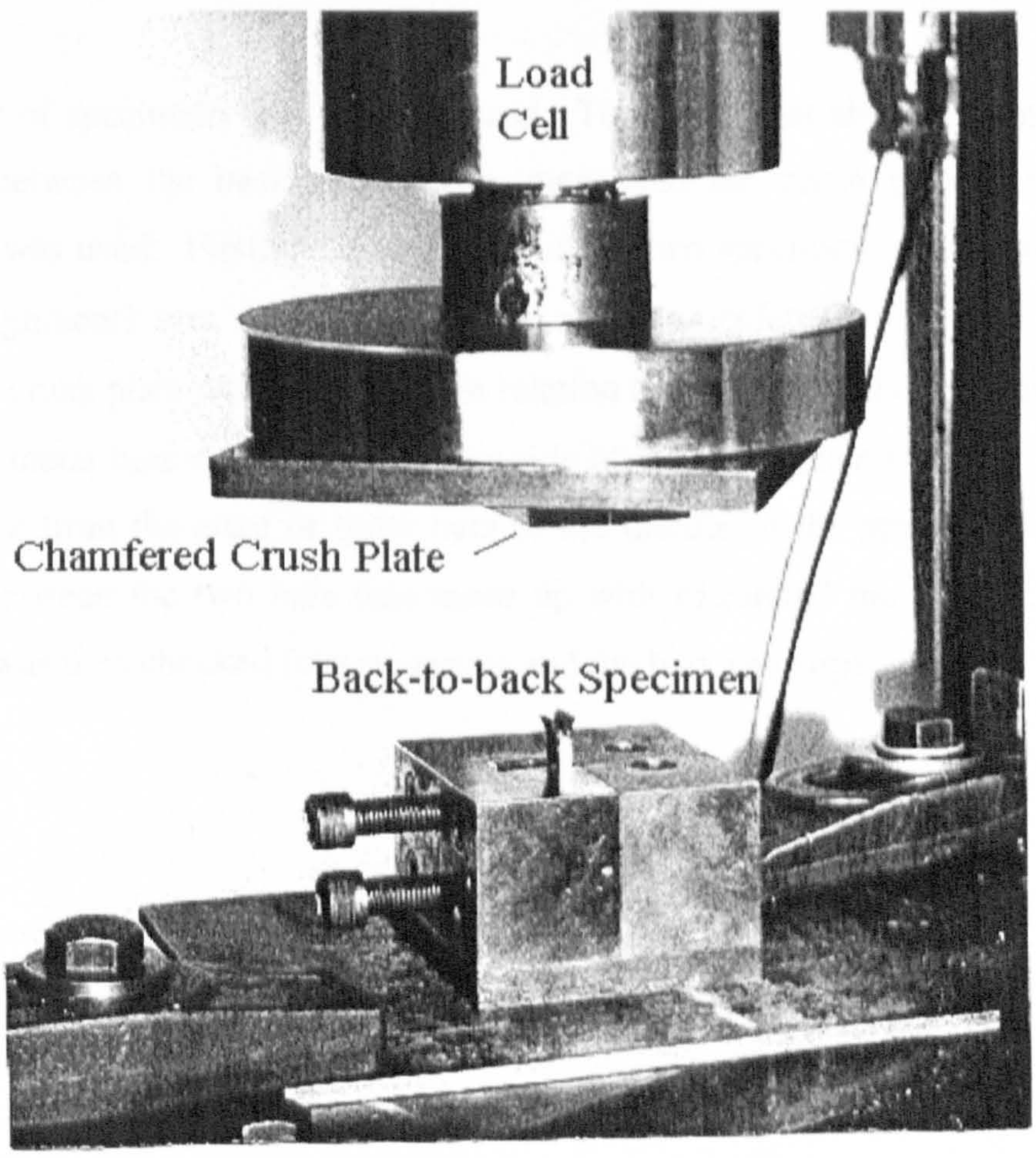

Figure 5.7 Photograph of "Back-to-Back" testing rig

Although the results from the first set of tests were scattered, possibly due to incorrect adjustment of the loading plate, several of the samples exhibited plateau stresses approaching those of the individual sandwich panel faces. One specimen exhibited a plateau stress of 25.6MPa compared with an average of 27MPa for the sandwich panel faces.

A second set of specimens was manufactured and the tests repeated, this time using a video camera to aid alignment of the crush plate in relation to the specimens. The peak loads recorded were high due to the fact that two specimens were crushed, on average 7330N. One set of samples, however, yielded a lower value of 4500N. The mean plateau loads varied between 670 and 730N, which corresponds to a stress in each of the skins of 33MPa. One sample yielded a value of 30MPa. Examination of the specimens after crushing still revealed a slight misalignment of the crush plate. The failure modes in the back-to-back specimens were the same as those seen in the sandwich faces; a bending/crushing mode.

A third set of specimens was manufactured. To ensure that absolute alignment was achieved between the back-to-back specimens and the crush plate the following procedure was used. Firstly, the thickness of the two specimens plus a metal spacer (to aid alignment) was measured and the centre calculated. Next the tip of the chamfered crush plate was ascertained in relation to the edge of the crush plate. A set of parallel metal bars was clamped either side of the crush plate (see Figure 5.8) and the distance from the edge of these bars to the middle of the specimens calculated. The gap between the two bars was made up with calibrated metal slips, the whole assembly was then checked for squareness and the bars and slips removed.

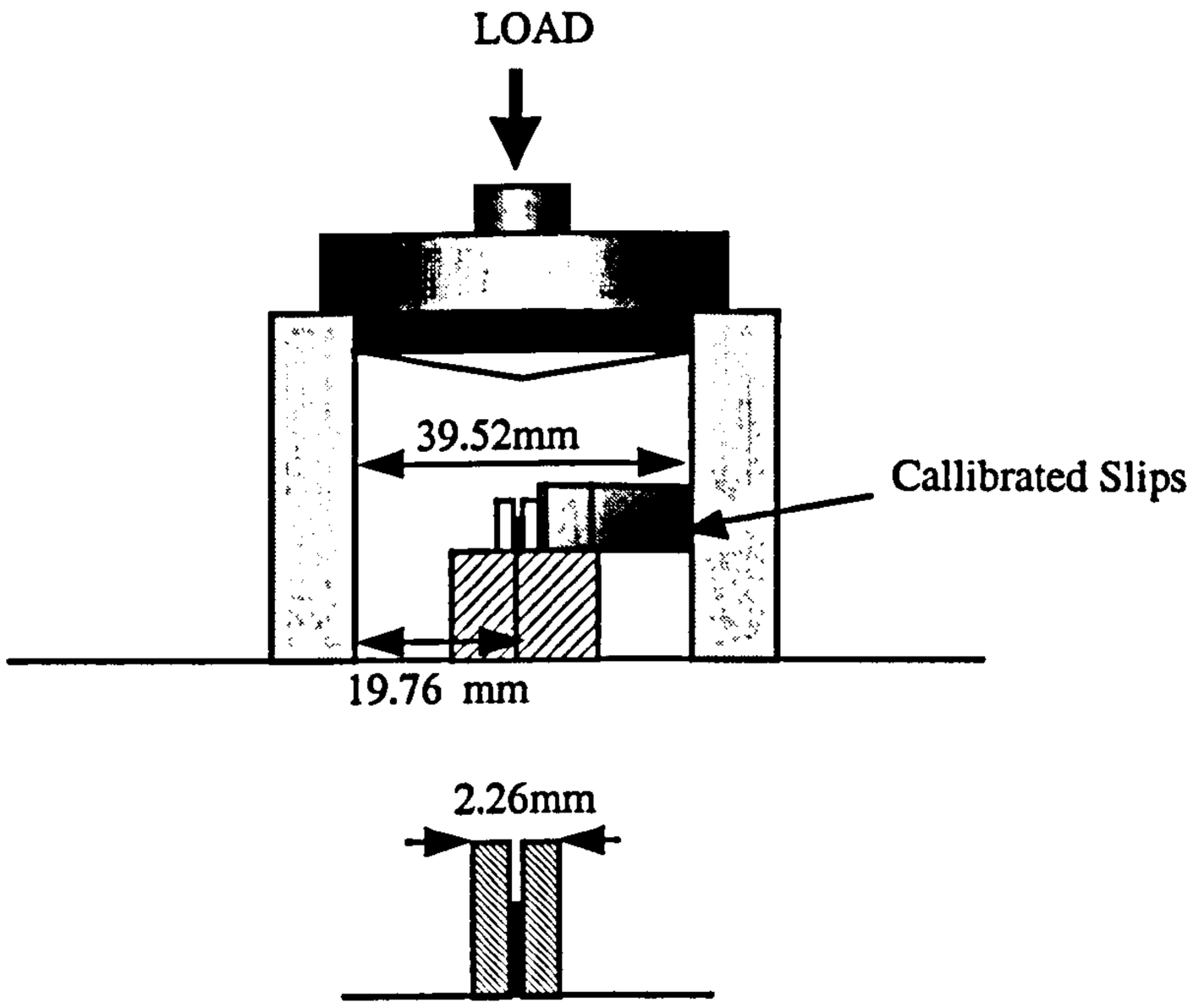

Figure 5.8 Alignment of "Back-to-Back" crush rig

Five pairs of specimens were tested, two pairs were 6mm in length, and three pairs were slightly shorter at 4.9mm. The crush plate was cleaned and sprayed with PTFE before each test was started.

Table 5.3, shows the average of the results obtained for the tests outlined below. The crushing modes seen in the back-to-back specimens were excellent, the two specimens crushed away from each other with no interaction. The metal spacer was not involved in the crushing, being located below the surface of the clamping fixture. The first of the 6mm specimen pairs had a plateau stress of 22.8MPa i.e. approximately 20% less than the average plateau stress for one face of a sandwich panel.

The second pair of specimens crushed equally as well and the real time plot showed that a similar plateau stress had been obtained. However, due to a data acquisition problem no data was recorded. The third pair of specimens had an un-supported length of 4.9mm. As can be seen from Figure 5.45, the peak and plateau loads were very high, the plateau stress was 45.3MPa. Once the specimen had been crushed it was removed from the test rig and examined. It became clear that when placing the specimen in the testing rig the metal spacer had moved and had interfered with the crushing process.

The fourth and fifth pairs of specimens crushed with plateau stresses of 27.1MPa and 26.4MPa, slightly higher than that seen for the first specimen, but this would be expected for a shorter specimen. The results for the back-to-back specimens are shown in Table 5.3. As shown, the average stress is 32.67 MPa, compared with 23.40MPa for the sandwich panels. However, this average is affected by the first few sets of tests when poor alignment of the specimens resulted in high stresses. A compilation graph of the last set of specimens tested is shown in Figure 5.32.

To conclude, once near perfect alignment of the back-to-back specimens had been achieved the failure modes seen were very similar to the sandwich panels, as were the plateau stresses. It would be expected that the stress in the sandwich panels would be higher than those in the face-skin specimens. The failure modes in the face-skin specimens are mainly delamination/fibre crushing, whereas in the sandwich panels there was also face-to-core debonding and core crushing contributing to the higher crush loads and therefore higher crush stresses. Load–displacement curves for back-to-back specimens are shown in Figures 5.46.

5.3 Skin-to-Core Bond Strength

The use of high performance, lightweight sandwich materials has increased significantly in recent years. Typically, carbon and glass fibre reinforced plastics are bonded to low density cores to produce strong, stiff, lightweight structures. The strength of the interface between the composite facing and the low density core is likely to be critical. Values of peel strength will vary considerably, depending upon: -

- Test method used
- Toughness of the adhesive
- Amount of adhesive used
- Density of the core
- Cell size of the core
- Direction of the peel (along or across the ribbon direction)
- Adequacy of the surface preparation

- Degradation of the adherend surface subsequent to bonding

To investigate the skin-to-core strength for the sandwich specimens two test methods were employed, namely, the climbing drum peel test [45] and the double cantilever beam test [46]. Two sizes of aluminium honeycomb core cell were tested, 6.35mm (1/4") and 3.175mm (1/8").

5.3.1 Climbing Drum Peel Tests

5.3.1.1 Introduction

Much of the published work relating to skin-core adhesion in sandwich structures has involved the use of the climbing drum peel test. This test has the virtue of being easily duplicated, as well as possessing an obvious relationship to the toughness whose value is sought. The test apparatus used (Figure 5.9) was in accordance with ASTM D1781-76 [45] and consisted of a flanged drum, flexible loading straps and clamps to hold the specimen.

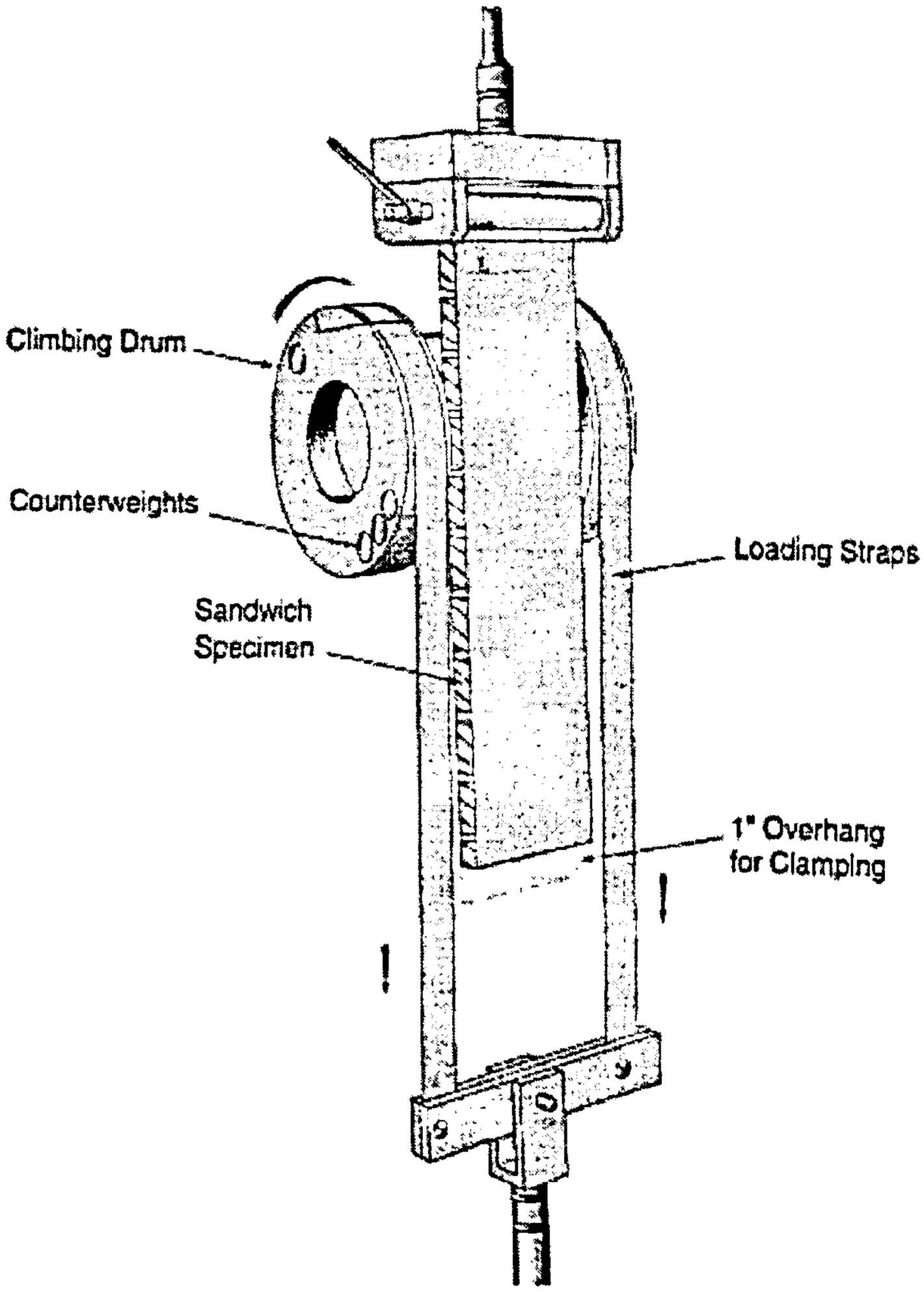

Figure 5.9 Climbing drum apparatus

5.3.1.2 Test Specimen

The climbing drum specimen (Figure 5.10) was 12mm thick, consisting of two 1mm HTA/913 faces and a 10mm thick core manufactured from 5052 aluminium alloy. The faces were quasi-isotropic and had a stacking sequence of $(-45°, 0°, 90°, +45°)_s$. The test specimen used was manufactured via the route outlined in Section 4.1 and was 285mm in length by 75mm wide. At each end of the specimen was a 25mm overhang of one face skin, produced by removing the top skin and the core of the panel to allow clamping of the specimen (Figure 5.9). Two different cell sizes were tested, i.e. nominally 3.175mm (1/8") and 6.35mm (1/4").

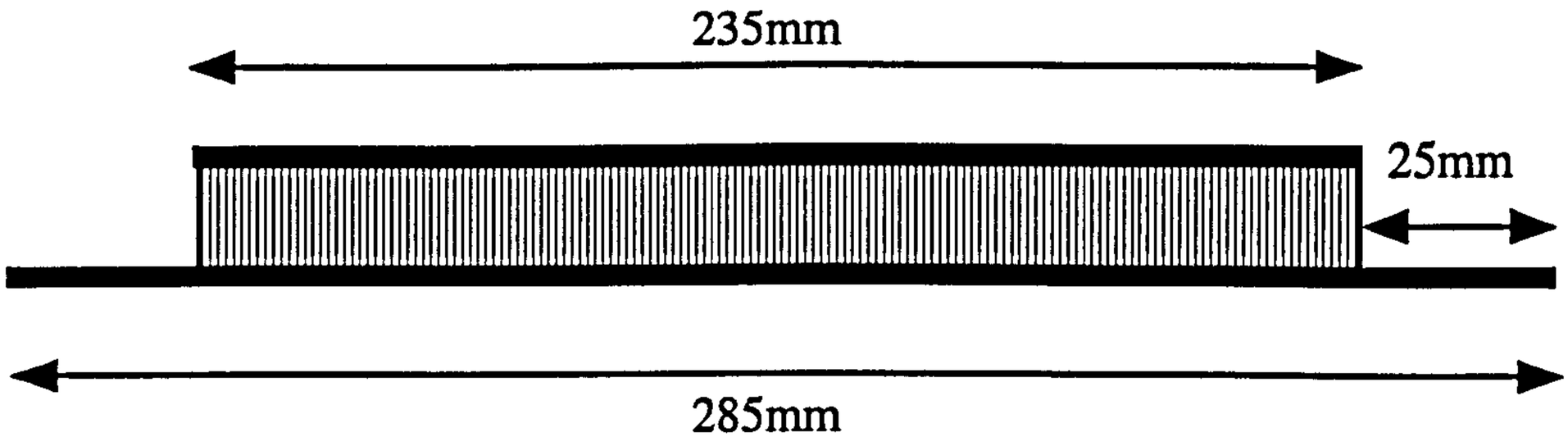

Figure 5.10 Climbing drum specimen

5.3.1.3 Test Method

The test specimen was clamped securely to the drum by means of drum clamps. The top and bottom clamps were connected to the upper and lower crossheads of an Instron universal testing machine respectively. The difference in diameter of the cylinders to which the loading straps were attached caused the drum to rotate clockwise, peeling the skin off the core when tension was applied by the movement of the upper crosshead. The crosshead speed was 25mm min^{-1}. The peel resistance was then calculated for both the honeycomb cell sizes over a bond distance exceeding 152mm. Five specimens of each of the two cell sizes were tested.

5.3.1.4 Results

To obtain a measure of the different torques to peel the sandwich skin from the core the following equation [45] was used: -

$$T^* = [(r_o - r_i)(F_p - F_o)]/W$$

Where: -

T^* = average peel torque, (mm. kg/mm of width)

r_o = radius of flange, including one half the thickness of the loading straps, (mm)

r_i = radius of drum plus one half the thickness of the adherend being peeled, (mm)

F_p = average load required to bend and peel adherend plus the load required to overcome the resisting torque (kg)

F_o = load required to overcome the resisting torque (kg)

W= width of specimen (mm)

$$\text{Therefore T* (6.35mm)} = \frac{[((62.95+0.23)-(50.03+0.5))(51.8-43.4)]}{75}$$

$$= 1.42 \text{ mm.kg/mm}$$

$$\text{Similarly T* (3.175mm)} = \frac{[((62.95+0.23)-(50.03+0.5))(44.0-23.9)]}{75}$$

$$= 3.39 \text{ mm.kg/mm}$$

The values of F_p and F_o were obtained graphically (Figure 5.11). F_p, the top curve represented the force needed to unpeel one of the skins from the sandwich panel plus the force required bending the skin around the drum. F_o,the bottom curve represented the force needed to wrap a single skin around the drum. The difference, therefore, between the area of the two curves was the energy needed to unpeel the skin from the core. As can be seen from the results above, the smaller sized cell was bonded more strongly to the face skin. This was due to the smaller cell having a greater cell wall length per given surface area than the larger cell. A greater torque was therefore needed to peel the face from the core. The torque value obtained for the 3.175mm cell size was only very approximate; as can be seen from Figure 5.12 the two traces did not show the typical load-displacement behaviour seen in Figure 5.11. The loads varied considerably and so the mean loads were obtained using KaleidaGraph®, a graph plotting software package.

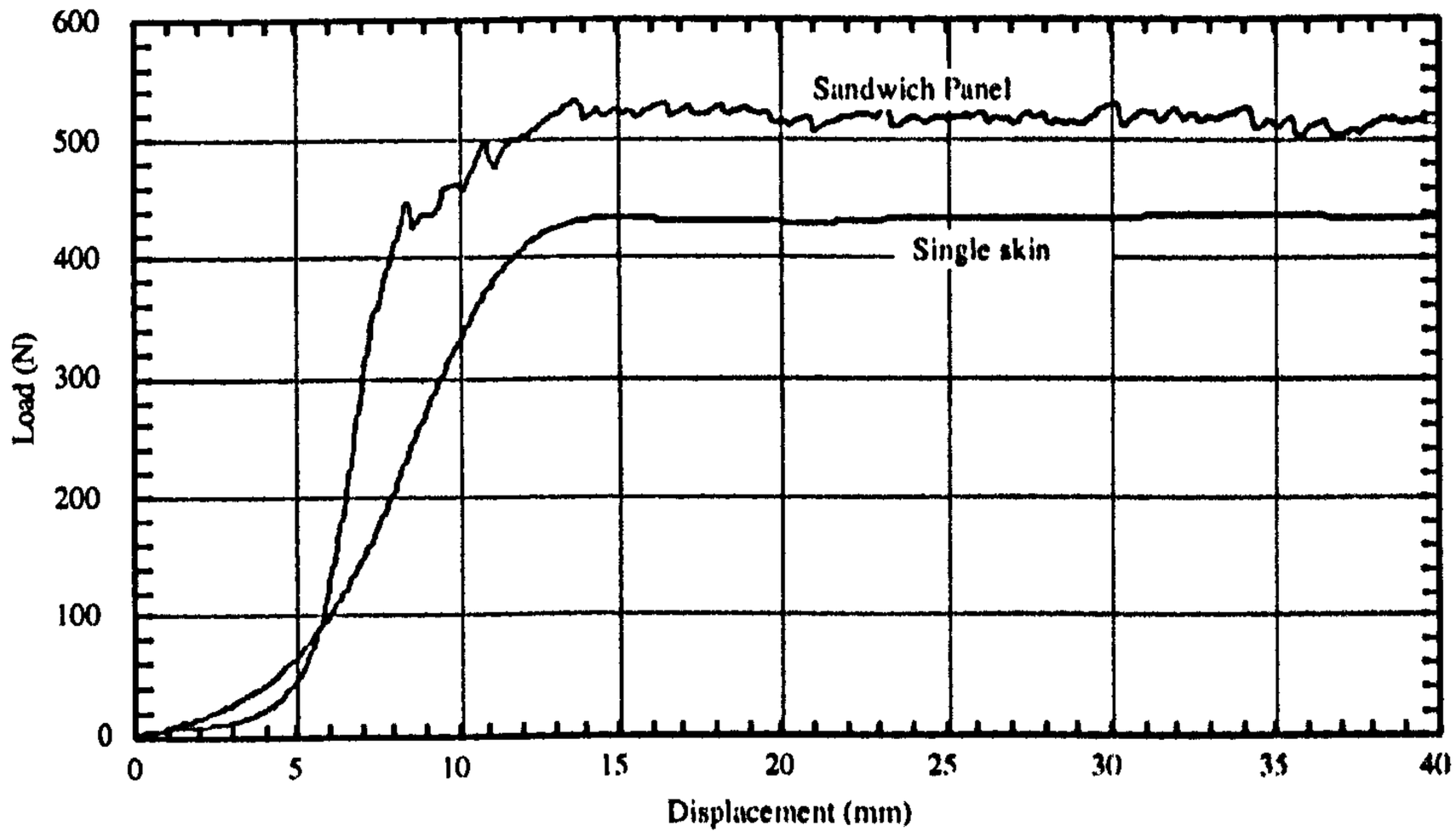

Figure 5.11 Climbing drum load - displacement curve for 6.35mm cell size honeycomb

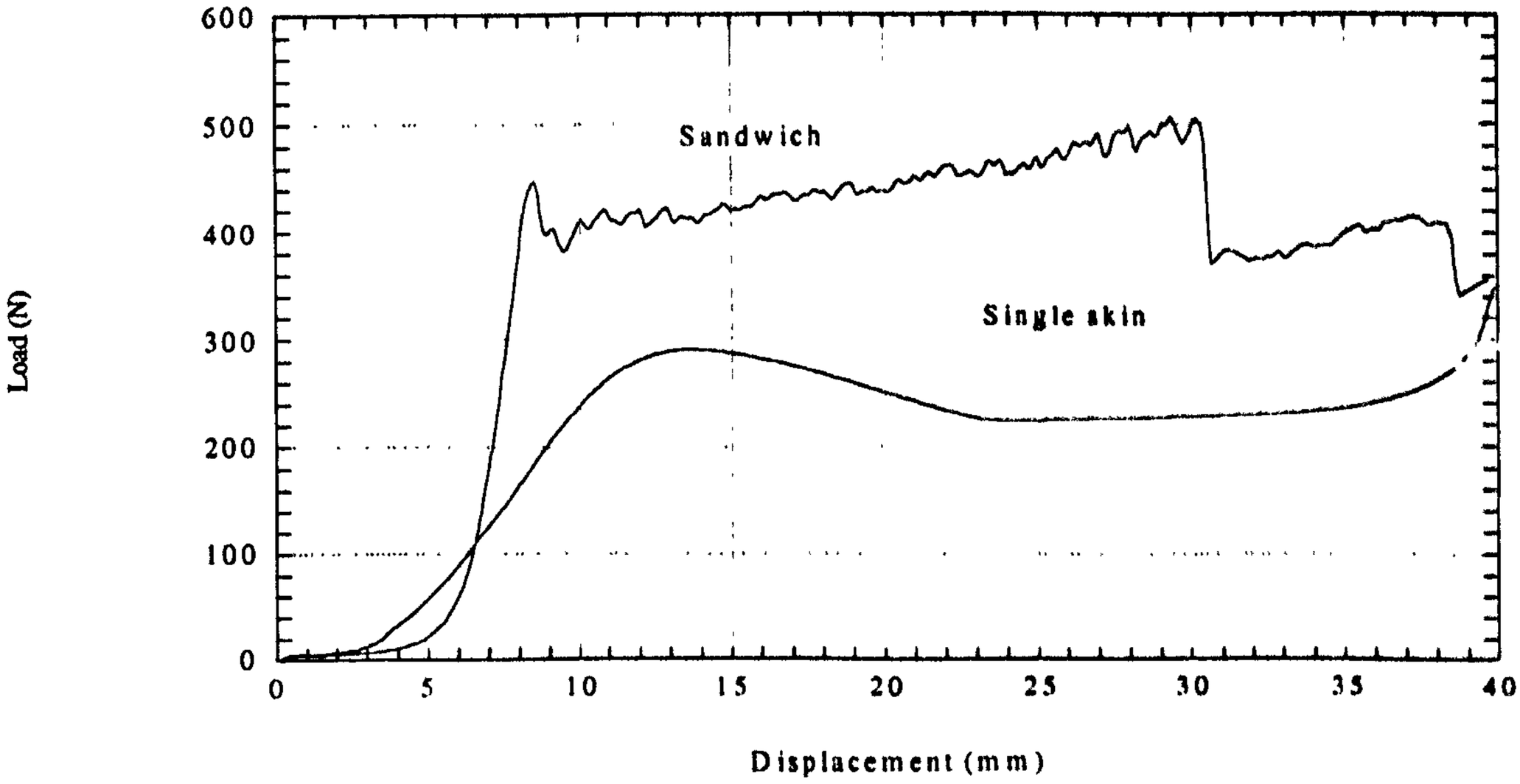

Figure 5.12 Climbing drum load - displacement curve for 3.125mm cell size honeycomb

As stated previously the difference in the areas of the two load-displacement curves represented the energy required debonding the face from the core. The average difference in the energy values for the five specimens with a 6.35mm cell size was 3.13 Joules. When this was divided by the effective debond area (120mm x 75 mm) a fracture toughness value of 348 Jm^{-2} was obtained. A similar calculation for the 3.175mm cell size was not possible. Inspection of these specimens after testing showed that damage to the skin had occurred during the peeling test, therefore, any results obtained would be a combination of the energy required for skin debonding from the core plus the energy required to cause delamination in the face skin. A load-displacement curve for the 3.175mm cell size showing the influence of the skin damage is shown in Figure 5.12.

5.3.2 Double Cantilever Beam Tests

5.3.2.1 Introduction

The test method outlined in ASTM D 5528-94a [46] describes the determination of the opening Mode I interlaminar fracture toughness G_{Ic} of unidirectional fibre-reinforced polymer matrix composites using the double cantilever beam (DCB) specimen. This type of specimen was used here to evaluate the face-to-core bond strength of the sandwich panel specimens.

5.3.2.2 Test Specimen

The double cantilever beam specimens tested were 12mm thick, consisting of two 1mm HTA/ 913 faces and a 10mm thick core manufactured from 5052 aluminium alloy. The faces were quasi-isotropic and had a stacking sequence of $(-45°, 0°, 90°, +45°)_S$. The test specimen used was manufactured via the route outlined in Section 4.1 and was 200mm long by 46mm wide (Figure 5.13).

Aluminium alloy loading blocks were bonded to the specimen using a cold-cured high strength epoxy adhesive (Araldite® 2015). Prior to this the composite substrate and the aluminium end blocks had been grit blasted and degreased to improve their

adhesion between the sandwich face and the aluminium blocks. A 50mm starter crack was machined into each specimen. To help monitor the position of the crack front, the sides of the specimen were painted using typewriter correction fluid, and marked at 5mm intervals. The DCB tests were carried out using an Instron universal testing machine fitted with a 5kN load cell.

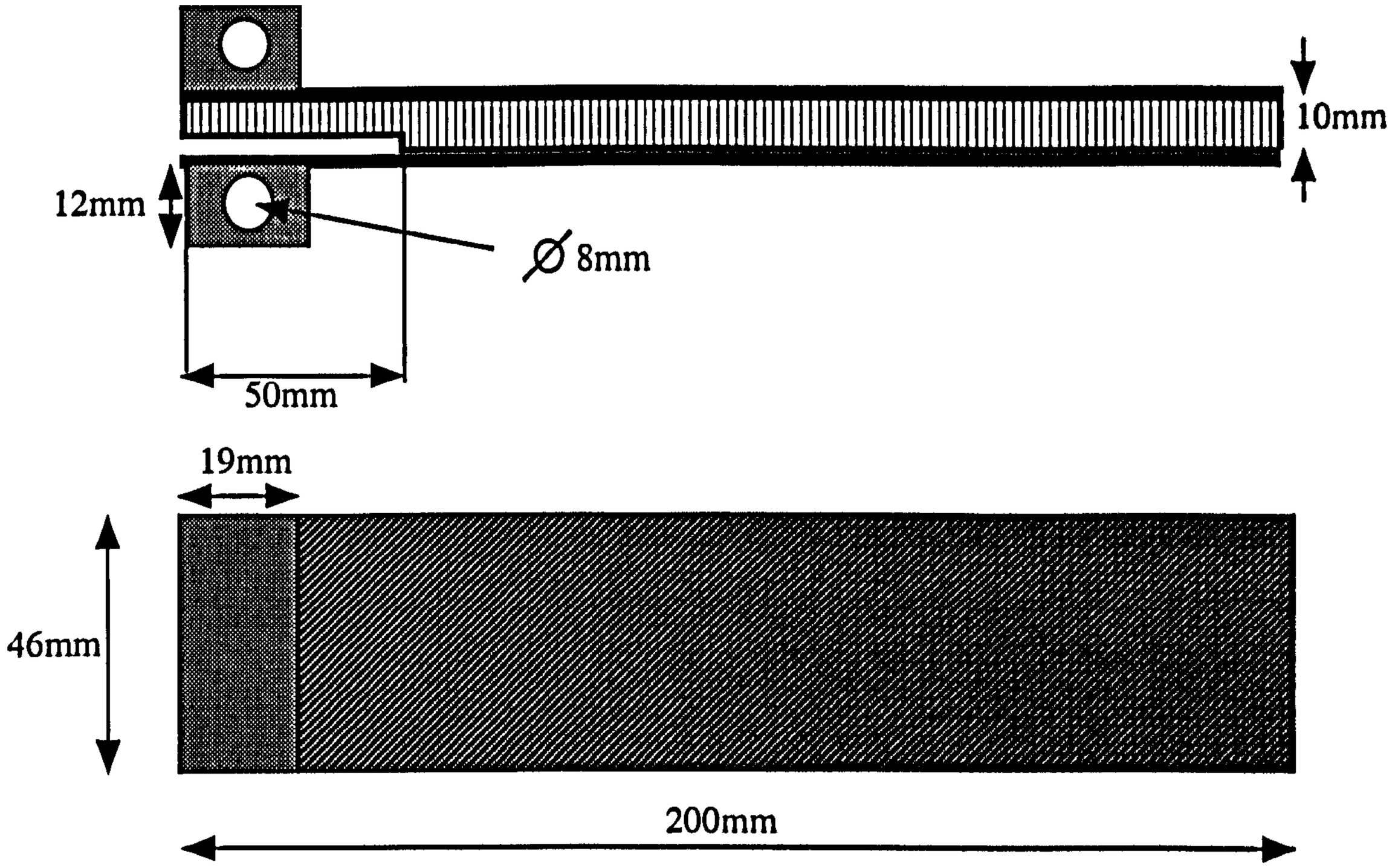

Figure 5.13 Double cantilever beam specimen

The DCB specimens were loaded at 10mm/min. The crack growth was observed using a travelling microscope. A typical load-displacement curve is shown in Figure 5.14 indicating that the crack growth was unstable as shown by the sharp drops in load.

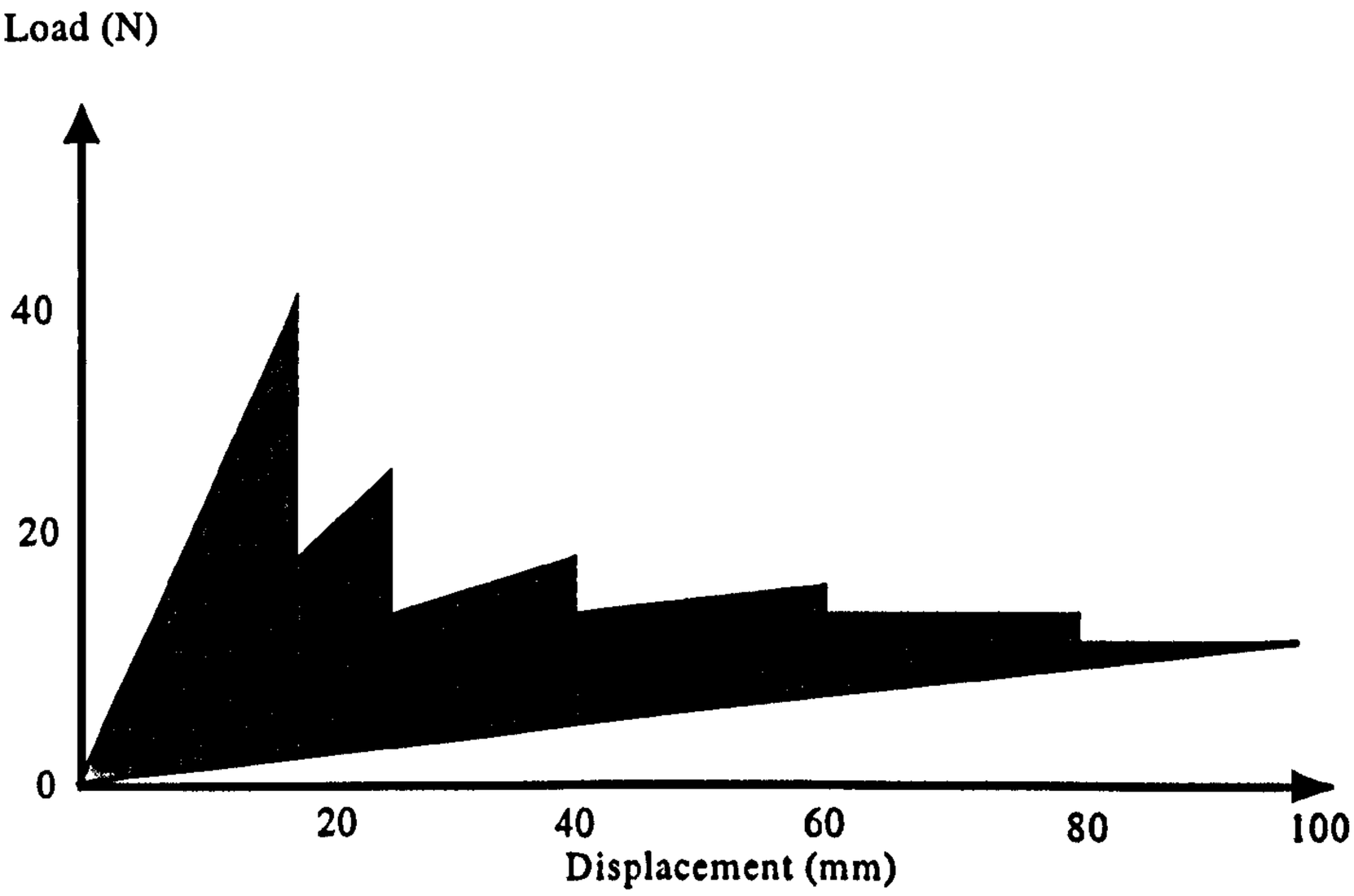

Figure 5.14 Typical load-displacement plot

5.3.2.3 Data Reduction

The method of data reduction used to calculate the fracture toughness values was the modified beam theory (MBT)[46]. The beam theory expression for the strain energy release rate of a perfectly built-in (that is, clamped at the delamination front) double cantilever beam is as follows:-

$$G_I = \frac{3P\delta}{2ba}$$

Where:

P = load,

δ = load point displacement,

b = specimen width

a = delamination length

In practice, this expression over estimates G_I because the beam is not perfectly built-in (that is, rotation may occur at the delamination front). One way to correct this is to treat the DCB as if it contained a slightly longer delamination, $a+\Delta$. Where Δ is determined by generating a least squares plot of the cube root of the compliance divided, in this case, by N, the loading block correction factor, i.e. $(C/N)^{1/3}$, as a function of the delamination length. The compliance, C, is the ratio of the load point displacement to the applied load, δ/P. To calculate the Mode I interlaminar fracture toughness the following expression was used.

$$G_I = \frac{3P\delta}{2b(a+\Delta)}$$

To account for the large displacement and loading blocks' stiffening effect a correction factor for the measured crack length and for measured values for the displacement are used. For the DCB specimen geometry the factors are as follows.

Large Displacement Effects [46]: -

$$F = 1 - \frac{3}{10}\left(\frac{\delta}{a}\right)^2 - \frac{3}{2}\left(\frac{\delta}{a^2}\right)$$

Loading Block Stiffening Effect [46]: -

$$N = 1 - \left(\frac{L'}{a}\right)^3 - \frac{9}{8}\left[1 - \left(\frac{L'}{a}\right)^2\right]\left(\frac{\delta t}{a^2}\right) - \frac{9}{35}\left(\frac{\delta}{a}\right)^2$$

Where corrected G_I = G_I (measured) x F/N

Where: -

L is the total length

L' is the distance from the middle to the edge of the loading block (see Figure 5.15)

t is the distance from the middle of the loading block to the mid-plane of the top skin (see Figure 5.15)

F is the correction factor for large displacements

N is the correction factor due to the inclusion of end blocks

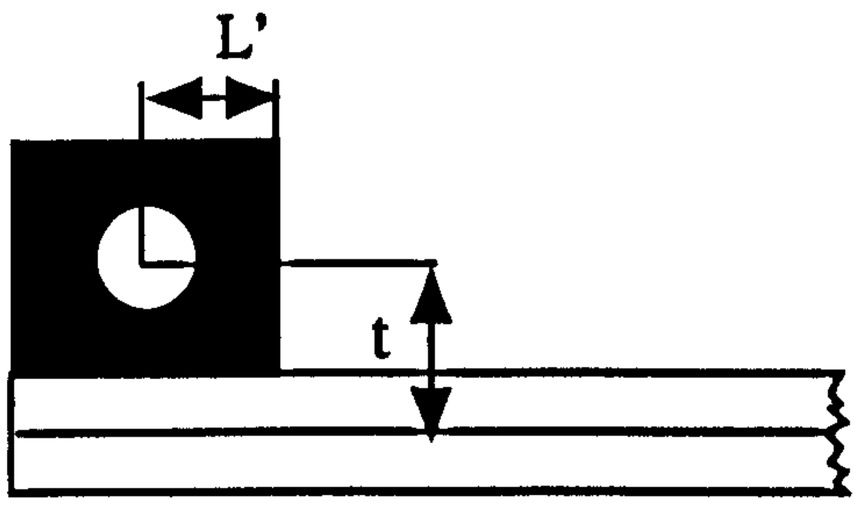

Figure 5.15 Schematic showing end block nomenclature

5.3.2.4 Sample Calculation

The first step when using the MBT method was to plot the factored measured compliance to the power of one third, $(C/N)^{1/3}$, against the corresponding crack length, a, the intercept yielding the correction factor Δ (Figure 5.16). In order to do this N was calculated, and then F.

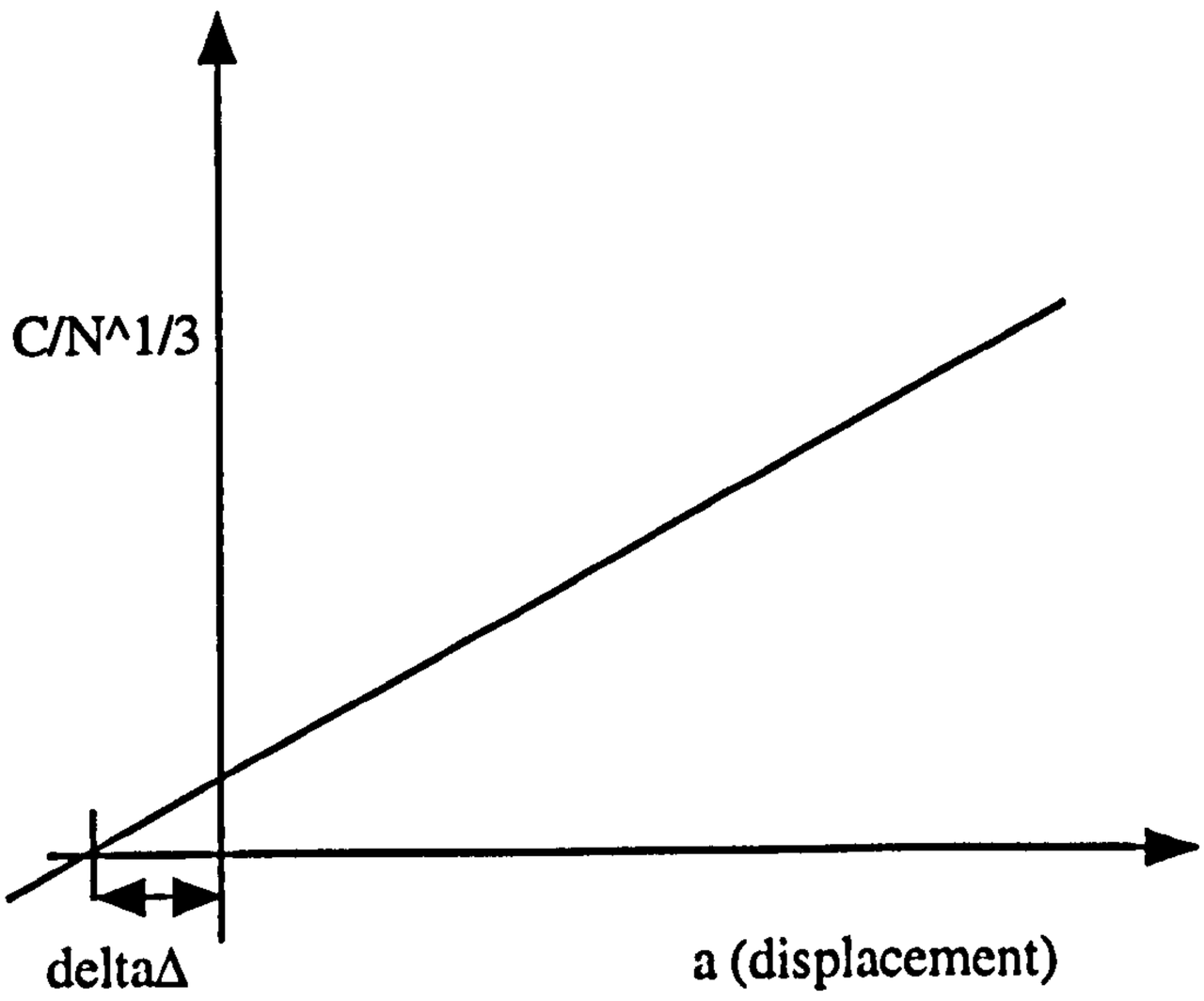

Figure 5.16 Graph of (C/N)^1/3 vs. crack displacement

If δ = 65mm, a = 90mm, L' = 10mm and t = 8mm and

$$N = 1-\left(\frac{L'}{a}\right)^3 - \frac{9}{8}\left[1-\left(\frac{L'}{a}\right)^2\right]\left(\frac{\delta t}{a^2}\right) - \frac{9}{35}\left(\frac{\delta}{a}\right)^2 \qquad N = 1\text{-}0.00137\text{-}0.0570\text{-}0.1341 =$$

0.80753

$$F = 1 - \frac{3}{10}\left(\frac{\delta}{a}\right)^2 - \frac{3}{2}\left(\frac{\delta t}{a^2}\right) \qquad F = 1\text{-}0.1565\text{-}0.0963 =$$

0.74720

therefore F/N = **0.9253**

A graph of $(C/N)^{1/3}$ versus (a) was plotted from the data taken from the chart recorder. A line was fitted using the Kaleidagraph® graph-plotting package. The fitted line had the following values, y = -0.0042242 + 1.475x, therefore if y = 0, x = **0.002864**

Substituting values into: -

$$G_{Ic} = \frac{3P\delta}{2b(a+\Delta)}$$

Gave a fracture toughness value of 412Jm^{-2}. Multiplying by the correction factor F/N gave a final G_I value of 381Jm^{-2}.

Four DCB tests were carried out on each of the two core cell sizes i.e. 6.35 and 3.175mm (1/4" and 1/8"). The results are shown below (Table 5.5): -

5.3.2.5 Discussion

The average fracture toughness for the 6.35mm (1/4") DCB specimens was 351 Jm^{-2} compared with an average value of 348 Jm^{-2} obtained using the climbing drum method for the same cell size. This was a very good correlation.

For the smaller cell size the results were very high, an average value of 2833 Jm^{-2} recorded. For two of the specimens, the growing crack jumped interfaces, growing through the aluminium core until the other face was reached, hence, the results were considered invalid. Examination of the 3.175mm (1/8") cell size specimens, as with the similarly sized climbing drum specimens, revealed a large amount of delamination in the face skins of the sandwich. Approximately 50% by surface area of the face remained adhered to the core (Figure 5.17).

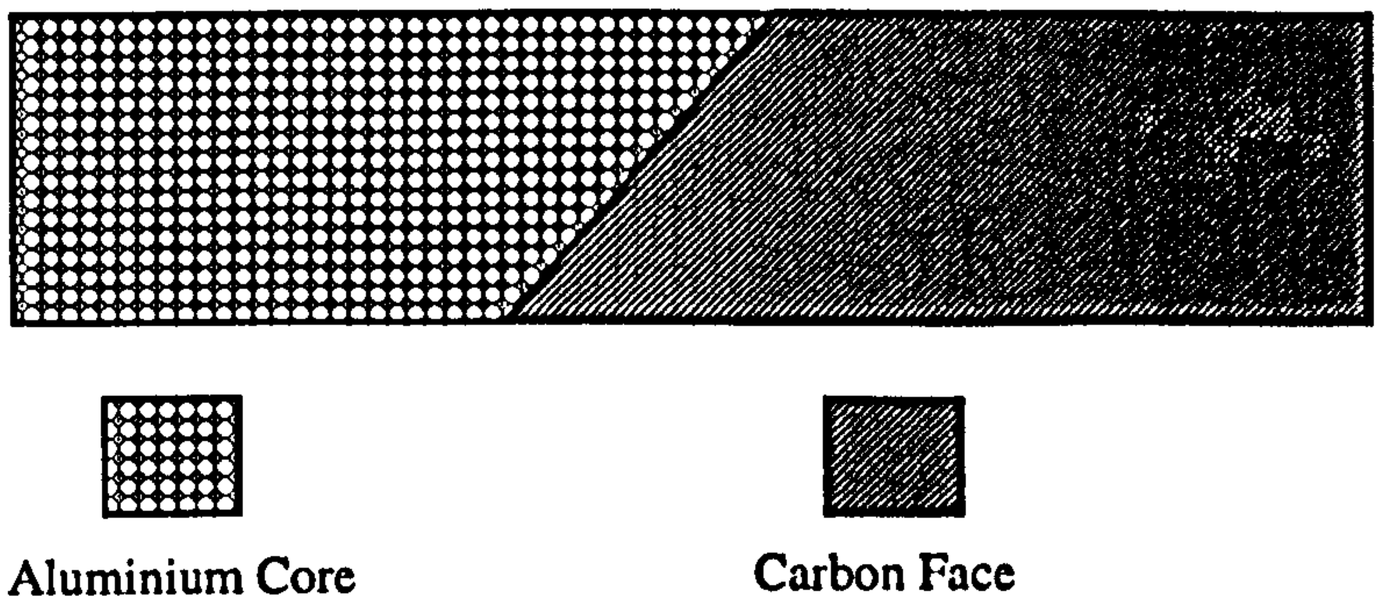

Figure 5.17 Failure surface of 3.175mm cell DCB specimen

As a result of the large amount of delamination in the specimens, the results obtained for the 3.175mm (1/8") specimens could not be used as an accurate measure of interfacial fracture toughness. Obviously, it can be surmised that the interfacial fracture toughness for the smaller cell specimen was greater than for the larger cell.

The modified beam theory used to calculate the fracture toughness assumes that the growing crack is loaded evenly from both end blocks. In the case of a sandwich panel this could only be achieved if a crack was placed in both skin-to-core interfaces. However, even this would not be satisfactory, as only one crack would ever grow under loading at one time.

As methods for comparing the interfacial fracture toughness (rather than specifically G_{Ic}) for the two cell sizes, both the methods used have their limitations. It was revealed by these tests that the interfacial fracture toughness was greatly affected by the core cell size or, more specifically, the effective bonding area.

5.4 Effective Bonding Area

To calculate the effective bond area for both cell sizes, the cell wall lengths were accurately measured using a microscope and a set of vernier callipers. It was found under closer inspection that the cells in some cases were not regular hexagons, (Figure 5.18). However, as the honeycomb core was measured at a number of places along its length and a mean value taken, the resulting measurements were as accurate as was needed for the comparison calculation below. An effective bond area was calculated and the ratio of the cell wall length to the effective bond area was obtained.

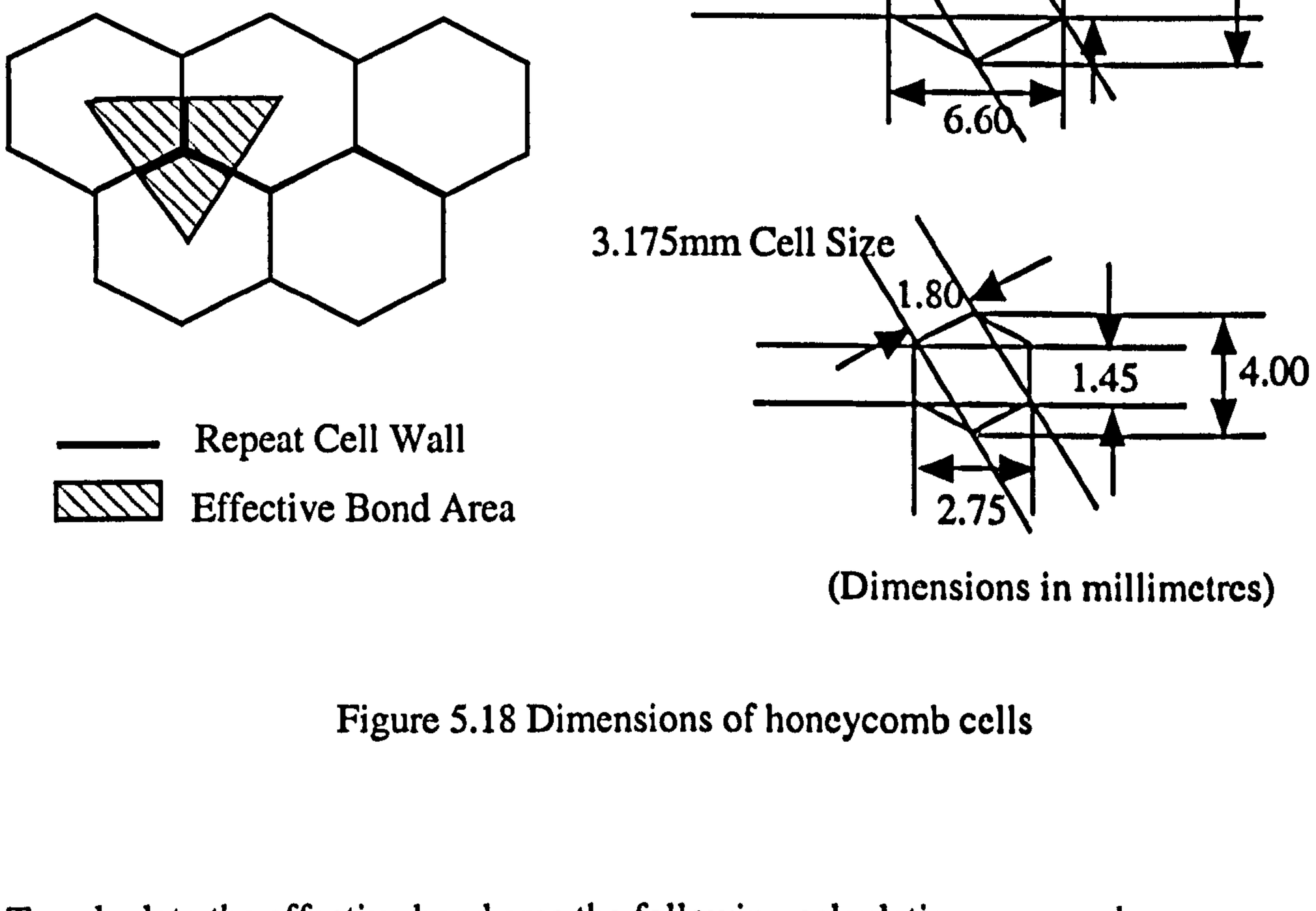

Figure 5.18 Dimensions of honeycomb cells

To calculate the effective bond area the following calculation was used: -

Effective cell wall length (3.175mm) = (3.30/2) + 2(2.05) = 2.525mm

Effective cell wall length (6.35mm) = (1.45/2) + 2(0.90) = 5.750mm

Effective bond area (3.175mm) = (0.5(6.60 x 8.50) = 5.50 mm^2

Effective bond area (6.35mm) = (0.5(2.75 x 4.00) = 28.05 mm^2

Therefore ratio of effective bond area to cell wall length for 3.175mm: 6.35mm was 2.24: 1. It was hoped that a correlation could be found between this ratio and the interfacial fracture toughness values as discussed above, but due to the problems encountered this was not possible. Based on the above ratio the G value for the 3.175mm (1/8") cell specimens would be in the region of 800 Jm^{-2}.

5.5 Effect of Sandwich Panel Skin Tearing on Energy Absorption

5.5.1 Introduction

As reported in Section 4.1 one of the energy absorbing mechanisms seen when crushing sandwich panels and cruciforms was tearing of the faces. The tearing was caused because of the need in various crush rigs to support the specimen with knife-edges whilst it was crushed. During crushing, friction can occur between the faces and the knife-edges. If the friction became too great tearing occurred. The contribution of tearing to the overall energy absorbed in a given test is investigated in this section.

5.5.2 Test Specimen and Procedure

The sandwich panels used were manufactured to the same configuration as the DCB and climbing drum specimens but had the larger 6.35mm cell size. Three widths of specimen were tested; 35, 55 and 100mm. All the specimens were 75mm in height and had saw-tooth triggers (Section 3.5) machined into them.

The specimens were crushed in a Boeing compression after impact rig (Figure 5.19). All the specimens were crushed trigger upper most, at a rate of 1mm min^{-1}, using a 20mm thick flat steel bar. The CAI rig was clamped to the bottom platen of an Instron universal test machine fitted with a 10kN load cell. Load and displacement data were recorded for all the specimens. The energy values quoted below were for 25mm of platen displacement.

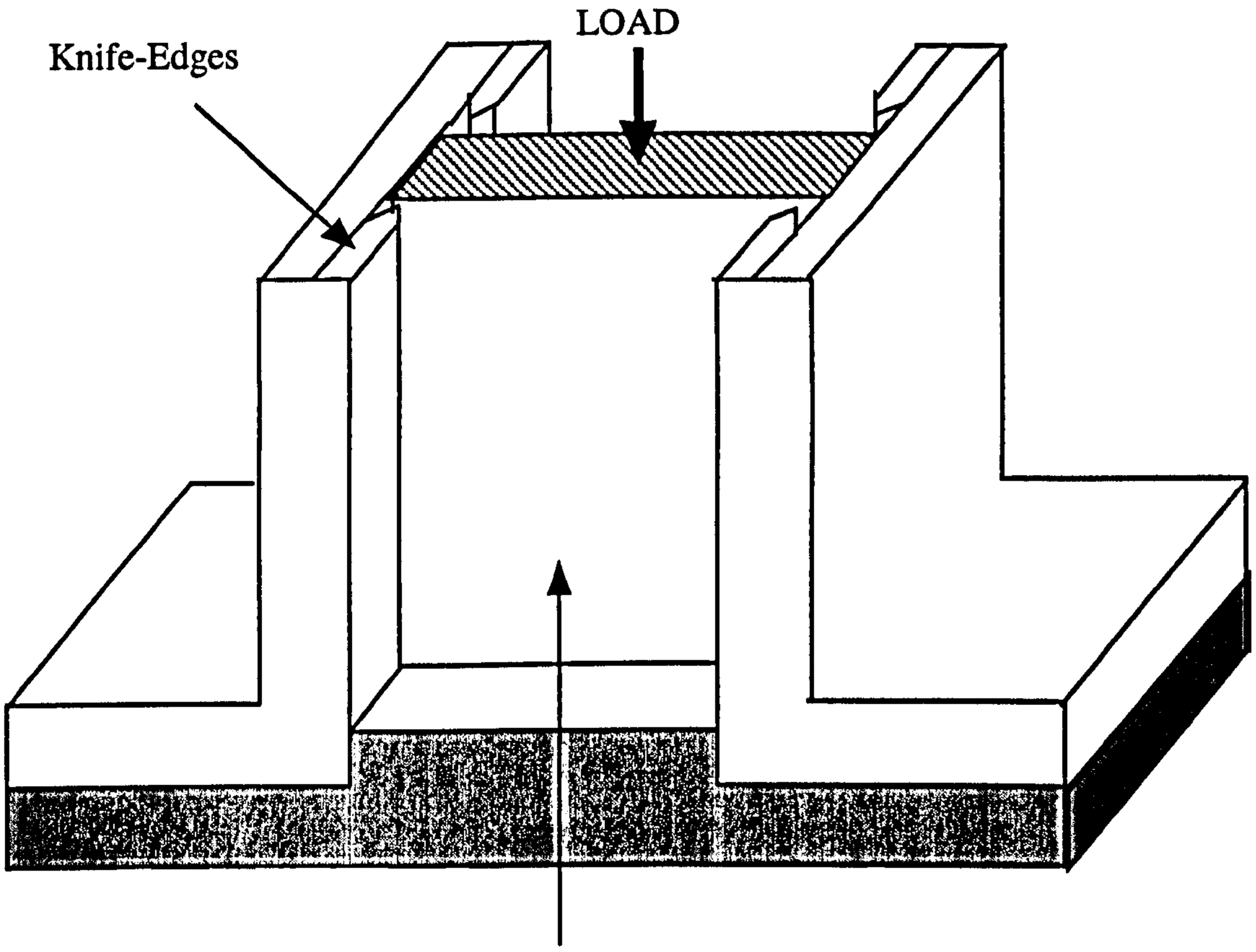

Figure 5.19 Boeing compression after impact rig

5.5.3 Results and Discussion

All the specimens exhibited four distinct tears in their faces, with the region of the sandwich panel supported inside the knife-edges remaining uncrushed. A graph of energy absorbed versus specimen width was plotted (Figure 5.20). Extrapolating back to the horizontal axis at zero width yielded the result that the energy absorbed just in the tearing of the skins was 96 Joules. For each specimen there were four separate tears and as the data was for 25mm displacement, 0.96 Joules/mm^2 were absorbed per tear. A typical load-displacement curve is shown in Figure 5.21. The results are detailed in Table 5.4.

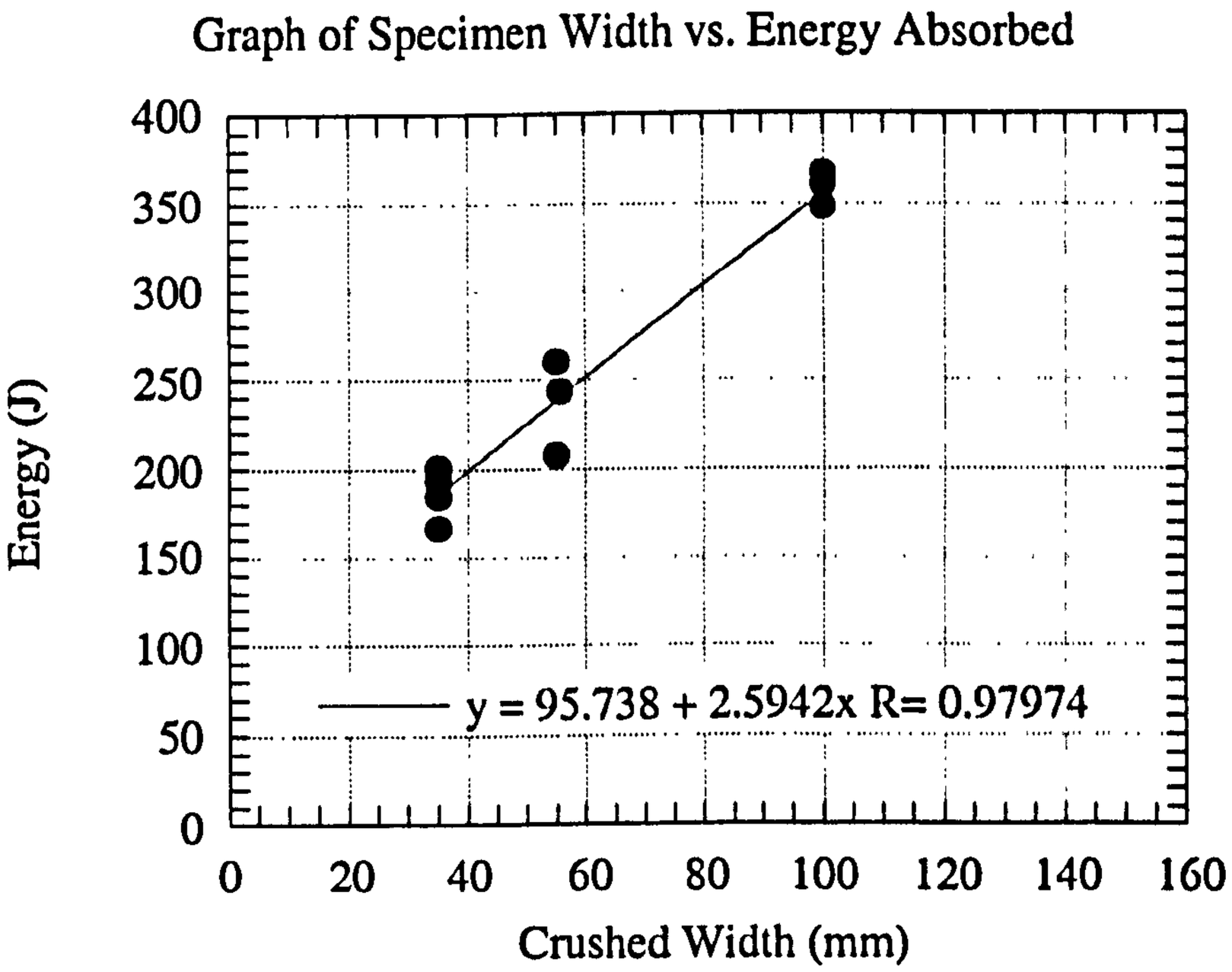

Figure 5.20 Graph of specimen width vs. energy absorbed

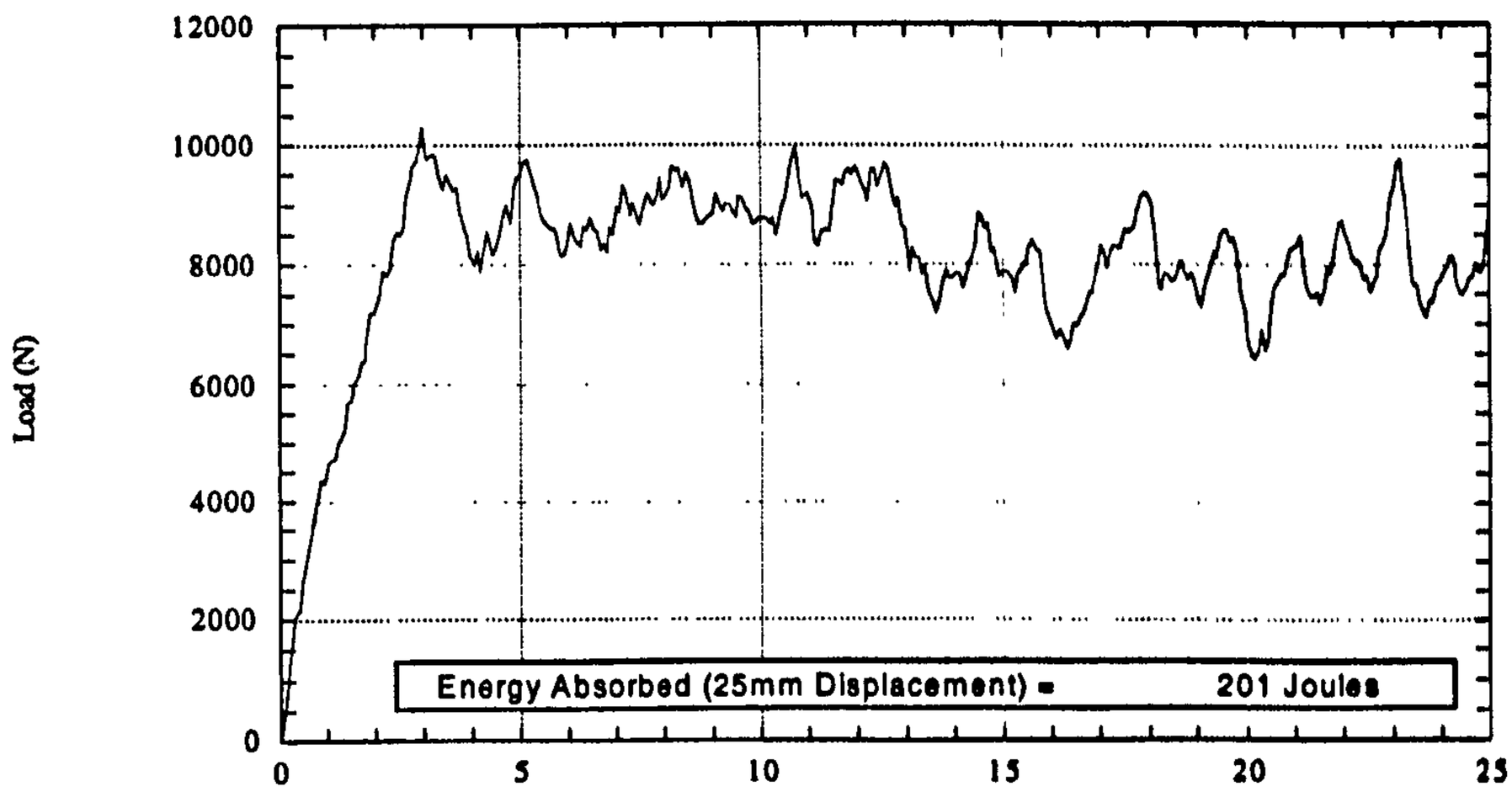

Figure 5.21 Load-displacement curve for 35mm wide panel

5.6 Angle Stiffener Crushing

The carbon fibre composite angle sections used to stiffen the sandwich cruciforms were separately crushed. Four stiffeners were arranged as shown in Figure 5.22 and crushed using a flat plate attached to an Instron universal testing machine at a crush speed of 1mm/min. To support the angle stiffeners during testing one end was potted in a mixture of epoxy resin, chopped glass fibres and aluminium powder. Prior to potting, both ends of the stiffeners were ground flat to ensure that the load was introduced evenly to the specimen. The stiffeners, although placed back-to-back with each other, were not bonded together, apart from where they were submerged in the potting resin. It was thought that the stiffeners would behave more like they would in the cruciform structure in this configuration. The angle sections failed by buckling, the reason for this failure mode was probably due to the fact that they were not bonded together, each stiffener being able to buckle and move away from the other stiffeners.

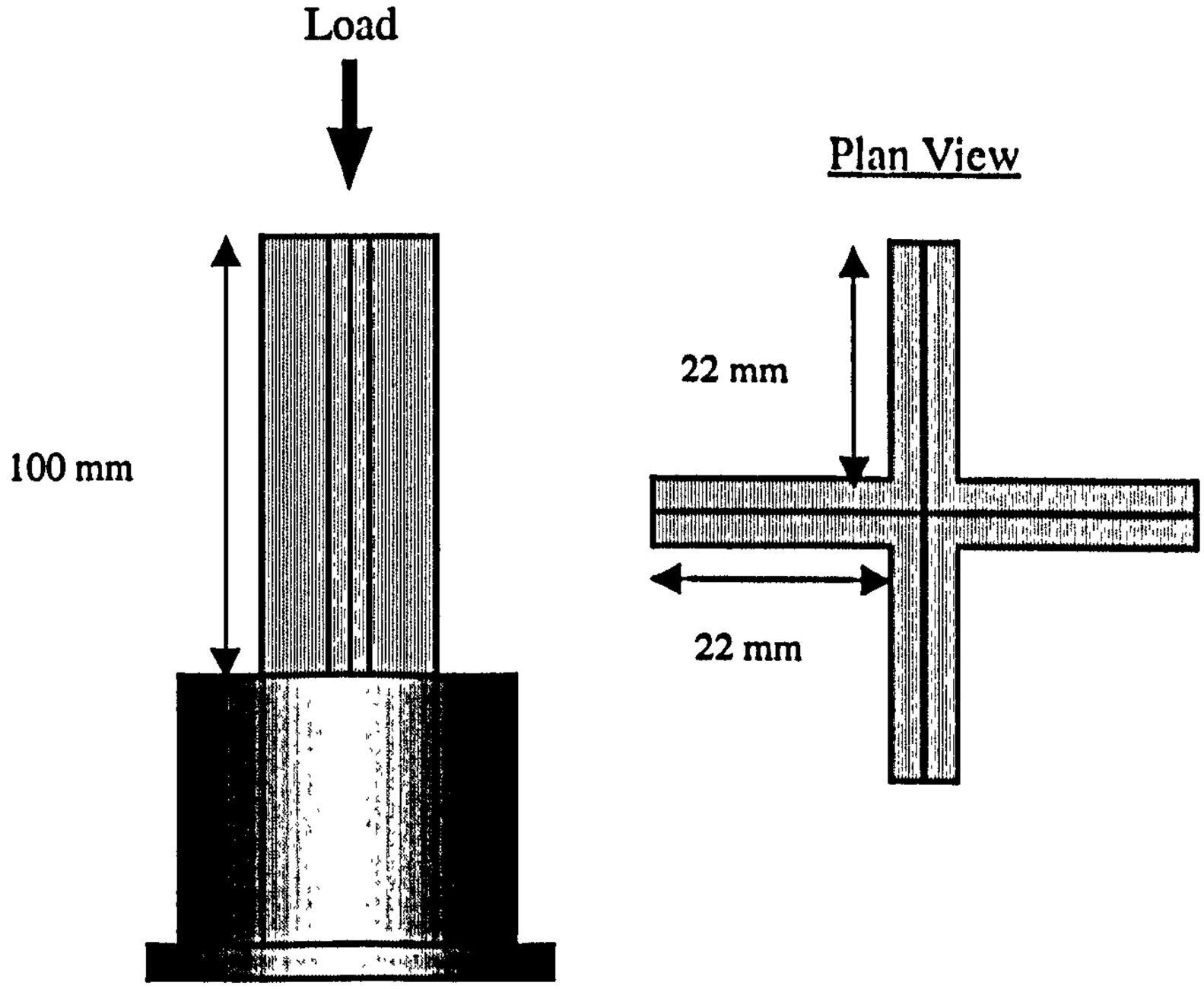

Figure 5.22 Angled stiffeners

As can be seen from the load - displacement curve (Figure 5.47) the peak load was high, a value of 70.6kN being recorded. The reason for this was that the ends of the stiffeners were not chamfered. After the peak load had been reached the stiffeners failed by buckling, the top 40mm of the stiffeners bent over and a large drop in load carrying capability was seen, the load dropping to 6kN. The load recovered again to a maximum value of 32kN, but after this it gradually decreased as the stiffeners crushed and delaminated until the test was stopped. The energy absorbed by the stiffeners crushing by 40mm was 883 Joules.

5.6.1 Chamfered Angled Stiffener Crushing

A new identical set of stiffeners was manufactured but this time the ends of the stiffeners were chamfered. The stiffeners were ground so that their thickness reduced from 2mm to zero over a distance of 10mm. The other end of the stiffeners were ground flat and potted as described in the previous section. The load-displacement curve is shown in Figure 5.48. A peak load of 31.1kN was reached, this being greatly reduced from the un-chamfered stiffeners. As previously, a large drop in load was recorded, the load dropping to a value of 15.5kN. The load recovered to a value of 39kN. The stiffeners gradually crushed and delaminated, the load decreasing as this happened, no buckling was observed. From the load-displacement graph it was calculated that the chamfered stiffeners absorbed 915 Joules in 40mm of crushing.

5.7 Conclusions

To conclude, this chapter reported on the failure modes of face skin specimens and also on several additional tests that were used to quantify energy absorbing mechanisms that were seen in the crushing of the sandwich panels, and more extensively in the in-plane crushing of the cruciform structures.

Un-triggered small specimens with various unsupported lengths and stacking sequences were subjected to in-plane crushing. The mode of failure, peak load, plateau stress and the energy absorbed were recorded. It was noted that the plateau stress for the various configurations tested were always higher than the stresses in the individual faces of the sandwich panels.

It was decided to crush two of the small specimens together in a "back-to-back" configuration so that the pair of specimens supported each other as they crushed, similarly to the support seen in a sandwich panel.

Initially, problems were encountered in aligning the "back-to-back" specimens so that both specimens crushed identically, and the resulting plateau stresses were still high compared with the crushing sandwich panel faces. The technique used to align the specimens was improved, and more specimens were crushed. With the improved alignment the pairs of specimens crushed in a similar manner to the sandwich panel faces and the plateau stresses were also similar; some pairs crushed with a lower plateau stress. The face skin specimens failed in a similar manner, and recorded similar crushing stress to the sandwich panels tested. We are therefore able to say that the "back-to-back" specimens could be used to study the face-skin failure modes seen in sandwich panel faces, without having to go to the time and expense of manufacturing sandwich panels.

The tests used to measure the skin-to-core bond strength were only partially successful in establishing the interlaminar bond strength for the two sizes of honeycomb cell size used. There was a good correlation between the fracture toughness results obtained for the 6.35mm cells using both the DCB and climbing drum methods. The results from the tests undertaken on the 3.175mm sized cells were, however, not conclusive. The smaller cells adhered more strongly to the faces of the sandwich panel and the failures seen were a mixture of skin-to-core debonding and face delamination, yielding erroneously large fracture toughness values.

The effect of face tearing on the energy absorbed by a sandwich panel was quantified, the various widths of panel producing consistent tears under in-plane compressive loading and it was possible to calculate the quantity of energy absorbed by this process.

The angled stiffeners, both chamfered and un-chamfered, were crushed and their load -displacement characteristics detailed. The stiffeners failed through buckling in conjunction with extensive delamination and fibre crushing.

Peak Load(kN)		Energy Absorbed (J) (2.5mm Disp.)		Mean Crush Load (N)	
Normal 5mm Unsupported Length $(-45°, 0°, 90°, +45°)_s$					
Average	Std.Dev.σ	Average	Std.Dev.σ	Average	Std.Dev.σ
2.60	0.36	1.96	0.27	567	124
5mm Unsupported Length, Load Plate Friction $(-45°, 0°, 90°, +45°)_s$					
Average	Std.Dev.σ	Average	Std.Dev.σ	Average	Std.Dev.σ
5.08	0.77	3.76	0.16	877	52
5mm Unsupported Length, Stacking Sequence $(+45°, -45°, 0°, 90°)_s$					
Average	Std.Dev.σ	Average	Std.Dev.σ	Average	Std.Dev.σ
3.50	0.57	3.17	0.46	796	116

Table 5.1 Effect of stacking sequence and friction on 5mm unsupported length specimens

Peak Load (kN)	Mean Crush Load (N)	Average Stress (MPa)
4mm Unsupported Length $(-45°, 0°, 90°, +45°)_s$		
2.78	572	57
6mm Unsupported Length $(-45°, 0°, 90°, +45°)_s$		
2.72	612	61
7mm Unsupported Length $(-45°, 0°, 90°, +45°)_s$		
2.65	534	53
9mm Unsupported Length $(-45°, 0°, 90°, +45°)_s$		
1.71	302	30

Table 5.2 Typical effect of unsupported length on the crushing characteristics of the face/skin specimens

Peak Load (kN)		Mean Crush Load (N)		Average Stress (MPa)	
"Back-to-Back" Specimens $(-45°, 0°, 90°, +45°)_S$					
Average	Std.Dev.σ	Average	Std.Dev.σ	Average	Std.Dev.σ
5.82	0.69	662	100	32.67	4.67
Sandwich Panels (one face) $(-45°, 0°, 90°, +45°)_S$					
Average	Std.Dev.σ	Average	Std.Dev.σ	Average	Std.Dev.σ
18.56	1.11	3522	452	23.40	3.01

Table 5.3 Crushing data for sandwich panels and 'Back-to-Back specimens

Specimen Width (mm)	Energy Absorbed (J)
35	167
35	194
35	185
35	201
55	208
55	246
55	260
100	348
100	361
100	344
100	368

Table 5.4 Results from Bocing rig

Fracture Toughness G_{Ic} (Jm^{-2})	
<u>3.175mm</u>	<u>6.35mm</u>
(Test 1) 2816	(Test 3) 308
(Test 2) 2850	(Test 4) 320
-----	(Test 5) 381 (Sample Calculation)
-----	(Test 6) 397
Av. 2833	Av. 351

Table 5.5 Fracture toughness results

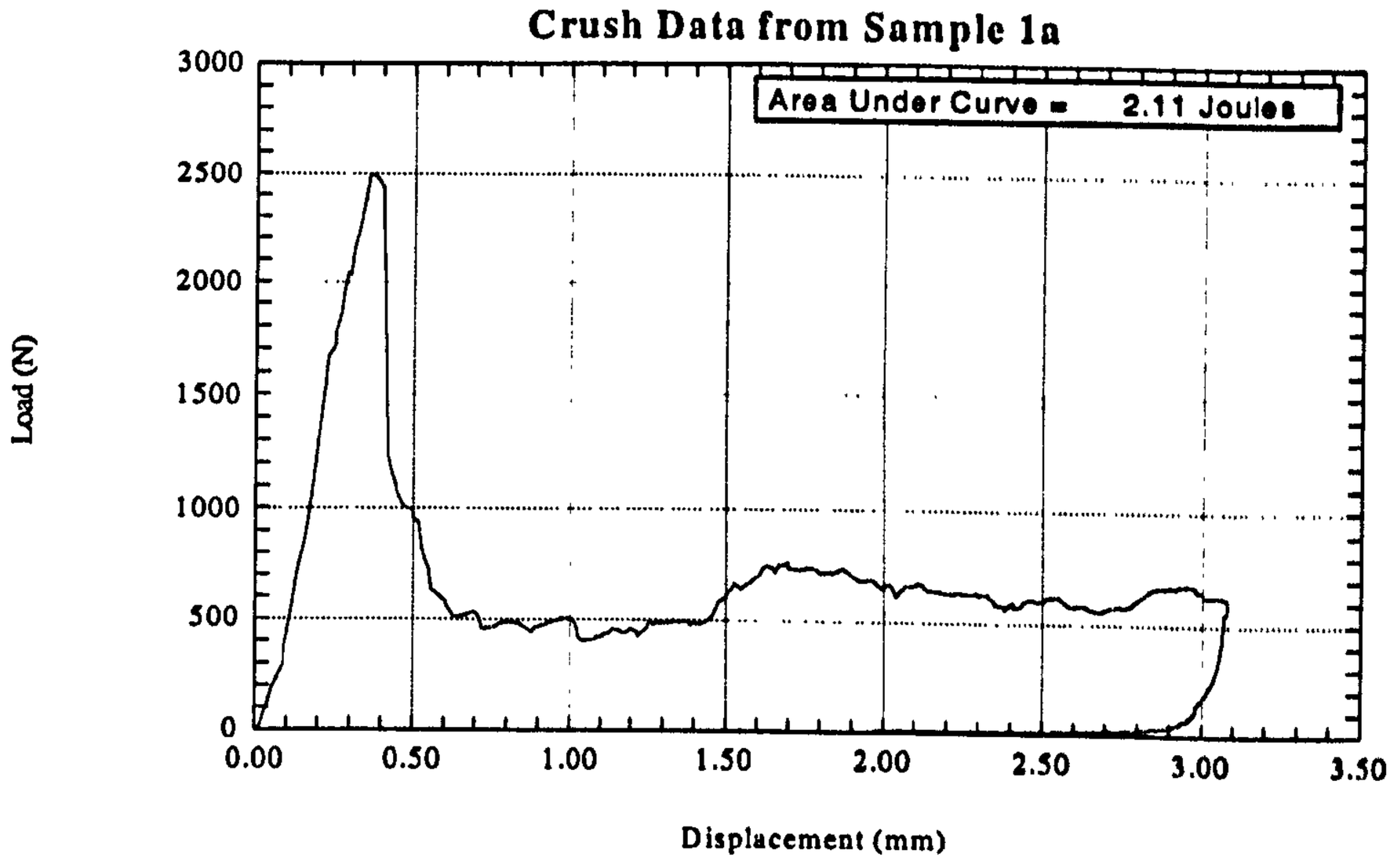

Figure 5.23

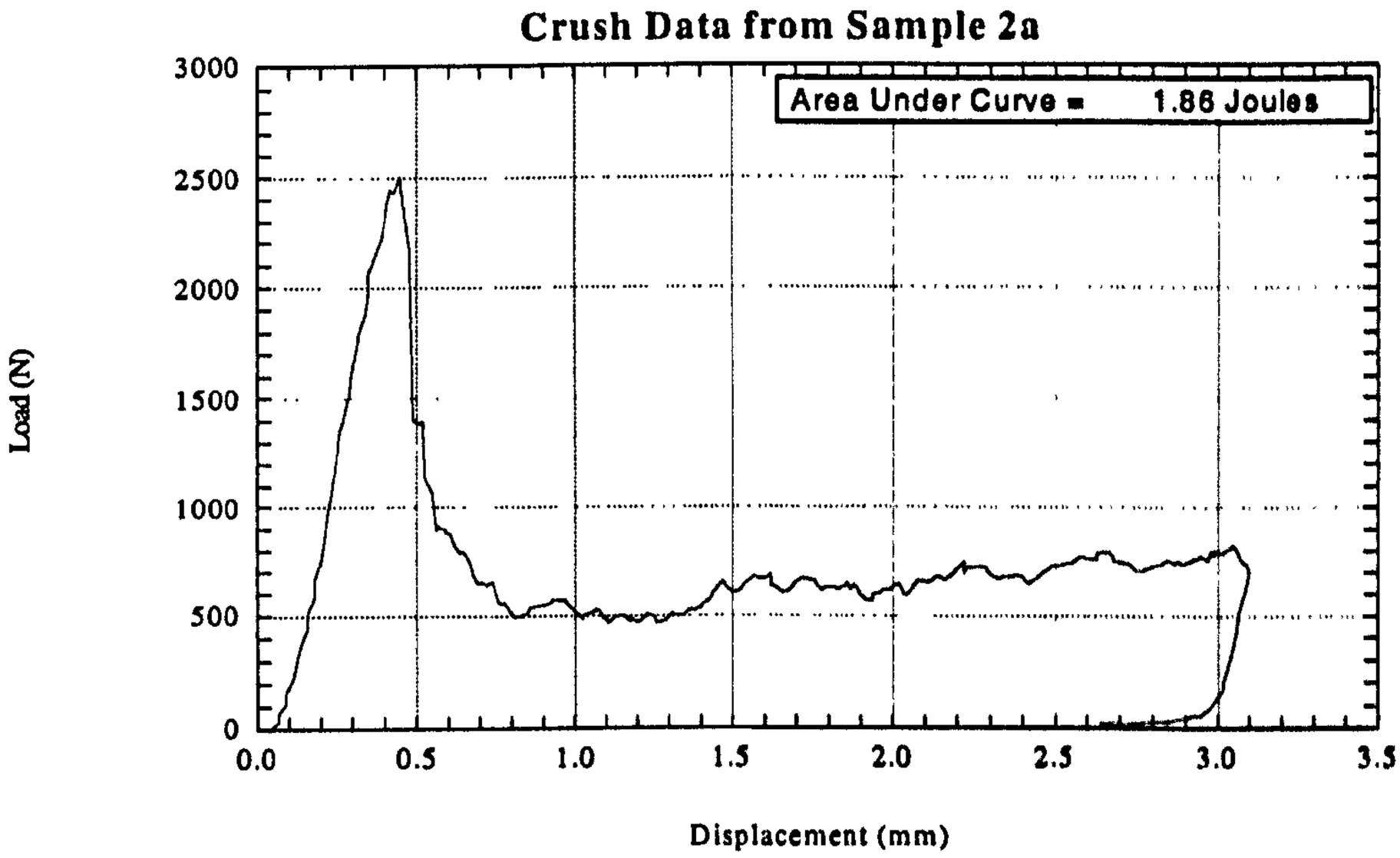

Figure 5.24

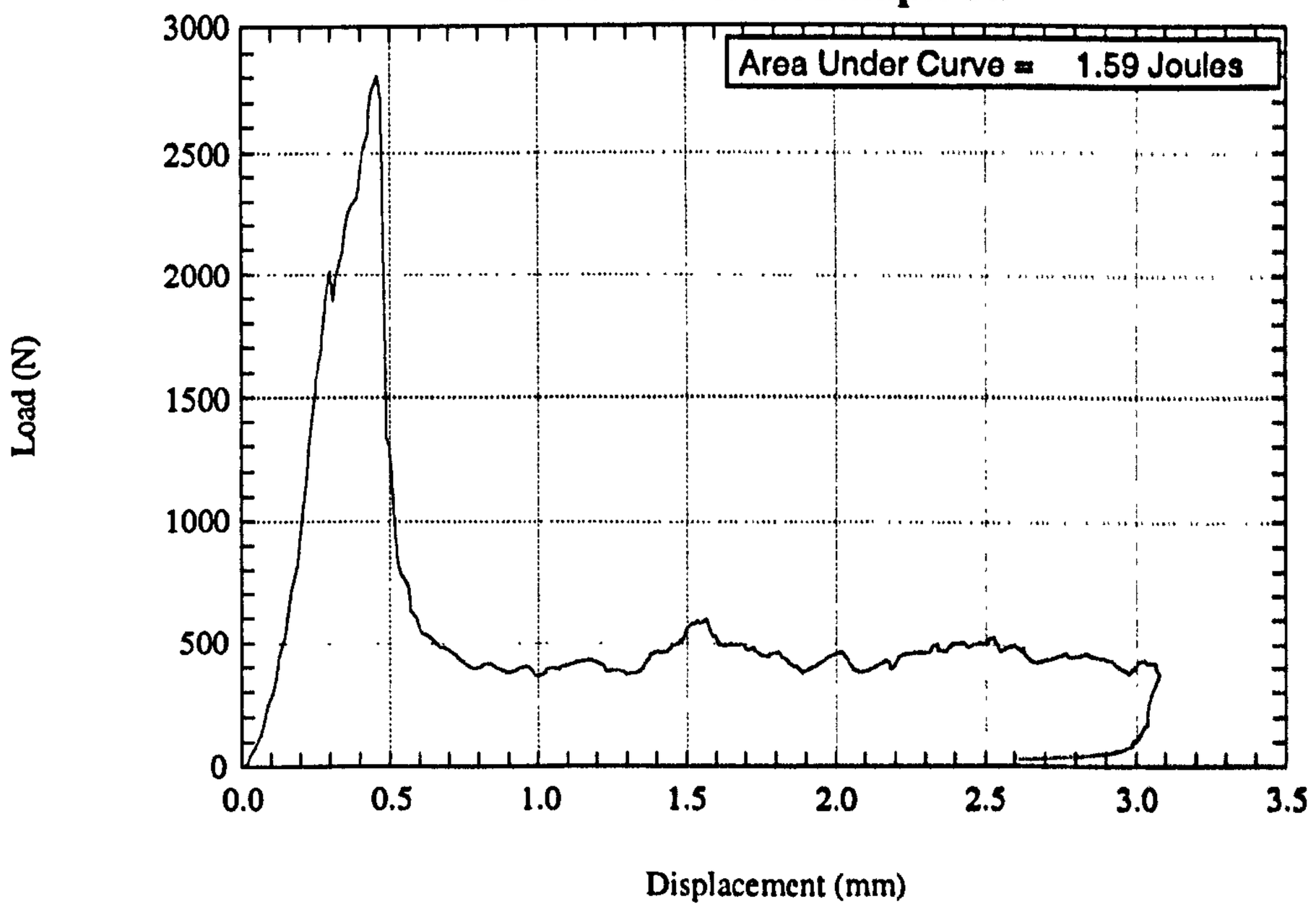

Figure 5.25

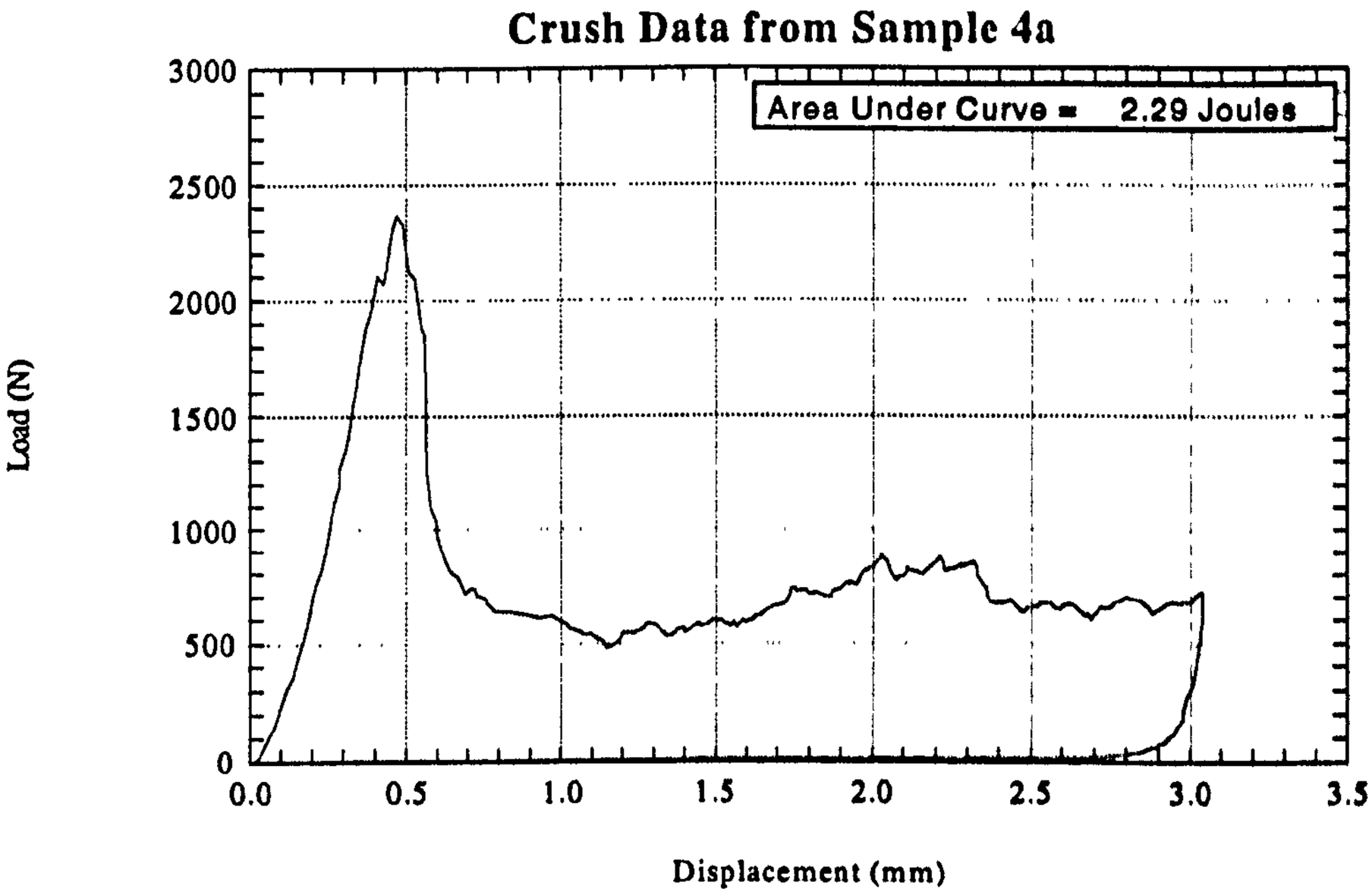

Figure 5.26

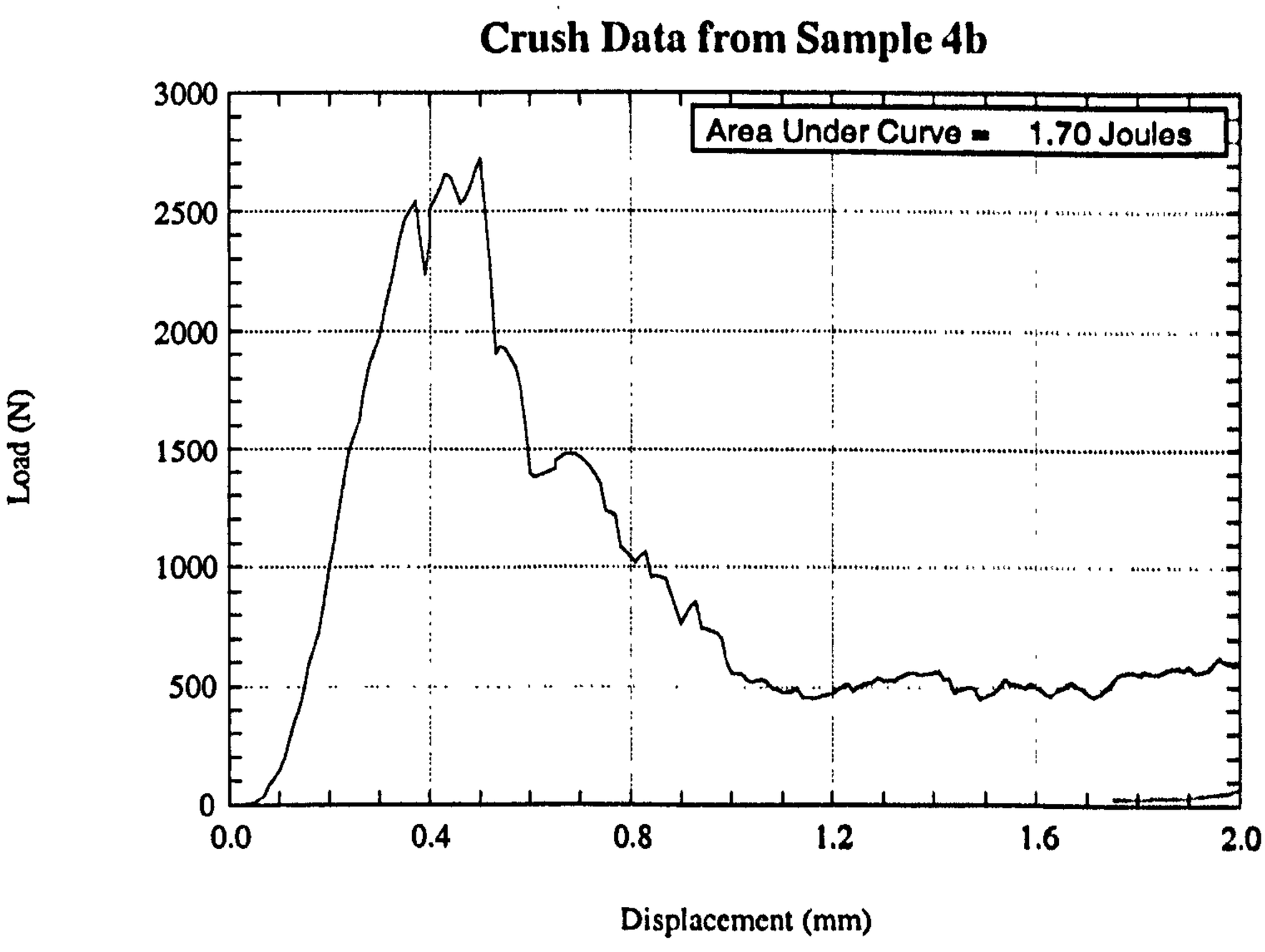

Figure 5.27

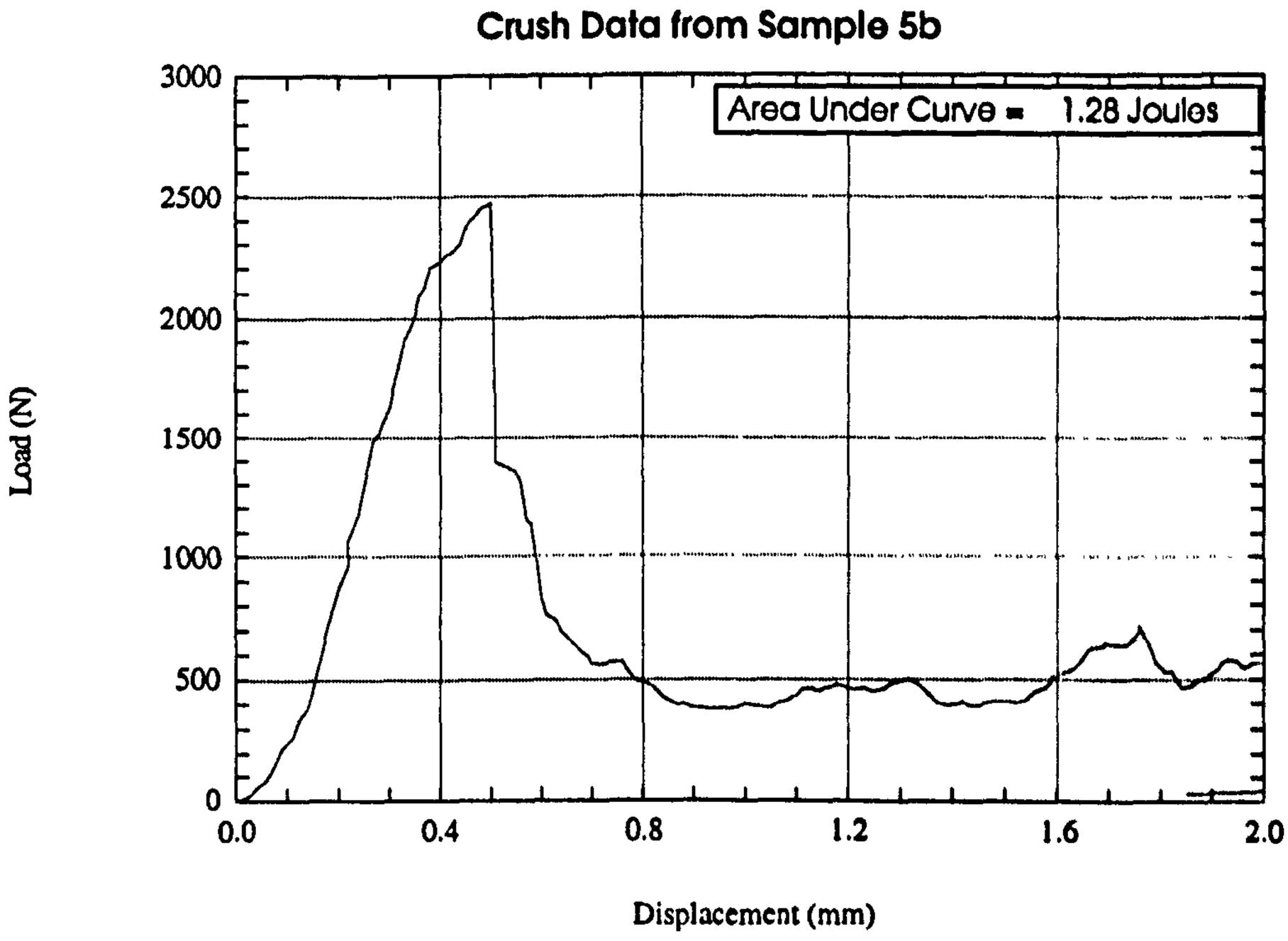

Figure 5.28

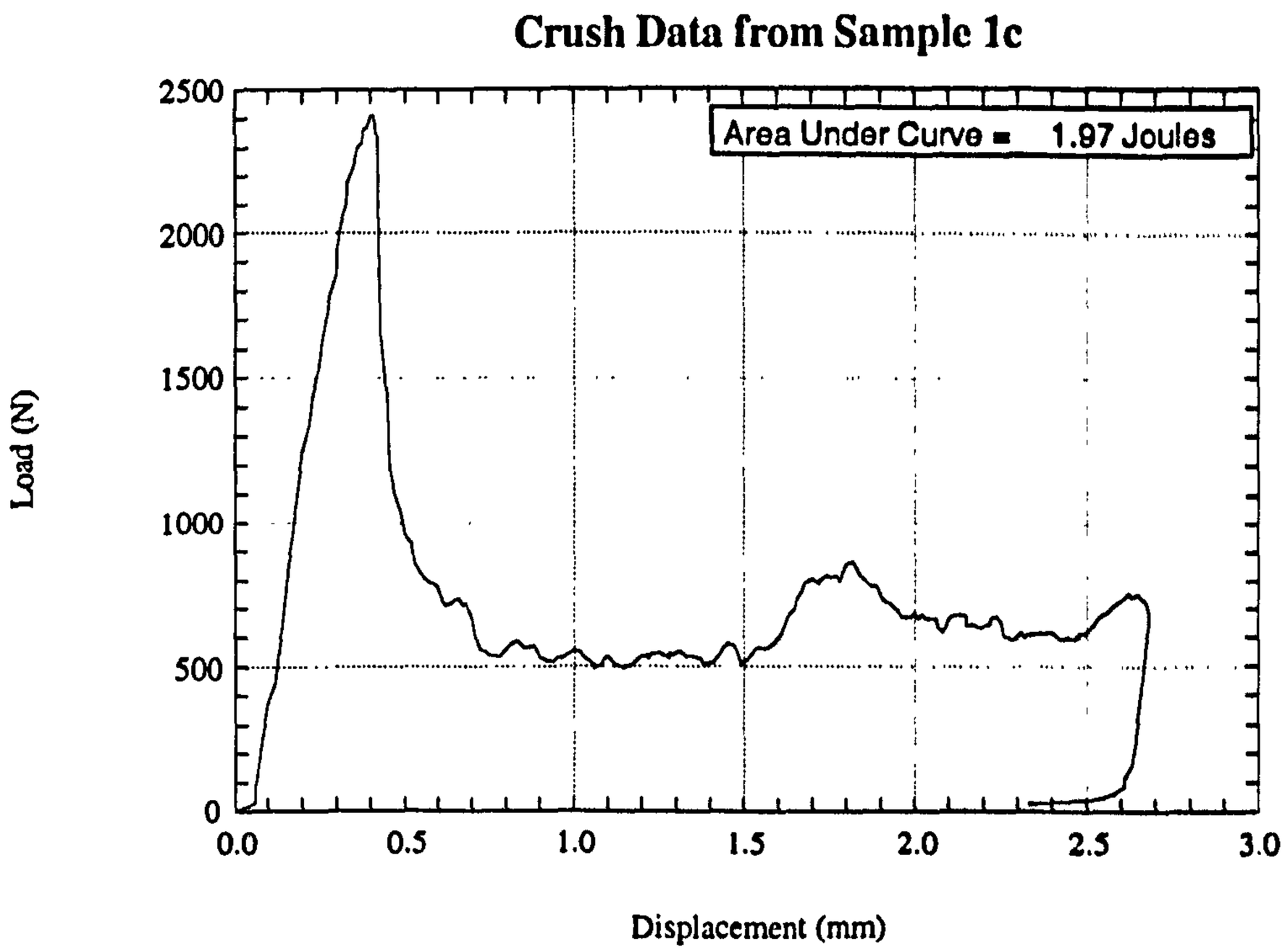

Figure 5.29

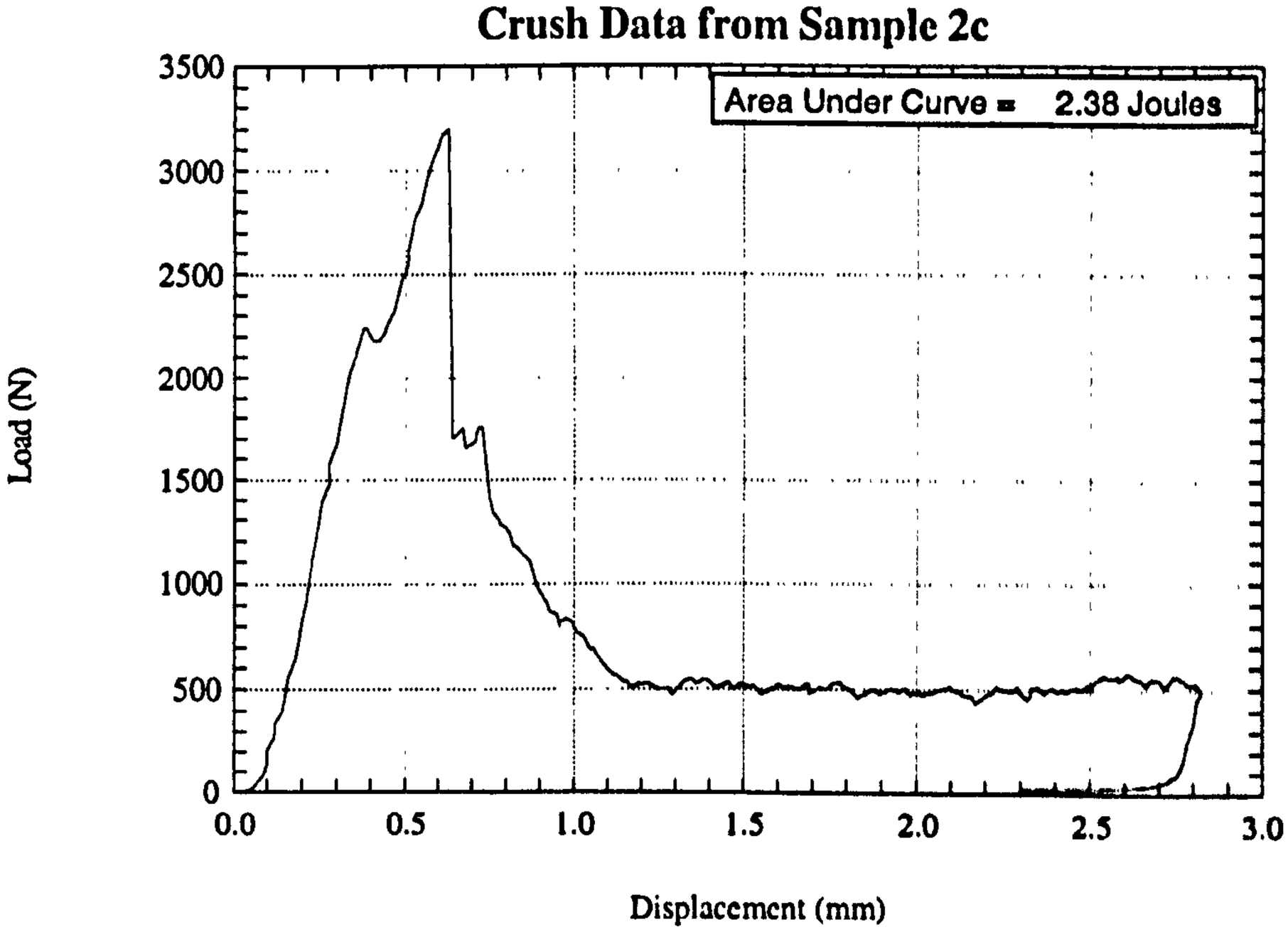

Figure 5.30

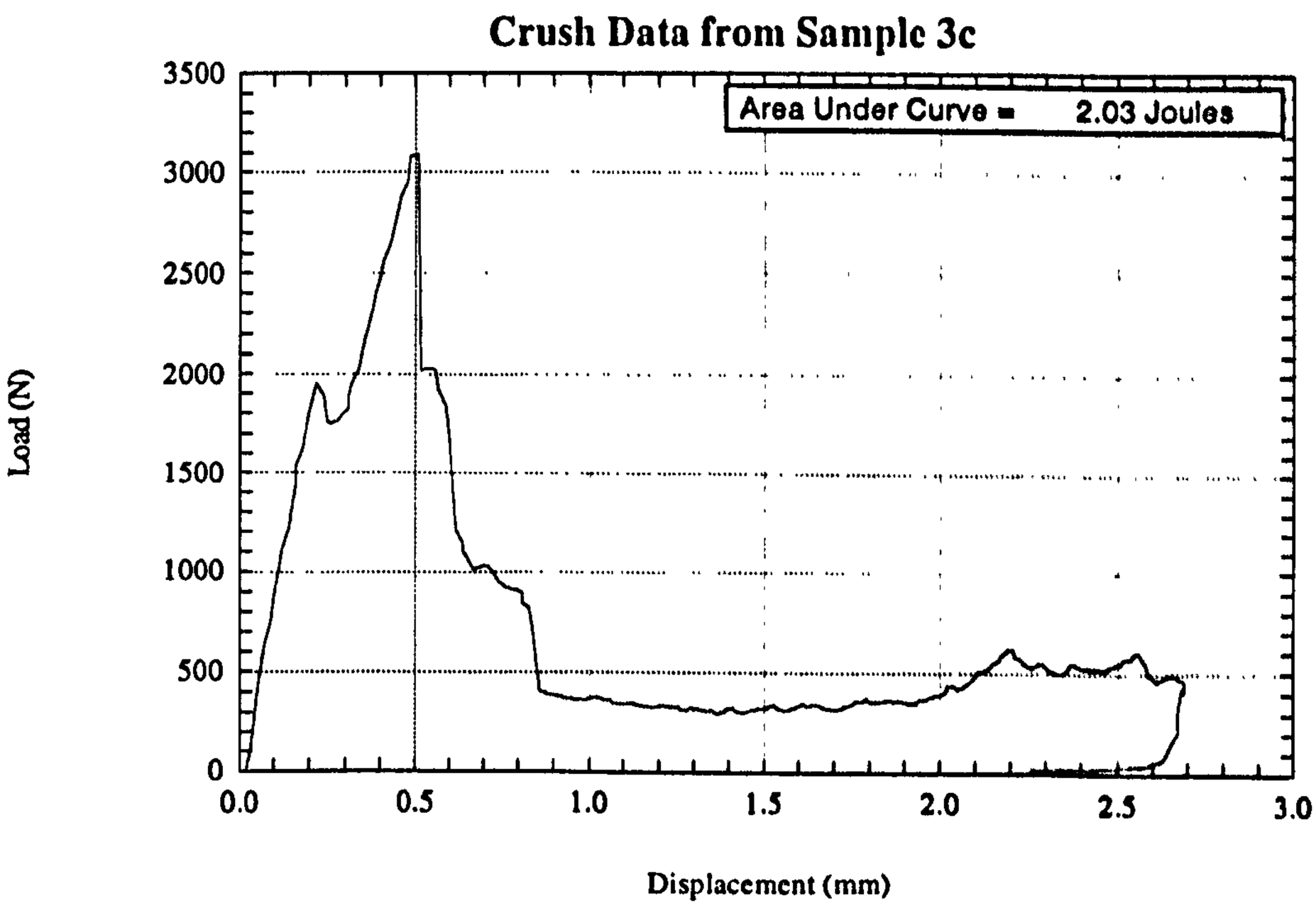

Figure 5.31

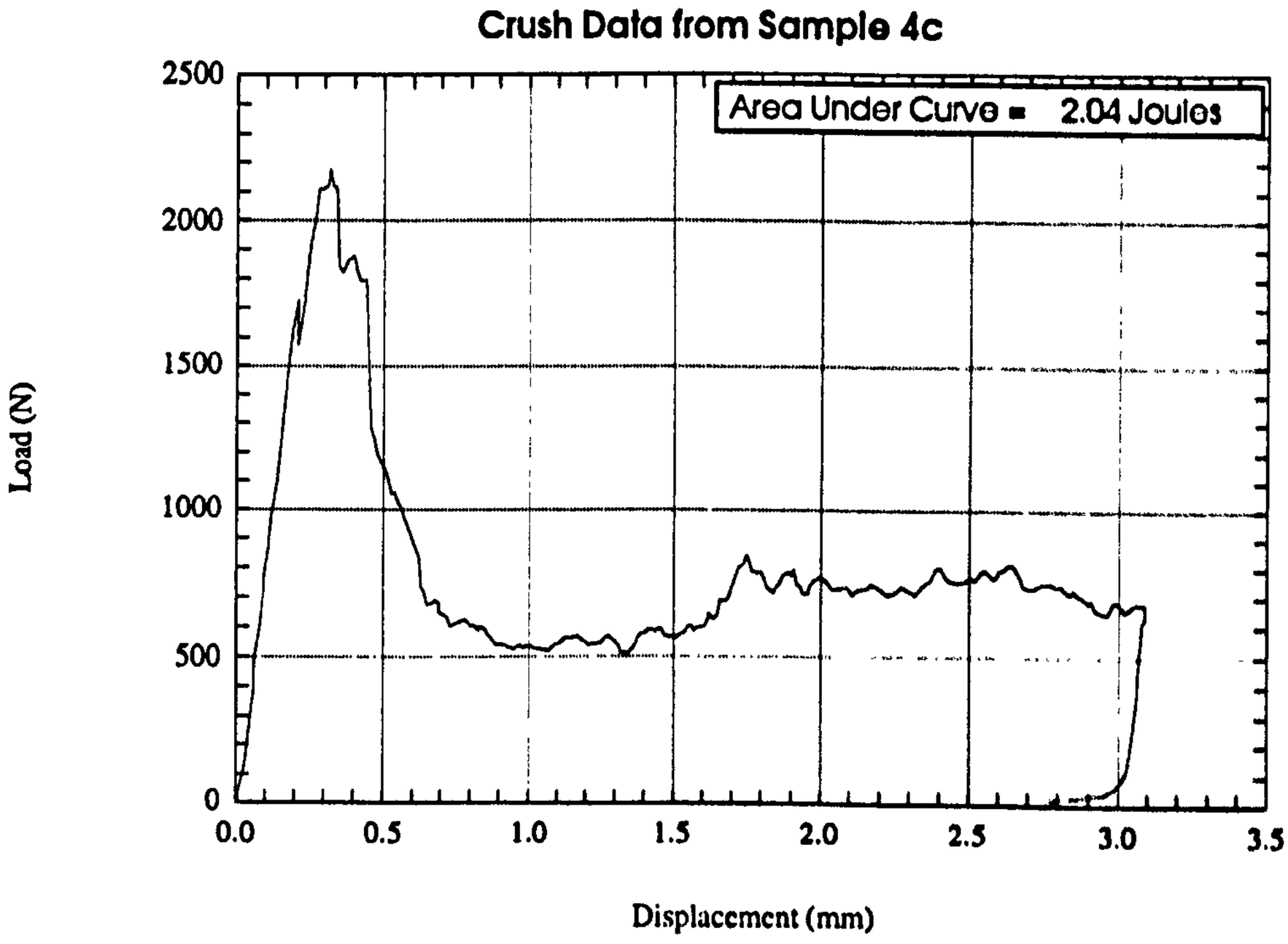

Figure 5.32

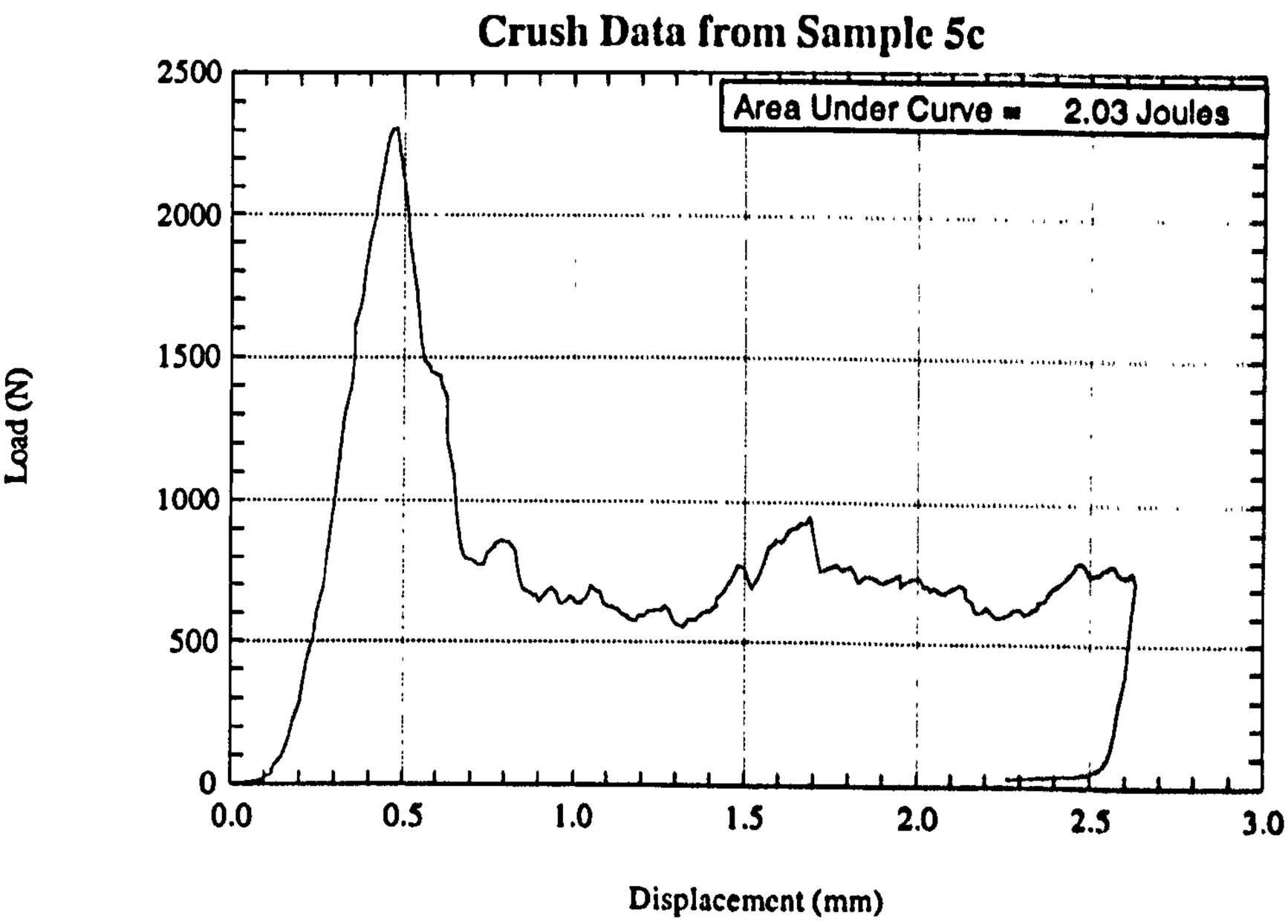

Figure 5.33

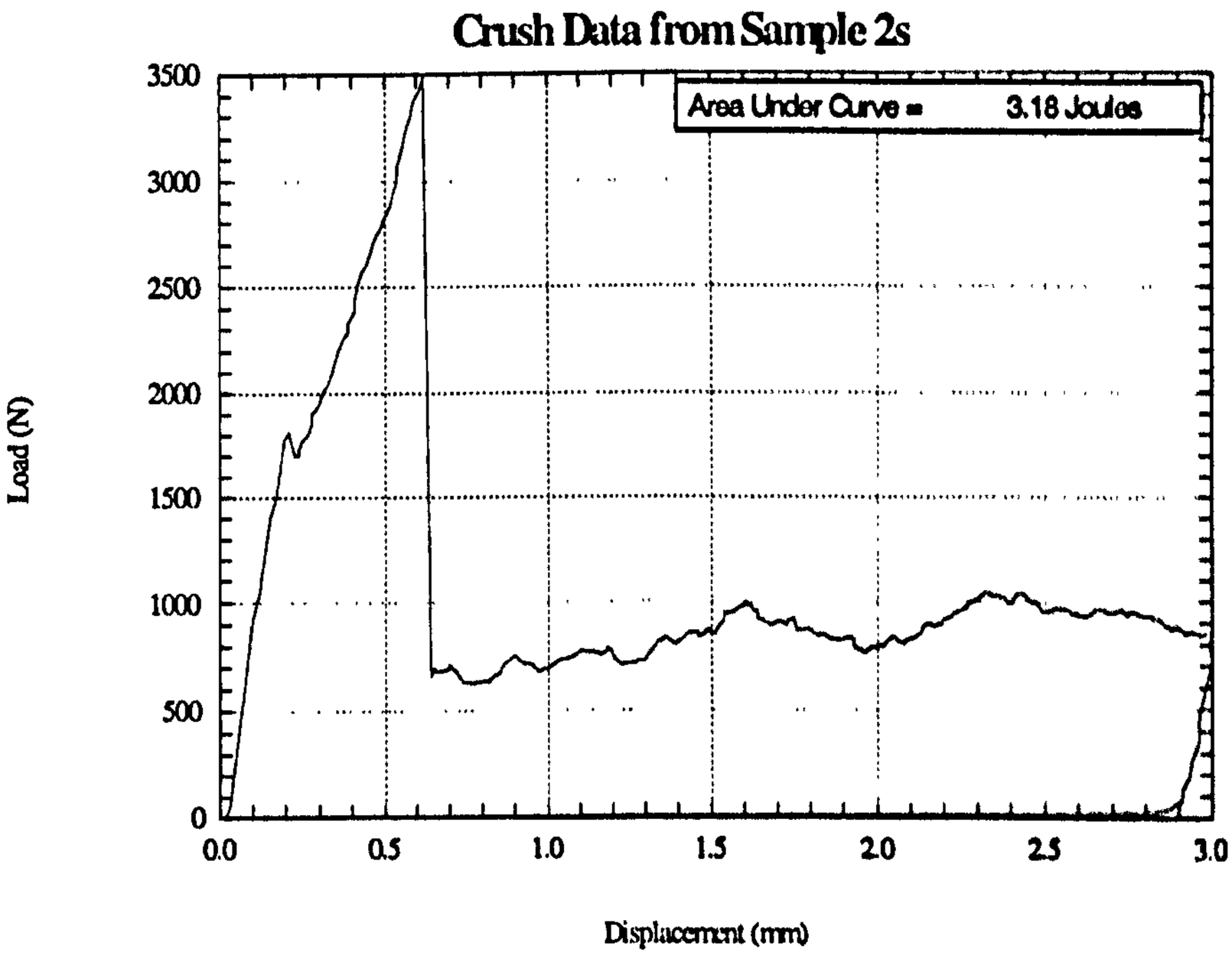

Figure 5.34

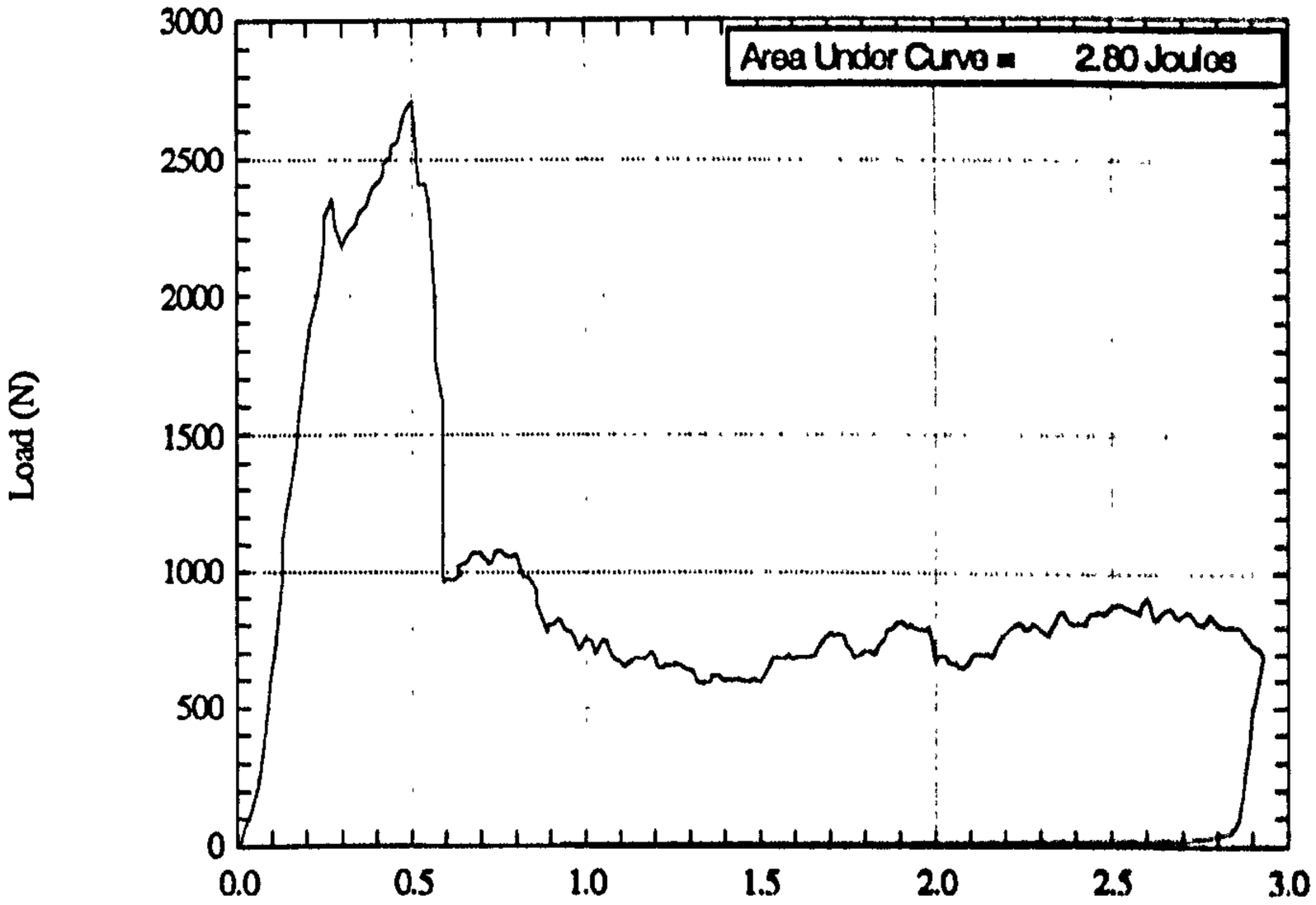

Figure 5.35

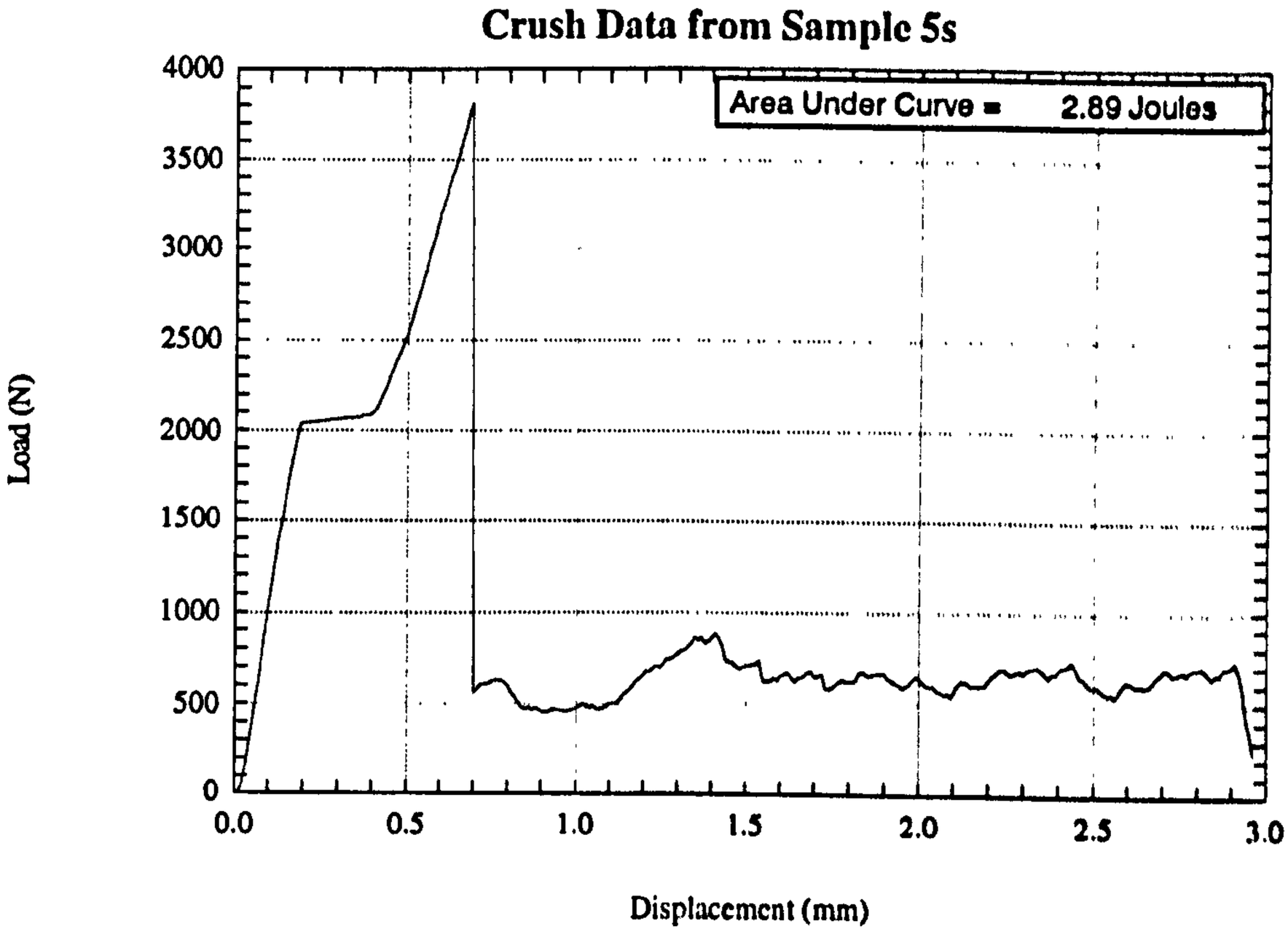

Figure 5.36

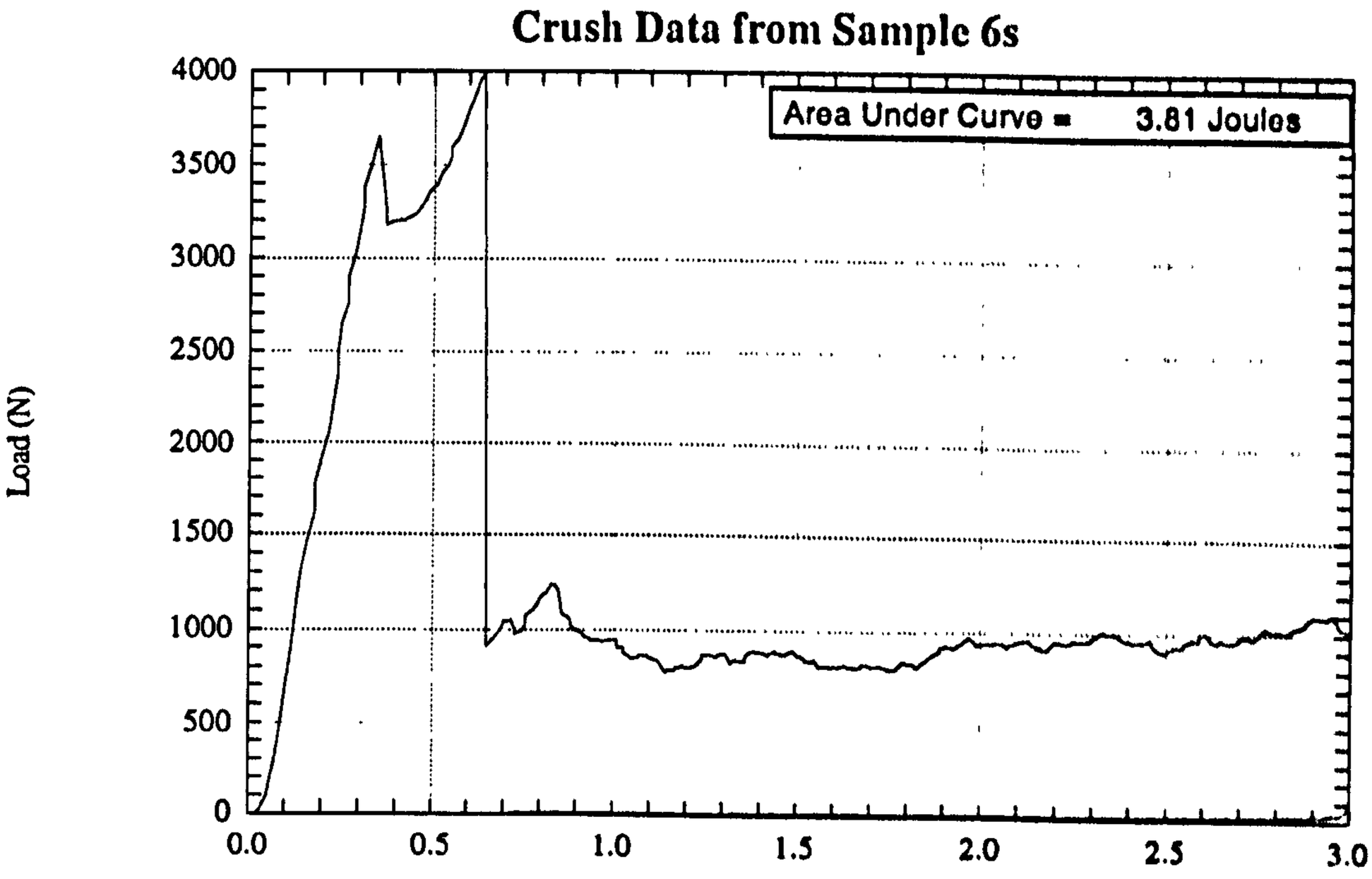

Figure 5.37

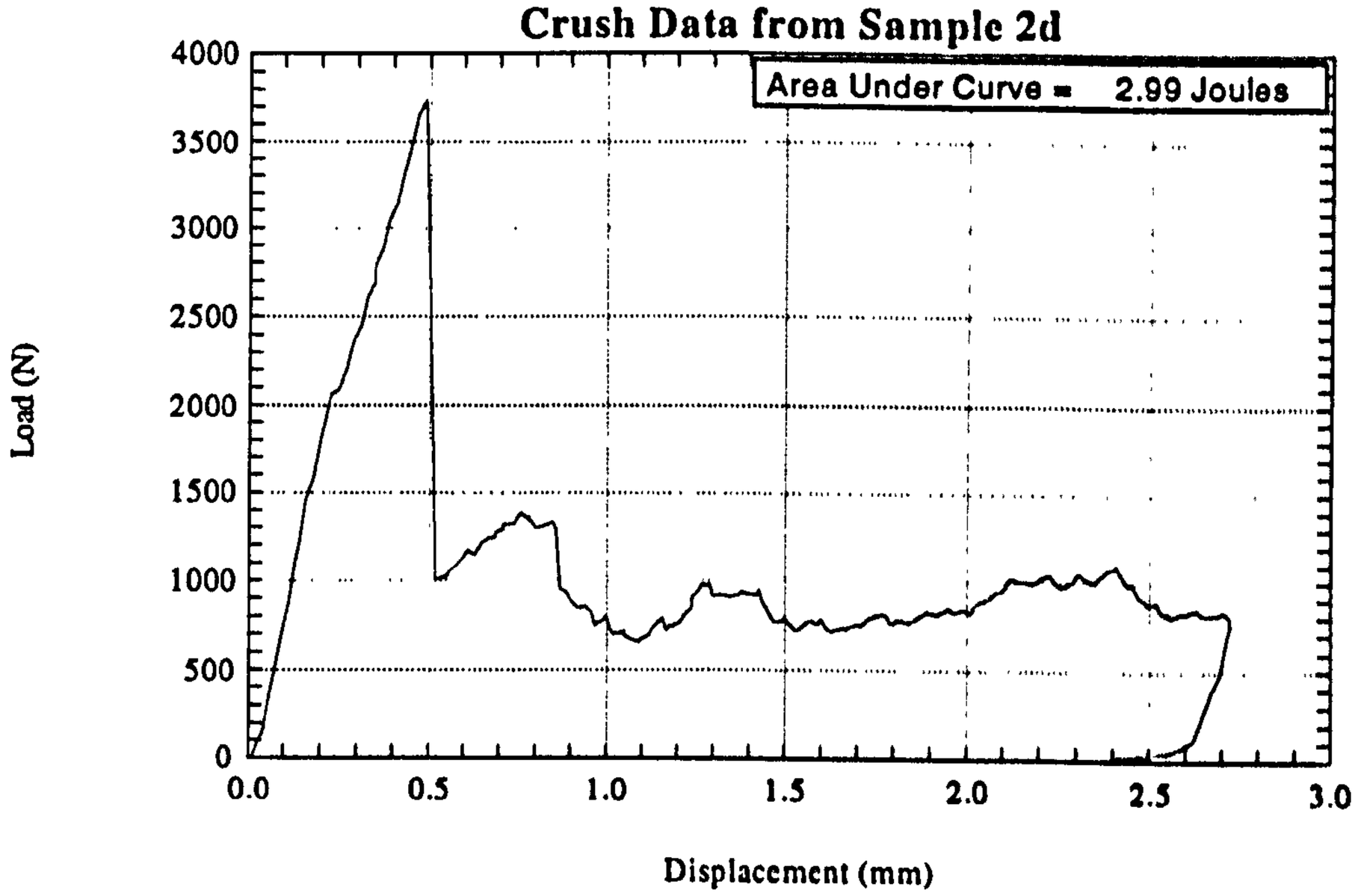

Figure 5.38

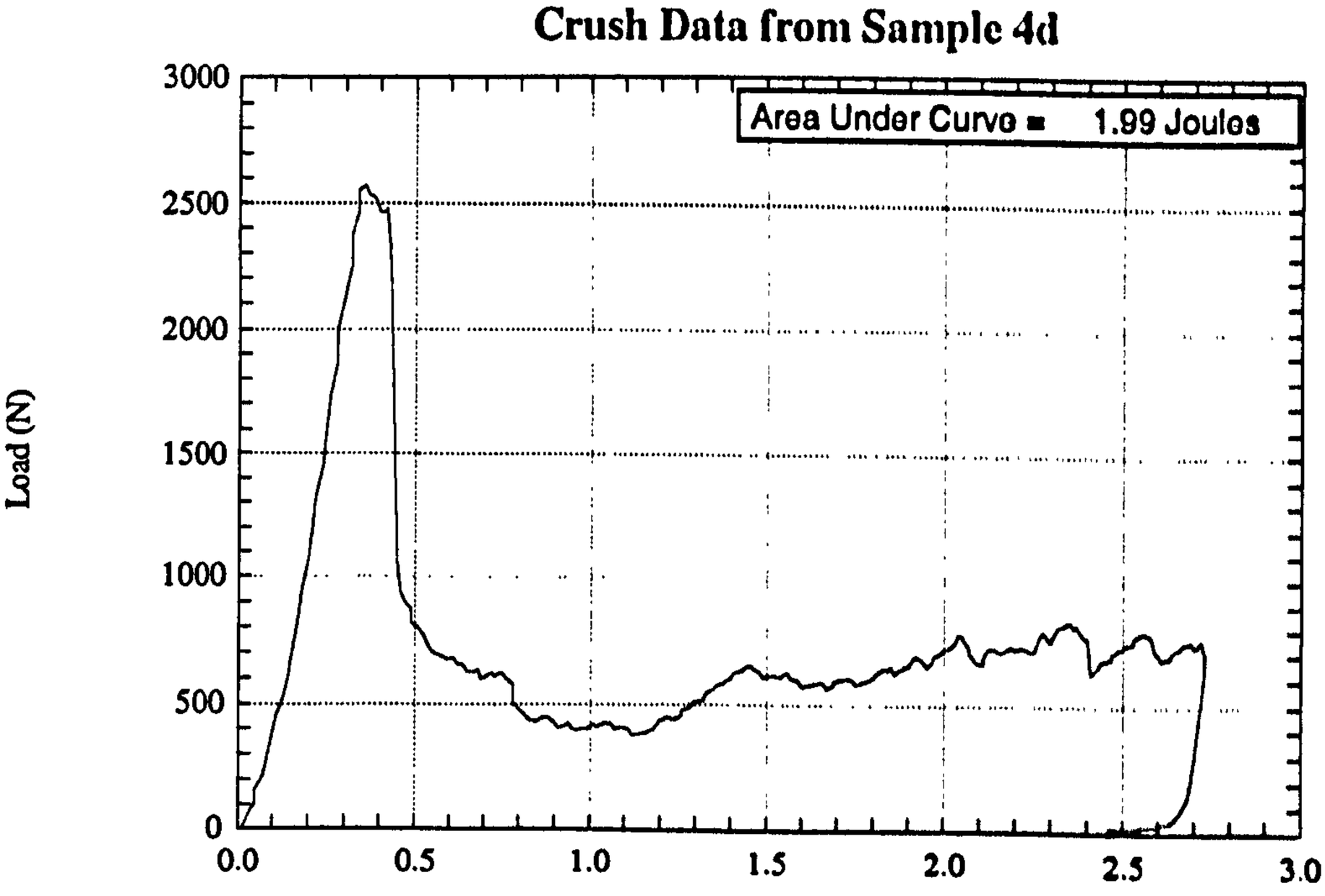

Figure 5.39

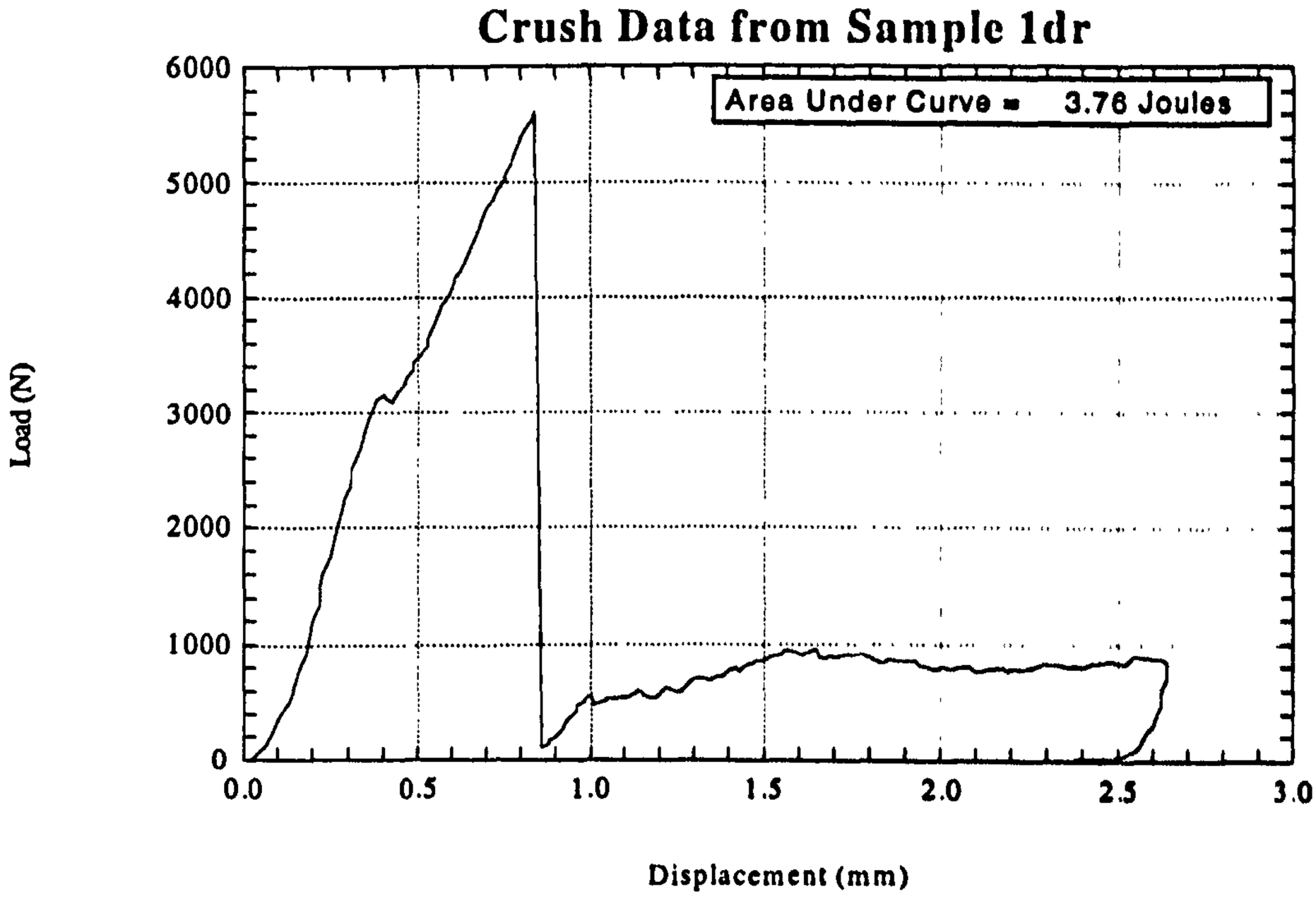

Figure 5.40

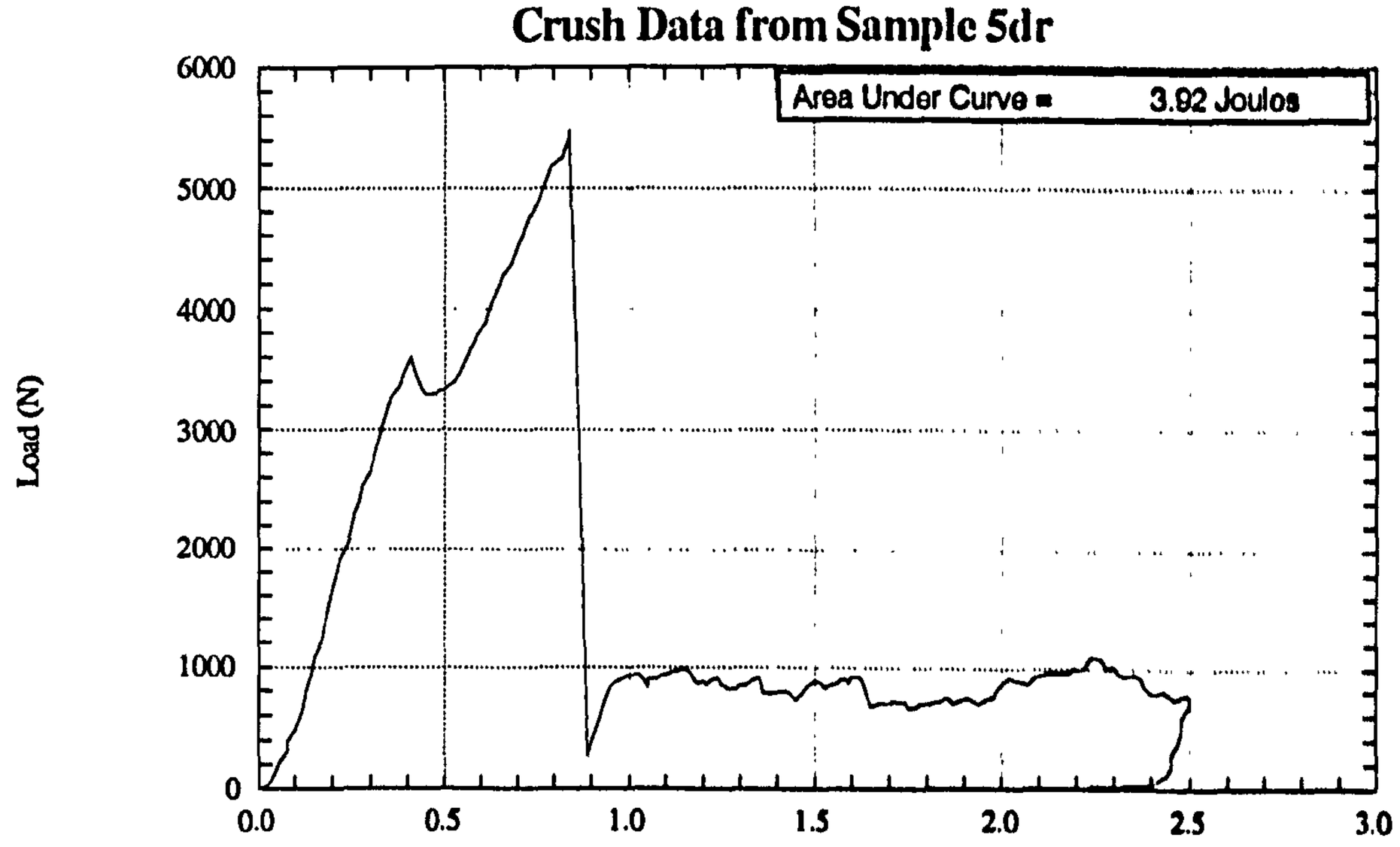

Figure 5.41

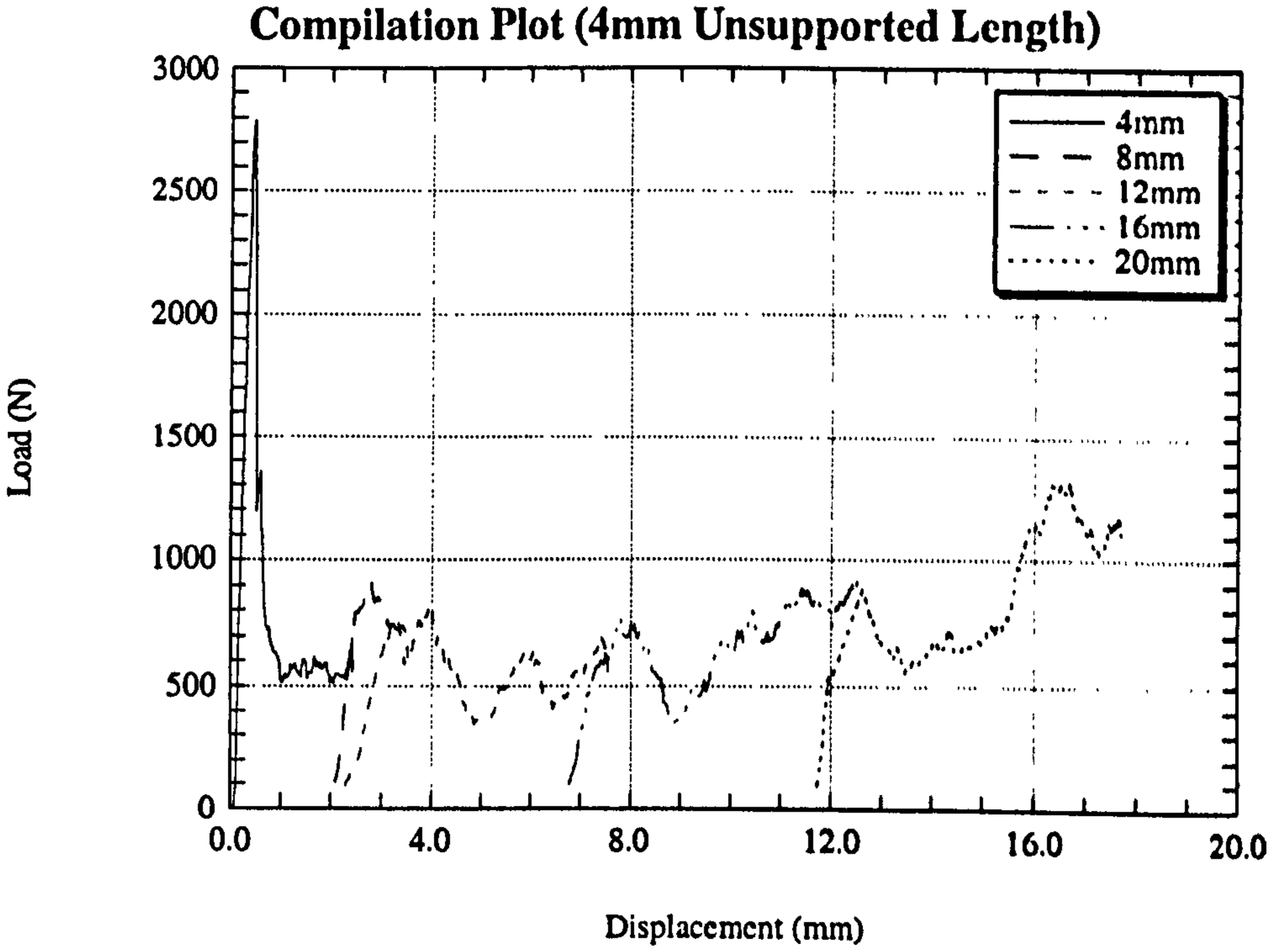

Figure 5.42

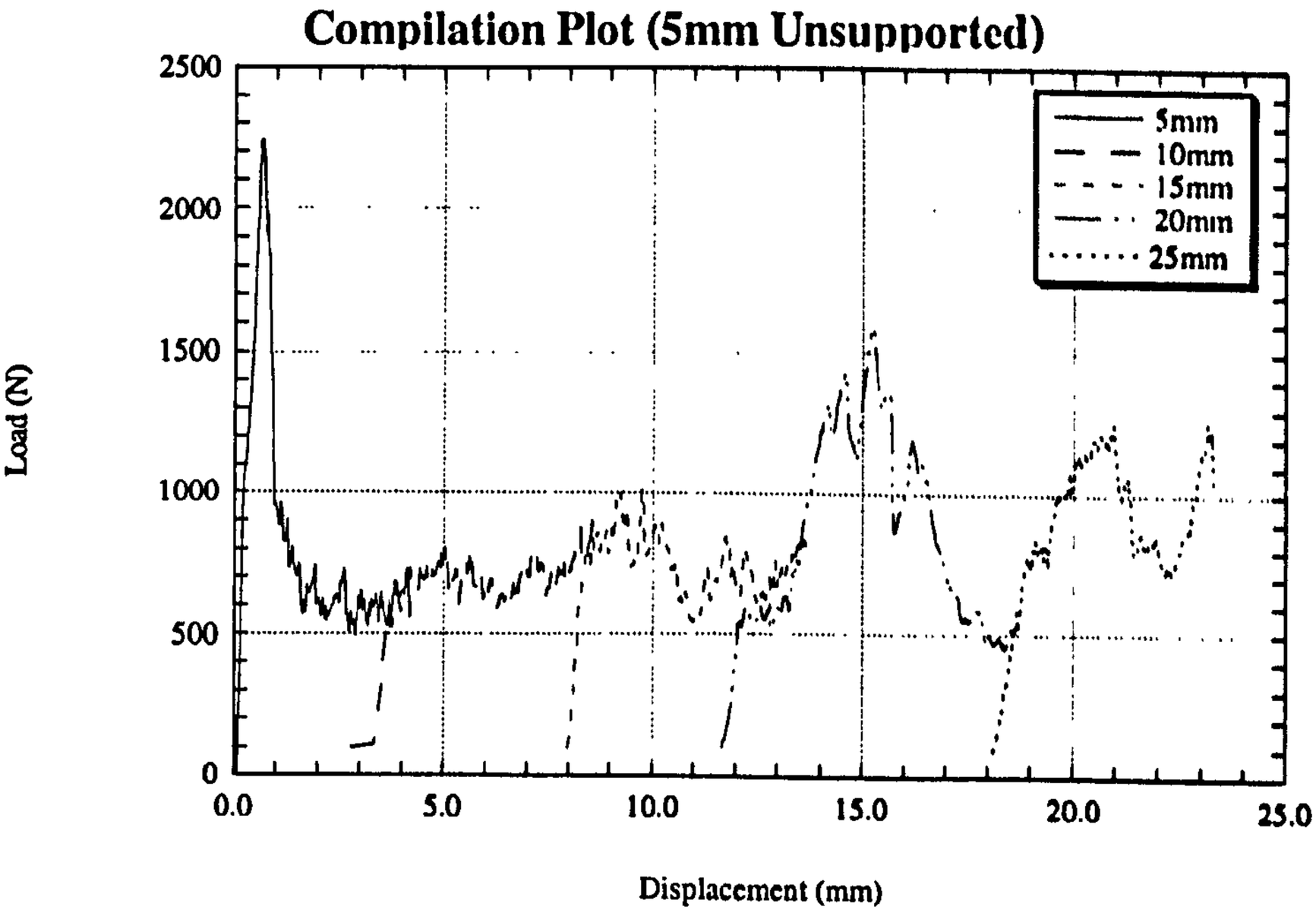

Figure 5.43

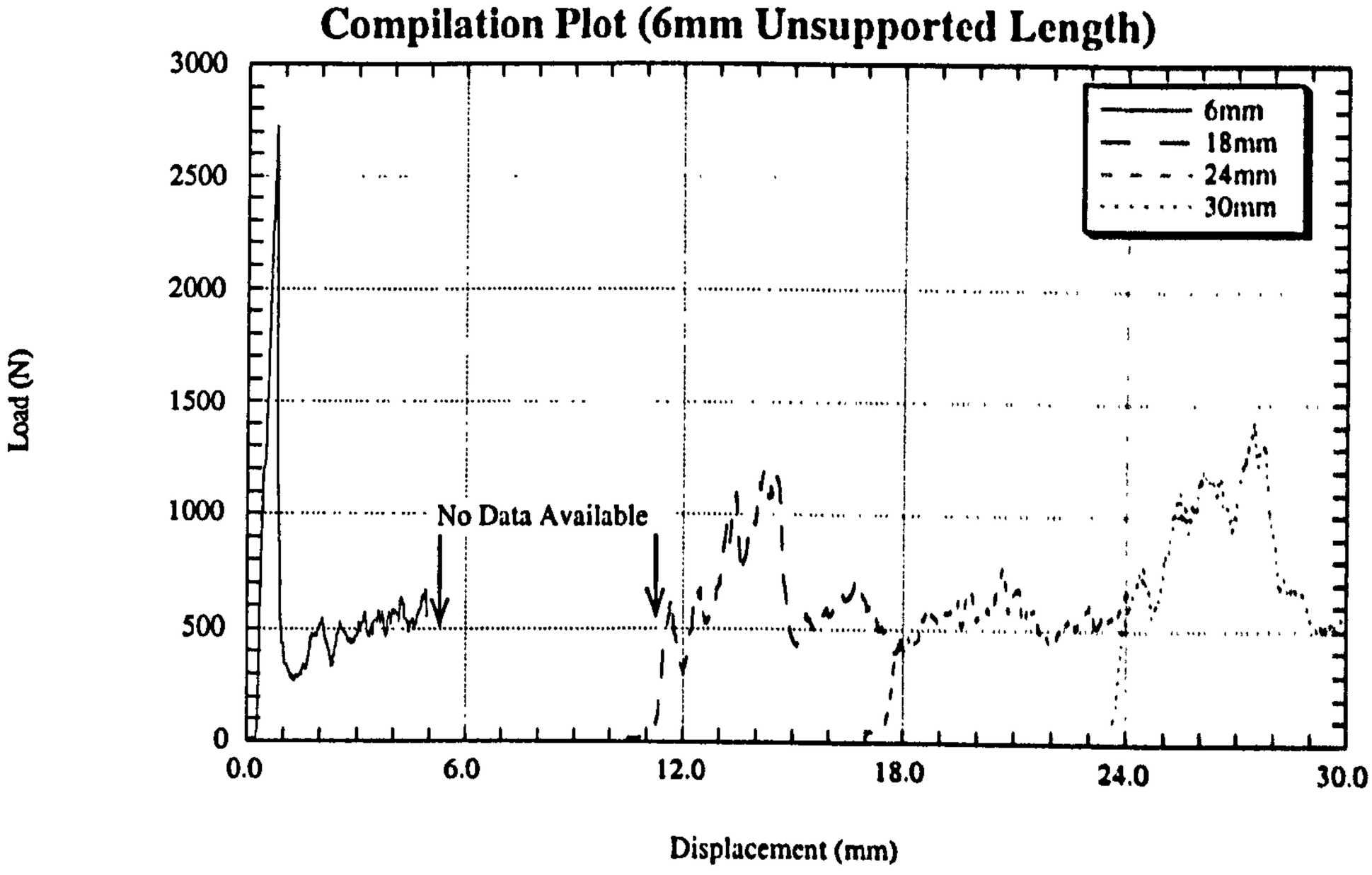

Figure 5.44

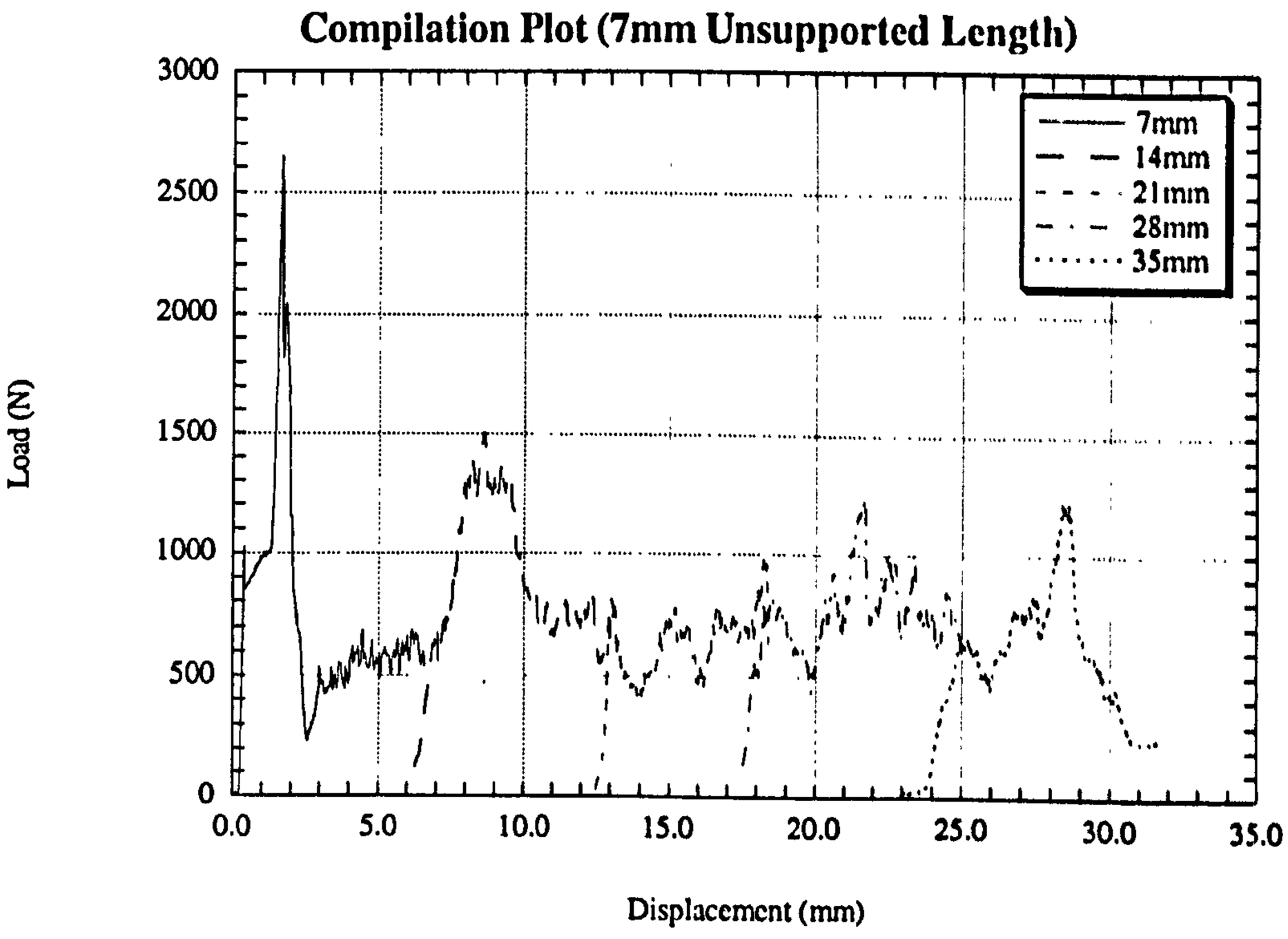

Figure 5.45

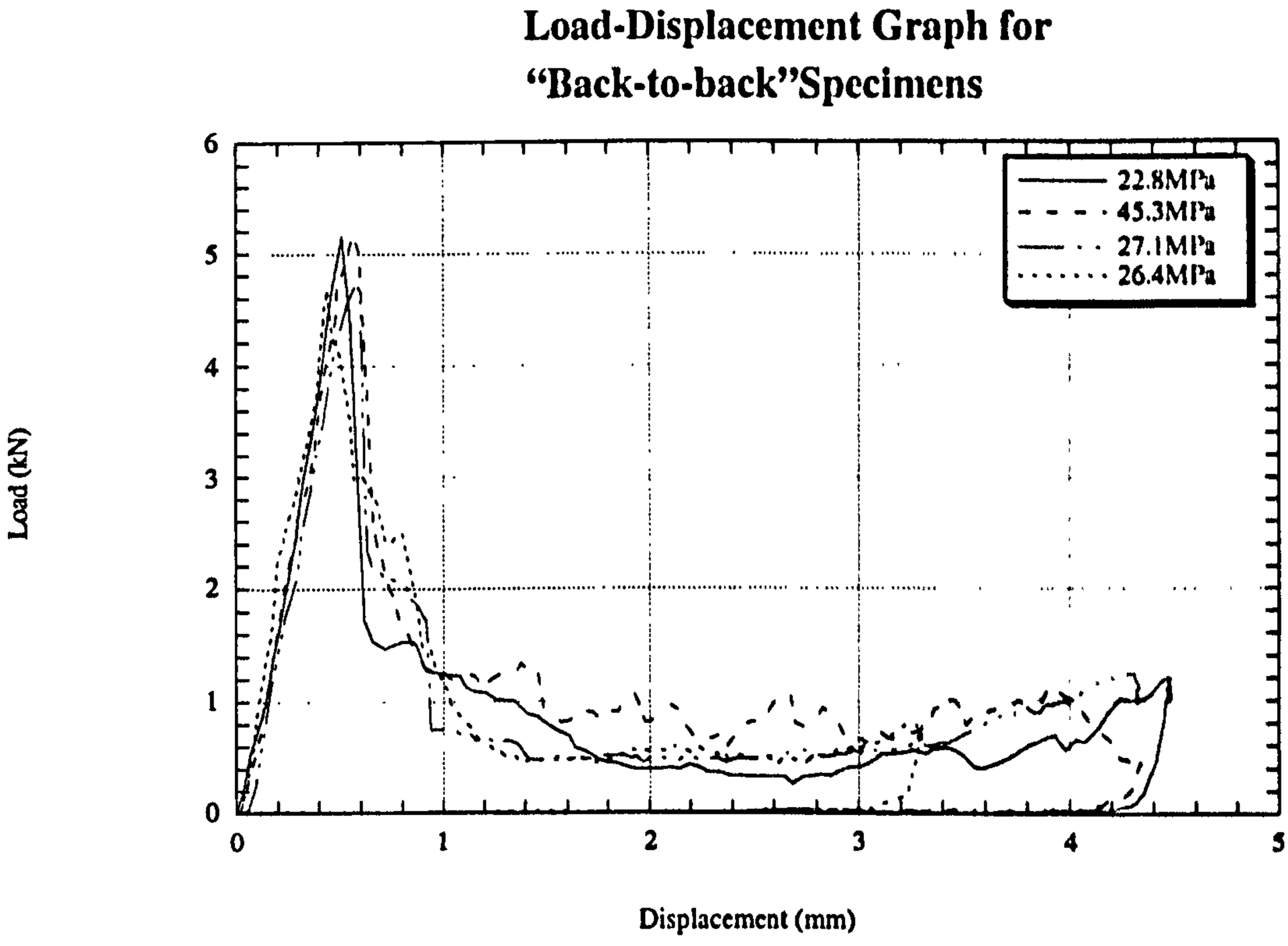

Figure 5.46

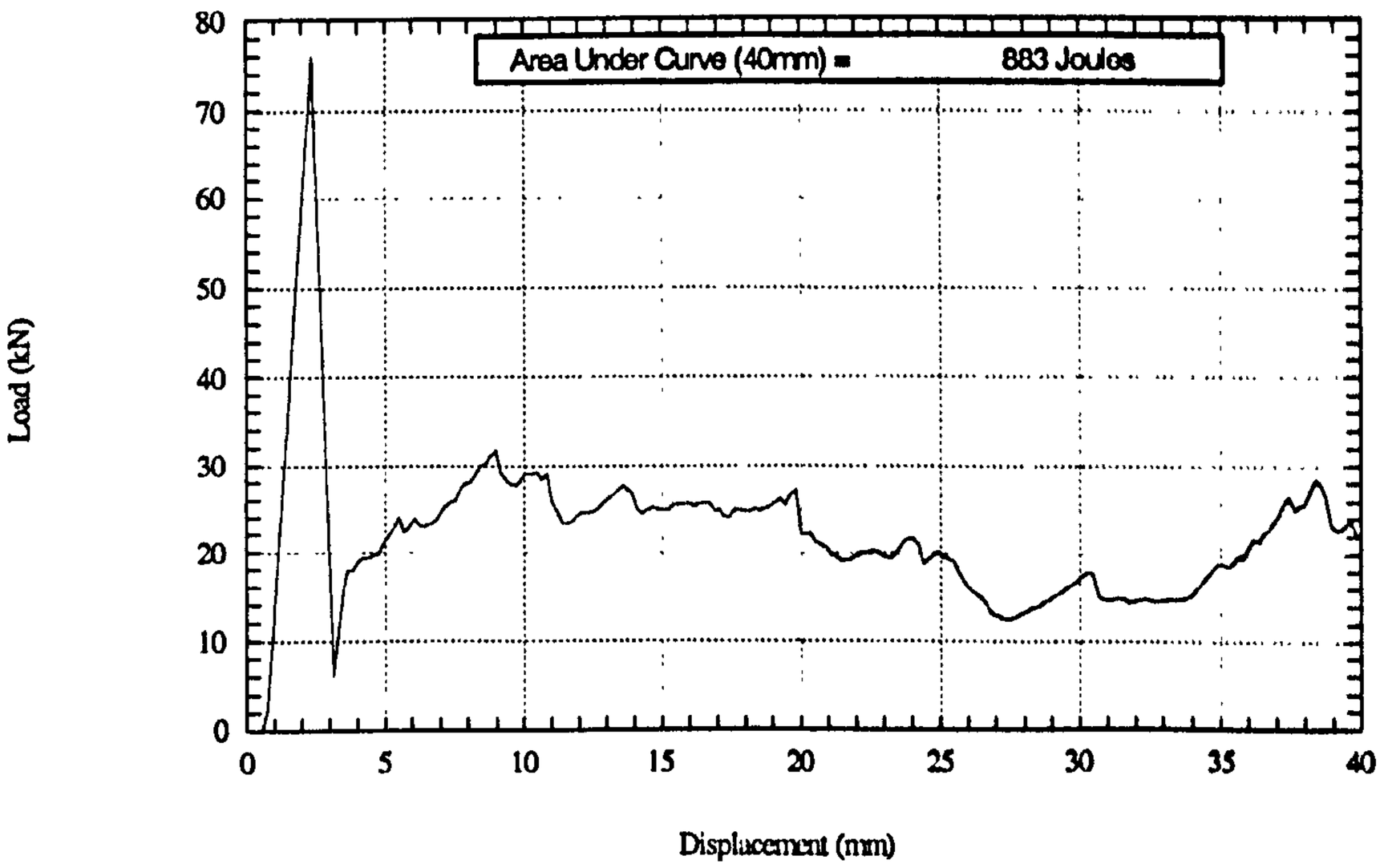

Figure 5.47 Load-Displacement Curve for Angled Stiffeners

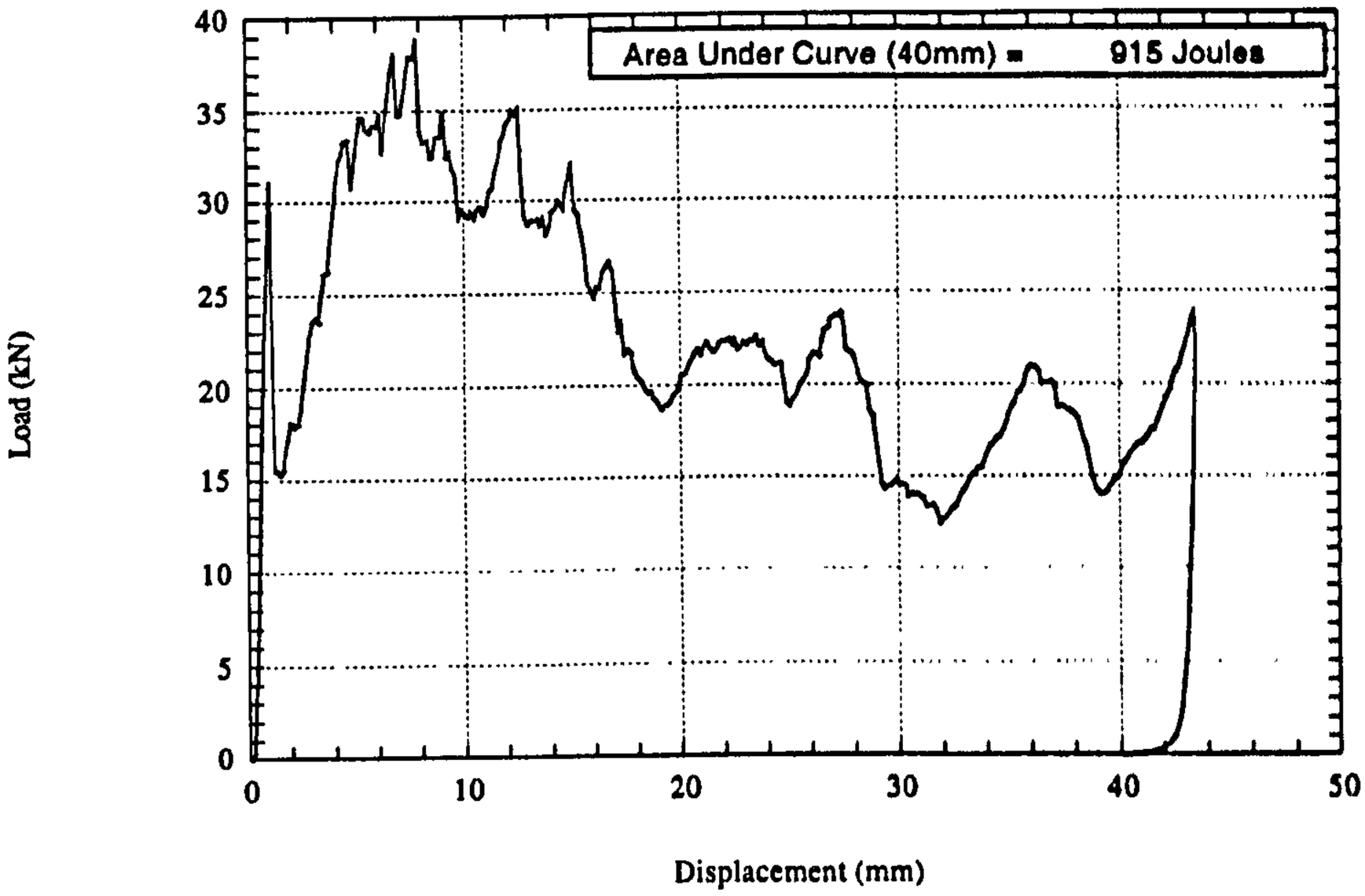

Figure 5.48 Load-Displacement Curve for Chamfered Stiffeners

CHAPTER 6

IN-PLANE CRUSHING OF CRUCIFORMS

6.1 Introduction

Structural intersections of keel beams and landing gear frames, for example, represent structural "hard points" under crash loading within the framework of an aircraft subfloor. In the event of a crash these stiff areas remain uncrushed and can penetrate into the cabin area, or they can transfer high levels of load to other areas of an aircraft structure. The "Black Hawk" helicopter (Figure 6.1) was one of the first helicopters to have been designed with crashworthiness in mind. As can be seen from the figure, the fuselage is primarily a box section, and crushable cruciforms, such as those discussed in this chapter, would be primarily used in this type of design to offer crashworthiness.

Sandwich cruciform structures were made via the manufacturing route outlined in Chapter 3 and subjected to in-plane crushing. The cruciform structures were stiffened at their intersecting points by the inclusion of carbon fibre composite angle stiffeners. It was decided, for reasons of time, to test free standing cruciforms rather than using clamps to represent the support that the cruciforms would see in a real fuselage structure. This free-standing configuration also helped simplify the analysis of the structural response of the cruciform.

The first four cruciforms were manufactured from HTA/913, the remaining 3 single cruciforms, 2 double cruciforms and 1 quadruple cruciform were (for reasons of material availability) manufactured from T300/914. Although a direct comparison between the structures manufactured from the different pre-preg systems would not be possible, the first 4 cruciforms tested as explained in the following text were used to alleviate any problems with cruciform support and crush fixtures.

6.2 Experimental Procedure

All of the cruciforms were crushed quasi-statically at a rate of 1mm/min between the platens of compressive testing machines. The first set tested were manufactured from HTA/913. The first two of four in this set were tested in an in-house built high stiffness compression test machine, the last two (for reasons of machine availability) in a Zwick testing machine fitted with a 180kN load cell (Figure 6.2).

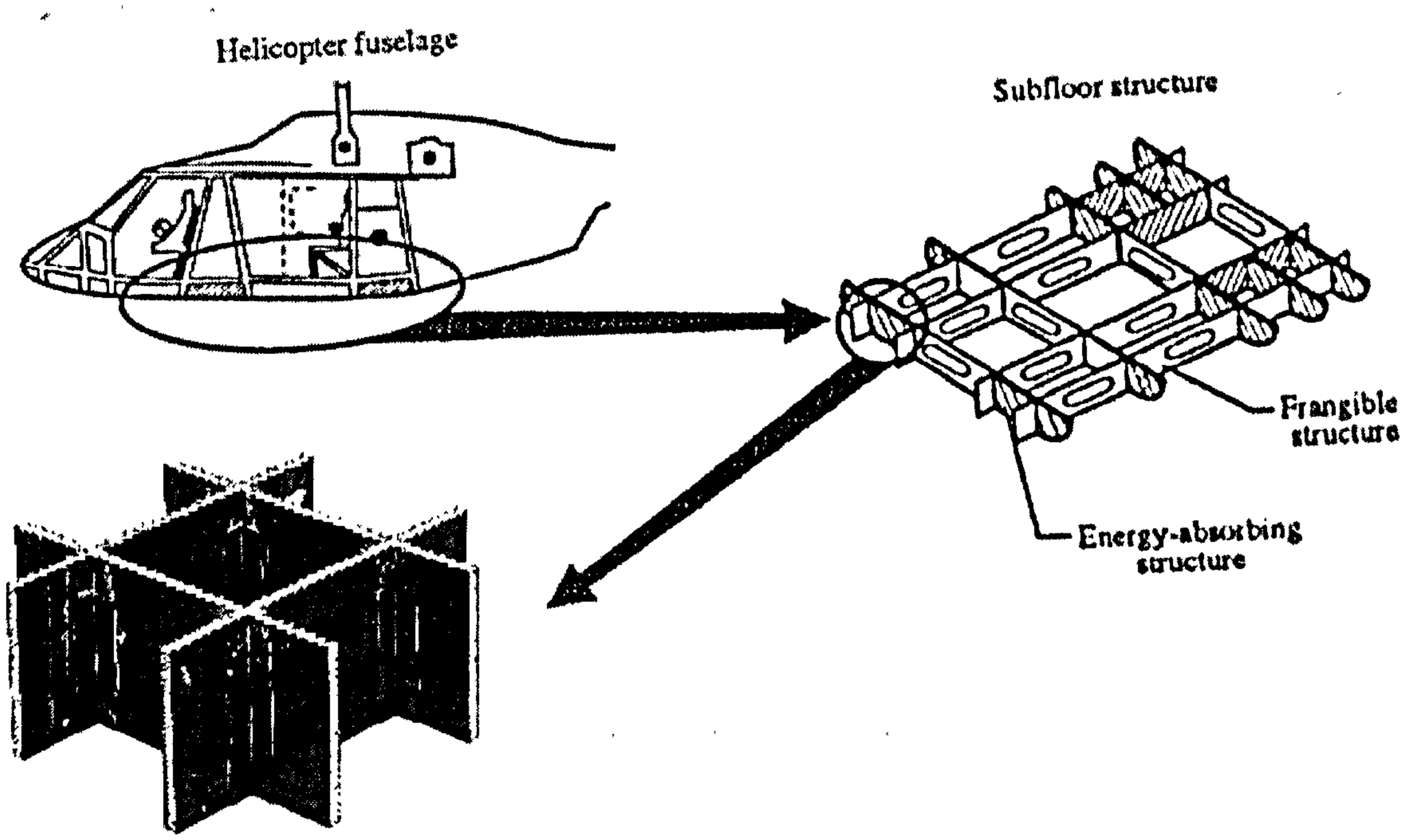

Figure 6.1 Fuselage of Black Hawk helicopter

In all cases the displacement was recorded manually using a dial displacement gauge (as well as by using the built-in LVDT available on the Zwick). The LVDT's available on the 250 tonne machine had a limited travel of approximately 25mm. A reading was taken every one revolution of the displacement gauge, which represented one millimetre of platen displacement. The effect of stiffener length on crush behaviour, cruciform support and crush plate configuration were investigated. All of the cruciforms bases were machined flat to ensure uniform crushing across the width of the cruciform.

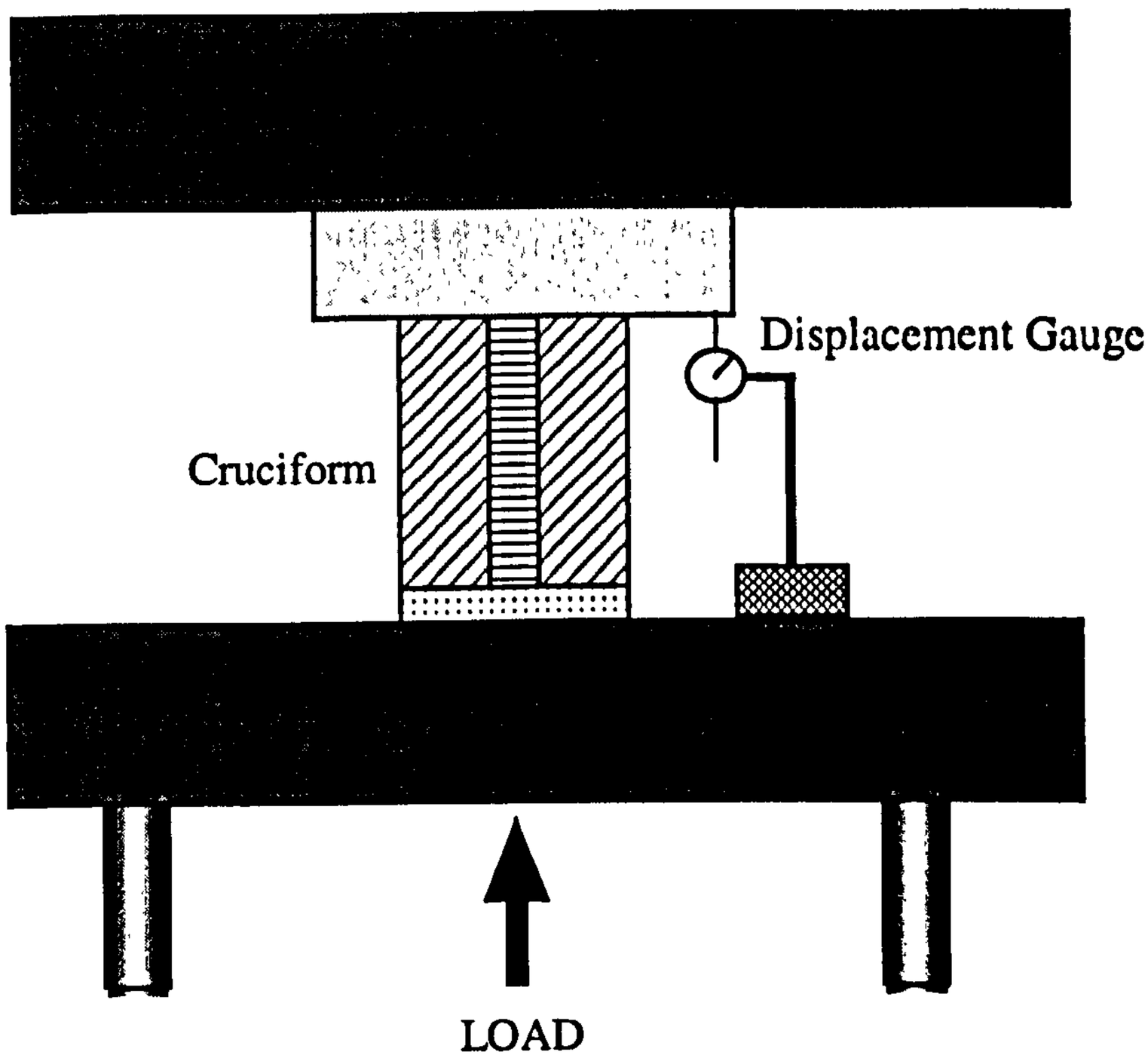

Figure 6.2 Test equipment configuration

6.3 Cruciform 1

The first cruciform crushed was of dimensions 150mm high x 162mm wide x 12mm thick (Figure 6.3), and was supported at its intersecting point by 2mm thick carbon fibre stiffeners 125mm in length (see Section 3.8 for the manufacturing method). The top of the cruciform contained saw-tooth triggers (Figure 3.4) machined as previously stated in Section 3.5, although not into the carbon stiffeners. Crushing was achieved using a 3mm thick flat steel plate. The cruciform was supported at its base by 12mm deep aluminium channels (Figure 6.4).

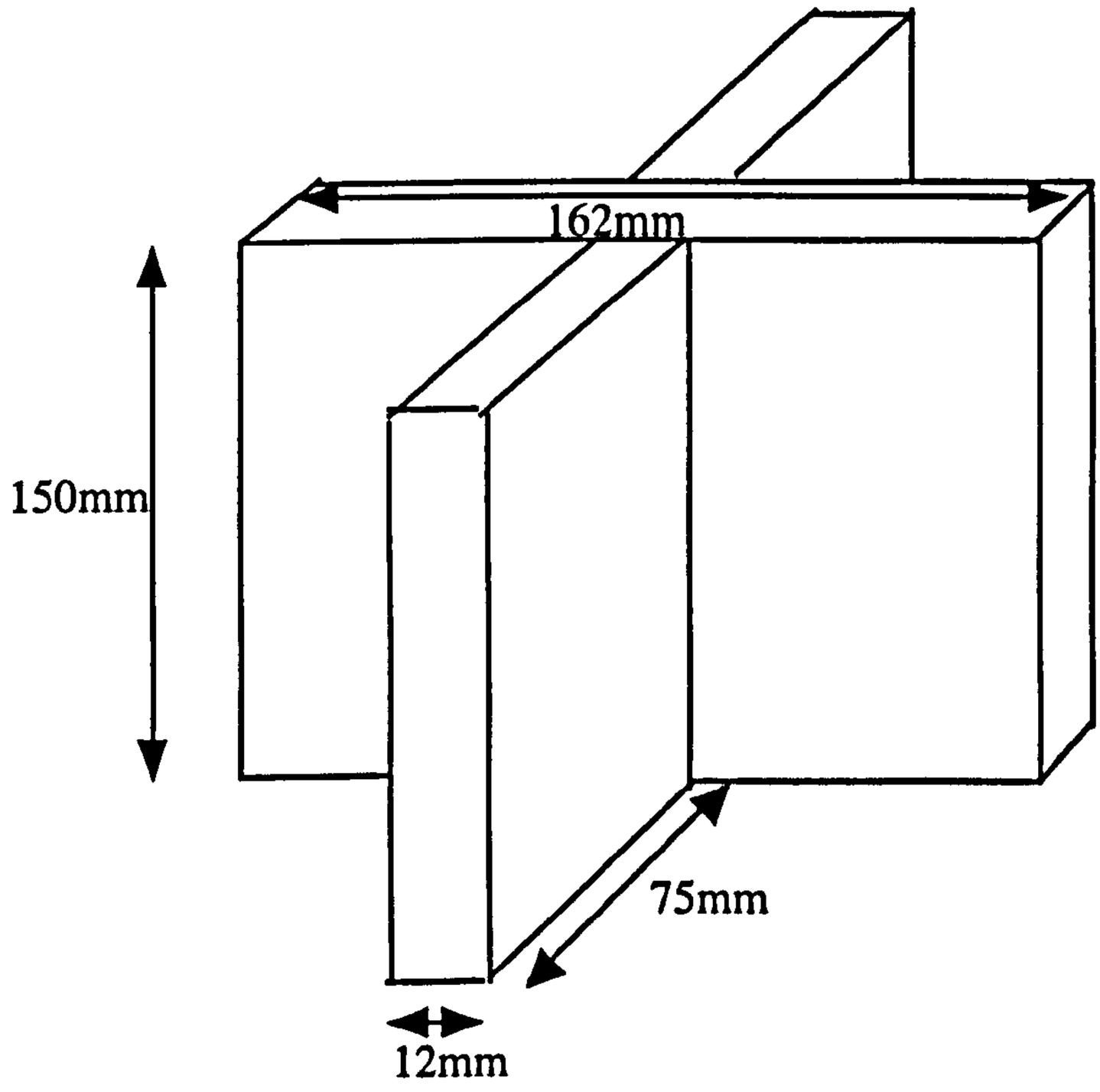

Figure 6.3 Schematic of cruciform

As can be seen from the load-displacement plot for the cruciform (Figure 6.12), the first 12mm displacement curve represented the un-stiffened part of the cruciform i.e. just the sandwich panel, the peak load recorded for this section being 110kN. The stiffened part of the cruciform failed at a peak load of 139kN. As indicated by Figure 6.12 the cruciform continued to crush steadily before reaching another peak of 132kN at 19.5mm displacement. A large decrease in load was then recorded, which was followed by a gradual decrease in load-carrying capability of the structure until the test was terminated.

The specimen was removed from the test machine and examined. As shown in Figure 6.4 below, and in more detail in Figure 6.5, the stiffeners debonded from the cruciform. At the outset of the test the ends of the stiffeners were 2mm above the aluminium support channels. Inspection of the bottom of the cruciform after testing

showed a degree of crushing, enough to have brought the stiffeners into contact with the support channels. This led to the debonding of the stiffeners from the cruciform.

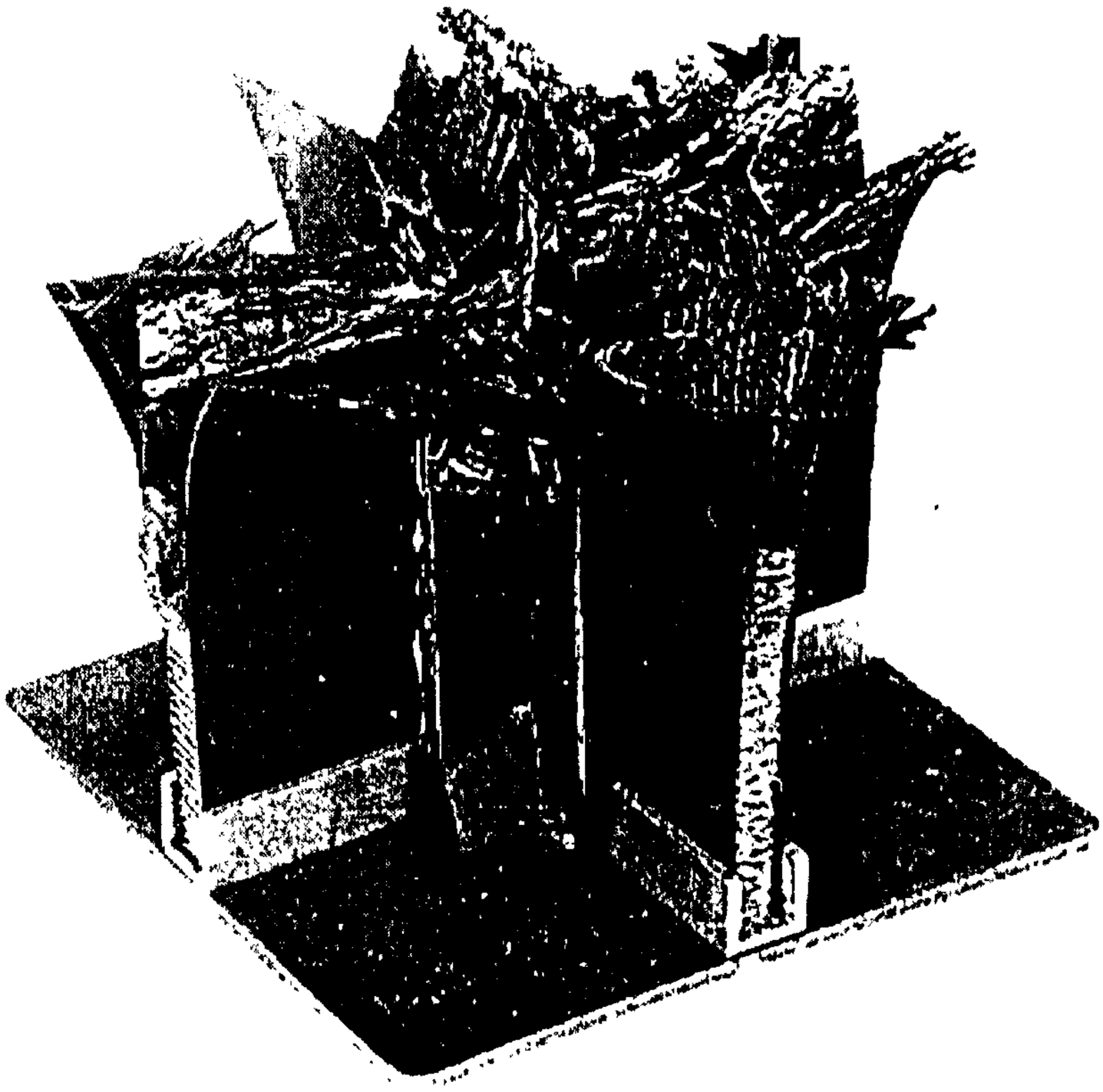

Figure 6.4 Crushed cruciform showing stiffener debond

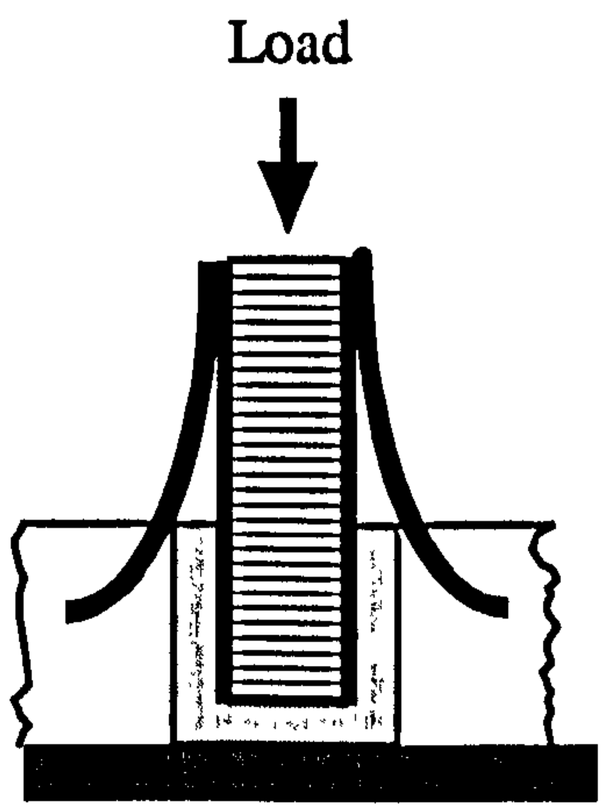

Figure 6.5 Schematic of stiffener debond

Once the stiffeners had become debonded one of the arms of the cruciform detached from the main cruciform section leading to a large drop in load carrying capability. Figure 6.4 shows that the main energy absorbing mechanisms in the crushing cruciform were extensive delamination, fibre crushing, debonding of the stiffeners and crushing of the aluminium core. From the load-displacement curve (Figure 6.12) it was calculated that for 25mm of crushing, the cruciform absorbed 2325 Joules of energy.

6.4 Cruciform 2

A second cruciform was manufactured and assembled. To prevent the stiffeners touching the support channel whilst crushing, the design of the support plate was altered. A slot was machined in each channel so that the each stiffener did not come into contact with the support channel. The stiffeners were therefore unsupported along their whole length, but the arms of the cruciforms were still supported by the U-shaped channel (Figure 6.6).

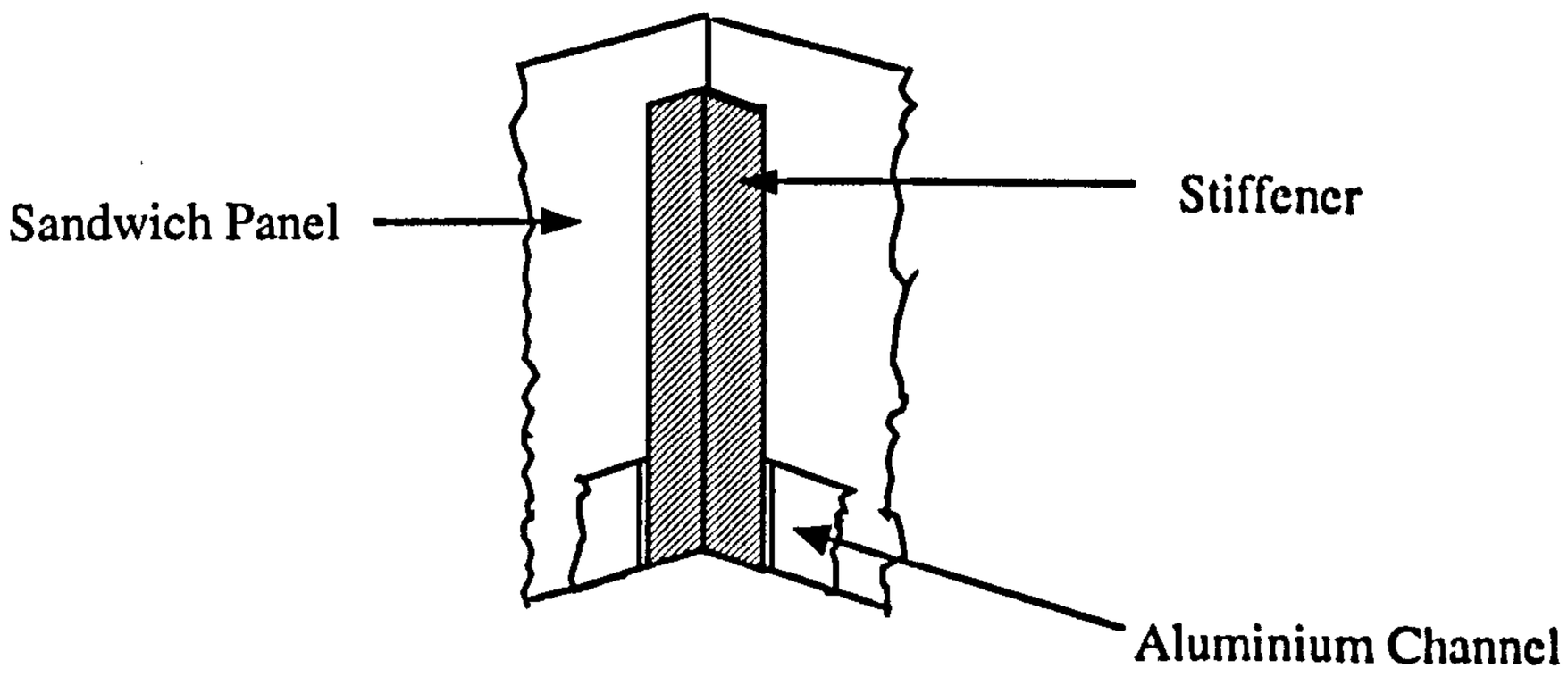

Figure 6.6 Schematic of altered support

The second cruciform had 20mm of un-stiffened sandwich panels above the stiffeners. The cruciform was again triggered using saw-tooth triggers. As can be seen from Figure 6.13 the un-stiffened region of the load-displacement curve was similar in shape to that of the first cruciform, but the peak load was lower at 96kN, the load decreasing to a minimum of 55kN before the stiffeners started to crush. The peak

load attained by the stiffened region of the cruciform was 150kN. The main energy absorbing modes of delamination, core and fibre crushing, and skin-to-core and stiffener debonding, were again seen. The energy absorbed by 25mm of crushing was 1846 Joules, lower than in the first cruciform. This can be explained by a larger proportion of un-stiffened panel being crushed in the first 25mm of cross-head displacement. The energy absorbed by 60mm of crushed cruciform was 5783 Joules.

6.5 Cruciform 3

The third cruciform had the same configuration as the second specimen, but was tested in a Zwick universal testing machine. The load-displacement trace is shown in Figure 6.14, and is very similar to that for Cruciform 2, the cruciform failing in a similar manner. The peak load reached by the un-stiffened part of the cruciform was 85kN, with the stiffened section reaching 160kN. The energy absorbed up to 25mm was 1477 Joules, lower than for the second cruciform. A reason for this may have been because the Zwick was not as structurally stiff as the 250 tonne machine, therefore some slight deflection of the cross heads may have occurred during crushing leading to an error in the displacement data collected and therefore ultimately to the absorbed energy calculated. The failure modes seen were the same as in the previous cruciforms.

6.6 Cruciform 4

The fourth cruciform was also tested on a Zwick universal testing machine. As with the second and third cruciforms there was 20mm of un-stiffened sandwich panel at the top of the cruciform. Saw-tooth triggers were again used, but this time in conjunction with a chamfered crush plate (Figure 6.7). The plate was chamfered at 2°, the same angle as was used to crush the individual sandwich panels. The chamfered plate was used to help promote an efficient mode of failure (Figure B.7 Appendix B) as with the sandwich panels in Chapter 4. A typical load-displacement curve can be seen in Figure 6.15.

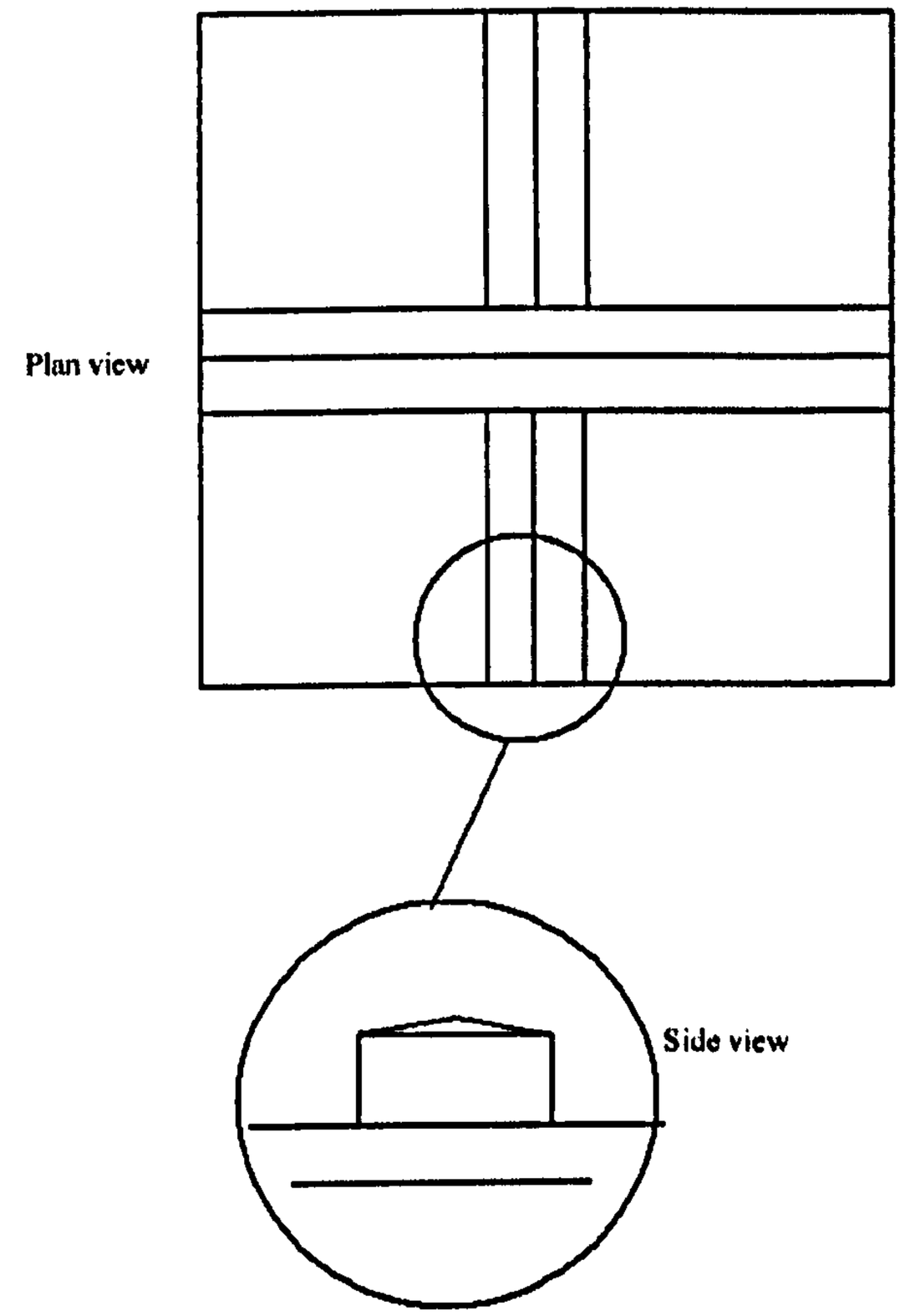

Figure 6.7 Chamfered crush plate.

As a consequence of using the chamfered crush plate there was a slight reduction in the initial peak load seen to 80kN and, similarly, in the second peak load to 150kN. Consequently the energy absorbed for a 25mm displacement was lower at 1342 Joules. The failure modes were the same as seen with the previous cruciforms.

6.7 Single Cruciform 5, 6 and 7.

As discussed in Chapter 3, for the cruciforms numbered 5–7, T300/914 pre-preg material system was used. The geometry of these single cruciform structures was identical to Cruciform 4. The cruciforms were tested in a 250 tonne press; the data

acquisition was the same as with the previous cruciform as were the support and crush conditions. The specimens were crushed at 1mm/min. Figure 6.16-6.18 shows the load displacement traces for Cruciforms 5, 6 and 7.

Due to the change in pre-preg system (see Chapter 3 for a comparison of mechanical properties) the peak loads for what was nominally an identical structure (in terms of crushable volume) were substantially reduced. The initial peak load for Cruciform 5 was 36kN as compared with 80kN, as a consequence the energy absorbed was also reduced. A crush displacement of 45mm absorbed 1384J. The shape of the load displacement curve was very similar to the previous four cruciforms tested. Cruciforms 6 and 7 also crushed in a similar manner to Cruciform 5. Up to a crush displacement of 45mm they absorbed 1351 and 1419J respectively. Their initial peak loads were 35 and 41 kN.

6.8 Double and Quadruple Cruciforms

To evaluate the energy absorption and crushing characteristics of larger subfloor structures double and quadruple cruciform structures were tested. As outlined in Chapter 3 these structures were manufactured from a different pre-preg material, namely T300/914. The double and quadruple cruciforms were designed such that the crushable volume of material was doubled and quadrupled (see Figures 6.8 and 6.9). The double and quadruple cruciforms were supported and crushed in the same manner as the single cruciforms. The support fixtures and crush plates being identical in detail to the single cruciform fixtures albeit doubled and quadrupled in size to accommodate the larger specimens.

Figures 6.19 and 6.20 show the load displacement traces for the crushed double cruciforms, good reproducibility was seen. In terms of the overall shape it can be seen that the load-displacement graph for the double cruciform was a similar shape to the single cruciforms (apart from the expected increase in load carrying capability).

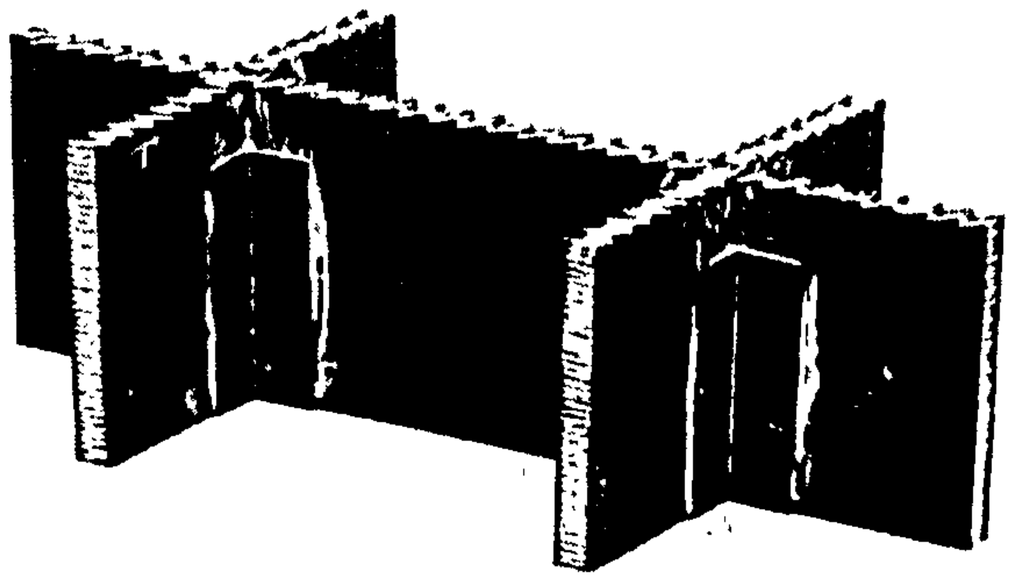

Figure 6.8 Double cruciform

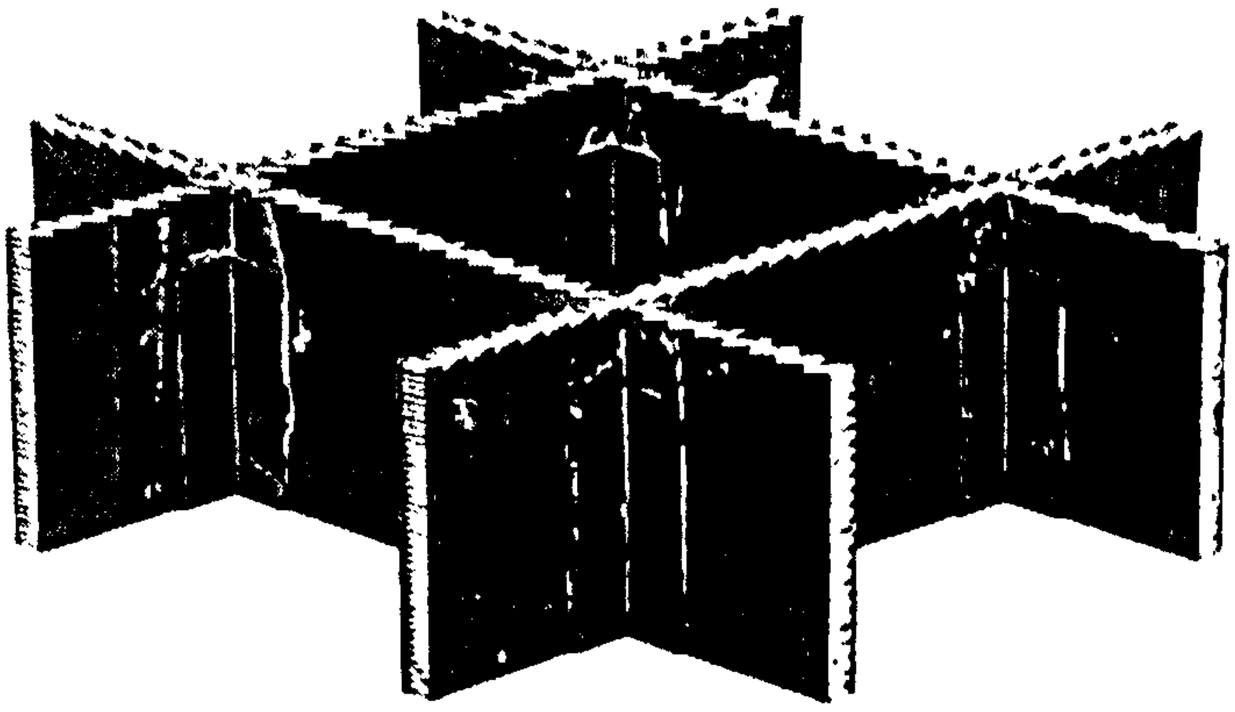

Figure 6.9 Quadruple cruciform

As can be seen from Figures 6.19 & 6.20, the initial peak loads and energy absorption for the two double cruciforms were similar. Figure 6.10 showed how the double cruciform crushed.

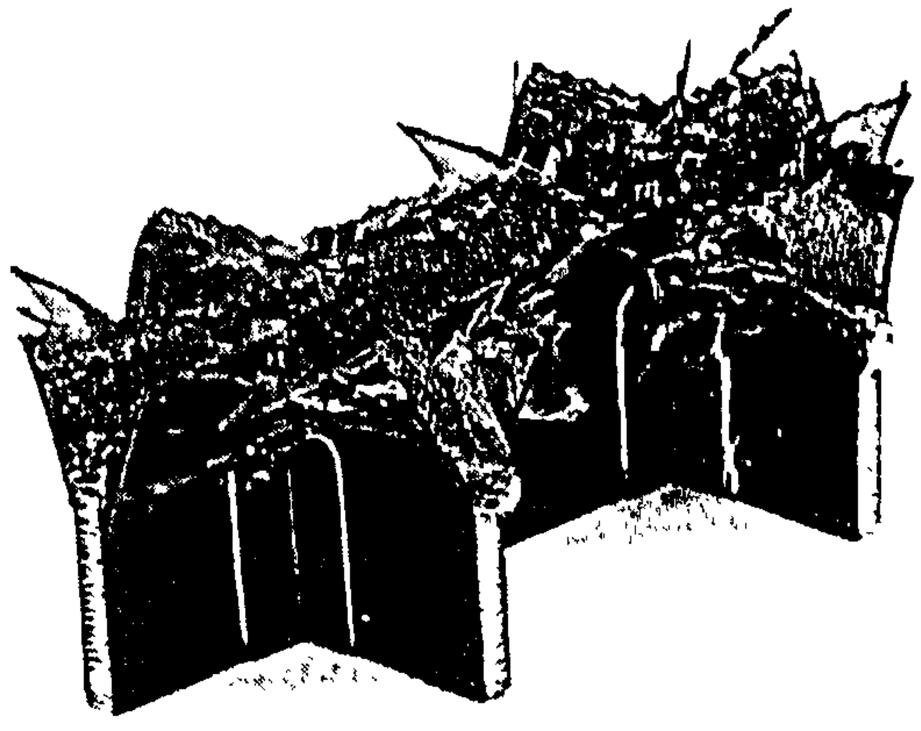

Figure 6.10 Crushed double cruciform

The double cruciforms failed as expected. The crush energy being absorbed by delamination, fibre tearing and crushing of the carbon faces and by in-plane crushing of the aluminium honeycomb core. The initial peak loads for the two double cruciforms were 90 and 95kN and the energy absorbed was 2612 and 2624 J.

To further scale up the cruciforms, a quadruple cruciform was manufactured (Figure 6.9) and crushed (Figure 6.11). The load-displacement graph is shown in Figure 6.21. As can be seen from comparing Figures 6.11 with 6.10, the quadruple cruciform absorbed the crush energy in a similar manner. The initial peak load was 181kN and the energy absorbed by 45mm of crushing was 4823J. A comparison of peak plateau loads and energy absorbed with increasing numbers of repeat cruciform units are shown in Figures 6.22 & 6.23.

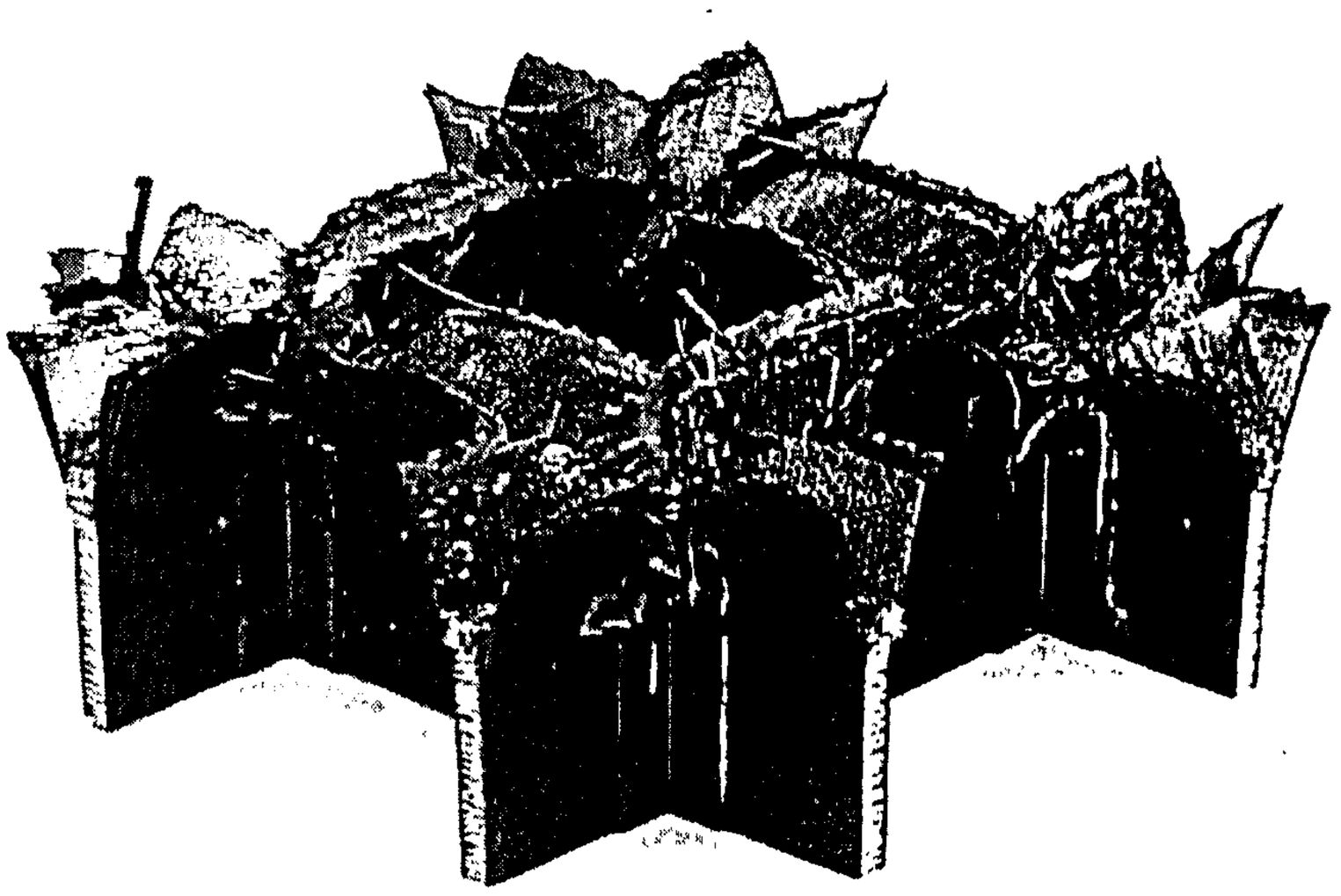

Figure 6.11 Crushed quadruple cruciform

6.9 Cruciforms' Performance Compared with Sandwich Panels and Stiffeners

In this section a comparison was made between the peak loads, energy absorption and crushing stresses for the cruciforms, sandwich panels and stiffeners.

6.9.1 Peak Loads

To compare the cruciforms' behaviour with that of the sandwich panels, it was assumed that a cruciform consisted of four sandwich panels and four stiffeners. This was not strictly correct, as one of the sandwich panels was continuous along the length of the cruciform.

Averaging the maximum peak loads of a set of standard sandwich panels tested as outlined in Chapter 4 gave a value of 18.58kN. The maximum peak load for the set of un-chamfered angled stiffeners tested was 79.6kN.

Sandwich panels = (4 (18.58)) + Stiffeners (79.6) = 153.92kN.

For the four cruciforms tested the maximum loads varied from 139 - 160kN, so the agreement between the actual and the synthesised maximum loads was very good.

6.9.2 Energy Absorption

To compare the energy absorbed by the various constituent parts of the cruciform with a complete cruciform, the second cruciform, which showed typical load-displacement characteristics of all the cruciforms, was used.

The energy absorbed by the second crushing cruciform was calculated and recorded at two points on the load-displacement graph i.e. 25mm and 60mm of cross head displacement. Intermediate values corresponding to changes in the cruciform structure were also calculated using the Kaleidagraph® graph plotting software.

The energy absorbed by the un-stiffened section of the cruciform was difficult to measure precisely. The crushing load rose steeply and it was seen that there was a degree of damage formation in front of the main crushing event caused by the crush plate. The minimum energy value recorded for the un-stiffened part of the cruciform was 835 Joules at 15mm displacement, where from Figure 6.13 it can be seen that the load-displacement response had yet to be influenced by the stiffeners. At 20mm the tops of the stiffeners were about to start being crushed and the energy absorbed rose to 1180 Joules.

In comparison with the cruciform, 4 separate sandwich panels which had the same crushed volume of material i.e. 20mm, absorbed only an average of 520 Joules.

Examination of typical graphs for the sandwich panels and cruciforms revealed where some of the discrepancy between the two energy values arose.

Firstly the single sandwich panels tested using the simplified testing rig (Chapter 4) showed typical behaviour for a crushing sandwich panel i.e. a peak load at crush initiation, a large drop in load followed by a recovery, and finally a level load plateau where the sandwich panel was progressively crushing.

The cruciform load-displacement graph does not exhibit a level load plateau. Instead of a sharp drop in load carrying capability, as seen typically with the sandwich panels tested, the load decreases gradually. The energy in this portion of the graph, (in the case of the second cruciform tested, approximately 100 Joules) accounting for a large percentage of the total extra energy seen for the un-stiffened panels of the cruciform compared with the sandwich panels when crushed by 20mm.

The second discrepancy is the magnitude of the load carried by the unstiffened region of cruciform. For the energies absorbed by the cruciform and its constituent pieces to be similar their load carrying capability must be of a similar level; it was not. Taking the second cruciform again as an example, as stated previously the load carried by the unstiffened region of the cruciform was not a level plateau. But, even taking the lowest value of about 55kN, this meant that each of the four sandwich panels that made up the cruciform would have had to carry 13-14kN to be equivalent. They actually carried 4-5kN.

The stiffened region of the cruciform also absorbed more energy than its constituent parts i.e. sandwich panels and stiffeners, as it required more load to crush by the same amount. The stiffened region of the cruciform showed a similar shape to the un-stiffened region. The difference in load levels being due to the stiffeners additionally crushing

From these results it was clear that the cruciform structure offered more support to the crushing sandwich panels enabling them to carry higher loads than the individually crushed sandwich panels.

At a cross head displacement value of 60mm the cruciform in question had absorbed 5783 Joules. In comparison the individual parts of the cruciform absorbed an estimated 2223 Joules. This can be broken down into the following contributions:- 40mm of crushed stiffeners absorbed 883 Joules and 60mm of crushed sandwich panel absorbed an estimated 1440 Joules, giving a total energy of 2323 Joules.

The energy absorbed up to 60mm had to be estimated, as the individual sandwich panel specimens tested in Chapter 4 were not long enough to be crushed by 60mm. The estimated value can be quoted fairly accurately as after the initial load peak the specimens exhibited sustained crushing and the load-displacement curve flattened out hence allowing the energy absorbed for the extra displacement up to 60mm to be calculated. The cruciforms were crushed to 60mm, rather than 40mm like the individual sandwich panels, to try and obtain more useful data from the load-displacement curves.

The energy absorbed by the constituent parts therefore totalled 2323 Joules, the cruciform 5783 Joules. The difference between the two energies was large. Apart from the reasons mention previously for the energy difference, new energy absorbing mechanisms were present in the crushing of the cruciform. Examination of the cruciform revealed two mechanisms that contributed to the differences in the energies absorbed.

Firstly as can be seen clearly in Figure 6.4 the stiffeners eventually became debonded from the cruciform. The breaking of the adhesive bond between the stiffeners and the cruciform over a distance of 30-40mm would absorb some energy, although it was difficult to quantify the exact amount. From work outlined in Chapter 5, on climbing drum and DCB tests, an average reliable G_{IC} value for the 913 resin adhered to honeycomb core was 350 Jm^{-2}. The bonded area of the stiffener to the cruciform was $1.6 \times 10^{-3} m^2$ giving a value of 0.5 Joules to debond a stiffener. Therefore, the energy absorbed in debonding the stiffeners would have been in the region of 2 Joules; not a significant amount.

Secondly, although not easily seen on Figure 6.4, a degree of panel skin tearing at the intersection point of the cruciform was present. It was calculated that to create a 1mm

tear in a 1mm thick skin absorbed approximately 1 Joule of energy, therefore a quantity of energy was absorbed in this manner. It was not easy to estimate the degree of tearing. The longest sandwich panel which made up two of the cruciform arms was torn in eight places over a distance of 50-60mm, which meant that at least 400 Joules was absorbed in tearing.

Although there were failure mechanisms in the cruciform that were not present in the individual constituent parts, the amount of energy absorbed by these additional mechanisms were not large, and did not fully account for the difference in the absorbed energy seen. The main difference, as explained previously, was due to the level of support given to the structures.

6.9.3 Mean Crushing Stresses

The crushing stresses of the individual cruciform parts did not add up to the stresses seen in the complete cruciform structure. The loads experienced by the cruciform were higher than the loads for the individual parts and therefore the stresses were also higher as it was assumed that a cruciform has the same crushable area as four sandwich panels and four angled stiffeners.

6.9.4 Comparison between Single, Double and Quadruple Cruciforms

As previously mentioned, the pre-preg material for the last 3 single cruciforms, 2 double and 1 quadruple cruciforms was different to the previous single cruciforms and individual sandwich panels due to reasons of material availability. A direct comparison between the first set of single cruciforms and any subsequent work is therefore not viable. However, if the last set of single cruciforms the double and quadruple cruciforms are compared some interesting results can be observed.

The initial peak loads, energy absorbed and plateau peak loads for the 3 different structural configurations were compared. Figs 6.22 and 6.23 show the peak plateau loads and energy absorbed respectively. The load-displacement data for these structures can be found in Appendix D.

6.10 Conclusions

This chapter described the work undertaken on the in-plane crushing of cruciform structures constructed from carbon fibre/epoxy faced, aluminium cored sandwich panels.

The cruciforms were manufactured as described in Chapter 3. Each of the cruciforms manufactured were crushed quasi-statically and their load-displacement response described. The cruciform structures were found to absorb energy by delamination and crushing of the carbon composite faces, debonding of the faces from the core and by crushing of the aluminium core, identical to the individually crushed sandwich panels. In addition to these energy absorbing mechanisms, debonding of the angle stiffeners and tearing of the sandwich faces were also identified.

The response of the single cruciform sandwich structures to in-plane compressive loading compared with their constitutive parts was described. The peak loads, energy absorbed and mean crushing stresses were compared. It was found that the peak loads encountered by the cruciform could be fairly accurately predicted from the peak load curves of the individually crushed sandwich panels and stiffeners. The energy absorbed and the mean crushing stresses summed for the individual parts of the cruciform were found to be a lot less than those for the complete cruciform. It was reasoned that the complete cruciform configuration is such that it gives greater support to the individual components than is achieved in the separate component tests. As a result of this the cruciform absorbed more energy and recorded higher crush stresses.

When the cruciform structures manufactured from T300/914 were compared with each other, the results obtained were excellent. The single, double and quadruple cruciforms all failed in the same progressive manner when subjected to compressive loading. When the initial peak, peak plateau loads and the energy absorbed was compared a linear relationship was seen. Figure 6.22 shows just how linear the relationship was, with an R^2 value of 0.9986. From this set of experiments it can be

seen that it may be possible to estimate the energy absorption of large sandwich cruciform structures from the testing of smaller cheaper cruciform units.

As stated previously, the crush loads (and therefore the energy absorbed) by the cruciforms manufactured from the T300/914 pre-preg were significantly lower than the cruciforms manufactured from HTA/913 pre-preg.

From Tables 3.1 and 3.2, (a comparison of mechanical properties for the two pre-pregs used) it is not immediately apparent where the difference in the failure loads might come from. The failed cruciforms were examined to try to explain the lower load carrying capability of the T300/914.

It was apparent that the face to core bond strength for the T300/914 was higher than that for the HTA/913 pre-preg. Figure 6.24 shows the two different sandwich panels manufactured. Figure 6.24 (A) is of the T300/914 sandwich panel; it can be seen that the adhesive fillets were much larger than those in (B) the HTA/913 sandwich panel. As a consequence of the increased face to core bond strength the fracture path in the T300/914 panel was through the aluminium honeycomb core. In the HTA/913 sandwich panel the faces peeled away from the core. In both cases the adhesive film used was the same thickness but in the case of the film used for the T300/914 it was able to be processed at a higher temperature.

From the above evidence it would be imagined that the T300/914 sandwich panels would fail at a higher load than the HTA/913, it being more difficult to fracture the aluminium honeycomb core than to debond the faces of the cruciform. This was not the case.

Secondly, the pre-preg faces of the two different sandwich panels were examined with the naked eye. It was seen that the T300/914 panels once debonded from the core had stayed intact, the individual layers of the faces delaminating, but, bending out of the way of the crush platen. The amount of fibre crushing/breakage was minimal. This was in contrast to the HTA/913 sandwich panels where a significant number of the pre-preg layers had crushed.

As the individual T300/914 pre-preg layers had delaminated to a greater extent than the HTA/913 sandwich panels it was decided to look at the strain energy release (G_{IC}) values for the two different pre-preg systems. Greenhalgh [47] compiled a comprehensive list of G_{IC} values for widely used pre-pregs and more recently Vernon [48] has worked on similar pre-preg systems to those used in the manufacture of the sandwich panels. Both authors quote a value of around $120Jm^{-2}$ -$140Jm^{-2}$ for T300/914 pre-preg with unidirectional interfaces. Vernon quotes a value of around $300Jm^{-2}$ - $400Jm^{-2}$ for multidirectional (±45°) interfaces for the same pre-preg material.

Although an extensive literature search was undertaken, similar values for HTA/913 were not found. However, Vernon reported upon values for HTA/6376. For unidirectional interfaces values of $250Jm^{-2}$ were measured, for multidirectional interfaces 300 - $900Jm^{-2}$. Greenhalgh reports on the XAS/913 pre-preg system quoting values of $225Jm^{-2}$ - $280Jm^{-2}$ for unidirectional interfaces and $280Jm^{-2}$ for multidirectional.

It is clear that there is a difference in the mode I strain energy release rates for the two pre-pregs. The values for T300/914 whether at a unidirectional or multidirectional interface could be half that of the HTA/913. The consequence of this is for the faces of the T300/914 panels to extensively delaminate and bend away from the crush platen, instead of initially supporting a higher applied load, (as in the case of the HTA/913 pre-preg), then crushing and fracturing therefore absorbing a higher amount of energy.

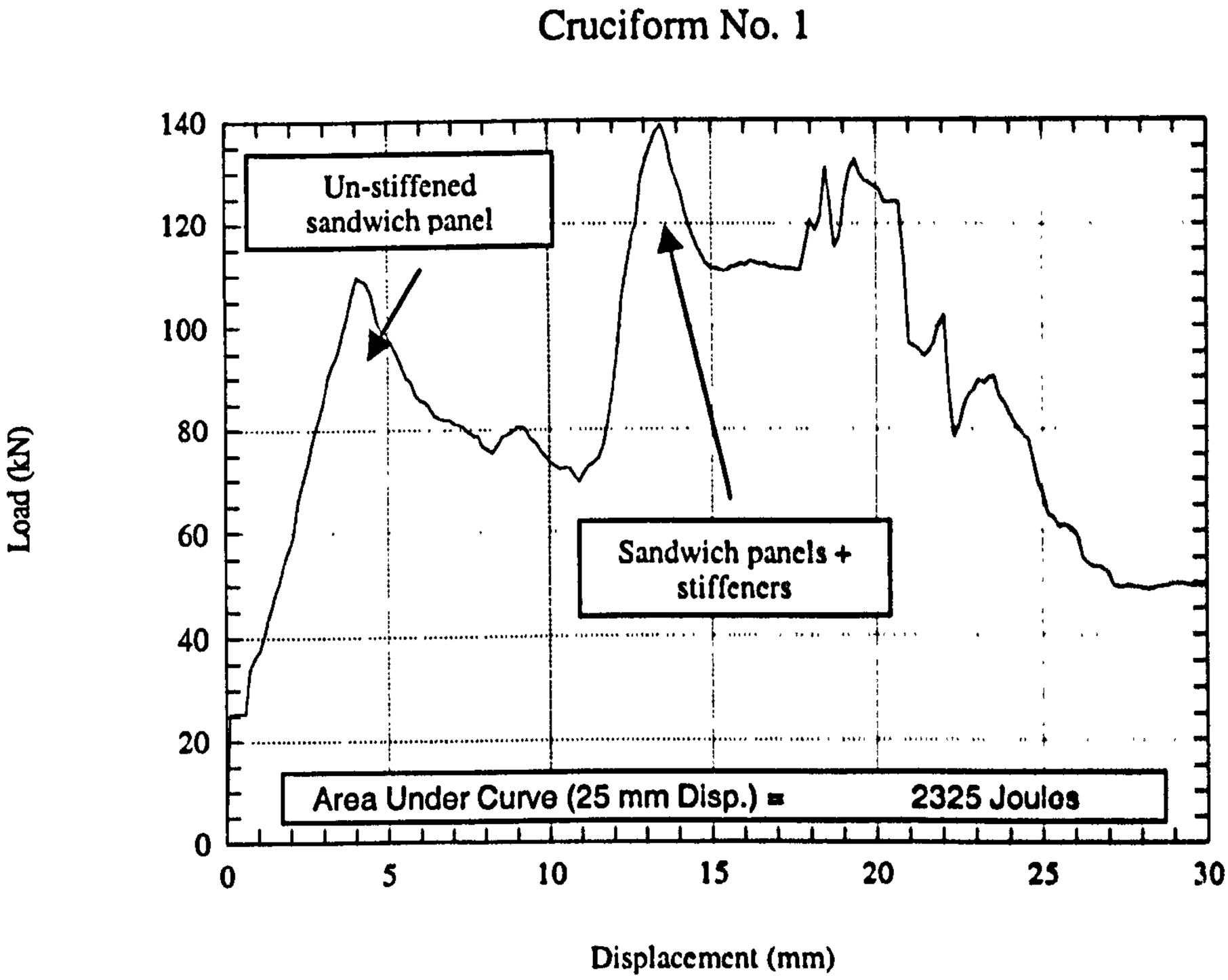

Figure 6.12 Load-Displacement Curve for Cruciform #1

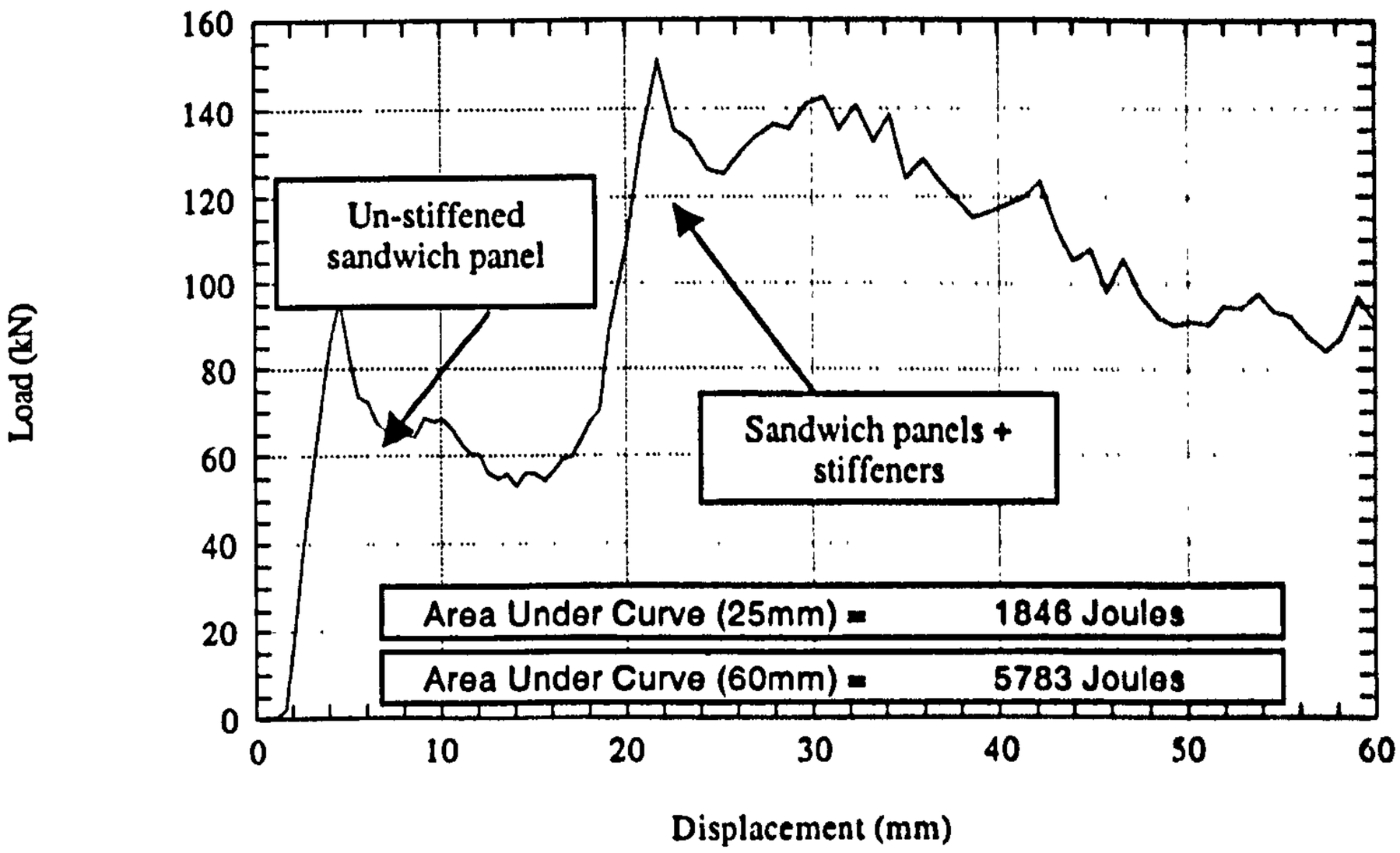

Figure 6.13 Load-Displacement Curve for Cruciform #2

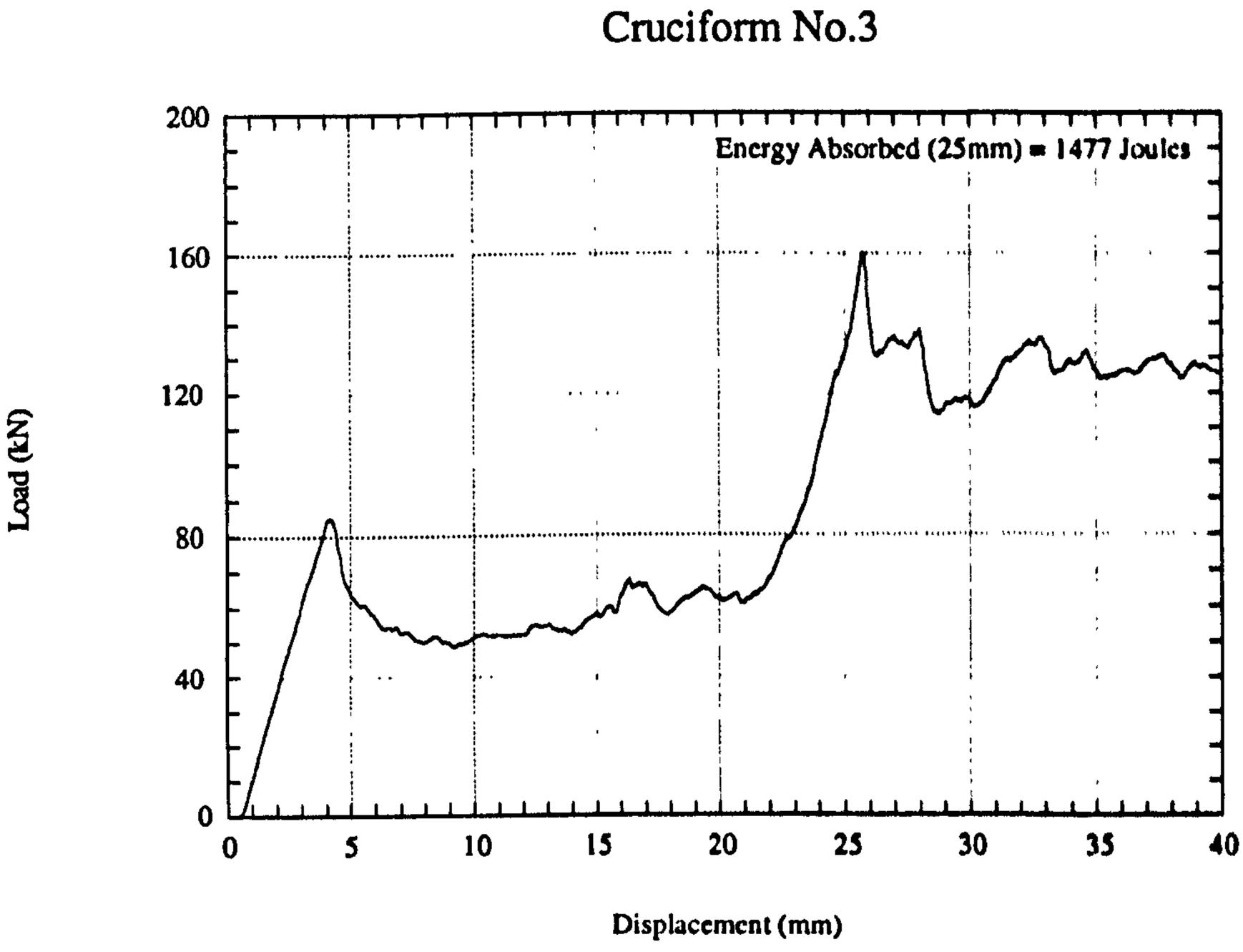

Figure 6.14 Load-Displacement Curve for Cruciform #3

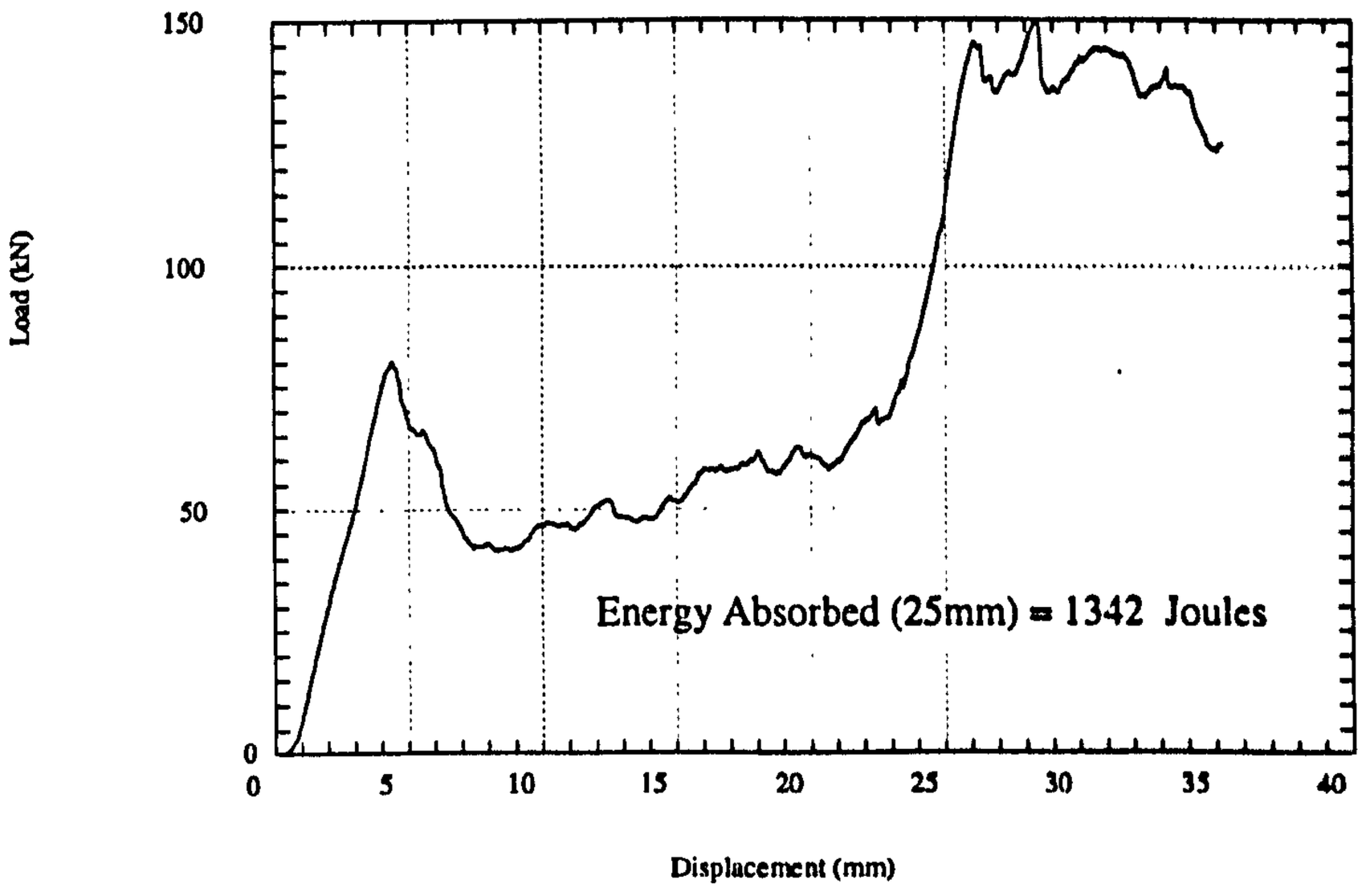

Figure 6.15 Load-Displacement Curve for Cruciform #4

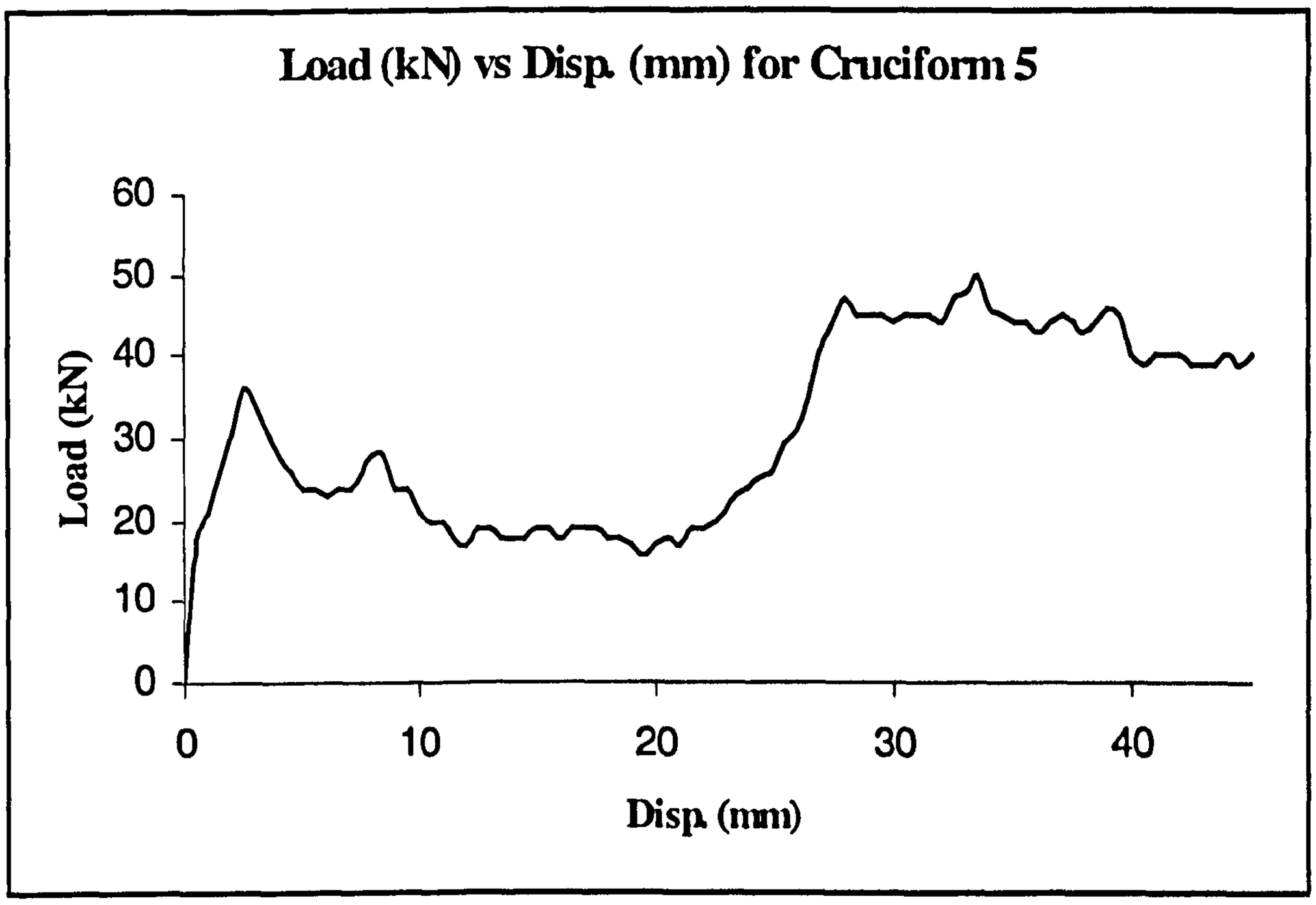

Figure 6.16 Load-Displacement Curve for Cruciform #5

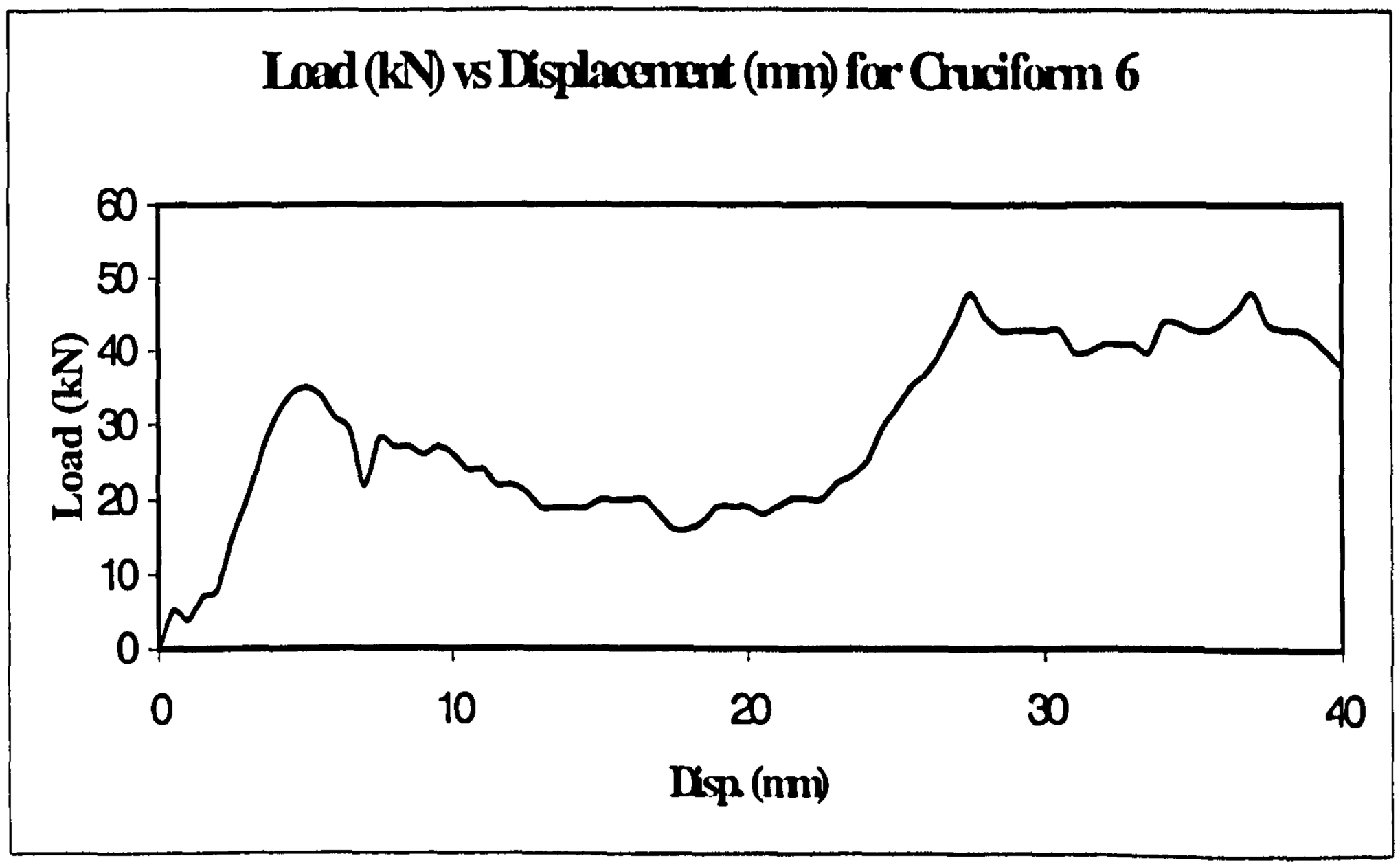

Figure 6.17 Load-Displacement Curve for Cruciform #6

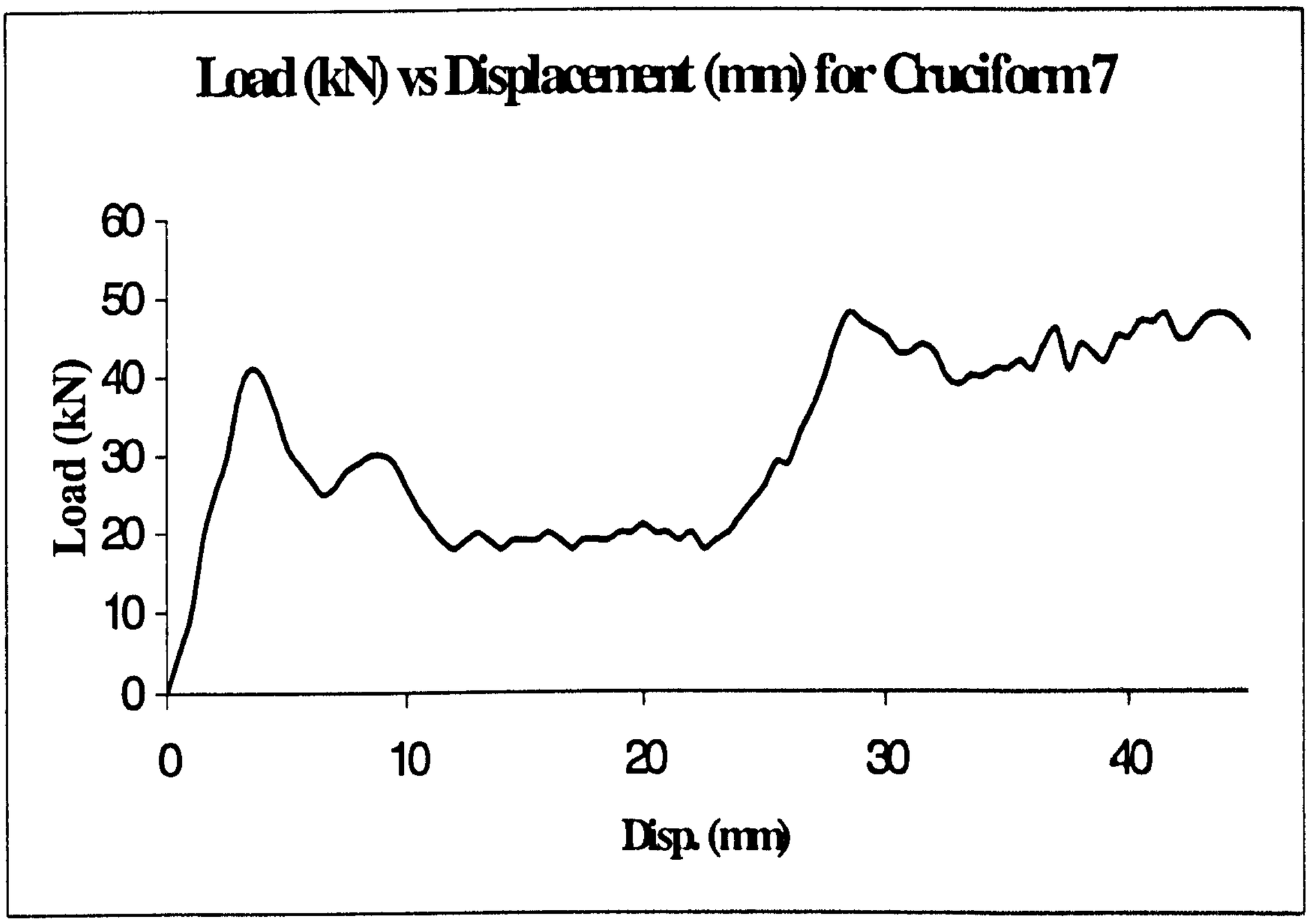

Figure 6.18 Load-Displacement Curve for Cruciform #7

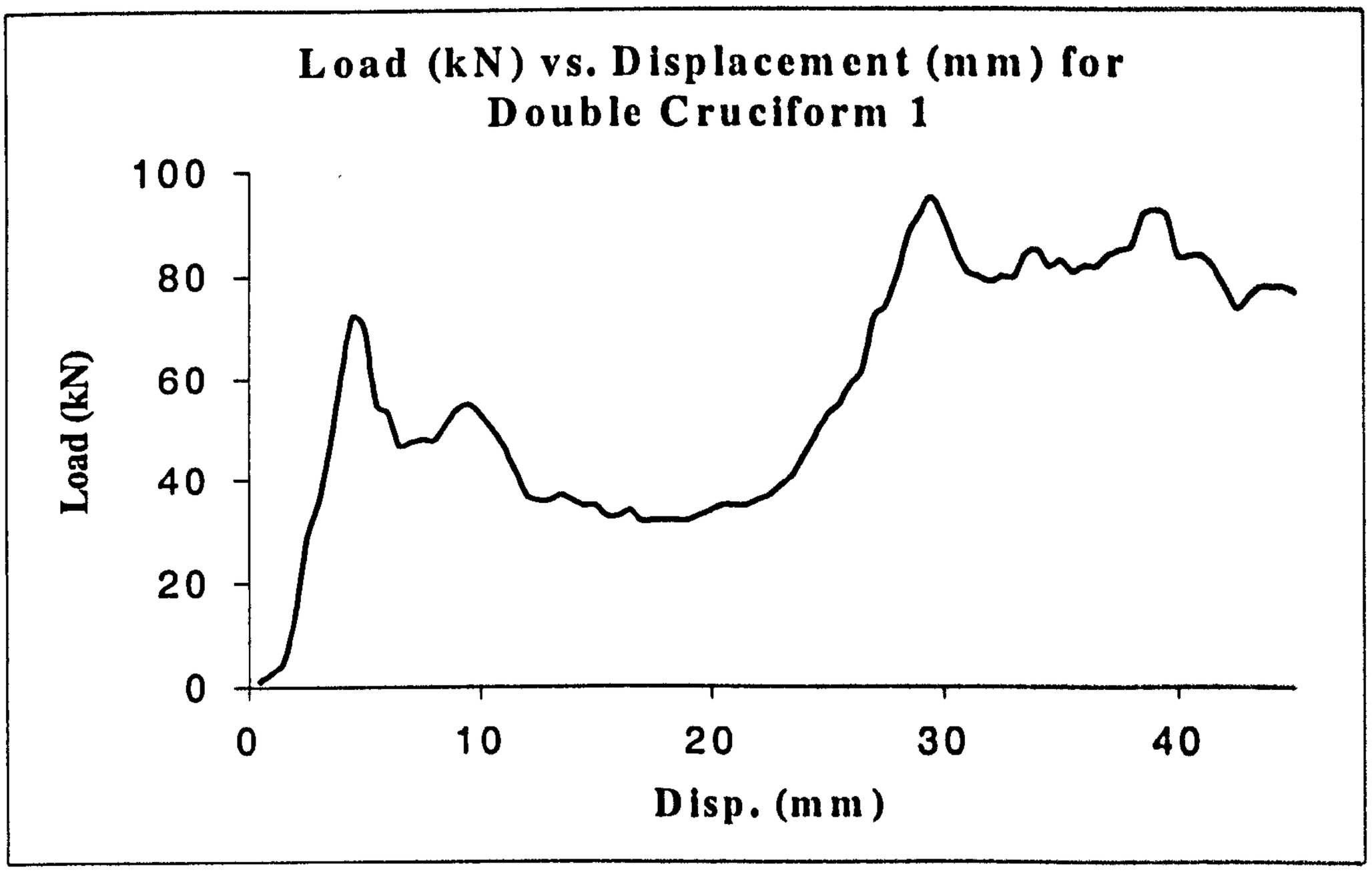

Figure 6.19 Load-Displacement Curve for Double Cruciform 1

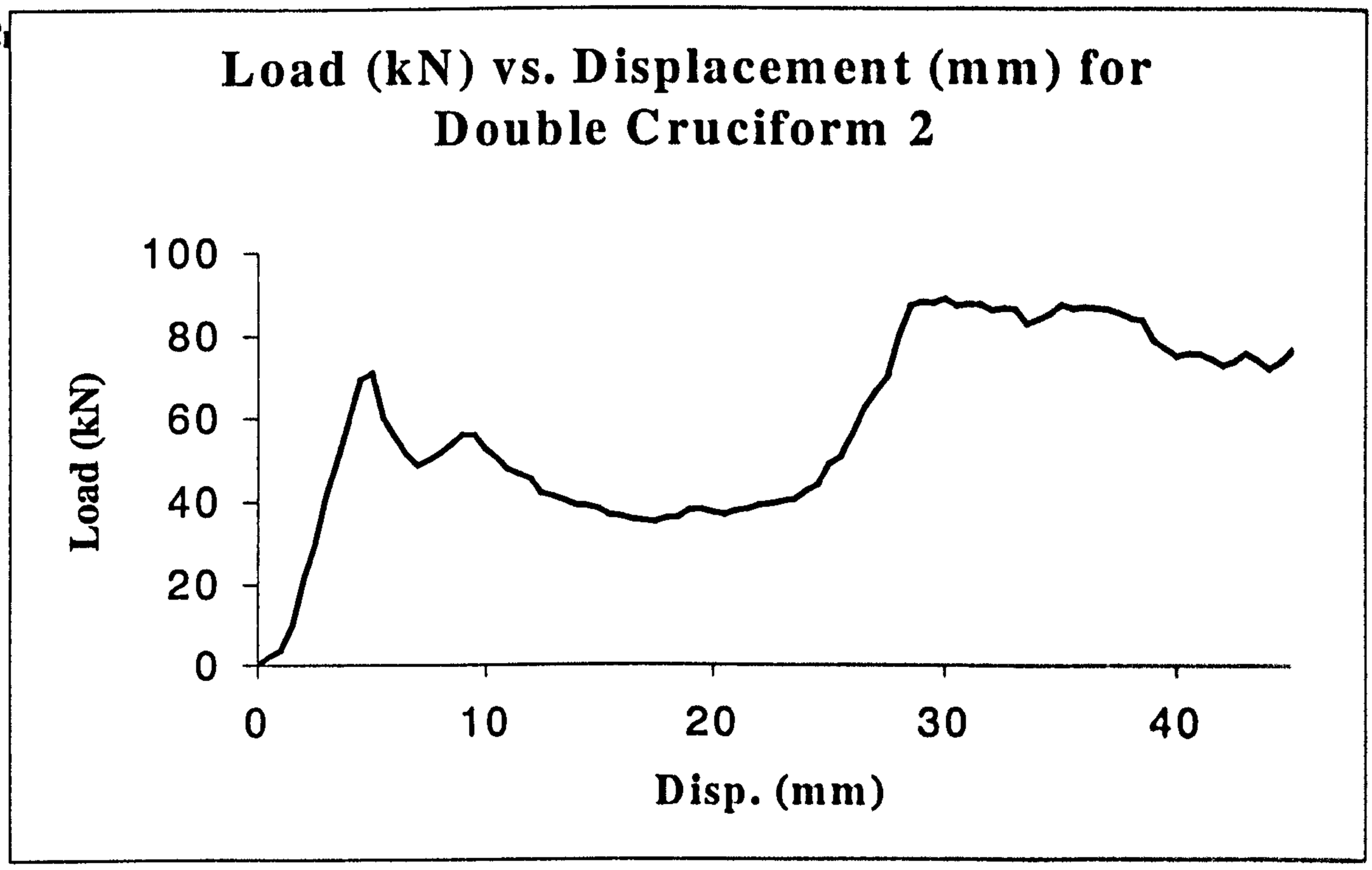

Figure 6.20 Load-Displacement Curve for Double Cruciform 2

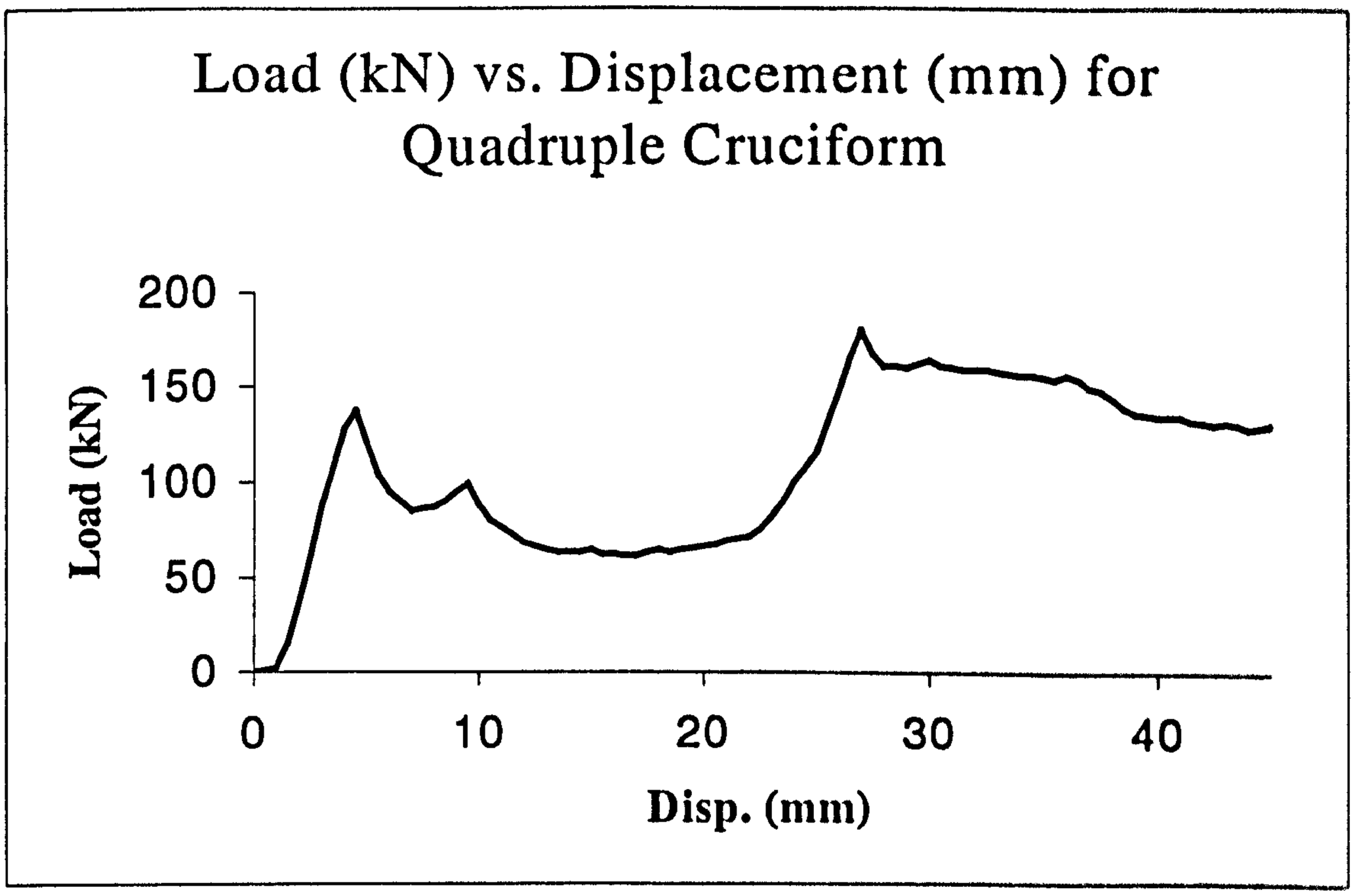

Figure 6.21 Load-Displacement Curve for Quadruple Cruciform

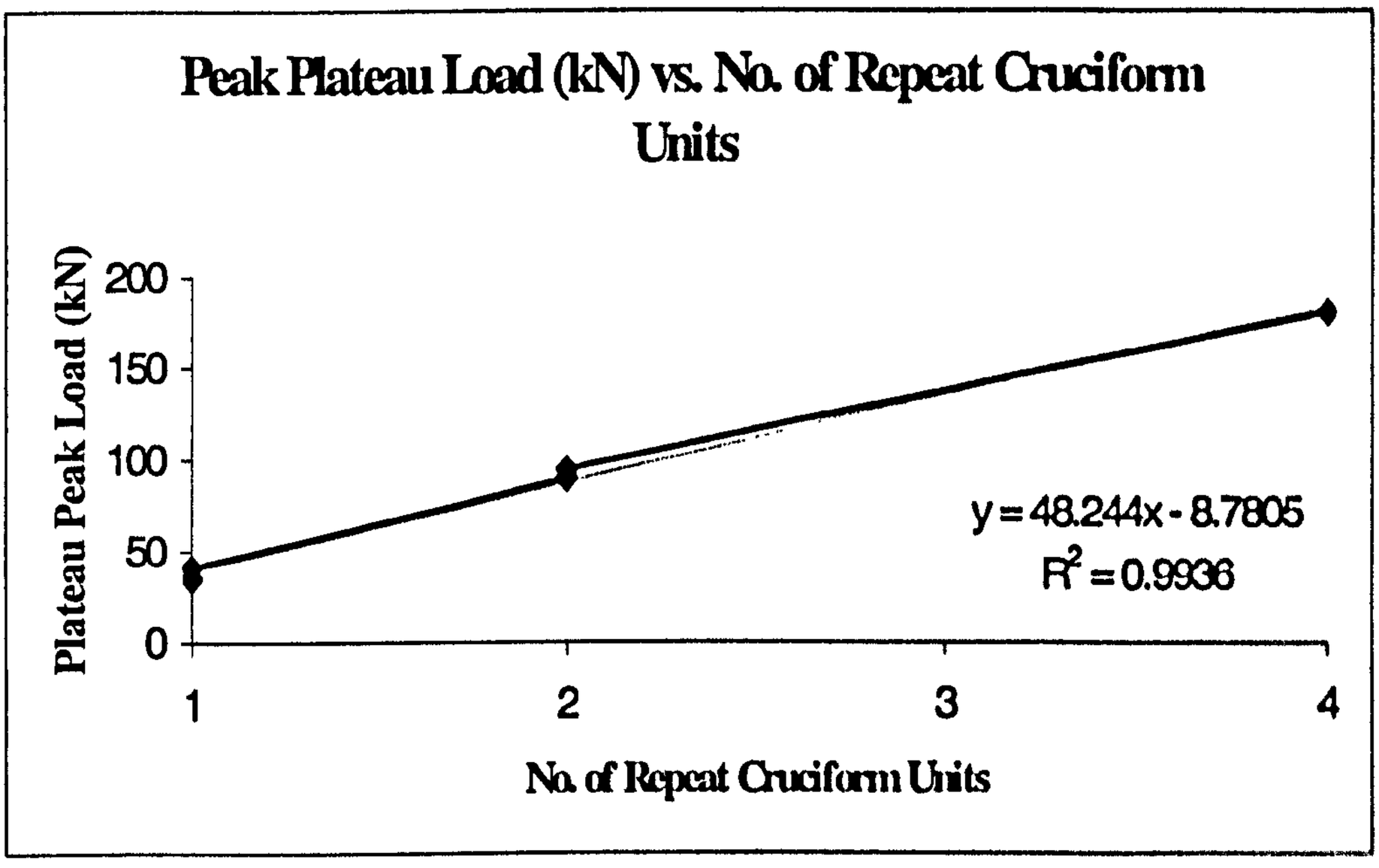

Figure 6.22 Peak Plateau Loads for Cruciform Units

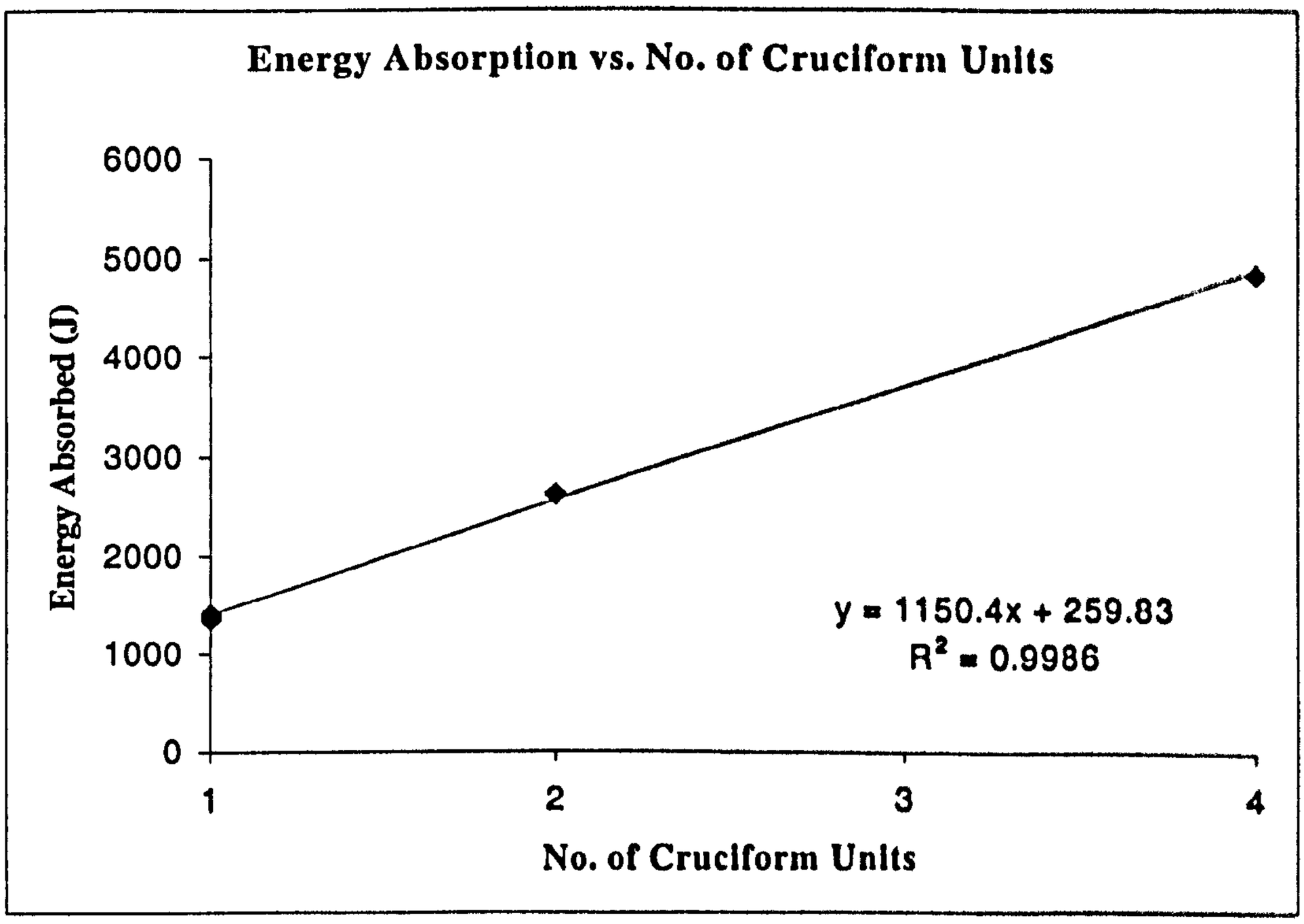

Figure 6.23 Energy Absorbed versus No. of Repeat Cruciform Units

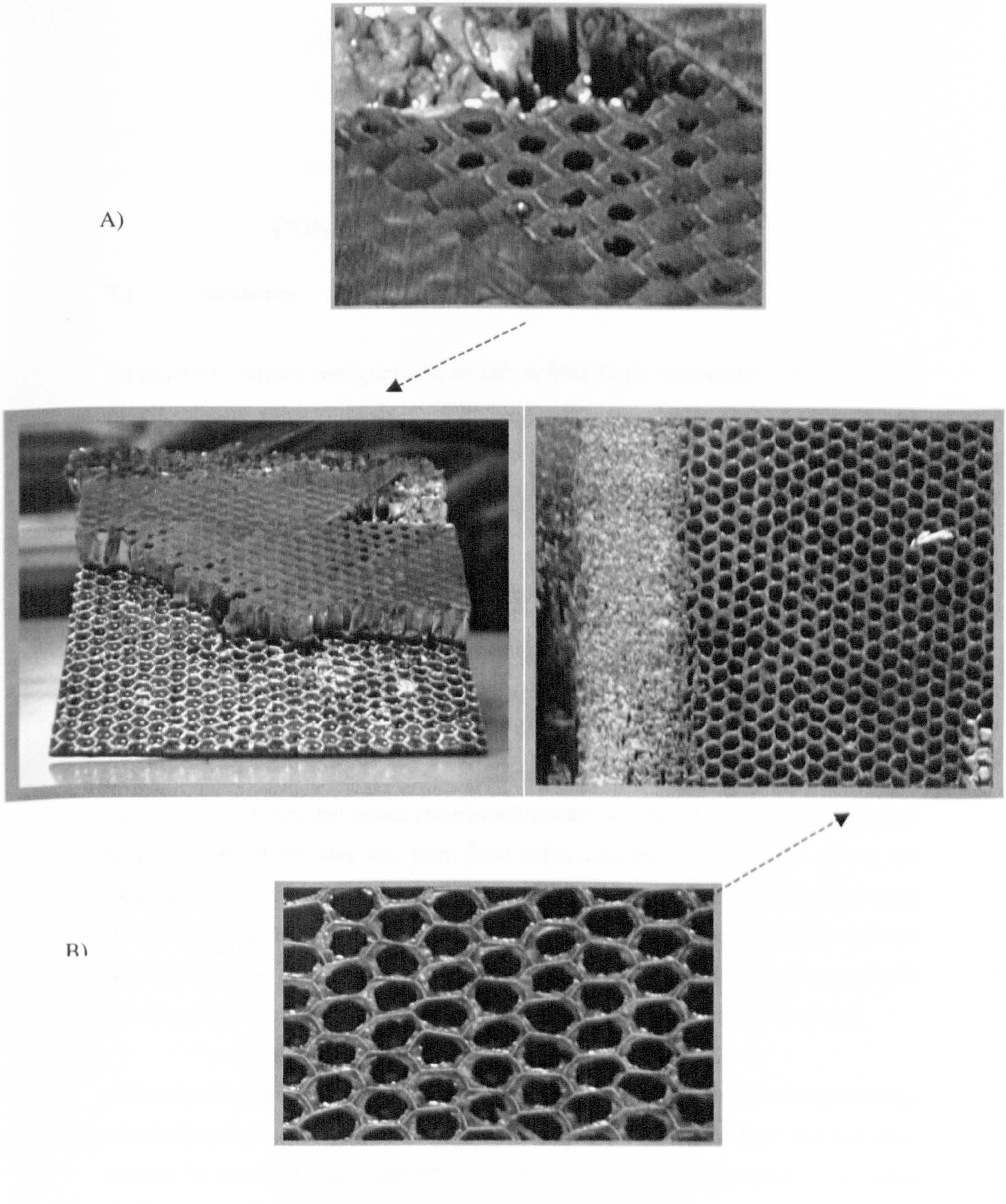

Figure 6.24 Comparison of Face-to-Core Bonding for the two Pre-preg Systems;
A) T300/914, B) HTA/913

CHAPTER 7

CONCLUSIONS AND FUTURE WORK

7.1 Conclusions

To conclude, various configurations of carbon fibre faced, aluminium cored sandwich panels, chosen using Taguchi methodology, were manufactured then subjected to quasi-static in-plane crushing in a compressive test rig, the panels were supported by two pairs of knife-edges whilst crushing. To initiate crushing saw-tooth type triggers were machined into the top of some of the panels.

From these tests it was found that of the two lay-ups tested (uni-directional and quasi-isotropic) the quasi-isotropic panels absorbed more energy, although, the uni-directional samples were able to support greater loads. It was seen that the quasi-isotropic panels maintained a higher level of structural integrity during the crushing process and were therefore able to withstand the crush loads for longer periods of time. The uni-directional panels fragmented quickly and their load carrying capability was soon lost. It was also seen from these initial tests that the role of the core in the sandwich panel was almost totally to support the sandwich faces and it absorbed very little energy. As discussed fully in Chapter 4 it was found that the knife-edge rig used to test the panels, over supported the panels during crushing, and friction between the crushing panels and the knife-edges complicated analysis of the results obtained.

A test rig which only supported the lower half of the sandwich panels during crushing was designed and manufactured. Although, some of the panels crushed in the desired manner i.e. a rolling fragmentation mode, some panels failed prematurely, the faces "ballooning" off. An examination of the failed specimens revealed that the initial movement of the loaded trigger was sometimes inwards, this eventually lead to debonding of the faces and to low values of energy absorption. To assure that the triggers always crushed outwards a symmetrical crush plate with a two degrees

chamfer was machined. Sandwich panels crushed with the simplified rig and the chamfered crush plate failed progressively. It was also found during this section of work that the core-to-bond strength contributed to the failure mode of the sandwich panel. If the bond was too strong then the faces of the sandwich panel would not peel away from the crushing core and the panel would not absorb much energy, conversely if the bond was too weak, the faces of the sandwich panel would rapidly debond from the core leading to the same outcome.

During the testing of the sandwich panels it was seen that most of the energy absorbed was in the faces of the sandwich panels not the core. To investigate parameters such as stacking sequence, friction and the un-supported length of the specimens, small specimens representing the faces of the sandwich panels were manufactured and tested as discussed in Chapter 5. It was shown that these specimens were useful in investigating parameters quickly and cheaply without having to manufacture sandwich panels. The parameters mentioned above were examined and reported on. It was shown that friction had a large effect on the load-displacement characteristics of the small specimens. The failure stresses for all the small specimens tested was larger than that seen for the sandwich panel faces. It was reasoned that as the small specimens did not have the support of a core during crushing, that they should fail at a lower load than the sandwich panel faces.

To recreate the support given to the sandwich panels, in the small specimen crush tests, two small specimens were arranged in a "back-to-back" configuration. Once problems of crush plate alignment had been overcome it was seen that the failure modes and crush stresses in both the small specimens and the sandwich panel faces were comparable. It has been shown that the small specimen tests are a viable alternative to full scale sandwich panel testing in terms of screening of different parameters. Angled stiffeners were also separately crushed.

In Chapter 6 the manufacture and testing of cruciform structures was discussed. Angled stiffeners were manufactured and bonded to the sandwich panels to produce the cruciforms. Ten cruciforms were tested, seven single, two double and a quadruple. Parameters such as the degree of support given to the cruciforms and length of the angled stiffeners were discussed. The load-displacement behaviour of

the cruciforms and its separate constituents i.e. stiffeners and sandwich panels was discussed. It was found that the peak loads of the cruciforms could be calculated from the peak loads of the constituent parts, but the energy absorbed and the stresses seen in the cruciforms were much higher than in the stiffeners and the sandwich panels added together. The load-displacement graphs for the cruciforms were examined, and from these it was reasoned that the cruciform offered more support to itself whilst it crushed and was able to withstand higher crush loads and hence stresses than the sum of its constituent parts, and therefore could absorb more energy.

For cruciforms manufactured from the same T300/914 pre-preg system a linear relationship was seen between all the usual parameters such as energy absorption and peak loads. It should therefore be possible to estimate the properties of larger sandwich subfloor structures from smaller representative structures. These would be less costly and quicker to manufacture.

Additional tests i.e. climbing drum, DCB and tearing tests were also conducted and reported on in Chapter 5. The results of these tests were used to establish the amount of energy absorbed in face-to-core debonding and face tearing both mechanisms seen during the crushing of the cruciforms.

7.2 Further Work

Experimentally, it would be beneficial to continue work on the role of the triggering mechanism. Although, the saw tooth triggering mechanism has been widely used and works well, it would not be feasible to use in a real structure. Perhaps, the triggers would be built in at the manufacturing stage rather than being machined into the finished part. Ideas such as resin rich and resin starved areas could be studied for example as a triggering point in a structure.

Apart from continuing the experimental side of the thesis, the crushing of a sandwich panel could be modelled either using Finite Element Analysis or using simple analytical equations. Appendix C outlines some ideas that may be an initial way to model the debonding of the faces from the sandwich panel core.

REFERENCES

1 **Olsson, Karl-Axel..** Testing of sandwich panels and structures. Report No.88-17, Dept. of Aeronautical Structures and Materials. The Royal Institute of Technology, Stockholm Sweden. March 1988.

2 **Davis, R.** Testing for crashworthiness, Aircraft. Eng. and Aerospace Technology Vol.67 (6) 1995.

3 **Kindervater, C.M. and Georgi, H.** Composite strength and energy absorption as an aspect of structural crash resistance. Proceedings of the International Conference on Structural Impact and Crashworthiness (Ed. N. Jones), Liverpool, 1993, pp189-235, Elsevier Applied Science.

4 **MIL-STD 1290A (AV).** Light fixed and rotary-wing aircraft crash resistance, Dept. of Defence, Washington, DC, Sept. 26, 1988.

5 **Burrows, L.T.** Variable design criteria for rotary wing aircraft crash resistance, Proceedings of the American Helicopter Society 49th Annual Forum, 1993, pp943-953.

6 **Farley, G.L.** The effect of fibre and matrix strain on the energy absorption of composite materials, J. Compos. Mater., 20,1986 pp322-333.

7 **Lavoie, J.A., Morton, J. and Jackson, K.** An evaluation of the energy absorption of laminated composite plates. Proc. Instn. Mech. Engrs. Part G Vol.209, 1995, pp185-194.

8 **Lavoie, J.A. and Kellas, S.** Dynamic crush tests of energy absorbing laminated composite plates, Composites Part A, 27A, 1996, pp467-475.

9 **Lavoie, J.A. and Morton, J.** Design and application of a quasi-static crush test fixture for investigating scale effects in energy absorbing composite plates. NASA CR 4526, August 1993.

10 **Fleming, D.C and Vizzini, A.J.,** The energy absorption of composite plates under off-axis loads. J. Compos. Mater., 30, No.18, 1996, pp1977-1995

11 **Vizzini, A.J and Dubey, D.D.,** Energy absorption of plates and tubes, J. Compos..Mater, 32, No.2, 1998, pp158-176

12 **Laananen, D.H and Bolukbasi, A.O.** Prediction of energy absorption in composite stiffeners. Composite Structures, 32, 1995, pp173-186.

13 **Laananen, D.H and Bolukbasi, A.O.** Energy absorption in composite stiffeners. Composites, 26, 1995 pp291-301.

14 **Ramany Bala Poubady, V.** Progressive crushing of woven carbon fibre/epoxy composite plates. MSc Project, Dept. of Aeronautics, Imperial College, 1997.

15 **Thornton, P.H., Harwood J. J., and Beardmore, P.** Fibre-reinforced plastic for energy absorption purposes. Compos. Sci. Technol., 24,1985 pp275-298.

16 **Hull, D.** A unified approach to progressive crushing of fibre-reinforced composite tubes. Compos. Sci. Technol., 40, 1991, pp377-421.

17 **Farley, G.L.,** The effect of specimen geometry on the energy absorption capability of composite materials. J. Compos. Mater., 20, 1986 pp390-400.

18 **Czaplicki, M.J., Robertson, R.E., and Thornton, P, H.,** Comparison of bevel and tulip triggered pultruded tubes for energy absorption. Compos. Sci. Technol., 40, 1991, pp31-46.

19 **Farley, G.L.,** The effects of crushing speed on the energy-absorption capability of composite tubes. J. Compos. Mater., 25, 1990, pp1314-1329.

20 **Thornton, P.H.,** Energy absorption in composite structures. J. Compos. Mater., 13 (1979) pp247-262.

21 **Farley, G.L.,** Energy absorption of composite materials. J. Compos. Mater., 17. 1983, pp267-279.

22 **Zenkert, D.** Damage tolerance of foam core sandwich constructions. Report No.90-8, Dept. of Aeronautical Structures and Materials. The Royal Institute of Technology, Stockholm Sweden. July 1990.

23 **Goldsmith, W. and Sackman, J.L,.**Energy absorption by sandwich plates: a topic in crashworthiness. Proceedings of the Symposium on Crashworthiness and Occupant Protection in Transportation systems. (Edited by T.Khalil et al.) AMD-Vol-126/BED-Vol 19, pp1-30, New York, ASME (1991).

24 **Brachos, V., Neogi, D. and Douglas, C.D.,** Analysis of Edge Loaded Sandwich Panels - Energy Absorption Characteristics, Proceedings of the 41st International SAMPE Symposium, pp. 800-813, 1996.

25 **Cronkhite, J. D., Berry, V. L.** Crashworthy airframe design concepts. NASA Contractor Report 3603, Sept 1992.

26 **Bannerman, D.C., and Kindervater, C.M.,** Crashworthiness investigation of composite aircraft subfloor beam sections. Proceedings of the International

Conference on Structural Impact and Crashworthiness (Ed. J. Morton), London, July 1984, pp710-722. Elsevier Applied Science.

27 **Hanagud, S., Craig, J I., Spiram P and Zhou, W.** Energy absorption behaviour of graphite epoxy composite sine webs. J. Compos. Mater., 23, 1989, pp448-459.

28 **Jimenez, M.A., Miravete, A., Larrode, E. and Revuelta D.** Effect of trigger geometry on energy absorption in composite profiles. Comp. Struct. 48, pp107-111. 2000.

29 **Barquet, H. and Sarlin, P.** The development of a crashworthy composite fuselage and landing gear. Proceedings of the American Helicopter Society 48th Annual Forum, 1992. pp1421-1430.

30 **Frese, J. Nitschke, D.,** Crushing behaviour of helicopter subfloor structures. AGARD-CP-443. 1988, paper 10, pp1-25.

31 **Jackson K. E. and Fasanella E. L.** Design of a scale model composite fuselage concept for improved crashworthiness. J of Aircraft, Vol. 38, No.1 Jan-Feb 2001.

32 **Bisagni, C,** Crashworthiness of helicopter subfloor structural components. Aircraft Engineering and Aerospace Technology, Vol.71 No.1 1999 pp 6-11.

33 **Magee, C.L. and Thornton, P.H.,** Design considerations in energy absorption by structural collapse, 1978, SAE Paper No.78-434.

34 **Kindervater, C. Gietl., A. and Muller, R.,** Crash investigations with sub-components of a composite helicopter lower airframe section. AGARD-CP-443. 1988, paper 11, pp1-18..

35 **Jones, L. and Carden, H.D.** Evaluation of energy absorption of new concepts of aircraft subfloor intersections, NASA Technical Paper 2951, November 1989.

36 **Farley G.L. and Jones R.M.,** Prediction of the Energy-Absorption Capability of Tubes, J. Compos.Mater, Vol. 26, No.3, 1992, pp388-404.

37 **Mamalis A.G, Manolakas D.E, Demosthenous G.A and Ioannidis M B.,** Analytical Modelling of the static and dynamic axial collapse of thin walled fibreglass composite conical shells, Int.J. Impact. Engng, Vol. 19, Nos. 5-6, 1997. pp477-492.

38 **Mamalis A.G, Manolakas D.E, Demosthenous G.A and Ioannidis M B.,** The static and dynamic axial collapse of composite automotive frame rails, Composite Structures 34, 1996, pp77-90.

39 **Mamalis A.G, Manolakas D.E, Demosthenous G.A and Ioannidis M B.,** Energy absorption capability of fibreglass composite square frustra subjected to static and dynamic axial collapse, Thin Walled Structures Vol. 25, No.4 1996, pp 269-295.

40 **Farley G.L. and Jones R.M.,** Analogy for the effect of material and geometrical variables on the energy-absorption capacity of tubes, J. Compos.Mater, Vol. 26, No.1, 1992, pp78-89.

41 **Kendall, K.,** Interfacial cracking of a composite, Part 1-Interlaminar shear and tension, J of Mat. Sci. 11, 1976, pp638-644.

42 **Hulway, J.A and Wineman, A.S.,** A model for the crush of polymer matrix composite tubes, Proceedings of the 8th Advanced Composites Conference, Chicago, Illinois, 2-5 Nov. 1992, pp167-178.

43 **Kendall K.,** Interfacial cracking of a composite, Part 2-bending, J of Mat. Sci. 11, 1976, pp1263-1266.

44 **Laananen D.H, and Bolukbasi A.O.,** Analytical and experimental studies of crushing behaviour in composite laminates, J. Compos.Mater, Vol. 29, No.8, 1995, pp1117-1138.

45 **ASTM D 1781-76** Standard Test Method for Climbing Drum Peel Test for Adhesives – ASTM 1976.

46 **ASTM D 5528-94a** Standard Test Method for Mode I Interlaminar Fracture Toughness of Unidirectional Fiber Reinforced Polymer Matrix Composites – ASTM 1994.

47 **Greenhalgh, E.S** Characterisation of Mixed Mode Delamination Growth in Carbon Fibre Composites. PhD Thesis, Imperial College of Science, Technology and Medicine, London 1996.

48 **Vernon, M.** An investigation into the use of side-delaminations in inter-laminar fracture, MSc Dissertation, Centre for Composite Materials, Imperial College, London University, September 2001

49 **Taguchi, G. and S.Koneshi.** Taguchi Methods, Orthogonal Arrays and Linear Graphs, American Supplier Institute, Dearborn MI.

50 **Williams J.G.,** Fracture mechanics of composite failure, Proceedings of the Institution of Mechanical Engineers, Vol. 204, March 1990, pp209-218.

51 **Roark R.J.,** Formulas for Stress and Strain, 5th Edition, 1975, Edited by McGraw-Hill.

APPENDIX A

Use of Taguchi Methodology to Optimise Sandwich Panel Response

Taguchi Methodology

Taguchi methods were developed by Genechi Taguchi [40] to improve the implementation of total quality control in Japan. They are based on the design of experiments to provide near optimal quality characteristics for a specific objective. The objective of the Taguchi method is process and product design improvement through the identification of easily controllable factors and their settings.

Taguchi methods were used in this project to maximise the energy absorbing capabilities of CFRP/aluminium honeycomb core sandwich panels.

The first point to establish in any type of experimental programme is that the objective of the programme is clear. Whatever the type of approach used, the most common cause of failed experiments is lack of clarity as to the reasons for doing them. The simplest, least effective, least efficient, but unfortunately most common way is to "follow your nose". In this, each experiment is decided on the basis of the previous one, almost invariably leading to "chasing your tail" and so to much wasted effort.

A more logical approach than the one above, is to use the "change one variable at a time" method of experimentation. Using this method the engineer observes the results of an experimental trial, having changed the setting (level) of only one factor whilst keeping every other factor fixed. A factor is a process variable or any uncontrolled source of variation, either quantitative or qualitative. The experimental process should start with the understanding that real life rarely allows the manipulation of only a single factor, this premise is particularly true of most of today's manufacturing processes, where the relationship between a large number of variables, with different levels, is always in need of systematic study for reliable effects to be obtained.

For a one factor at a time experiment to be reliable, all possible combinations of level settings should be incorporated. But, the effort and the experimental cost required for such an experiment, termed a full factorial, could be prohibitively large and unrealistic (unless only a few factors are under study). For example, in the case of a 7 two-level factors, a full factorial experiment would require 128 trial runs. A more efficient type of factorial which retains much of the effectiveness of the full factorial is the orthogonal array, as described in recent years by Taguchi. Although Taguchi did not originate orthogonal arrays, he has done much to promote their use. In essence, they are fractional factorials (that is, subsets of full factorials) possessing the following properties:-

1) Balance: the different levels of each factor occur the same number of times.

2) Estimability: every factor effect must be capable of being estimated.

3) Orthogonality: This property is satisfied if, for example, for each pair of factors, every combination of factor levels exists and occurs equally often. As an example of the type of design which can be used, for a programme involving seven variables (A-G) at two levels each, the L_{12} orthogonal array (Table A.1) would require twelve experiments for a simple optimisation objective (-1 and +1 are levels of the variables, -1 indicating that the variable is held at a low value e.g. 1mm face skin thickness, +1 a high level, e.g. a 3mm skin thickness).

TRIAL	A	B	C	D	E	F	G
1	+1	+1	-1	+1	+1	+1	-1
2	+1	-1	+1	+1	+1	-1	-1
3	-1	+1	+1	+1	-1	-1	-1
4	+1	+1	+1	-1	-1	-1	+1
5	+1	+1	-1	-1	-1	+1	-1
6	+1	-1	-1	-1	+1	-1	+1
7	-1	-1	-1	+1	-1	+1	+1
8	-1	-1	+1	-1	+1	+1	-1
9	-1	+1	-1	+1	+1	-1	+1
10	+1	-1	+1	+1	-1	+1	+1
11	-1	+1	+1	-1	+1	+1	+1
12	-1	-1	-1	-1	-1	-1	-1

Table A.1 L_{12} Orthogonal array

These methods can be used or adapted for a wide range of experimental needs. They are ideal for optimising conditions either to achieve a desired level of a quality characteristic or to minimise variation.

Taguchi Methods Operation

The basic procedure for planning and carrying out experimental programmes is broadly the same whatever the needs. There are certain steps which must be followed in every case.

The essential steps are:

1. Define the overall objective.
2. Define and agree the questions which need to be answered.
3. Formulate the objectives of the experiment.

4. Define the type of experiment (Taguchi appropriate ?)
5. Define the assessment characteristics.
6. Define the variables/control factors, and their levels.
7. Predict possible interactions.
8. Select an array.
9. Assign factors/interactions to columns.
10. Run the programme.
11. Prepare response tables.
12 Select factors to reduce variation.
13. Select factors to set level.
14. Refer to objective.
15. Determine the preferred level of factors.

Although orthogonal arrays can be used to analyse interactions between factors, in the case of maximising the energy absorption of sandwich panels it was used to establish the main effects (on the response of interest) of the associated factors. By main (factor) effect it was meant the individual contribution of the factor to the total variability inherent in the experimental results.

An L_{12} orthogonal was chosen as the basis for the analysis, which allows the analysis of up to 7 main effects (A-G in Table A.1), although in our case we had 4, namely:- face thickness, core thickness, inclusion of trigger mechanism (or not) and lay-up. An L_8 array would also be able to analyse 7 main effects in 8 experiments, but it was thought that it would be beneficial to manufacture slightly more panels to familiarise ourselves with the manufacturing process. As all rows and columns in the array have to be full for the array to be balanced, 3 interactions between the factors were also included (Table A.2). Each factor had 2 levels (except interactions).

Variables	FACTORS	LEVEL -1	LEVEL +1
A	Face thick.	1mm	3mm
B	Core thick	10mm	20mm
C	Trigger	No	Yes
D	Lay-up	Unidirectional	Quasi-isotropic
E	Interactions	Interactions	Interactions
F	Interactions	Interactions	Interactions
G	Interactions	Interactions	Interactions

Table A.2 Main effects

In this example A to G will be used to represent the names of the factors. Then each row of +1's and -1's signs show how to set the variables for one of the runs. The first row has + + - + + + - in the 7 columns; therefore for trial #1 A, B, D, E and F, will be set high (+1) and C, and G low (-1) (see Table A.3 below). The output of these tests was the energy absorbed measured in Joules.

TRIAL	A	B	C	D	E	F	G	En(J)
1	+1	+1	-1	+1	+1	+1	-1	1972
2	+1	-1	+1	+1	+1	-1	-1	1946
3	-1	+1	+1	+1	-1	-1	-1	462
4	+1	+1	+1	-1	-1	-1	+1	1082
5	+1	+1	-1	-1	-1	+1	-1	1222
6	+1	-1	-1	-1	+1	-1	+1	1594
7	-1	-1	-1	+1	-1	+1	+1	322
8	-1	-1	+1	-1	+1	+1	-1	413
9	-1	+1	-1	+1	+1	-1	+1	283
10	+1	-1	+1	+1	-1	+1	+1	2345
11	-1	+1	+1	-1	+1	+1	+1	887
12	-1	-1	-1	-1	-1	-1	-1	660

Table A.3 Table of variable levels and energy absorbed by each panel

Method of Analysis

To eliminate unwanted factors the "b coefficients" are calculated by the following process.

- Compute **sum** (+1) and **sum** (-1) and the **difference** for each column.
- **Check sum** is (sum +) + (sum -).
- Compute **effect** by dividing the difference by T/2, which is the number of trials/2 T=12 here. T is always an even number.
- Compute the **b's** by dividing each effect by 2.

So for example:- Referring back to the previous table column A has the following order from top to bottom +1 +1 -1 +1 +1 +1 -1 -1 -1 +1 -1 -1. If all the response values are added together the total will be 13,188 (Third row down in table below). If all the response values corresponding to a +1 are added the total will be 10,161 (First row down in table below). Similarly for the response values for the minuses. The difference is then obtained by subtracting the + value from the - value i.e. 10,161 - 3027 = 7134 The difference is then divided by T/2 (T = 12 in this case) to compute the effect i.e. 7134/6 = 1189. Lastly each effect is divided by 2 to compute the b coefficient i.e. 1189/2 = 594.5

	A	B	C	D	E	F	G
Sum (+)	10,161	5908	7137	7330	7095	7161	6513
Sum (-)	3027	7280	6053	5858	6093	6027	6675
Check	13,188	13,188	13,188	13,188	13,188	13,188	13,188
Diff.	7134	-1372	1081	1472	1002	1134	-162
Effect	1189	-229	180	245	167	189	-27
b	595	-115	90	123	84	95	-14

Table A.4 Results

Once the b coefficients have been calculated the smallest b's can be eliminated. The biggest factors whether + or - should be retained. In the example Factor A (skin

thickness) is the largest with a b of 595. A negative sign means that the response (energy absorption in this case) increases more when the factor is held at its minus limit than at its plus limit, therefore from this experiment it would seem that the thickness of the core increases the energy absorption decreases. There is a benefit in knowing the factor's size whether its b is positive or negative.

Conclusions from Taguchi Trial

The conclusions from the Taguchi trial are discussed in Chapter 4.

APPENDIX B

Video Stills of Various Crushing Composite Structures

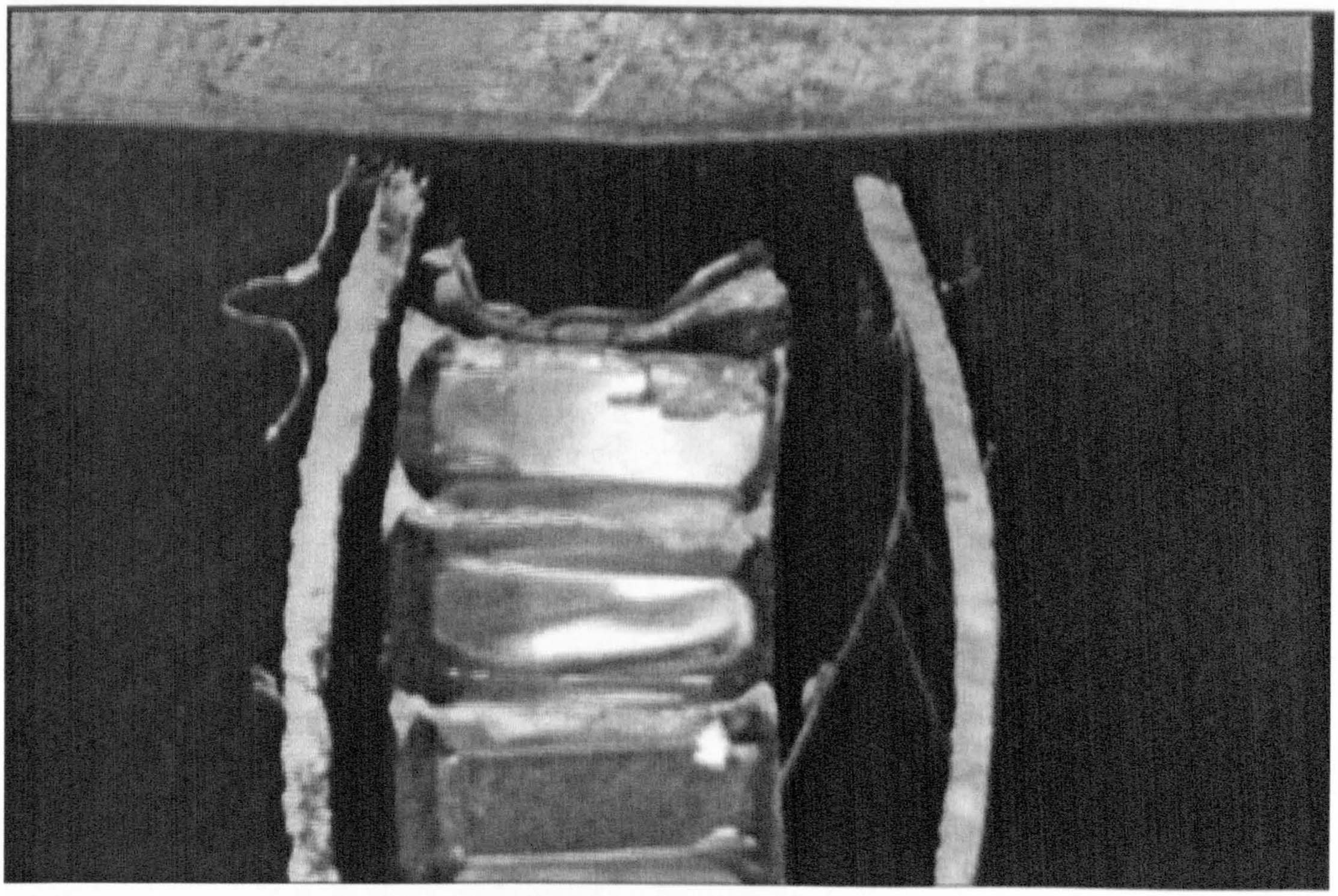

Figure B.1

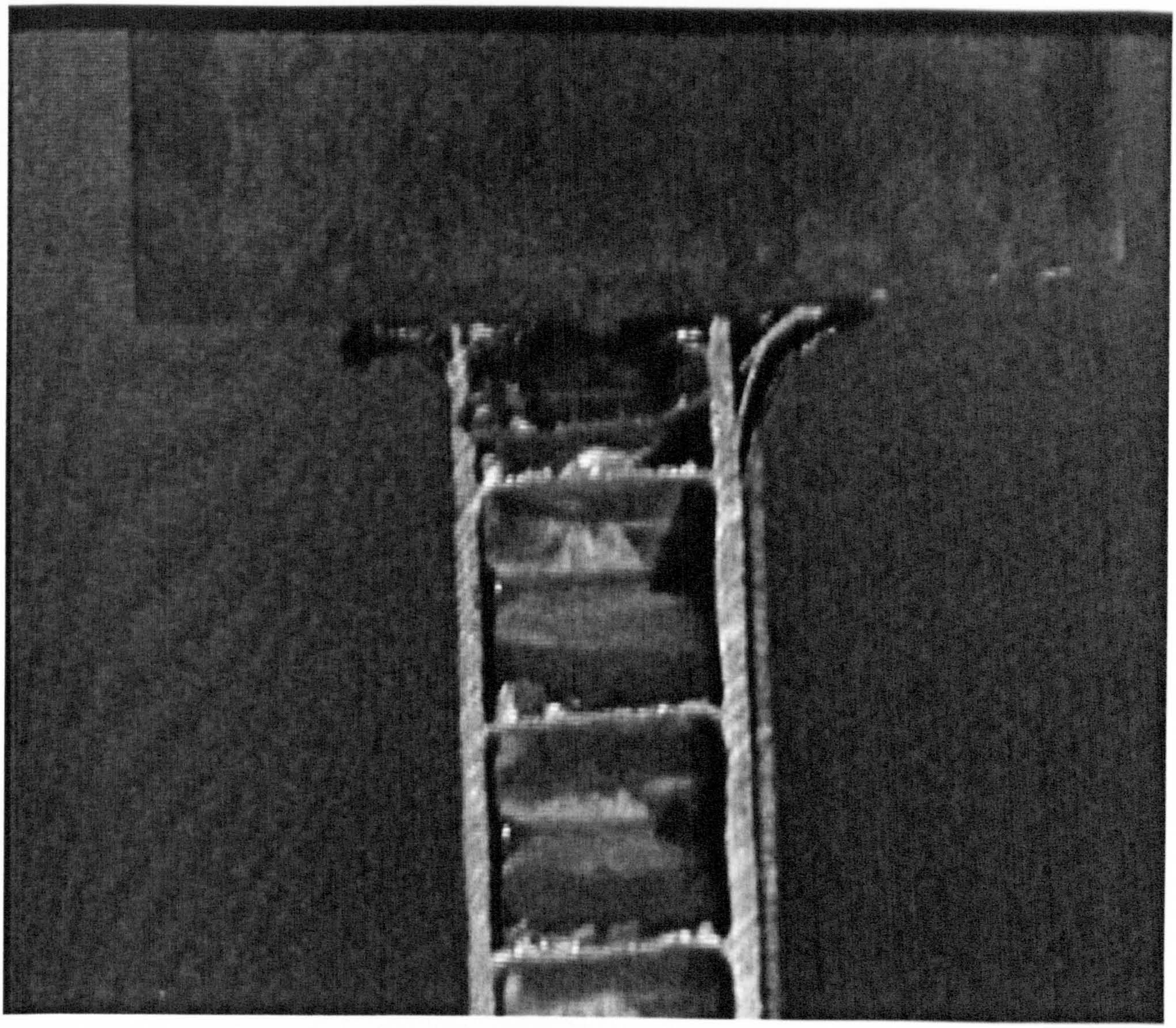

Figure B.2

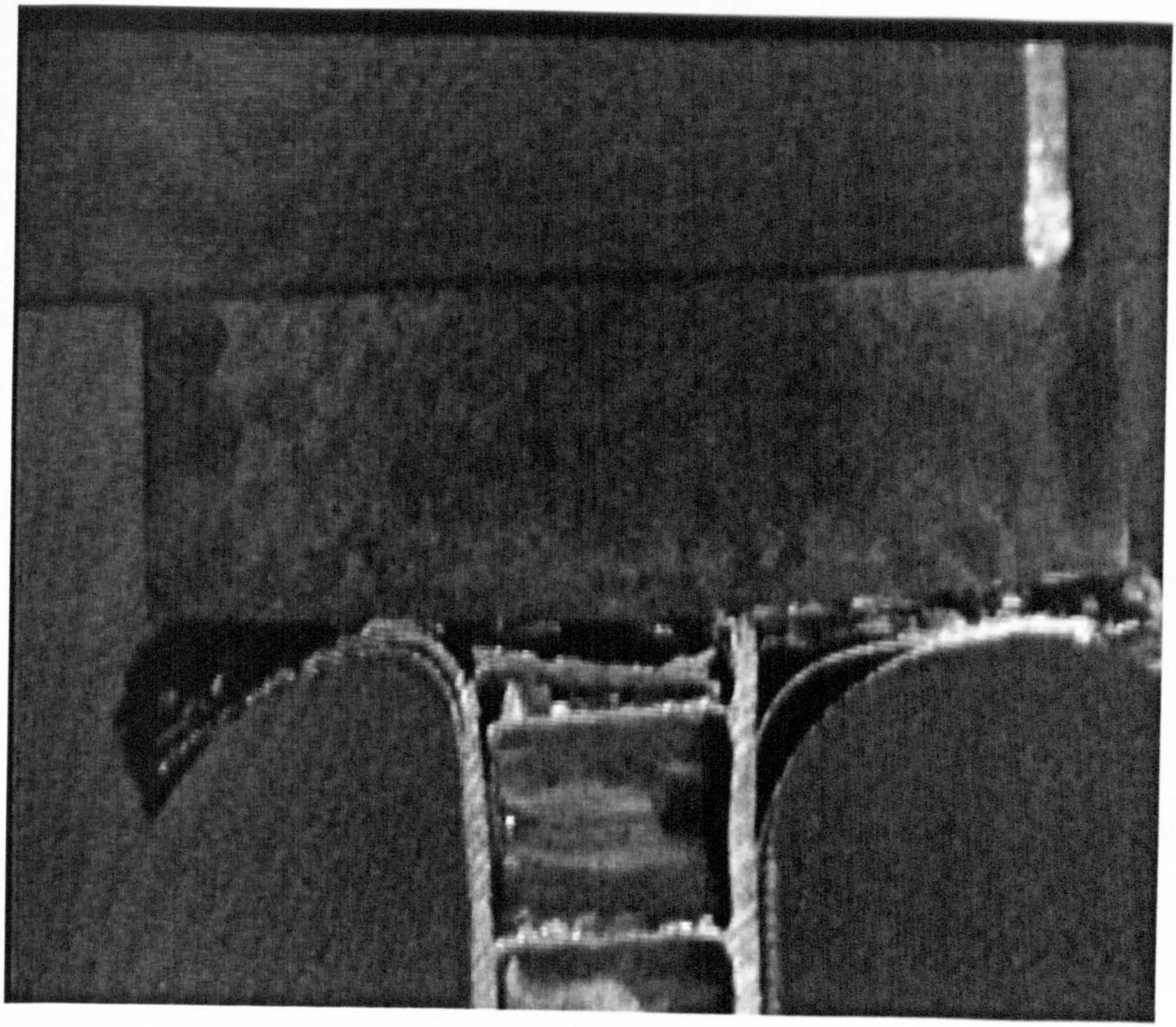

Figure B.3

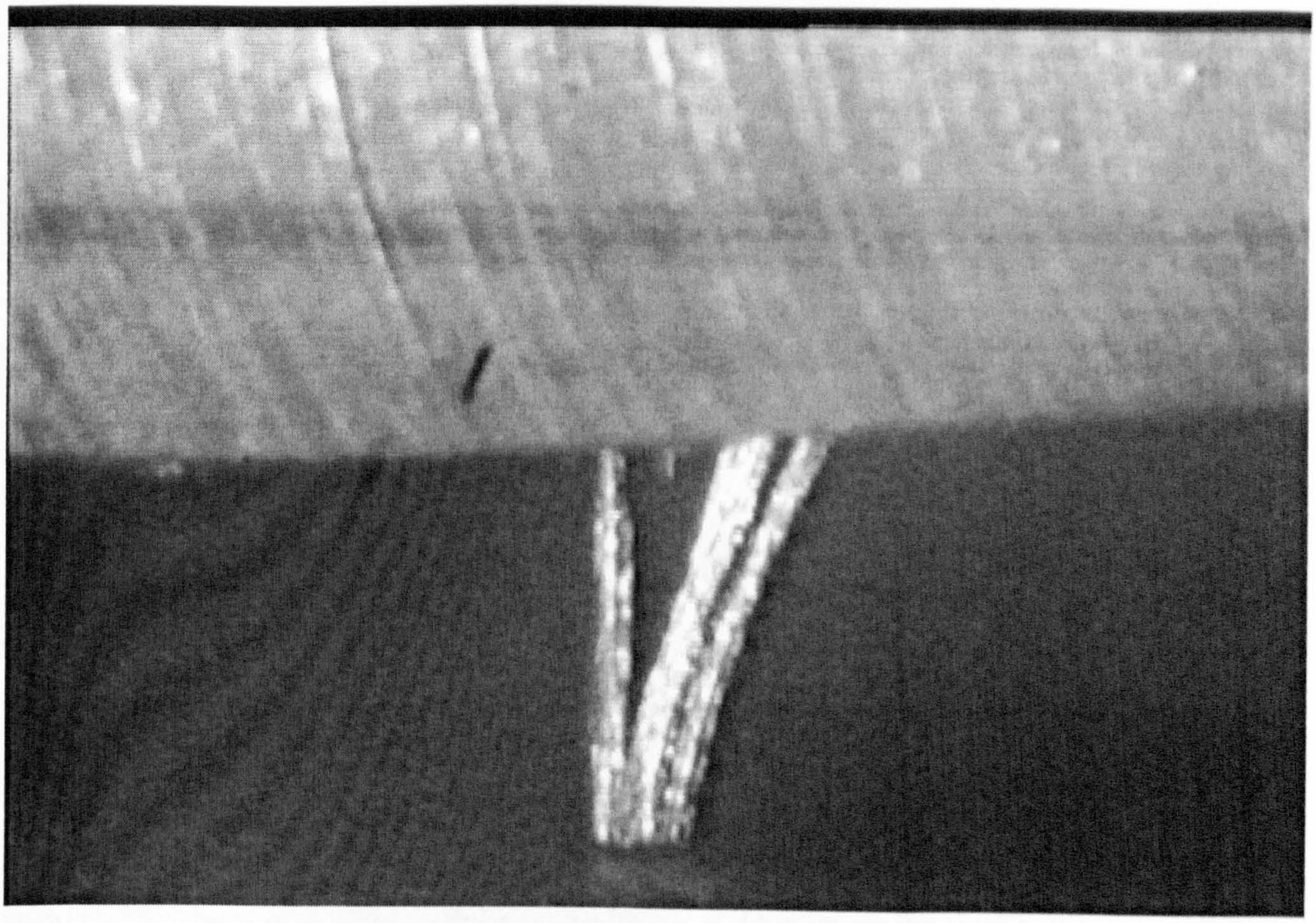

Figure B.4

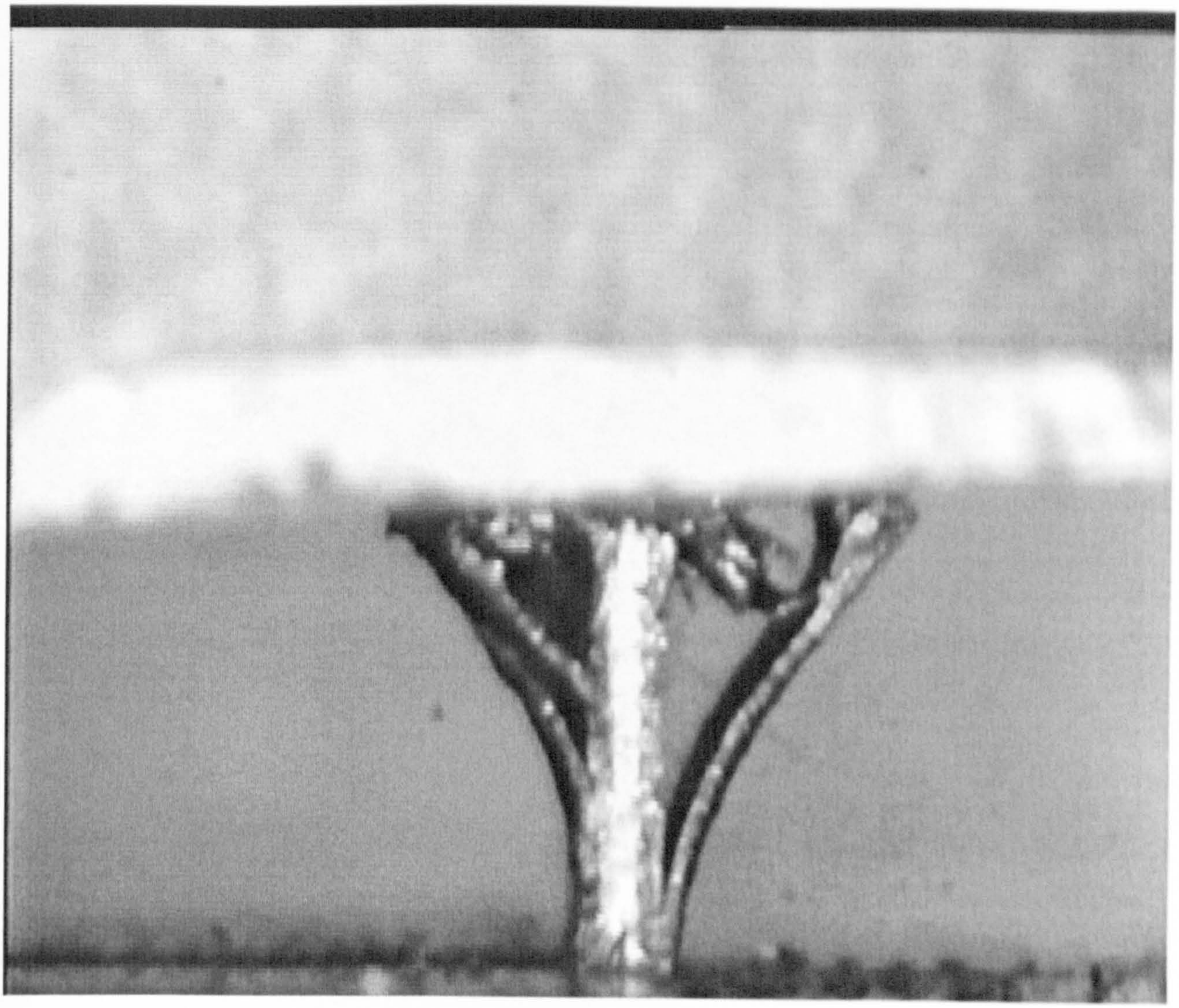

Figure B.5

Figure B.6

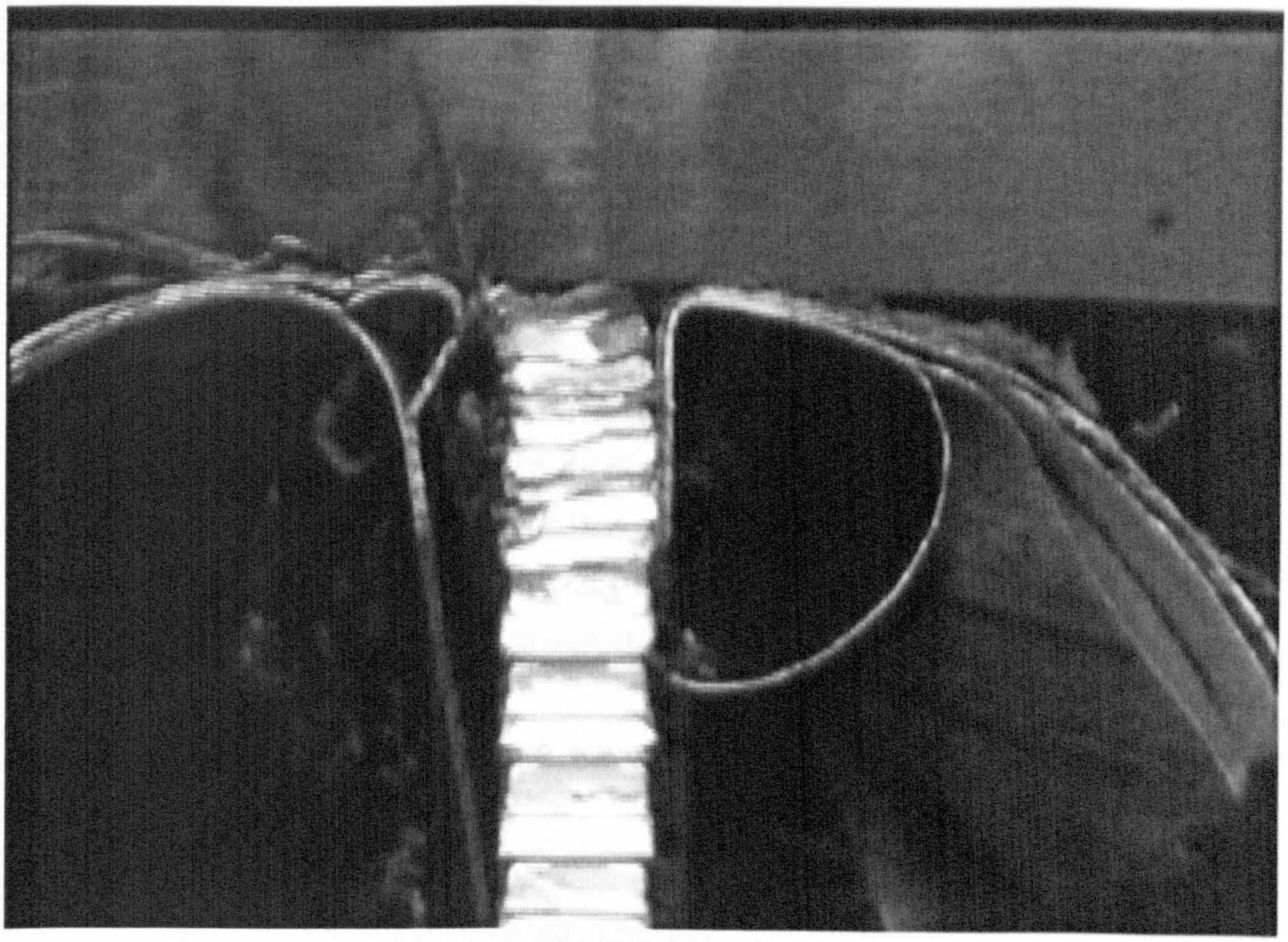

Figure B.7

APPENDIX C

Outline Method for Modelling the Compressive Failure of a Sandwich Panel

The work detailed below is a first approximation of a method for modelling the face-to-core debonding which was seen during the in-plane crushing of a sandwich panel. The sandwich panel could initially be represented by a beam being compressed by a known load. It has been assumed that friction between the arms of the beam, and between the arms and the crushing plate is zero. It has also been assumed that as the cross-head progresses a distance δ the crack advances a distance δ, under a constant load P, (Figure C.1) therefore the crack growth is steady.

Linear elastic fracture mechanics ideas developed by Williams[50] may be applied in this situation e.g.

Work done = Work consumed in fracture - loss of strain energy

$$P\delta = G_{Ic}\delta B - \frac{P^2\delta}{E2Bd}$$

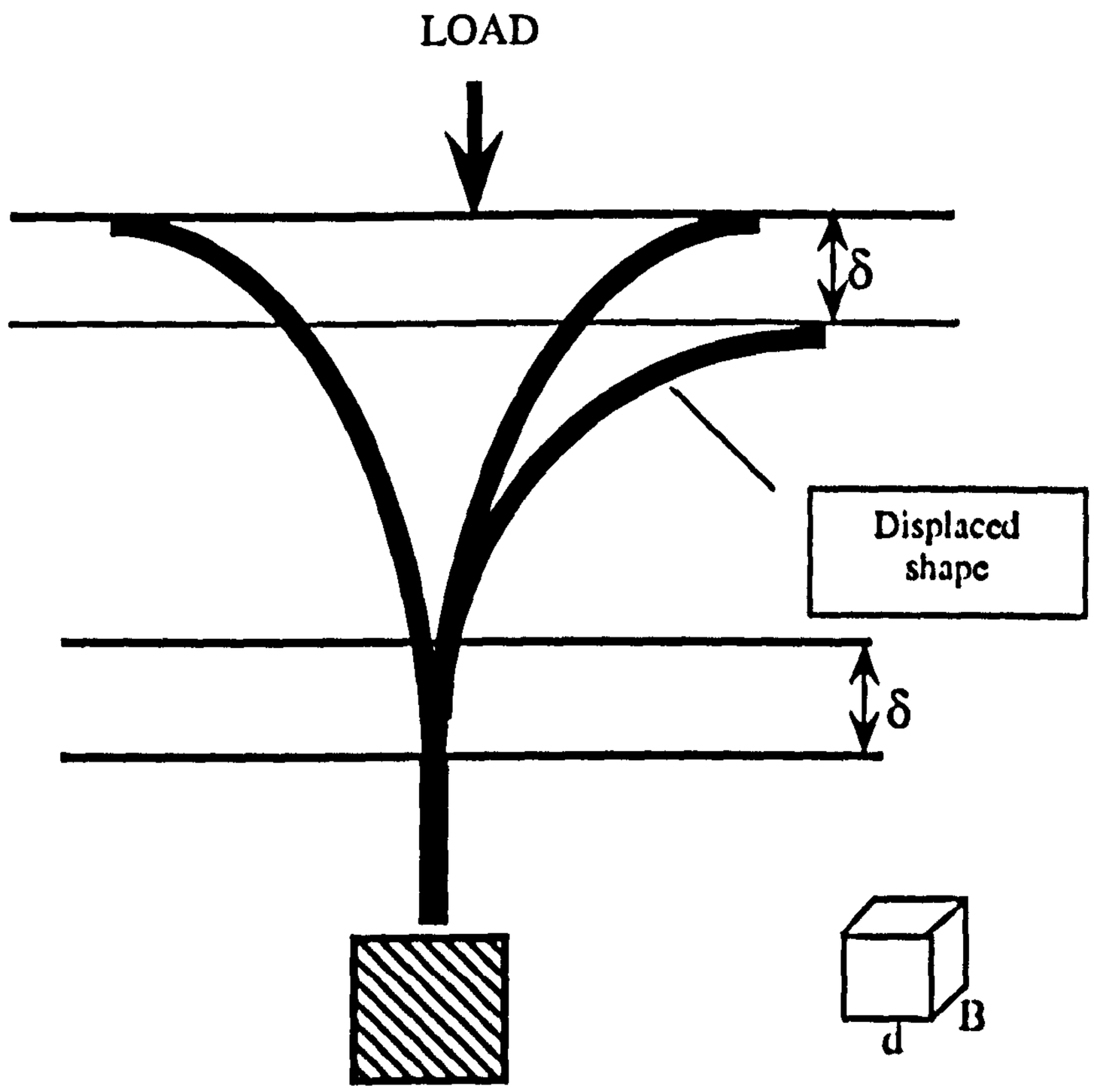

Figure C.1 Steady state geometry

As load is applied to the top of the beam, several things could happen. The beam could crush catastrophically, buckle or, a crack could form in the beam, if this occurs, then as the loading continues the central crack could continue to grow, or, secondary cracks could develop in the arms of the beam. To establish the sequence of events, the geometry of the crushing beam and the values of G in the two areas indicated in Figure C.2 would have to be calculated.

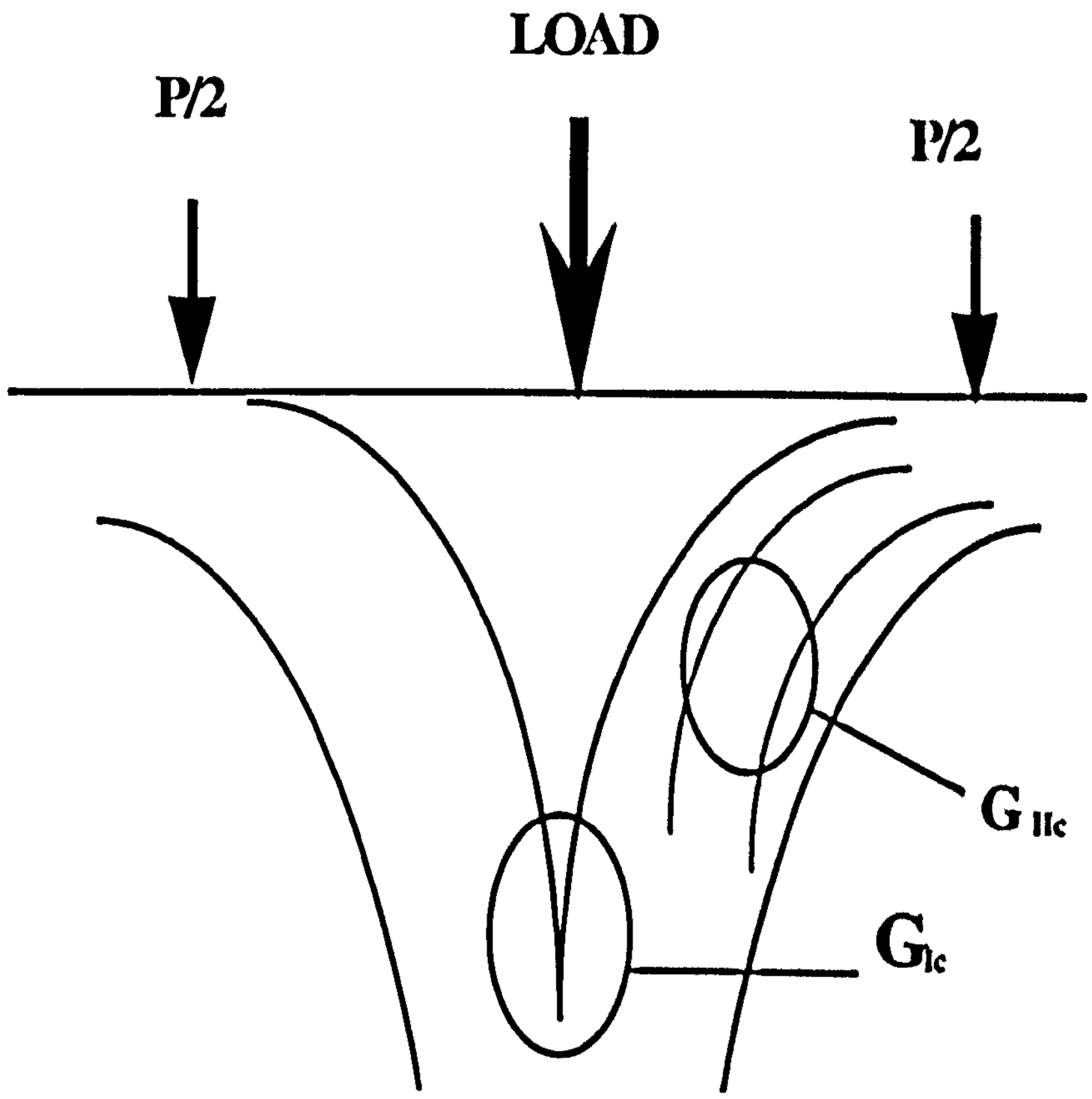

Figure C.2 Position of beam cracks

The Elastica Theory [51] for large deflections of buckled beams may be suitable to ascertain the beam geometry, assuming at steady state that $\alpha = 90°$, the length of the bar "l" can be calculated using:-

$$l = \int_0^{\alpha} \frac{d\theta}{k\sqrt{2}\sqrt{\cos\theta - \cos\alpha}} = \frac{1}{2k}\int_0^{\alpha} \frac{d\theta}{\sqrt{\sin^2\frac{\alpha}{2} - \sin^2\frac{\theta}{2}}}$$

Knowing "l" the elastica theorem would then enables us to calculate the x and y displacements of the beam under a given load, hence G_{Ic} could be calculated.

The Elastica Theorem [51] may also be able to be used to model crack growth in the tops of the arms where Mode II cracking may occur. By assuming a reduced stiffness (EI) in the top half of the arms the effect of cracks secondary to the main central crack could be modelled. If the geometry of the crushing arms could be found, then for a given applied load the moment acting on the arms could be found, leading to the calculation of G_{IIc}. Once the fracture energies for the two areas had been calculated the behaviour of the beam under compressive loading could start to be understood, parameters such as friction could then be added.

APPENDIX D

Load-Displacement-Energy Data for Single, Double and Quadruple Cruciforms manufactured from T300/914 Pre-preg.

Cruciform 5			Cruciform 6			Cruciform 7		
Disp (mm)	Load (kN)	Energy (J)	Disp (mm)	Load (kN)	Energy (J)	Disp (mm)	Load (kN)	Energy (J)
0	0		0	0		0	0	
0.5	18		0.5	5		0.5	5	
1	21	9.75	1	4	2.25	1	10	3.75
1.5	26	11.75	1.5	7	2.75	1.5	19	7.25
2	31	14.25	2	8	3.75	2	25	11
2.5	36	16.75	2.5	15	5.75	2.5	30	13.75
3	34	17.5	3	20	8.75	3	38	17
3.5	31	16.25	3.5	26	11.5	3.5	41	19.75
4	28	14.75	4	31	14.25	4	40	20.25
4.5	26	13.5	4.5	34	16.25	4.5	36	19
5	24	12.5	5	35	17.25	5	31	16.75
5.5	24	12	5.5	34	17.25	5.5	29	15
6	23	11.75	6	31	16.25	6	27	14
6.5	24	11.75	6.5	29	15	6.5	25	13
7	24	12	7	22	12.75	7	26	12.75
7.5	26	12.5	7.5	28	12.5	7.5	28	13.5
8	28	13.5	8	27	13.75	8	29	14.25
8.5	28	14	8.5	27	13.5	8.5	30	14.75
9	24	13	9	26	13.25	9	30	15
9.5	24	12	9.5	27	13.25	9.5	29	14.75
10	21	11.25	10	26	13.25	10	28	13.75
10.5	20	10.25	10.5	24	12.5	10.5	23	12.25
11	20	10	11	24	12	11	21	11
11.5	18	9.5	11.5	22	11.5	11.5	19	10
12	17	8.75	12	22	11	12	18	9.25
12.5	19	9	12.5	21	10.75	12.5	19	9.25
13	19	9.5	13	19	10	13	20	9.75
13.5	18	9.25	13.5	19	9.5	13.5	19	9.75
14	18	9	14	19	9.5	14	18	9.25
14.5	18	9	14.5	19	9.5	14.5	19	9.25
15	19	9.25	15	20	9.75	15	19	9.5
15.5	19	9.5	15.5	20	10	15.5	19	9.5
16	18	9.25	16	20	10	16	20	9.75
16.5	19	9.25	16.5	20	10	16.5	19	9.75
17	19	9.5	17	18	9.5	17	18	9.25
17.5	19	9.5	17.5	16	8.5	17.5	19	9.25
18	18	9.25	18	16	8	18	19	9.5
18.5	18	9	18.5	17	8.25	18.5	19	9.5
19	17	8.75	19	19	9	19	20	9.75
19.5	16	8.25	19.5	19	9.5	19.5	20	10
20	17	8.25	20	19	9.5	20	21	10.25
20.5	18	8.75	20.5	18	9.25	20.5	20	10.25
21	17	8.75	21	19	9.25	21	20	10
21.5	19	9	21.5	20	9.75	21.5	19	9.75
22	19	9.5	22	20	10	22	20	9.75
22.5	20	9.75	22.5	20	10	22.5	18	9.5

Cruciform 5			Cruciform 6			Cruciform 7		
Disp (mm)	Load (kN)	Energy (J)	Disp (mm)	Load (kN)	Energy (J)	Disp (mm)	Load (kN)	Energy (J)
23	21	10.25	23	22	10.5	23	19	9.25
23.5	23	11	23.5	23	11.25	23.5	20	9.75
24	24	11.75	24	25	12	24	22	10.5
24.5	25	12.25	24.5	29	13.5	24.5	24	11.5
25	26	12.75	25	32	15.25	25	26	12.5
25.5	29	13.75	25.5	35	16.75	25.5	29	13.75
26	31	15	26	37	18	26	29	14.5
26.5	35	16.5	26.5	40	19.25	26.5	33	15.5
27	41	19	27	44	21	27	36	17.25
27.5	44	21.25	27.5	48	23	27.5	40	19
28	47	22.75	28	45	23.25	28	45	21.25
28.5	45	23	28.5	43	22	28.5	48	23.25
29	45	22.5	29	43	21.5	29	47	23.75
29.5	45	22.5	29.5	43	21.5	29.5	46	23.25
30	44	22.25	30	43	21.5	30	45	22.75
30.5	45	22.25	30.5	43	21.5	30.5	43	22
31	45	22.5	31	40	20.75	31	43	21.5
31.5	45	22.5	31.5	40	20	31.5	44	21.75
32	44	22.25	32	41	20.25	32	43	21.75
32.5	47	22.75	32.5	41	20.5	32.5	40	20.75
33	48	23.75	33	41	20.5	33	39	19.75
33.5	50	24.5	33.5	40	20.25	33.5	40	19.75
34	46	24	34	44	21	34	40	20
34.5	45	22.75	34.5	44	22	34.5	41	20.25
35	44	22.25	35	43	21.75	35	41	20.5
35.5	44	22	35.5	43	21.5	35.5	42	20.75
36	43	21.75	36	44	21.75	36	41	20.75
36.5	44	21.75	36.5	46	22.5	36.5	44	21.25
37	45	22.25	37	48	23.5	37	46	22.5
37.5	44	22.25	37.5	44	23	37.5	41	21.75
38	43	21.75	38	43	21.75	38	44	21.25
38.5	44	21.75	38.5	43	21.5	38.5	43	21.75
39	46	22.5	39	42	21.25	39	42	21.25
39.5	45	22.75	39.5	40	20.5	39.5	45	21.75
40	40	21.25	40	38	19.5	40	45	22.5
40.5	39	19.75	40.5	38	19	40.5	47	23
41	40	19.75	41	39	19.25	41	47	23.5
41.5	40	20	41.5	38	19.25	41.5	48	23.75
42	40	20	42	39	19.25	42	45	23.25
42.5	39	19.75	42.5	36	18.75	42.5	45	22.5
43	39	19.5	43	37	18.25	43	47	23
43.5	39	19.5	43.5	38	18.75	43.5	48	23.75
44	40	19.75	44	37	18.75	44	48	24
44.5	39	19.75	44.5	34	17.75	44.5	47	23.75
45	40	19.75	45	33	16.75	45	45	23
Energy (J)		1384			1351			1419

Double Cruciform 1			Double Cruciform 2			Quadruple Cruciform		
Disp (mm)	Load (kN)	Energy (J)	Disp (mm)	Load (kN)	Energy (J)	Disp (mm)	Load (kN)	Energy (J)
0	0		0	0		0	0	
0.5	1.13	0.9475	0.5	2.23		0.5	0.93	
1	2.66	1.9975	1	3.8	1.5075	1	2.4	0.8325
1.5	5.33	4.8875	1.5	9.79	3.3975	1.5	15.11	4.3775
2	14.22	10.695	2	21.57	7.84	2	37	13.0275
2.5	28.56	16.02	2.5	29.9	12.8675	2.5	61.49	24.6225
3	35.52	20.63	3	41.38	17.82	3	88	37.3725
3.5	47	27.1625	3.5	50.5	22.97	3.5	107	48.75
4	61.65	33.455	4	59.92	27.605	4	128	58.75
4.5	72.17	35.5425	4.5	69.48	32.35	4.5	137	66.25
5	70	31.25	5	71.04	35.13	5	120	64.25
5.5	55	27.1125	5.5	60.29	32.8325	5.5	104	56
6	53.45	25.1125	6	55.43	28.93	6	95	49.75
6.5	47	23.625	6.5	51.47	26.725	6.5	90	46.25
7	47.5	23.875	7	48.8	25.0675	7	85	43.75
7.5	48	24	7.5	49.9	24.675	7.5	86	42.75
8	48	24.75	8	51.73	25.4075	8	87	43.25
8.5	51	26.25	8.5	53.6	26.3325	8.5	90	44.25
9	54	27.25	9	56.09	27.4225	9	95	46.25
9.5	55	27	9.5	55.93	28.005	9.5	99	48.5
10	53	25.81	10	52.7	27.1575	10	98	46.75
10.5	50.24	24.31	10.5	50.44	25.785	10.5	80	42
11	47	22.25	11	47.84	24.57	11	76	39
11.5	42	19.75	11.5	46.51	23.5875	11.5	72	37
12	37	18.25	12	45.31	22.955	12	68	35
12.5	36	18	12.5	41.91	21.805	12.5	66	33.5
13	36	18.25	13	41.28	20.7975	13	64	32.5
13.5	37	18.25	13.5	40.22	20.375	13.5	63	31.75
14	36	17.75	14	39.14	19.84	14	63	31.5
14.5	35	17.5	14.5	38.95	19.5225	14.5	63	31.5
15	35	17	15	38.32	19.3175	15	64	31.75
15.5	33	16.5	15.5	36.75	18.7675	15.5	62	31.5
16	33	16.75	16	36.39	18.285	16	62	31
16.5	34	16.5	16.5	35.75	18.035	16.5	61	30.75
17	32	16	17	35.42	17.7925	17	61	30.5
17.5	32	16	17.5	35.16	17.645	17.5	63	31
18	32	16	18	35.92	17.77	18	64	31.75
18.5	32	16	18.5	36.22	18.035	18.5	63	31.75
19	32	16.25	19	37.82	18.51	19	64	31.75
19.5	33	16.75	19.5	37.92	18.935	19.5	65	32.25
20	34	17.25	20	37.29	18.8025	20	66	32.75
20.5	35	17.5	20.5	36.82	18.5275	20.5	67	33.25
21	35	17.5	21	37.65	18.6175	21	69	34
21.5	35	17.75	21.5	38.05	18.925	21.5	70	34.75
22	36	18.25	22	39	19.2625	22	71	35.25
22.5	37	19	22.5	39.22	19.555	22.5	75	36.5
23	39	20	23	40	19.805	23	81	39
23.5	41	21.5	23.5	40.42	20.105	23.5	89	42.5
24	45	23.5	24	42.28	20.675	24	100	47.25
24.5	49	25.5	24.5	44	21.57	24.5	107	51.75
25	53	27	25	48.74	23.185	25	115	55.5
25.5	55	28.5	25.5	50.67	24.8525	25.5	132	61.75
26	59	30.25	26	56.29	26.74	26	149	70.25
26.5	62	33.5	26.5	62	29.5725	26.5	166	78.75

Double Cruciform 1			Double Cruciform 2			Quadruple Cruciform		
Disp (mm)	Load (kN)	Energy (J)	Disp (mm)	Load (kN)	Energy (J)	Disp (mm)	Load (kN)	Energy (J)
27.5	74	38.5	27.5	70.18	34.115	27.5	167	86.75
28	80	42	28	80	37.545	28	161	82
28.5	88	45	28.5	87	41.75	28.5	161	80.5
29	92	46.75	29	87.89	43.7225	29	160	80.25
29.5	95	46.5	29.5	87.62	43.8775	29.5	162	80.5
30	91	44	30	88.62	44.06	30	164	81.5
30.5	85	41.5	30.5	87.02	43.91	30.5	161	81.25
31	81	40.25	31	87.39	43.6025	31	160	80.25
31.5	80	39.75	31.5	87.36	43.6875	31.5	159	79.75
32	79	39.75	32	85.92	43.32	32	159	79.5
32.5	80	40	32.5	86.32	43.06	32.5	159	79.5
33	80	41	33	86.16	43.12	33	158	79.25
33.5	84	42.25	33.5	82.69	42.2125	33.5	157	78.75
34	85	41.75	34	83.89	41.645	34	156	78.25
34.5	82	41.25	34.5	85.02	42.2275	34.5	156	78
35	83	41	35	87.23	43.0625	35	155	77.75
35.5	81	40.75	35.5	86.26	43.3725	35.5	154	77.25
36	82	41	36	86.59	43.2125	36	156	77.5
36.5	82	41.5	36.5	86.29	43.22	36.5	154	77.5
37	84	42.25	37	86.19	43.12	37	150	76
37.5	85	42.75	37.5	85.19	42.845	37.5	148	74.5
38	86	44.5	38	84	42.2975	38	144	73
38.5	92	46.25	38.5	83.39	41.8475	38.5	139	70.75
39	93	46.25	39	79	40.5975	39	136	68.75
39.5	92	44	39.5	76.7	38.925	39.5	135	67.75
40	84	42	40	75	37.925	40	134	67.25
40.5	84	42	40.5	75.54	37.635	40.5	134	67
41	84	41.5	41	75.44	37.745	41	134	67
41.5	82	40	41.5	74.27	37.4275	41.5	132	66.5
42	78	38	42	72.76	36.7575	42	131	65.75
42.5	74	37.5	42.5	73.54	36.575	42.5	130	65.25
43	76	38.5	43	75.54	37.27	43	131	65.25
43.5	78	39	43.5	74.07	37.4025	43.5	130	65.25
44	78	39	44	72.07	36.535	44	128	64.5
44.5	78	38.75	44.5	73.61	36.42	44.5	129	64.25
45	77	38.25	45	76.14	37.4375	45	130	64.75
Energy (J)		2624			2612			4823